Reanalysis of Surface Geophysical Exploration Resistivity Data for the 241-T Tank Farm

Prepared by **Dale Rucker and Gillian Noonan** of hydroGEOPHYSICS, Inc.
and **Colin Henderson** of Columbia Energy & Environmental Services, Inc.

Prepared for
Washington River Protection Solutions
Richland, WA 99352
U.S. Department of Energy Contract DE-AC27-08RV14800

EDT/ECN:	DRF	UC:	
Cost Center:		Charge Code:	
B&R Code:		Total Pages:	156

Key Words: SGE, resistivity, geophysics, T Farm, long electrode, inversion

Abstract: This report presents the results of a reanalysis (including processing and inversion) of electrical resistivity data collected in and around the T tank farm at the U.S. Department of Energy's (DOE) Hanford Site in Washington State in 2005 and 2006. Given the extent of near-surface metallic infrastructure that could potentially mask any interpretable waste plume, it was necessary to use the large number of wells around the site as long electrodes. To accommodate the long electrodes, the resistivity inversion code was modified to allow low resistivity values to be assigned to the well's location. The results of the T tank farm field survey showed large low resistivity plumes beneath the disposal areas that coincided with the conceptual hydrogeological models developed about the releases. Additionally, in areas of minimal infrastructure, the long electrode method was able to match the results of a three-dimensional surface resistivity survey with reasonable fidelity. Based on these results, the long electrode resistivity method may provide a new strategy of environmental characterization at highly industrialized sites, provided a sufficient number and density of wells exist. In summary, the reprocessing of T tank farm SGE resistivity data was a success. The well-to-well models showed greater coherency and targets matched conceptual models.

TRADEMARK DISCLAIMER. Reference herein to any specific commercial product, process, or service by trade name, trademark, manufacturer, or otherwise, does not necessarily constitute or imply its endorsement, recommendation, or favoring by the United States Government or any agency thereof or its contractors or subcontractors.

Nancy A Fouad 10-8-09
Release Approval Date

OCT 0 8 2009
DATE:
STA: 15
HANFORD RELEASE
ID: 65
Release Stamp

Approved For Public Release

EXECUTIVE SUMMARY

Electrical resistivity data acquired in the T tank farm was reprocessed using advanced software algorithms and enhanced computer hardware. The resistivity datasets for T tank farm included surface-to-surface data acquired in the summer of 2005, and well-to-well and well-to-surface acquired in January 2006. Limitations in both software and hardware forced the modeling effort to split the T farm domain into smaller subsets.

Since the initiation of the Surface Geophysical Exploration program, significant advances have been made in modeling resistivity data that encompass large tank farm domains in one single inversion model. The current scope of reprocessing the T tank farm data included reprocessing the well-to-well, surface-to-surface, and well-to-surface data using these enhanced tools with an upgraded version of the upgraded software code, RES3DINV, developed by Geotomo Software located in Penang, Malaysia.

The reprocessing of the T farm data was divided into three tasks. The first task was to model the well-to-well data, and several subsets of the well-to-well data were modeled including a pole-pole array dataset of all groundwater and vadose zone wells, pole-pole dataset for groundwater wells alone, dipole-dipole data for both groundwater and vadose zone wells, and a mixed pole-pole with dipole-dipole for groundwater and vadose zone wells. Several trials for pole-pole data on all well types were completed to test the effects of various well parameters on the outcome. One model was selected which produced the best results, which showed targets that were coherent and met hydrologic expectations compared to the site conceptual model and direct characterization data. The outcome with the RES3DINV model were far superior to the previous outcome using EarthImager3D®.

Figure ES-1 shows the results of the well-to-well inversion with RES3DINV. In general, the well-to-well model shows several low resistivity targets around known disposal areas. The most significant target is found in the southwest corner of the grid around cribs T-5, T-7, and T-32. Given the large volume of disposal for these trenches, the target matches hydrogeologic expectations. The exact shape and position of the large target, however, is likely influenced by the distribution and density of the wells. Another significant target is found at the southeast corner of the T-106 tank, which matches the conceptual model discussed in RPP-23752, *Field Investigation Report for Waste Management Areas T and TX-TX*. This target is elongated from the northwest corner of T-106 (and directly south of T-103) to the northwest corner of T-111.

® EarthImager3D is a registered trademark of Advanced Geosciences, Inc.

Figure ES-1. Example of the WTW Reprocessed Data.

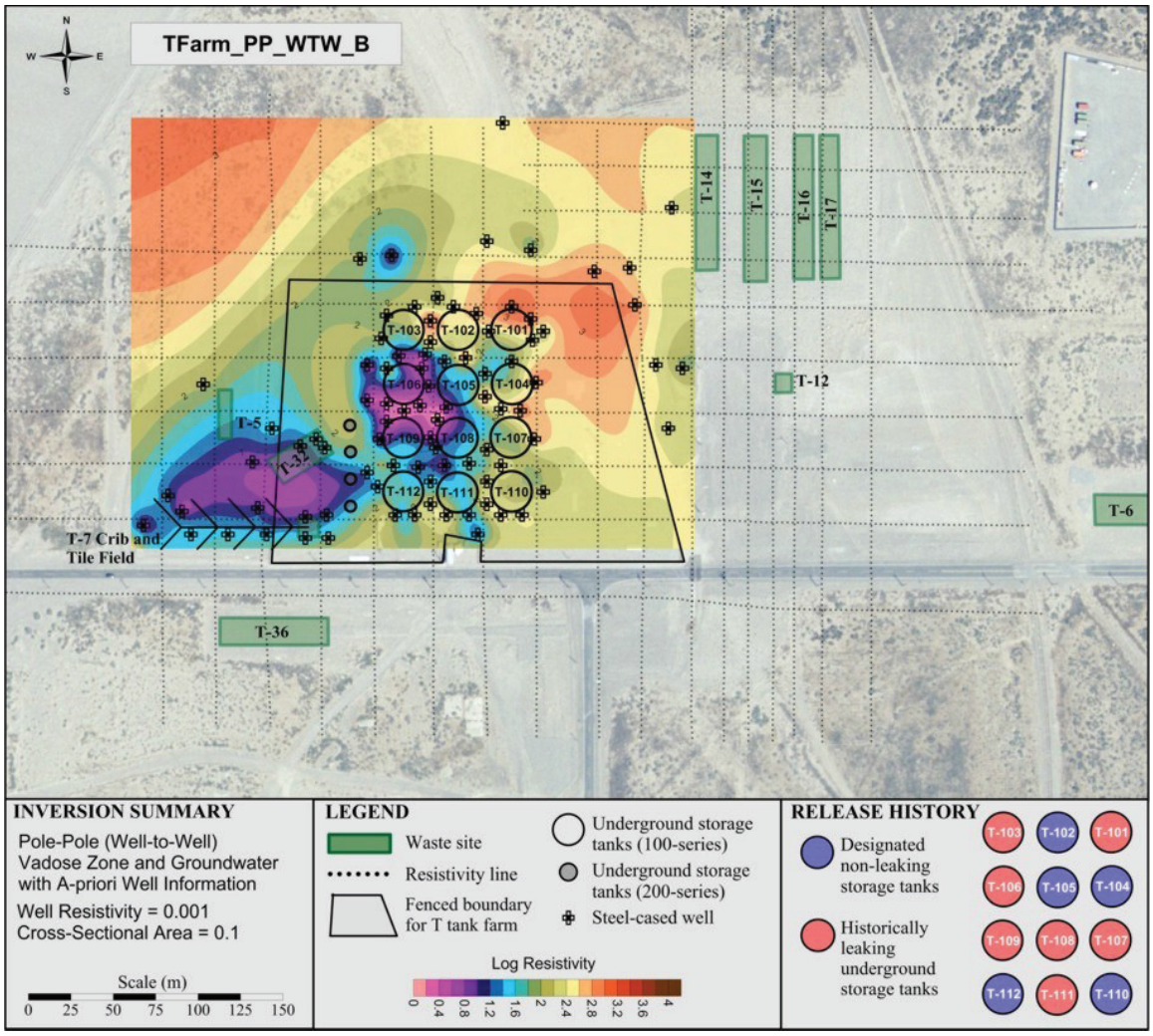

The second task was to model the surface-to-surface data. The effort was divided into three subtasks to investigate the western trenches area, northeastern trenches area, and the entire domain. The first two subtasks were meant to investigate areas of minimal infrastructure to ensure a good model with reasonable error statistics could be generated in simple areas before moving on to complex areas. The model of the western trenches showed a significant target beneath T-7 and T-32 cribs. These cribs received approximately 35 million gallons of liquid waste and it was expected that a large low resistivity target would be located here. The model of the northeastern trenches also showed a significant target, which appeared to match information from the sole characterization well in the area (W11-45). Figure ES-2 shows a slice at a depth of 38 meters for the northeast domain, with the majority of the low resistivity feature towards the south end of the trenches.

Figure ES-2. Horizontal Slice Showing Resistivity Distribution at 38M For the Northeast Region Model.

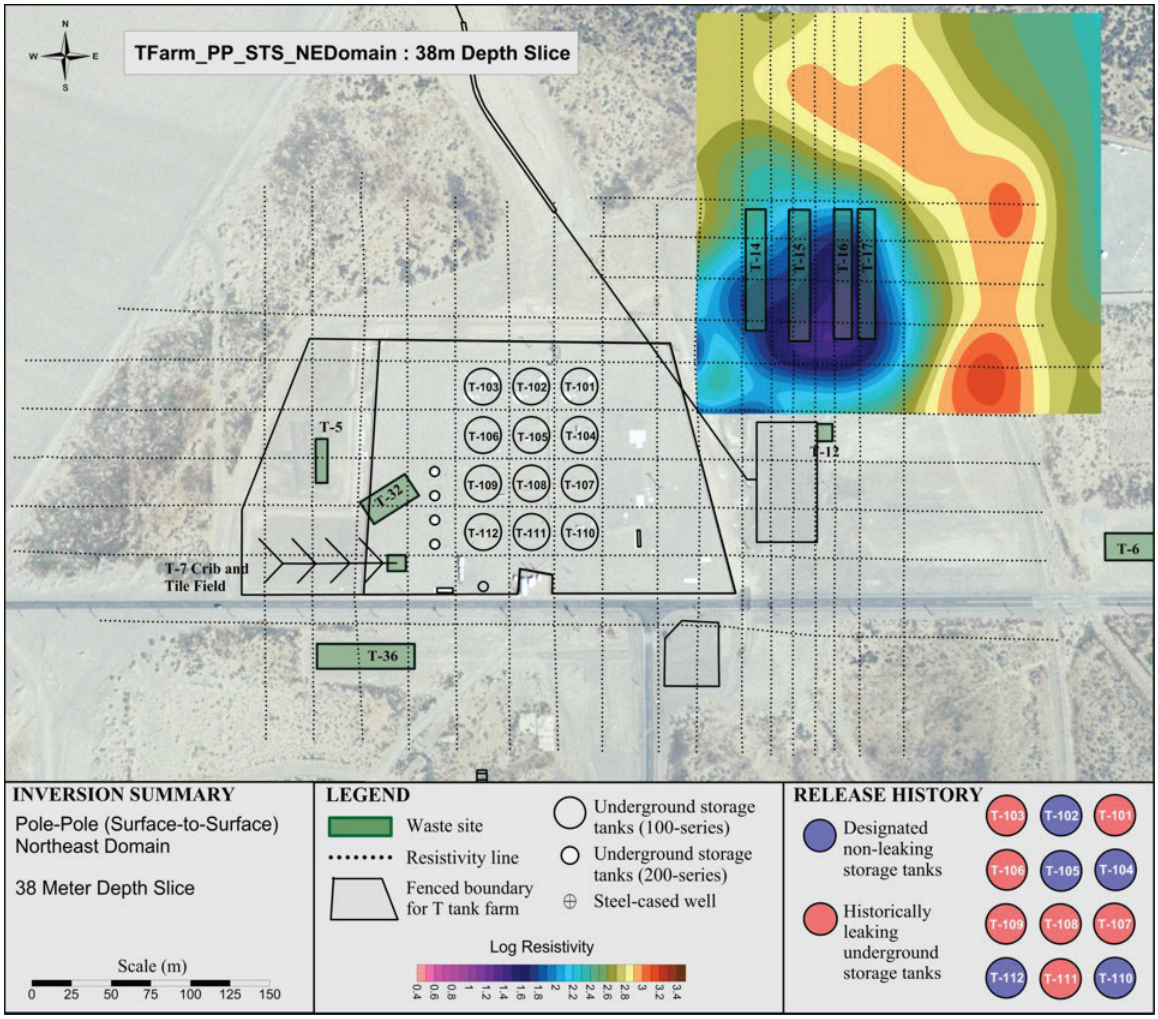

The last model for surface-to-surface was completed on the entire domain, including data that went directly through the tank farm. The T tank farm has a considerable amount of infrastructure that could cause interference with electrical resistivity measurements. The resistivity results reflect much of this infrastructure in that the low resistivity appears to coincide with the footprint of the tanks. Unlike the well-to-well models which identified segregated areas of low resistivity, the surface-to-surface model of the entire domain shows only large undifferentiated targets that do not match hydrologic expectations.

The third task was to model the well-to-surface data. The surface lines for the well-to-surface acquisition coincided with the locations of 5N and 5E from the surface-to-surface acquisition. The results showed a high degree of incoherency, or noise that may or may not coincide with historical leaks. These noise sources are likely due to a majority of the surface electrodes running directly through the tank farm where metallic infrastructure could be causing interference. A few trials were conducted with the well-to-surface geometry including adding

well-to-well data and removing surface electrodes that are within the tank farm (leaving electrodes outside the farm intact). Adding well-to-well data did not affect the outcome of the resistivity distribution.

However, removing a subset of surface electrodes had a profound effect. Figure ES-3 shows the model results. Many low resistivity targets were shown to be at logical locations with respect to contamination sources. A few low resistivity targets existed at unexpected locations, which simply could mean that even though the electrodes were outside the farm fence, piping could still be causing significant noise. If placed properly, the well-to-surface method could expand the success of the well-to-well method to areas of no or minimal well coverage. An example is the TX/TY tank farm Surface Geophysical Exploration project, where surface electrodes were placed on the periphery of the domain.

Figure ES-3. Mixed WTS and WTW Inversion Results Using a Subset of Surface Electrodes.

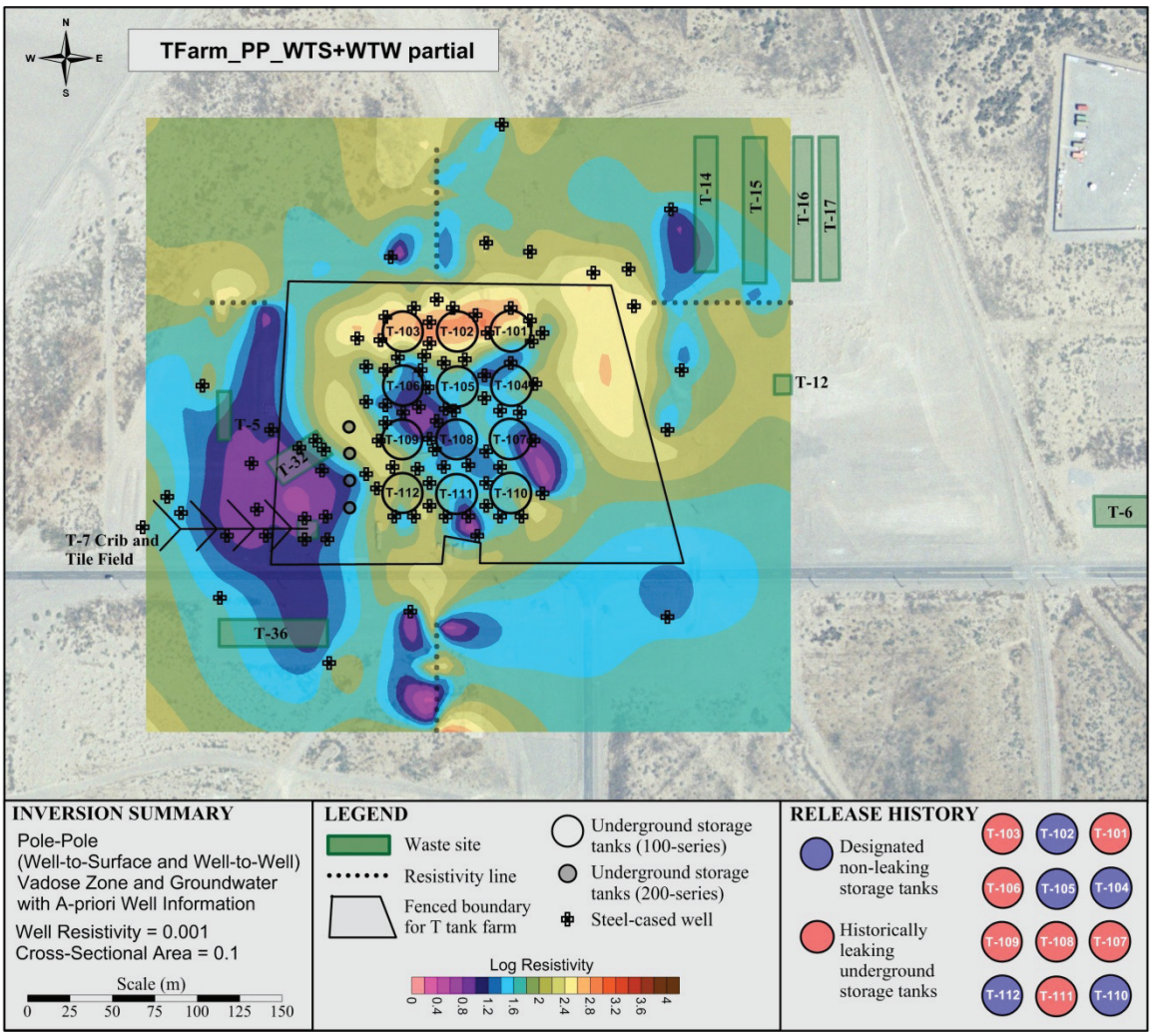

In summary, the reprocessing of T tank farm Surface Geophysical Exploration resistivity data was a success. The well-to-well models showed greater coherency and targets matched

conceptual models. The surface-to-surface models of domains in areas of minimal infrastructure were also quite successful. It is recommended, at the minimum, to reprocess all previous well-to-well data from the various Surface Geophysical Exploration project using RES3D.

TABLE OF CONTENTS

1.0 INTRODUCTION 1-1
1.1 SCOPE 1-1
1.2 OBJECTIVES 1-2
1.3 REPORT LAYOUT 1-2

2.0 BACKGROUND 2-1
2.1 SITE DESCRIPTION 2-1
2.2 OPERATIONAL HISTORY 2-1
2.3 ENVIRONMENTAL SETTING 2-12
2.4 HISTORICAL CHARACTERIZATION EFFORTS 2-12

3.0 QUALITY ASSURANCE FOR DATA PROCESSING AND REDUCTION 3-1

4.0 THEORY 4-1
4.1 RESISTIVITY INVERSION PRINCIPLES 4-1
4.2 WELL-TO-WELL INVERSION EXAMPLES 4-5
4.2.1 Example with Pole-Pole Array 4-5
4.2.2 Example with Dipole-Dipole Array 4-9
4.3 MECHANICS OF INVERSION MODELING AND VISUALIZATION 4-11
4.3.1 Geospatial Database Management and Queries 4-11
4.3.2 Inverse Modeling With RES3D Inversion Code 4-12
4.3.3 Inversion Parameters 4-14
4.3.4 Resistivity Visualization 4-17
4.3.5 Resistivity Color Scales 4-17

5.0 METHODOLOGY 5-1
5.1 RESISTIVITY EQUIPMENT 5-1
5.2 SURVEY AREA AND LOGISTICS 5-3
5.2.1 Task 1 – Well-to-Well Measurements 5-4
5.2.2 Task 2 – Surface-to-Surface Resistivity Mapping 5-5
5.2.3 Task 3 – Well-to-Surface Measurements 5-7
5.3 DATA PROCESSING 5-8
5.3.1 Task 1 – WTW Processing 5-8
5.3.2 Task 2 – STS Processing 5-10
5.3.3 Task 3 – WTS Processing 5-14

6.0 RESULTS AND INTERPRETATION 6-1
6.1 PREVIOUS T FARM WELL-TO-WELL INVERSION RESULTS 6-1
6.2 REPROCESSED 3D RESISTIVITY INVERSION MODELING 6-4
6.2.1 Task 1 – WTW Inversion Results 6-4

6.2.2 Task 2 – STS Inversion Model Results 6-17
6.2.3 Task 3 – WTS Inversion Model Results 6-36

7.0 CONCLUSIONS 7-1

8.0 LIMITATIONS AND RECOMMENDATIONS 8-1
8.1 DATA ACQUISITION 8-1
8.1.1 Logistics 8-1
8.1.2 Equipment 8-1
8.2 DATA PROCESSING 8-2
8.2.1 Infrastructure Interference 8-2
8.2.2 Inversion Modeling 8-2

9.0 REFERENCES 9-1

LIST OF APPENDICES

A DATA PROCESSING AND REDUCTION ..... A-i
B ELECTRICAL RESISTIVITY INVERSION FORMS ..... B-i

LIST OF FIGURES

2-1. Location of the T Tank Farm in the 200 West Area 2-2
2-2. T Tank Farm and Surrounding Facilities 2-3
2-3. General Configuration of Tanks in Waste Management Area T 2-4
2-4. Liquid Waste Volumes Discharged/Leaked Around the T, TX, and TY Tank Farms 2-6
2-5. Estimates of Major Cations in Wastes Disposed of or Leaked in and Around T Tank Farm 2-9
2-6. Estimates of Major Anions Disposed of or Leaked in and Around T Tank Farm 2-10
2-7. Infrastructure Map of Waste Management Area T 2-11
2-8. Nitrate and Sodium Concentrations and Soil Moisture in Selected Vadose Zone Samples Collected Around T Tank Farm 2-15
4-1. a) Discretized Earth for Inversion, b) Overhead View of Meshing Showing Relationship Between Nodes, Mesh Lines, and Blocks 4-2
4-2. Numerical Model Results of a Conductor of Finite Length and Diameter Compared to the Analytical Solution of an Infinite Conductor of Infinitesimal Diameter 4-4
4-3. Comparison of WTW inversion with RES3DINVx64 (RES3D64) and EarthImager3D (EI3D) 4-6
4-4. Example Models Showing the Resistivity Inversion Results for Surface and Long Electrodes 4-8

4-5. Pole-Pole Transfer Resistance Data Used to Calculate Dipole-Dipole Data For the Example Model With and Without Any Target 4-10
4-6. Dipole-Dipole Transfer Resistance Data With a Simple Target 4-10
4-7. Inversion Results of the Dipole-Dipole Array with a Simple Target 4-11
4-8. Flowchart of the Resistivity Inversion Process With RES3D Code 4-13
4-9. Example Histogram of Inversion Model Resistivity Data 4-18
5-1. Resistivity Equipment Showing Use of Lockout/Tagout Safety Equipment 5-1
5-2. Setup of Remote Electrodes for Pole-Pole Acquisition 5-2
5-3. Physical Connection of Wells for Acquisition 5-2
5-4. Location of the Completed High-Resolution Resistivity Survey Lines 5-3
5-5. Wells Used in the WTW Data Collection at T Tank Farm 5-4
5-6. STS Resistivity Line Layout for STS Data Collection at T Tank Farm 5-6
5-7. Example of Road Crossing Setups 5-7
5-8. Line Layout and Wells Used in WTS Data Collection in the T Tank Farm 5-8
5-9. Transfer Resistance Measured in WTW Data Collection 5-10
5-10. Transfer Resistance Data Measured in STS Data Collection 5-13
5-11. Transfer Resistance Measured in WTS Data Collection 5-15
6-1. Previous T Tank Farm WTW Inversion Results Using Vadose Zone Wells Only 6-1
6-2. Previous Results From WTW Inversion at T Tank Farm Using Groundwater Wells Only 6-3
6-3. Convergence Curves for the WTW Models 6-4
6-4. WTW Inversion Results for Reprocessed Data Using Well Resistivity of 0.001 OHM-M and Well Diameter of 0.04M 6-6
6-5. WTW Inversion Results for Reprocessed Data Using Well Resistivity of 0.001 OHM-M and Well Diameter of 0.1M 6-7
6-6. WTW Inversion Results for Reprocessed Data Using Well Resistivity of 0.05 OHM-M and Well Diameter of 0.5M 6-8
6-7. WTW Inversion Results for Reprocessed Data Using Well Resistivity of 0.1 OHM-M and Well Diameter of 0.5M 6-9
6-8. WTW Inversion Results for Reprocessed Data Using Well Resistivity of 0.006 OHM-M and Well Diameter of 0.1M 6-10
6-9. WTW Inversion Results for Reprocessed Data Using Groundwater Wells Only With Well Resistivity of 0.006 OHM-M And Well Diameter of 0.1M 6-12
6-10. Nitrate in Groundwater for Select Wells Around the T Tank Farm 6-13
6-11. Ratio of Nitrate to Technetium in Groundwater for Select Wells 6-14
6-12. WTW Inversion Results for Dipole-Dipole Array Reprocessed Data Using Well Resistivity of 0.006 OHM-M and Diameter of 0.1M 6-15
6-13. WTW Inversion Results for Mixed Pole-Pole and Dipole-Dipole Array Reprocessed Data Using Well Resistivity of 0.006 OHM-M and Well Diameter of 0.1M 6-16
6-14. Domain Boundaries for the STS Inversion Models 6-17
6-15. Convergence Curves for the STS Models 6-18

6-16. Horizontal Slice Showing Resistivity Distribution at 5M for the Western Region STS Inversion Model 6-19
6-17. Horizontal Slice Showing Resistivity Distribution at 16M For The Western Region STS Inversion Model 6-20
6-18. Horizontal Slice Showing Resistivity Distribution at 38M for the Western Region STS Inversion Model 6-21
6-19. Horizontal Slice Showing Resistivity Distribution at 56M for the Western Region STS Inversion Model 6-22
6-20. Horizontal Slice Showing Resistivity Distribution at 78M for the Western Region STS Inversion Model 6-23
6-21. Horizontal Slice Showing resistivity Distribution at 5M for the Northeast Region STS Inversion Model 6-24
6-22. Horizontal Slice Showing Resistivity Distribution at 16M for the Northeast Region STS Inversion Model 6-25
6-23. Horizontal Slice Showing Resistivity Distribution at 26M for the Northeast Region STS Inversion Model 6-26
6-24. Horizontal Slice Showing Resistivity Distribution at 38M for the Northeast Region STS Inversion Model 6-27
6-25. Horizontal Slice Showing Resistivity Distribution at 56M for the Northeast Region STS Inversion Model 6-28
6-26. Horizontal Slice Showing Resistivity Distribution at 78M for the Northeast Region STS Inversion Model 6-29
6-27. Horizontal Slice Showing Resistivity Distribution at 5M for the Entire T Farm 6-31
6-28. Horizontal Slice Showing Resistivity Distribution at 16M for the Entire T Farm 6-32
6-29. Horizontal Slice Showing Resistivity Distribution at 26M for the Entire T Farm 6-33
6-30. Horizontal Slice Showing Resistivity Distribution at 38M for the Entire T Farm 6-34
6-31. Horizontal Slice Showing Resistivity Distribution at 56M for the Entire T Farm 6-35
6-32. Horizontal Slice Showing Resistivity Distribution at 78M for the Entire T Farm 6-36
6-33. Convergence Curves for the WTS Models 6-37
6-34. WTS Inversion Model Results 6-38
6-35. Results of Combined WTS and WTW Inversion Model 6-39
6-36. Mixed WTS and WTW Inversion Model Results Using a Subset Of Surface Electrodes 6-40

LIST OF TABLES

2-1. Liquid Disposal Facilities and Discharge Volumes Near T Tank Farm 2-5
2-2. T Tank Farm Tanks Classified as Assumed/Confirmed Leakers and Estimated Leak Volumes 2-7
5-1. Summary of Resistivity Acquisition Stats at the T Tank Farm 5-4
5-2. STS Resistivity Data Acquisition Parameters 5-12

6-1. Details of the WTW Models and Naming Convention..... 6-5

LIST OF TERMS

Abbreviations and Acronyms

2D	two-dimensional
3D	three-dimensional
CCu	Cold Creek Unit
DOE	U.S. Department of Energy
EI3D	EarthImager3D®
EI3DCL	EarthImager3D®CL
ERC	electrical resistivity characterization
RES2D	RES2DINV
RES3D	RES3DINV
RES3D64	Res3DINVx64
RMS	root-mean-square
SGE	Surface Geophysical Exploration
SST	single-shell tank
STS	surface-to-surface
WMA	waste management areas
WTS	well-to-surface
WTW	well-to-well

Units

ft	foot or feet
in.	inch
m	meter
mg/L	milligrams per liter

1.0 INTRODUCTION

This report presents the results of a reanalysis (including processing and inversion) of electrical resistivity data collected during an investigation of the T tank farm at the U.S. Department of Energy's (DOE) Hanford Site in Washington State and surrounding areas for subsurface contamination. The original T tank farm resistivity project was conducted in 2005 and 2006 and the results were reported in RPP-RPT-28955, *Surface Geophysical Exploration of T Tank Farm*. The current scope includes a reanalysis of the original data to make use of advances in Surface Geophysical Exploration (SGE) computing capability and software that have been implemented since 2005. This investigation was specifically designed to apply both new analytical software and hardware to T farm data and to provide an assessment of the changes, if any, in the analysis of T farm resistivity anomalies.

The T farm was the first tank farm in which resistivity and other geophysical tools were deployed to help define the extent of subsurface contamination specifically within a tank farm environment. The T tank farm was identified as the first candidate for construction of an interim surface barrier to inhibit or stop the migration of mobile contaminants in the vadose zone. SGE results for the region were used to augment existing field information to design and implement the barrier as it was constructed. SGE identified additional anomalies within the farm which were not included beneath the interim barrier. In the time since this first deployment of SGE in the tank farm environment, numerous improvements have been made in the analysis of the data.

For the resistivity analysis conducted in 2005, it was necessary to parse the data into subareas, treat each subarea as an individual unit, and then stitch the information back together to form a complete image of the subsurface. This approach, while necessary at the time, can result in numerical boundary errors impacting the final analysis, "High Resolution Resistivity (HRR) delineation of a liquid waste plume at a former radioactive waste disposal site, Hanford, Washington." See *Geophysics,* 2009 (in review), "Electrical resistivity characterization of an industrial site using long electrodes. The present analysis uses all information together in hopes of mitigating previous issues associated with the possible numerical errors introduced along subarea boundaries. Additionally, lessons learned from previous SGE projects at Hanford regarding noise and potentially suspect data from measurement errors, were applied to the raw T farm data in order to formulate a new processed data set ready for inversion.

1.1 SCOPE

The scope for this effort was to provide an assessment of the changes, if any, in the analysis of T farm resistivity anomalies using the latest generation of computer hardware and software designed explicitly to model large electrical resistivity datasets. The scope was divided into three modeling tasks that included reanalysis of the previously acquired well-to-well (WTW), surface-to-surface (STS), and well-to-surface (WTS) data.

Task 1 – The T tank farm was the first SGE project to use the WTW technique to image the resistivity within infrastructure rich areas. In the previous effort, code modifications to the

EarthImager3D® (EI3D) inversion software were necessary to use the steel wells (drywells and groundwater wells) as long electrodes. Additionally, several types of arrays were employed with the WTW technique including the pole-pole and dipole-dipole arrays. The scope of the current task reprocesses all data with the Res3DINVx64 (RES3D64) code on a computing platform capable of inverting the entire T farm domain.

Task 2 – The previous T tank farm effort was the first SGE project to conduct the STS technique over an infrastructure rich area and the data were obviously affected by the large amount of metal associated with infrastructure in the subsurface. The original processing steps to accommodate the noisy data in 2005 were applied ad hoc and without much prior knowledge of this type of site. The current task reprocesses the original raw data in the four years of investigations in other tank farms. Additionally, the data are inverted as a whole using the RES3D64 code on a computing platform capable of inverting the entire T farm domain.

Task 3 – During the original WTW acquisition, two lines of electrodes were placed on the surface for a WTS acquisition. The lines followed 5E and 5N, but with a 6m electrode separation. Past efforts using EI3D to combine the surface and well data were performed, but with difficulty. Under the new task, the previously acquired data are reprocessed and inverted with the improved version of RES3D64. Unfortunately, the data quality of the surface electrodes in the farm were low and the results were not sufficiently coherent for direct interpretation.

1.2 OBJECTIVES

The main objective of the current work was to reprocess the original T farm data acquired in 2005 and 2006 using the new algorithms, processing methodologies, different acquisition modalities, and computing platforms available to current SGE projects.

1.3 REPORT LAYOUT

This report is divided into several main sections.

- **Section 1.0, Introduction** – Describes the scope and objectives of the investigation.
- **Section 2.0, Background** – Describes the setting of the T tank farm, with geology and hydrology, and information regarding the disposal activities in and around the tank farm.
- **Section 3.0, Quality Assurance** – Discusses the project-specific quality assurance plans that conform to applicable requirements from the Columbia Energy quality assurance procedures.
- **Section 4.0, Theory** – Discusses the theory behind the resistivity methods employed at the T tank farm.
- **Section 0, Methodology** – Discusses briefly the acquisition methodology and processing of the geophysical data at the T tank farm.
- **Section 6.0, Results and Interpretation** – Presents the results from the surveying effort.

® EarthImager3D is a registered trademark of Advanced Geosciences, Inc.

- **Section 7.0, Conclusions** – Provides conclusions drawn from the results, interpretations, and subsequent assessment of results.
- **Section 8.0, Limitations and Recommendations** – Provides limitations and recommendations for improving follow-on SGE efforts.
- **Section 9.0, References** – Lists reference documents cited in the report.
- **Appendix A, Data Processing and Reduction** – Discusses the details of the data processing and reduction of the T farm data.
- **Appendix B, Electrical Resistivity Inversion Forms** – Inversion tracking forms that lists detailed information regarding each inversion.

2.0 BACKGROUND

2.1 SITE DESCRIPTION

The T tank farm is one of 12 single-shell tank (SST) farms on the Hanford Site. The T tank farm is in the northern portion of the 200 West Area near the T plant, as shown in Figure 2-1, and is surrounded by a number of cribs and trenches (Figure 2-2). Most of the cribs and all of the trenches received waste directly from SSTs. Refer to WHC-MR-0227, *Tank Wastes Discharged Directly to the Soil at the Hanford* Site.

Washington River Protection Solutions, LLC has responsibility for vadose zone characterization at the tank farms under the direction of the DOE, Office of River Protection. The following documents provide background on T tank farm vadose zone characterization.

- RPP-23752, *Field Investigation Report for Waste Management Areas T and TX-TX*
- RPP-7578, *Site-Specific SST Phase 1 RFI/CMS Work Plan Addendum for WMAs T and TX-TY.*

The T tank farm consists of the following:

- 12 100-series SSTs
- 4 200-series SSTs
- Waste transfer lines
- Leak detection systems
- Tank ancillary equipment.

The 100-series SSTs are 23 meters or 75 feet (23m or 75 ft) in diameter. The four 200-series SSTs are 6.1m (20 ft) in diameter. The 12 larger SSTs are approximately 9m (30 ft) tall from base to dome. The smaller SSTs are approximately 8m (26 ft) tall. The general configuration of tanks in the T tank farm is shown in Figure 2-3. As noted in Figure 2-1, 7 of the 16 SSTs in T tank farm are designated as assumed leakers. See HNF-EP-0182, *Waste Tank Summary Report for Month Ending December 31, 1998* and RPP-7578.

2.2 OPERATIONAL HISTORY

Facilities in the T tank farm released liquid wastes to the vadose zone. Adjacent waste management facilities intentionally discharged liquid wastes to the vadose zone. These discharges led to contaminant plumes distributed in the vadose zone in and around the tank farm.

Figure 2-1. Location of the T Tank Farm in the 200 West Area.

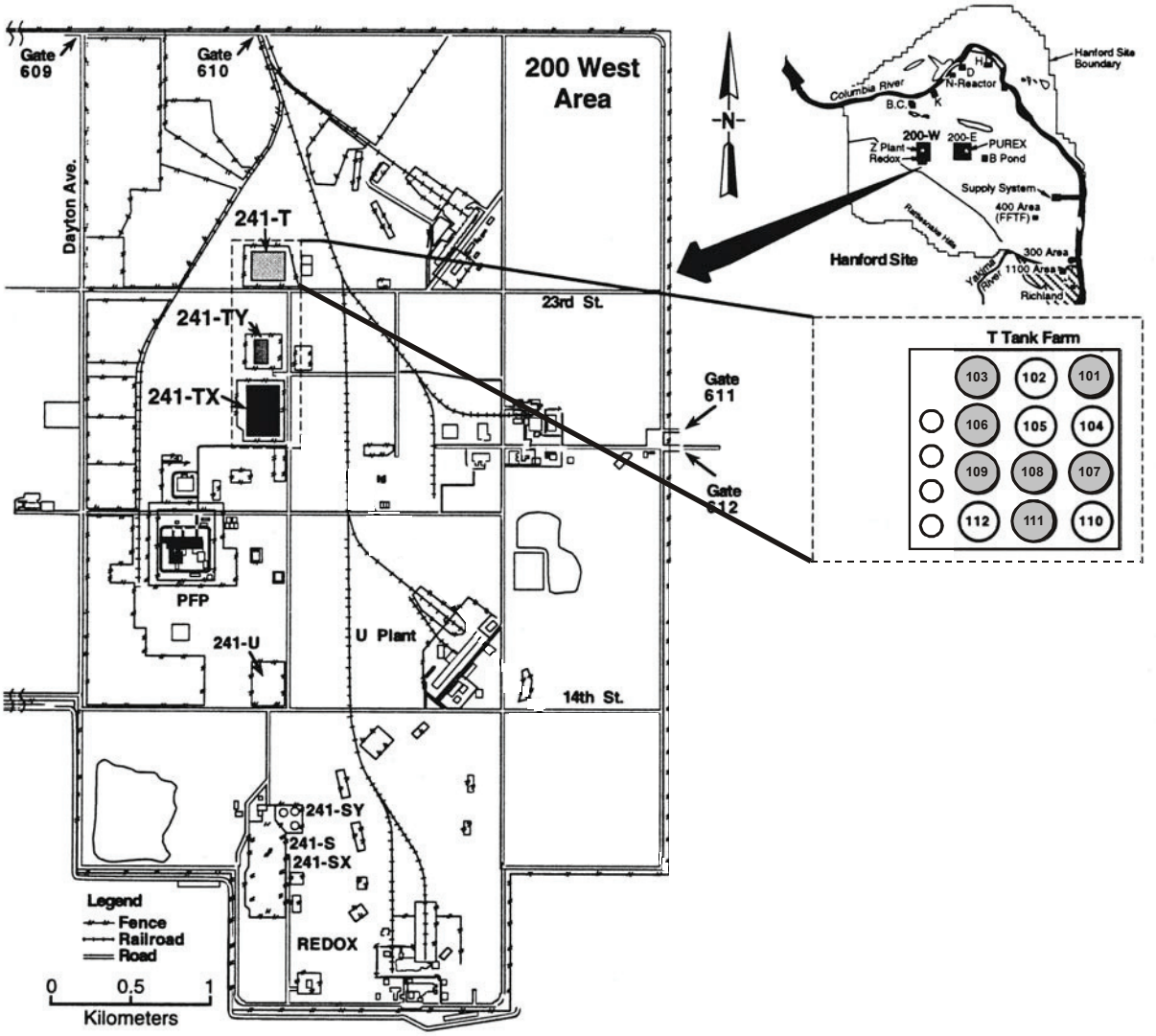

K:\CH2M\28090\Task 8\T-Farm SGE\Graphics\Fig2-1.cdr

Note: Shaded tanks are assumed or confirmed leaking tanks. Small 200-series tanks are not thought to have leaked.
Source: Modified from RPP-23752, *Field Investigation Report for Waste Management Areas T and TX-TY.*

Figure 2-2. T Tank Farm and Surrounding Facilities.

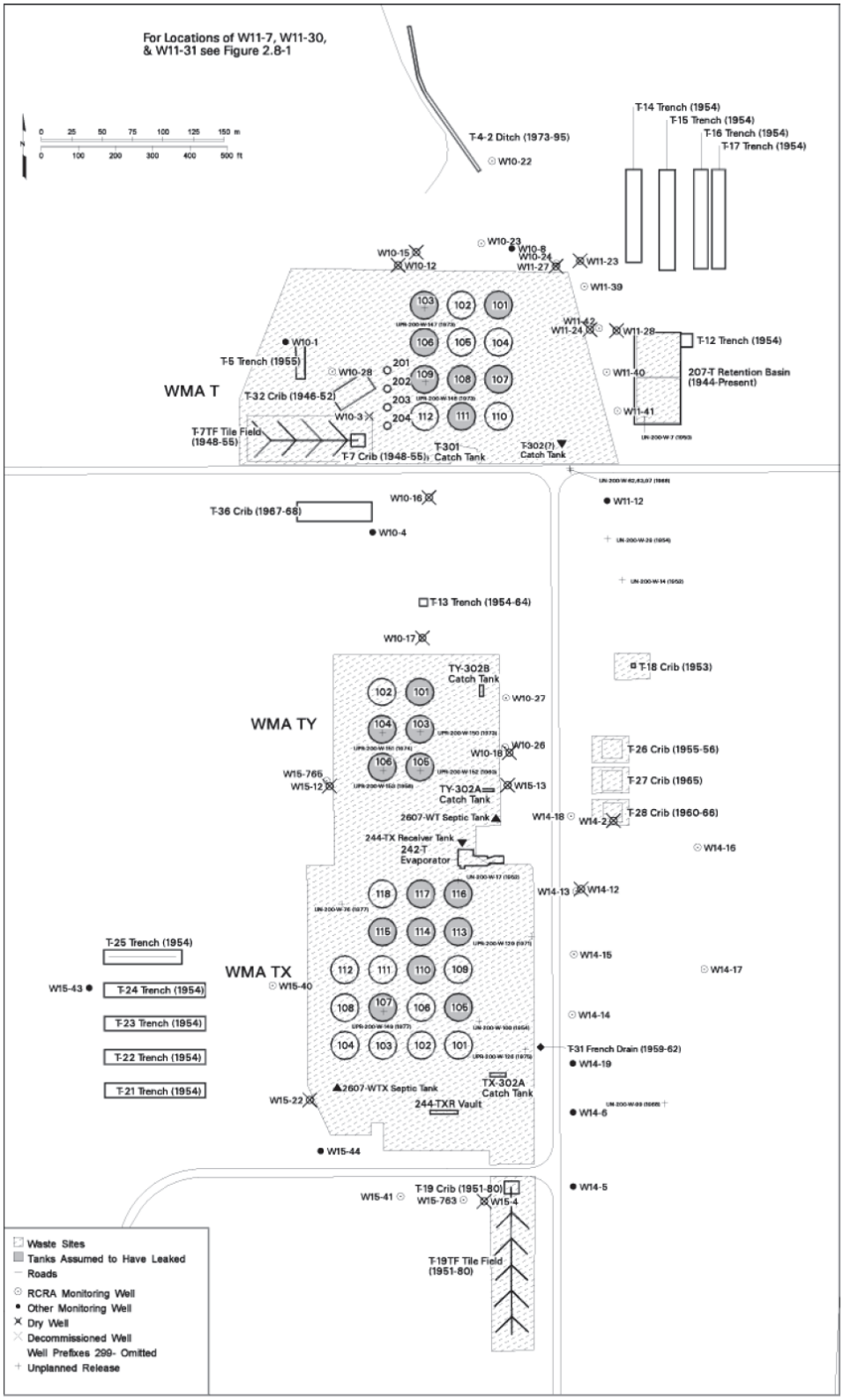

Source: RPP-23752, 2005, *Field Investigation Report for Waste Management Areas T and TX-TY*.

Figure 2-3. General Configuration of Tanks in Waste Management Area T.

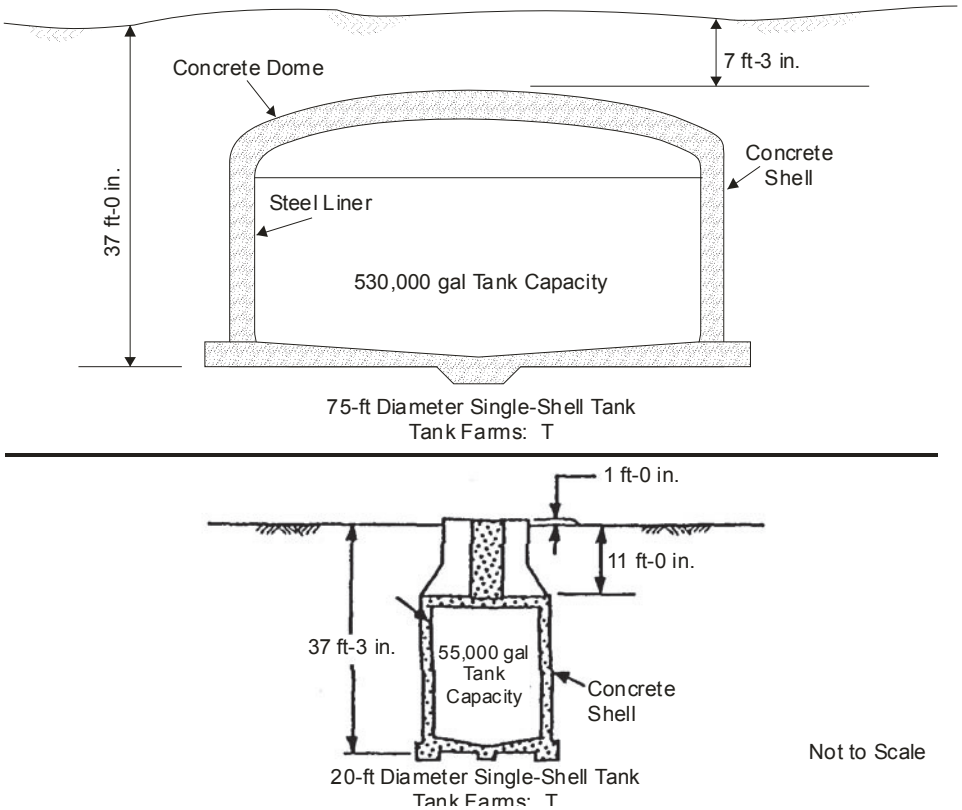

Source: HNF-EP-0182, *Waste Tank Summary Report for Month Ending February 28, 2006.*

The T tank farm was constructed between 1943 and 1944. In 1944, the T tank farm started receiving waste from T plant. The tanks were filled to capacity soon after they entered service. Because of limited tank space, liquid waste from the T tank farm was discharged to the 216-T-32 crib, T-7 trench, and T-5 trench. From 1948 through 1955, the T-7 crib/tile field was the primary discharge facility, receiving approximately 10 billion liters (29 million gallons) of waste (RPP-23752). During waste management operations, substantial volumes of liquid wastes were discharged to the cribs and trenches near the T tank farm as shown in Table 2-1.

Table 2-1. Liquid Disposal Facilities and Discharge Volumes Near T Tank Farm. (2 Sheets)

Facility/Component	Liquid Waste Discharge Volume (gallons)	Operational Period
T-5 trench	845,000	1955
T-32 crib	7.9 million	1946-1952
T-7 crib/tile field	29 million	1948-1955
T-12 trench	1.32 million	1954
T-14 trench	1 million	1954
T-15 trench		
T-16 trench		
T-17 trench		
T-36 crib	140,000	1967-1969

Source: RPP-23752, *Field Investigation Report for Waste Management Areas T and TX-TY.*

The distribution of discharged waste around the T tank farm and nearby TX and TY tank farms varies. Figure 2-4 shows the disposal volumes and tank leak volumes graphically depicted as relative-sized circles. The smaller the circle, the smaller the discharged, or released, volume. The figure shows that the significant proportion of the liquid waste volume was disposed in the trenches and cribs west of T tank farm. Approximately 144 million liters (38 million gallons) of waste were discharged to the T-5 and T-7 trenches and to the T-32 and T-36 cribs. Another area of significance is to the northeast of T tank farm, where 3.8 million liters (1 million gallons) of waste were discharged to four parallel trenches. As a result, groundwater samples have high nitrate concentrations, as well as other pertinent ions. The following documents show that nitrate concentrations have risen in the last five years in wells 299-W10-4 (south of the T tank farm) and 299-W10-28 (near the T-32 crib):

- PNNL-15070, *Hanford Site Groundwater Monitoring for Fiscal Year 2004*.
- RPP-20303, *Preliminary Data from 216-B-26 Borehole in BC Cribs Area*.

During active waste management operations, 7 of the 16 T tank farm tanks were identified as assumed leakers (HNF-EP-0182). This prompted a decision to take the tanks out of service and remove all pumpable liquid from the tanks. A leak from tank T-106 occurred in the early 1970's that released 435,000 liters (115,000 gallons). This leak is one of the most thoroughly documented SST leaks. Estimated leak volumes for the T tank farm tanks are provided in Table 2-2. Estimated leak volumes from two separate source documents are provided in Table 2-2 to show the uncertainty associated with volume estimates and leak dates.

Generally, the liquid tank waste is considered more concentrated than the waste disposed directly to the adjacent cribs and trenches. Tank T-106, for example, has been reported to have sodium concentrations of approximately 4 molar and nitrate concentrations of 0.77 molar. Figures 2-5 and 2-6 show a spatial distribution of major cations and anions discharged to the vadose zone.

Figure 2-4. Liquid Waste Volumes Discharged/Leaked Around the T, TX, and TY Tank Farms.

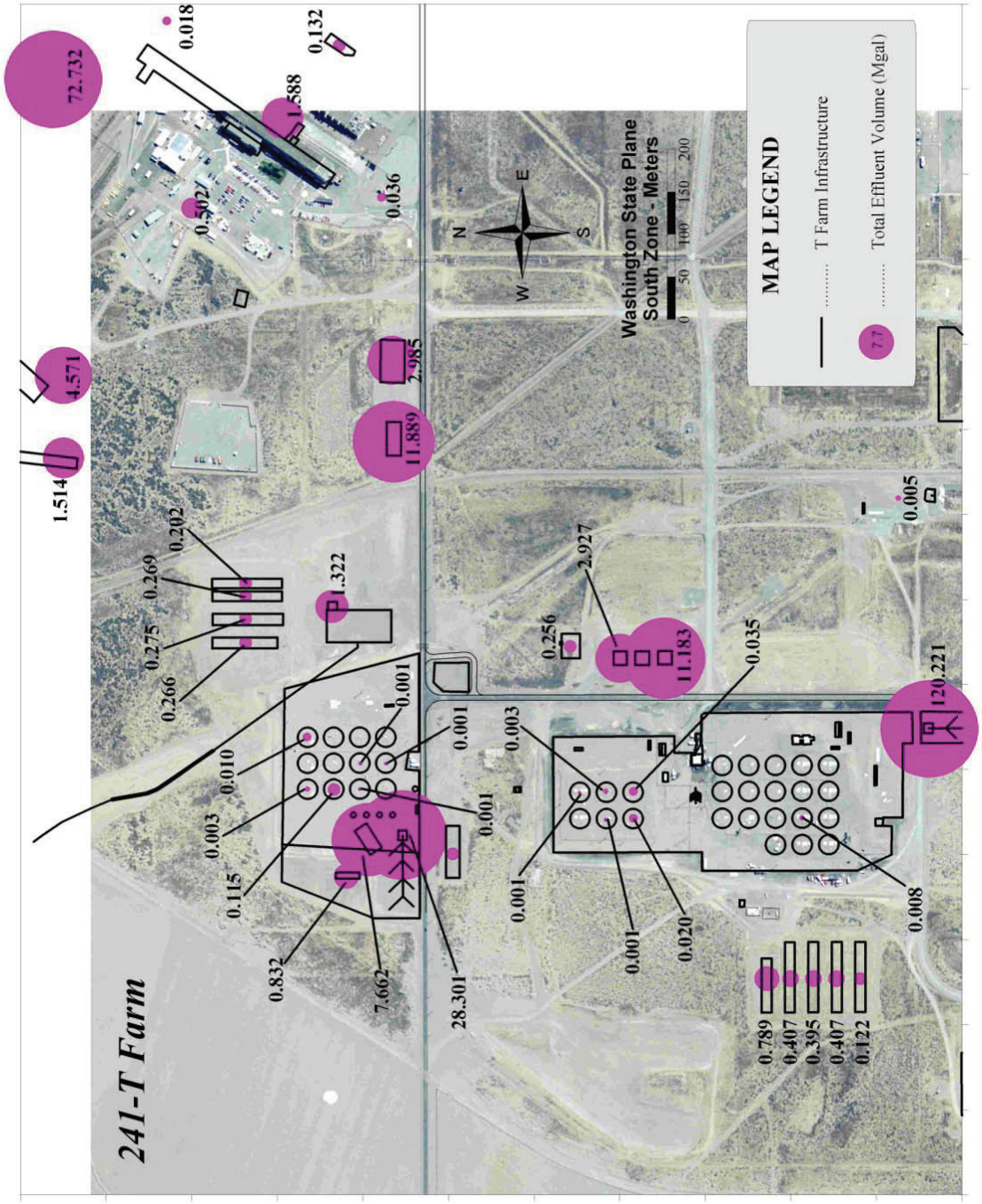

Table 2-2. T Tank Farm Tanks Classified as Assumed/Confirmed Leakers and Estimated Leak Volumes.

Tank	RPP-23405		HNF-EP-0182	
	Estimated Leak Volume (gallons) [a]	Estimated Leak Date	Estimated Leak Volume (gallons) [b]	Estimated Leak Date
T-101	10,000	1969	7,500	1992
T-103	3,000	1973	<1,000	1974
T-106	115,000	1973	115,000	1973
T-107	–[c]	1984	–[d]	1984
T-108	1,000	1974	<1,000	1974
T-109	1,000	1974	<1,000	1974
T-111	1,000	1971	<1,000	1979, 1994

Notes:
[a] From RPP-23405, *Tank Farm Vadose Zone Contamination Volume Estimates*.
[b] From HNF-EP-0182, *Waste Tank Summary Report for Month Ending February 28, 2006.*
[c] This tank is classified as an assumed leaker, although no liquid level decreases were observed for any of these tanks. RPP-23405 concludes that, in general, vadose zone activity near these tanks is negligible and does not support a volume inventory.
[d] Based on 19 tanks with the assumption that the cumulative leak volume was 150,000 gallons from these tanks for an average volume of 8,000 gallons for each of the 19 tanks.

Electrical resistivity methods are used to map the extent of subsurface contamination by contrasting electrical properties that appear anomalous relative to a background. At the T tank farm, these anomalies should be the result of water soluble inorganics from the waste, migrating through the vadose zone. The most appropriate property for comparing resistivity data is ionic strength. At the T tank farm as well as the 216-BC cribs and trenches site and to waste sites adjacent to the PUREX facility, sodium nitrate contributed more than 90 percent of the total ionic strength of the waste. In 1973, Griffin and Jurinak suggested that a linear relationship exists between ionic strength and electrical conductivity (reciprocal of resistivity) from soil extracts. In 1976, Marion and Babcock found better correlation with log-transformed values. A correlation coefficient, therefore, can be calculated between electrical resistivity and ionic strength. Refer to the four references below.

- PNNL-14948, *Plume Delineation in the BC Cribs and Trenches Area*.
- HGI-2005-062, *Geophysical Characterization of the PUREX Facility*.
- *Soil Science*, 1973, "Estimation of activity coefficients from the electrical conductivity of natural aquatic systems and soil extracts."
- *Soil Science*, 1976, "Predicting specific conductance and salt concentration in dilute aqueous solutions."

In addition to the intentional liquid waste discharges and unplanned waste releases, leaks from water distribution lines in and around the tank farm and known meteorological events

(i.e., 1978–1979 Chinook) may have contributed to waste migration in the vadose zone. Figure 2-7 shows the infrastructure, including pipes, tanks, and diversion boxes used to transfer waste and supply the tank farm with water.

Figure 2-5. Estimates of Major Cations in Wastes Disposed of or Leaked in and Around T Tank Farm.

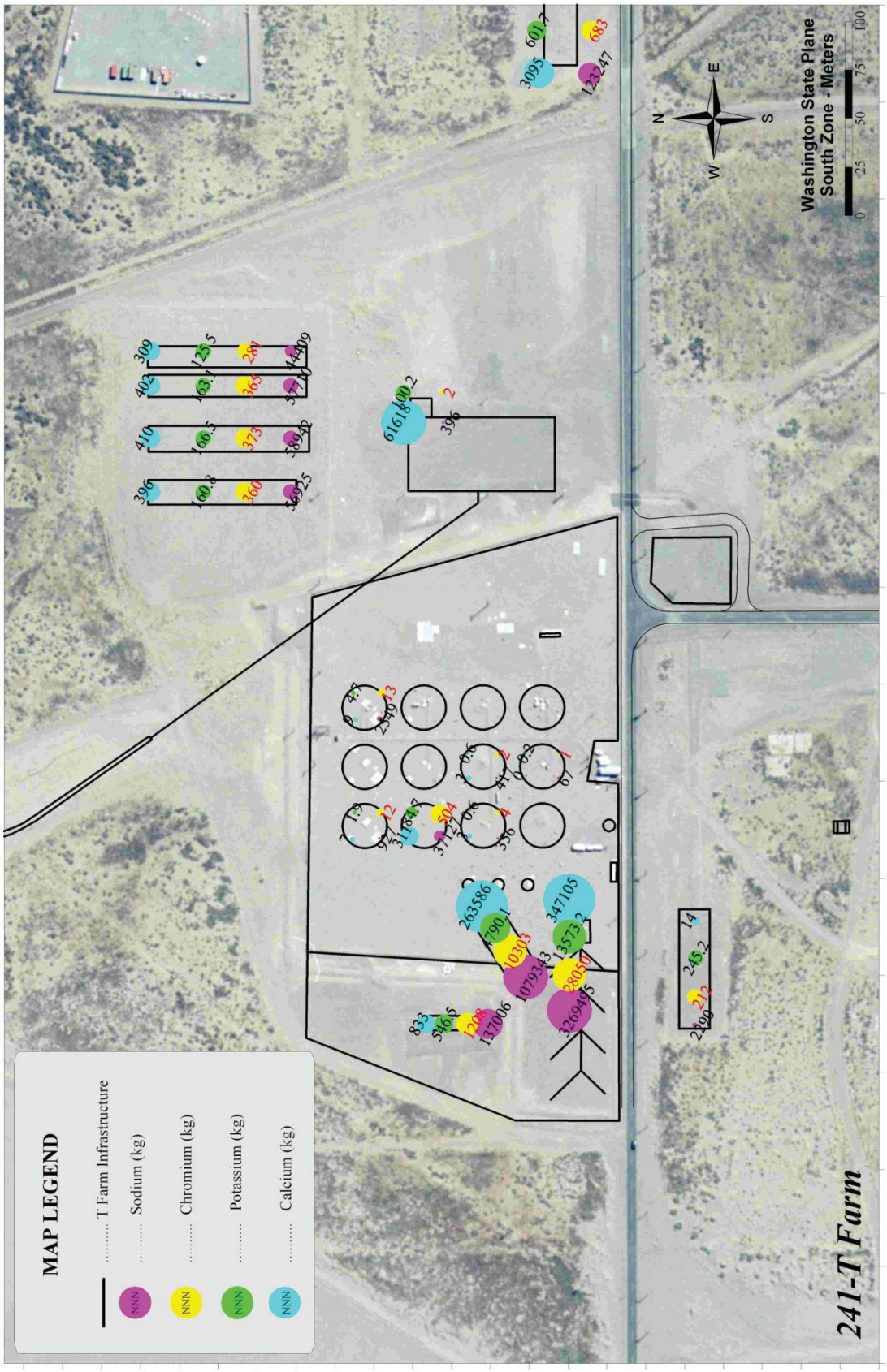

Figure 2-6. Estimates of Major Anions Disposed of or Leaked in and Around T Tank Farm.

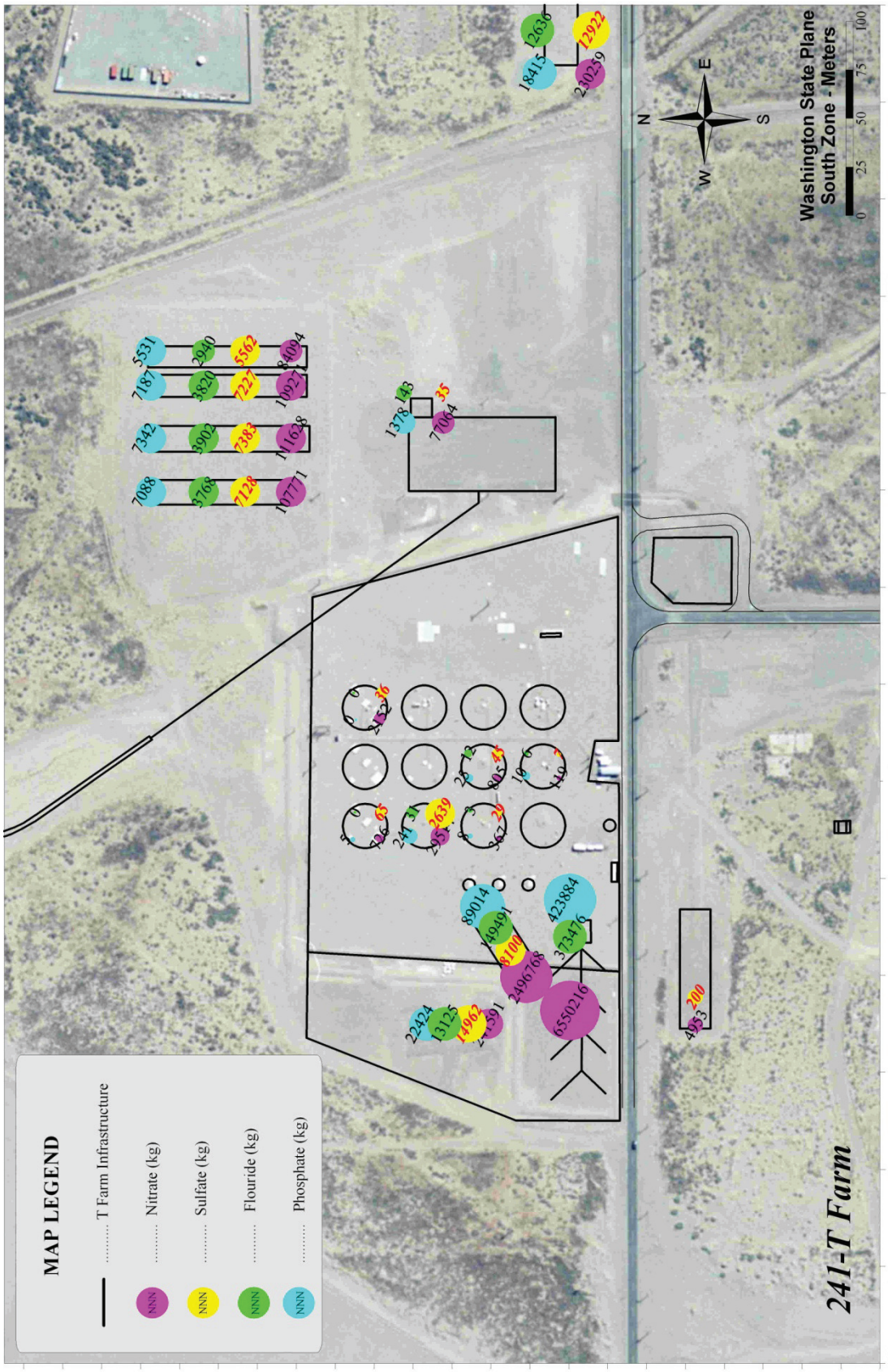

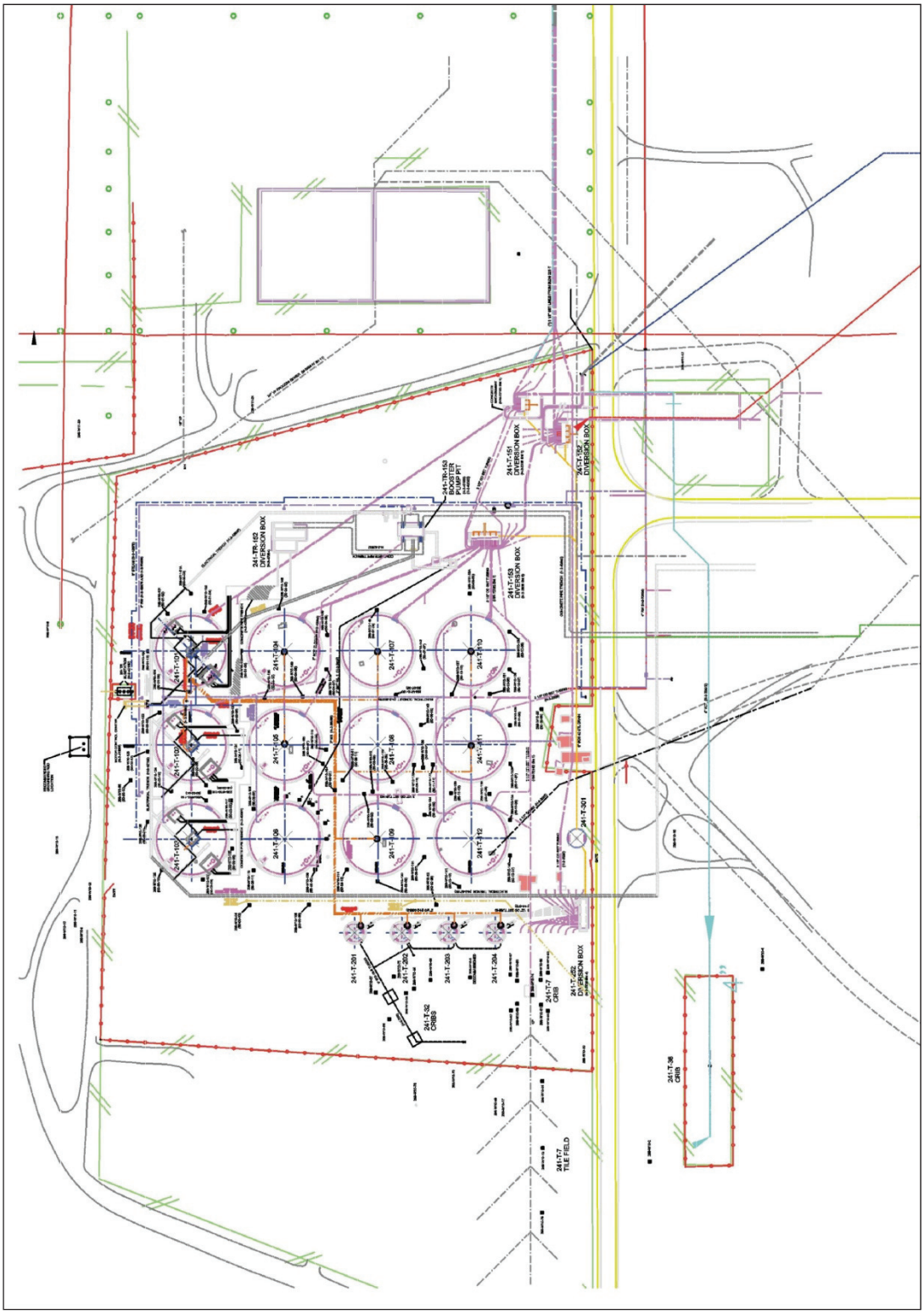

Figure 2-7. Infrastructure Map of Waste Management Area T.

2.3 ENVIRONMENTAL SETTING

As a result of decades of site characterization activities, the geology of the T tank farm and vicinity is well understood and has been described in numerous reports, including the following:

- ARH-LD-135, *Geology of the 241-T Tank Farm*.
- GJO-HAN-27, *Hanford Tank Farms Vadose Zone: T Tank Farm Report*.
- PNL-6820, *Hydrogeology of the 200 Areas Low-Level Burial Grounds – An Interim Report*.
- PNL-7336, *Geohydrology of the 218-W-5 Burial Ground, 200 West Area, Hanford Site*.
- RHO-ST-23, *Geology of the Separations Areas, Hanford Site, South Central Washington*.
- RPP-7123, *Subsurface Conditions Description of the T and TX-TY Waste Management Areas*.
- RPP-8531, *Vadose Zone Geology of Boreholes 299-W10-27 and 299-W11-39 T-TX-TY Waste Management Area, Hanford Site, South-Central Washington*.
- RPP-23748, *Geology, Hydrogeology, Geochemistry, and Mineralogy Data Package for the Single-Shell Tank Waste Management Areas at the Hanford Site*.
- RPP-23752, *Field Investigation Report for Waste Management Areas T and TX-TX.*
- WHC-SD-EN-TI-014, *Hydrogeologic Model for the 200 West Groundwater Aggregate Area*.

Information about geologic strata underlying the Hanford Site and the tank farms comes from boreholes and analyses of the sediments and contaminants.
Four major stratigraphic units underlie the T tank farm. In ascending order they include: igneous Columbia River Basalt Group (three sedimentary units), the Miocene- to Pliocene-age Ringold Formation (members of Wooded Island), the Cold Creek Unit (CCu), and the Hanford formation. Also, backfill materials consisting of poorly sorted cobbles, pebbles, and coarse to medium sand are distributed around the tanks and tank infrastructure.
The backfill, Hanford formation, CCu, and the upper portion of the Ringold Formation make up the vadose zone. The unconfined aquifer is contained within the lower portion of the Ringold Formation. All major stratigraphic units are inferred to be continuous in this area, although unit thicknesses vary and some subunits are not present at a few boreholes.

2.4 HISTORICAL CHARACTERIZATION EFFORTS

The SSTs are regulated under various DOE orders and policies in addition to the "Hazardous Waste Management Act," RCW 70.105, *Revised Code of Washington*, as amended, and its implementing requirements in WAC 173-303, "Dangerous Waste Regulations," *Washington Administrative Code*. The SSTs are operating under interim status permit pending closure. For regulatory compliance purposes, the SST farms are grouped into waste management areas (WMA).

The T tank farm was placed in assessment groundwater monitoring in 1993 because of elevated specific conductance (a measure of electrical conductivity of water), in downgradient monitoring wells (WHC-SD-EN-AP-132, *Interim-Status Groundwater Quality Assessment Plan for the Single-Shell Tank Waste Management Areas T and TX-TY*.) Technetium-99, chromium, iodine-129, tritium, fluoride, and nitrate are constituents that have exceeded Title 40 CFR 141, "National Primary Drinking Water Regulations," *Code of Federal Regulations*, at the T tank farm. The drinking water exceedances are currently limited to two wells (299-W11-41 and 299-W11-42) located along the southeast side of T tank farm. Refer to PNNL-15070.

Spectral gamma logging (i.e., collection of baseline gamma-specific radioisotope information in the upper vadose zone) was completed at the T tank farm in fiscal year 1999. The spectral gamma-logging program builds on a previous program in which gross gamma data were collected as a secondary means of leak detection from the SSTs. Both programs used the network of drywells installed around each tank.

The September 1999 final report on spectral gamma logging at the T tank farm (GJO-HAN-27) indicates that gamma-emitting contaminants Cesium-137, cobalt-60, and europium-154 were detected in the drywells. The network of drywells installed around each tank was intended for leak detection and was generally installed between depths of 22.8 and 45.7m (75 to 150 ft) below ground surface; thus, the maximum detection depth is limited by the drywell depth.

A groundwater assessment report on contaminants in the underlying unconfined aquifer indicates that WMA T is a source of groundwater contamination. See PNNL-11809, *Results of Phase 1 Groundwater Quality Assessment for Single-Shell Tank Waste Management Areas T and TX-TY at the Hanford Site*. WMA TX-TY is also a source of groundwater contamination. The sources for these contaminants are difficult to determine because of the many possible waste sources in the region (i.e., T and U ponds, cribs, trenches, and the tank farm facilities).

Two vertical boreholes along with a near-surface investigation near tank T-106 were recently completed as a part of field investigation activities (RPP-23752). Key findings include the following:

- Recent groundwater measurements northeast of the T tank farm indicate extremely high concentrations of nitrate and technetium-99. However, the source of these contaminants is not certain.
- Several vadose zone geologic layers can act to restrict vertical moisture flow and promote lateral spreading of fluids. Lateral migration of leakage from T-106 has been more extensive and longer lasting in the Hanford formation and CCu than previously hypothesized.

The results of field investigation and historical characterization activities have been used to develop a conceptual model for the nature and extent of contamination in the vadose zone beneath the T tank farm. RPP-23752 identifies two major contamination zones in the T tank farm. These include waste losses near tanks T-106 and T-103 and waste losses near tank T-101. A detailed discussion of the leak events and subsequent investigations is provided in RPP-23752. The following generalizations are intended to provide an overview of the contaminant plumes from the two major contamination sources within the T tank farm.

The contamination zone near tanks T-106 and T-103 results from the combined effects of an estimated 435,000-liter (115,000-gallon) leak from tank T-106 and an 11,400-liter (3,000-gallon) transfer line leak from tank T-103. The contaminant plume from these sources is estimated to be approximately 76m (250 ft) in diameter centered near the southeast quadrant of tank T-106 and extending to a depth of approximately 27 to 30m (90 to 100 ft) below ground surface.

Historical process records indicate that waste losses from tank T-101 were the result of overfilling the tank in 1969 by as much as 38,000 liters (10,000 gallons) (RPP-23752). Based on historical data and spectral gamma data, the contaminant plume from the tank T-101 leak extends to a depth of approximately 36.6m (120 ft) below ground surface and has migrated in a southerly direction. Groundwater monitoring data collected around the T tank farm indicate that some contamination has reached the unconfined aquifer.

During the fiscal years 2004 and 2006, several drilling and sampling activities within WMA T have further characterized inorganic contamination in the vadose zone. These include boreholes C4104 and C4105 near tank T-106 and wells 299-W11-25B, 299-W11-41, 299-W11-45, and 299-W11-47 outside the fence surrounding the farm. Figure 2-8 shows the sulfate and nitrate concentrations and soil moisture in selected vadose zone samples as a function of depth. In general, the sulfate and nitrate concentrations are highest close to waste management facilities. See PNNL-14849, *Characterization of Vadose Zone Sediments Below the T Tank Farm: Boreholes C4104, C4105, 299-W10-196, and RCRA Borehole 299-W11-39*.

Figure 2-8. Nitrate and Sodium Concentrations and Soil Moisture in Selected Vadose Zone Samples Collected Around T Tank Farm.

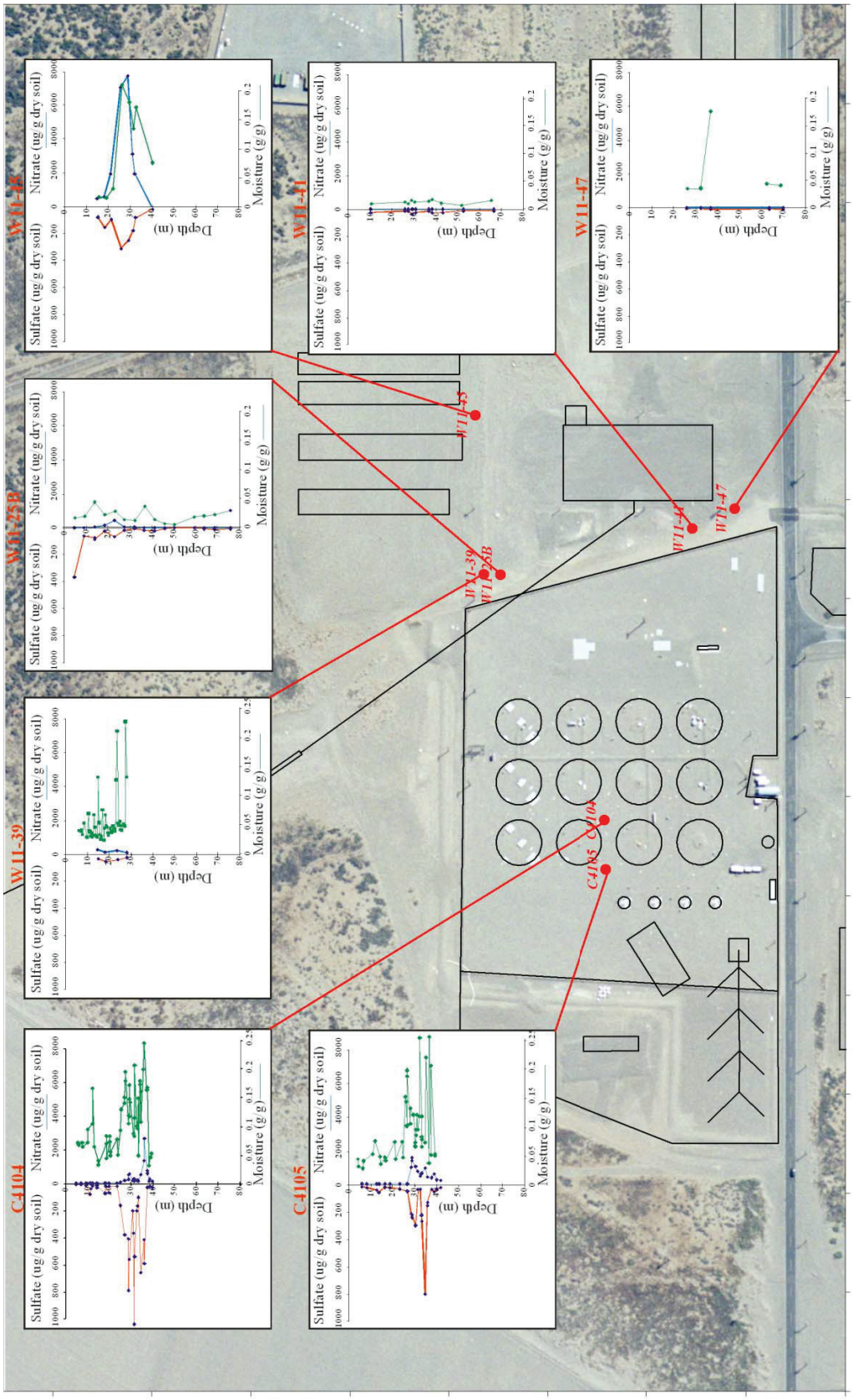

3.0 QUALITY ASSURANCE FOR DATA PROCESSING AND REDUCTION

Data processing is performed using a number of software packages. The requirements and responsibilities for the identification, evaluation, development, testing, and maintenance of quality-affecting software acquired, developed, or modified in support of the SGE efforts are defined in the CEES-0338, *Software Management Plan for Surface Geophysical Exploration Projects*.

Verification and testing of the software modifications made for the SGE projects was performed and documented in RPP-34974, *Verification and Testing of the EarthImager Series of Electrical Resistivity Inversion Codes – A Benchmark Comparison*. A detailed description of the test performed and the results are provided in RPP-34974. Verification and testing was performed on the existing two-dimensional (2D) and 3D versions of the software, as well as the upgraded version developed for the previous tank farm area SGE analysis.

The objective of the verification and testing study was to demonstrate that the EarthImager series of resistivity inversion codes, developed by Advanced Geosciences, Inc., were comparable to an industry standard or to known conditions from a pilot-scale field resistivity experiment. The industry standard was established by showing RES2DINV (RES2D) and RES3DINV (RES3D) (developed by Geotomo Software, Penang, Malaysia) (designated as RES#INV as reference to both codes) are used ubiquitously and accepted by geophysicists. RES2D and RES3D use has been cited in a large body of scientific literature. Subsequently, a benchmark study between the industry standard and the EarthImager series was conducted in both two and three dimensions for a variety of geological conditions with the same pole-pole array system and conditions deployed at SGE sites.

At the time of this project, RES3D64 a 64-bit version of the commercially available, industry standard RES3D software was available. Prior experience and testing as part of the verification and validation of EarthImager3D CL® (EI3DCL) as described in RPP-34974 showed that RES3D contained some mesh and a-priori modeling features that were superior to EarthImager. However, prior versions of RES3D operated on a 32-bit platform and therefore could not support the large SGE modeling domains. The newly released version, RES3D, provides support for multiple processors and large memory, but retains the same modeling routines. A side-by-side comparison between EI3DCL and RES3D64 was completed to ensure suitable results. Three-dimensional (3D) inversion of hypothetical WTW data were completed using the RES3D64 software. A detailed discussion of the inversion software and data processing operations and methodology can be viewed in Sections 4.0 and 5.0.

® EarthImager3DCL is a registered trademark of Advanced Geosciences, Inc.

4.0 THEORY

This chapter provides summary level descriptions for the resistivity inversion modeling. To read a summary of the theory behind the various resistivity techniques, refer to RPP-RPT-28955.

4.1 RESISTIVITY INVERSION PRINCIPLES

The modern application of the electrical resistivity characterization (ERC) method uses numerical modeling and inversion theory to estimate the electrical resistivity distribution of the subsurface from the acquired dataset. The inverse modeling is necessary, as measuring the resistivity is not a direct process. The acquired dataset only contains positions of the electrodes and the measured potential normalized to the injected current. However, the potential values are a result of the spatial resistivity distribution, allowing them to be used indirectly to back-calculate, using an inversion algorithm, an estimate of the true resistivity that gives rise to those potential measurements.

A common resistivity inverse method incorporated in commercial codes is the regularized least squares optimization method. Refer to *Geophysics*, 1989, "Two-dimensional joint inversion of magnetotelluric and dipole-dipole resistivity data," as well as, *Exploration Geophysics,* 2003, "A comparison of smooth and blocky inversion methods in 2D electrical imaging surveys." The objective function aims to minimize the difference between measured and modeled potentials or apparent resistivities (subject to certain constraints) and the optimization is conducted iteratively due to the nonlinear nature of the model that describes the potential distribution. The relationship between the subsurface conductivity σ and the measured potential ϕ is given by equation (1) which is from *Geophysics*, "Resistivity modeling for arbitrarily shaped three-dimensional structures.):

$$-\nabla\cdot\left[\sigma(x,y,z)\nabla\phi(x,y,z)\right]=\left(\frac{I}{U}\right)\delta(x-x_s)\delta(y-y_s)\delta(z-z_s) \qquad (1)$$

Where:

I is the current applied over an elemental volume U specified at a point (x_s, y_s, z_s) by the Dirac delta function. Common methods of solving Equation (1) include:

- the finite difference method (*Geophysics*, 1979, "Resistivity modeling for arbitrarily shaped three-dimensional structures.")
- the finite element method (*Geophysics* 1989, as mentioned earlier, and *Geophysics*, 2009, "Explicit expressions for the Fréchet derivatives in 3D anisotropic resistivity inversion.")
- the analytical element method, Vadose Zone Journal, Volume 1, "*Electrical potential distributions in response to applied current in a heterogeneous subsurface, solution for circular inclusions"*

- and the finite volume approach (*Geophysics*, 2007, "RESINVM3D: A 3D resistivity inversion package.

The finite-difference method was used in this research.

Regardless of the numerical method, a mesh is created whereby the subsurface is discretized into blocks and nodes. Equation (1) is solved for ϕ at every node with the appropriate boundary conditions. Additional requirements of the numerical model include explicitly assigning every block a resistivity value and every node a current source (if any). Figure 4-1a shows a typical mesh for a three-dimensional volume that has been discretized into rectangular blocks over several layers. Figure 4-1b shows a more detailed overhead view of the relationship between the mesh lines (in the x- and y-directions), model blocks, and nodes. The potentials are calculated at the nodes that are located at the intersections of the mesh lines, but the resistivity is assigned for the block bound by the mesh lines. Numerical methods work such that finer (or smaller) mesh sizes with more nodes give rise to more accurate solutions, with the trade-off of solution efficiency and computer memory requirements.

Figure 4-1. a) Discretized Earth for Inversion, b) Overhead View of Meshing Showing Relationship Between Nodes, Mesh Lines, and Blocks.

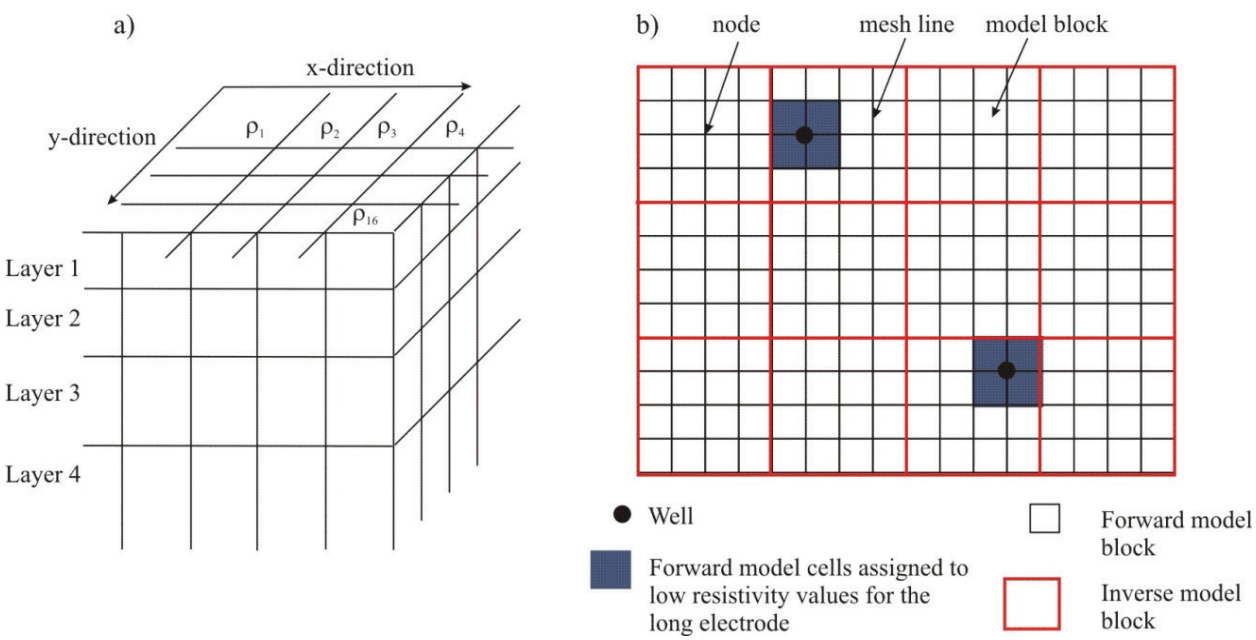

For the inversion code, the inverse mesh is separate from the forward mesh when using the long electrode module.

Accommodating long electrodes in commercial resistivity modeling codes can be accomplished easily by taking advantage of the existing code structure. Although, formally, the long electrodes act as linear sources and receivers, they can be modeled as a point source on the surface and by assigning to the long electrode's position a series of very conductive cells, say 0.01 ohm-m to simulate a metallic well. The current source is located at a node and the adjacent four cells are assigned the low resistivity values (Figure 4-1b). The high contrast between the well's resistivity and that of the surrounding medium can cause adverse effects in the numerical model such as accuracy and stability. In order to reduce this problem, the forward model mesh is

discretized more finely relative to the inverse model mesh so that a more gradual transition of electrical resistivity occurs between the well and the host medium.

An example of the capability of the resistivity code is demonstrated by placing a single long electrode in a 100 ohm-m background. The numerical results of transfer resistance using the finite difference method are compared to an analytic solution of an infinite conductor of infinitesimal diameter. This is taken from:

- GE-25, 1987, "Resistivity response of a homogeneous earth with a finite-length contained vertical conductor: IEEE Transactions on Geoscience and Remote Sensing
- *Water Resources Research*, Volume 35, "Effects of source cavity shape on steady, three-dimensional flow of soil gases."

$$R = \frac{V}{I} = \frac{\rho}{4\pi b} \ln\left[\frac{\left[r^2 + b^2\right]^{0.5} + b}{\left[r^2 + b^2\right]^{0.5} - b}\right] \qquad (2)$$

Where:

ρ = the resistivity of the background

b = the length of the long electrode (or well) extending from the surface of the earth

r = the distance between the center of the well and the potential measurement location.

Equation (2) can be shown to revert to the solution of a purely homogeneous half-space for b→0. For the numerical modeling, the length of the long electrode was simulated as 44m. The transfer resistance results in Figure 4-2 show that the resistivities of between 0.01 and 0.001 ohm-m assigned to the long electrode produce the most accurate results. Specifically for this example, the resistivity of 0.006 ohm-m is the most accurate with a difference of less than four percent from the analytical values for the entire distance of 1 to 50m away from the well. The differences are likely partially due to the assumptions of the infinite conductor and infinitesimal diameter for the analytical solution compared to the finite conductor and diameter for the numerical models (Figure 4-2).

Figure 4-2. Numerical Model Results of a Conductor of Finite Length and Diameter Compared to the Analytical Solution of an Infinite Conductor of Infinitesimal Diameter.

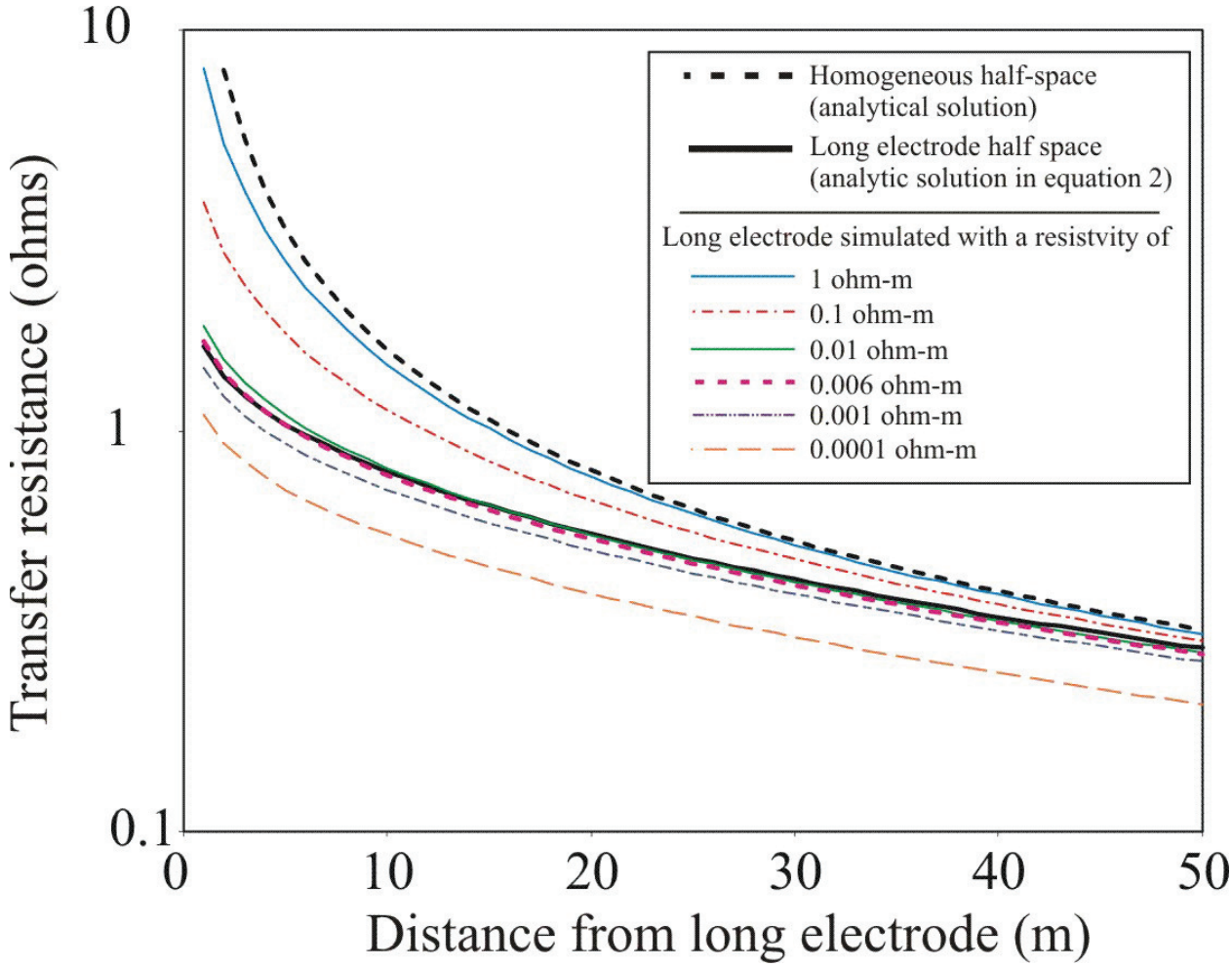

It is interesting to note that the numerical results with the lowest resistivity of 0.0001 ohm-m are very inaccurate. We suspect that the contrast between the 0.0001 ohm-m and the 100 ohm-m background (a resistivity contrast of 1:1,000,000) is too large such that the numerical method breaks down, either due to numerical round-off errors or the poor assumption of linear variation of the potential within each finite-difference cell.

The inversion of long electrode data is similar to that presented in *Geophysics*, 2002a, "A 3-D resistivity investigation of a contaminated site at Lernacken, Sweden." as well as Loke's *Exploration Geophysics,* 2003, with either the L_2 norm smoothness-constrained least squares that aims to minimize the square of the misfit between the measured and modeled data (*Geophysics,* "Occam's inversion to generate smooth, 2D models from magnetotelluric data," and Applied geophysical inversion: Geophysical Journal International.

$$\left(J_i^T J_i + \lambda_i W^T W\right)\Delta r_i = J_i^T g_i - \lambda_i W^T W r_{i-1} \quad (3)$$

or the L_1 norm that minimizes the sum of the absolute value of the misfit:

$$\left(J_i^T R_d J_i + \lambda_i W^T R_m W\right)\Delta r_i = J_i^T R_d g_i - \lambda_i W^T R_m W r_{i-1} \quad (4)$$

where:

G = data misfit vector containing the difference between the measured and modeled data

J = Jacobian matrix of partial derivatives

W = the roughness filter

R_d and R_m = weighting matrices to equate model misfit and model roughness

Δr_i = the change in model parameters for the ith iteration

r_i = the model parameters for the previous iteration, i

λ_i = the damping factor.

The logarithms of the model resistivity and measured apparent resistivity values are used as the model parameters and data respectively in the above equations. The long electrode module implemented in RES3D64, developed by Geotomo Software allows the wells to be located at an arbitrary grid point, separate from the discretization used for the inversion model blocks (Figure 4-1). The arbitrary grid modification simplifies the problem by eliminating the need to calculate the resistivity on a large number of small blocks.

4.2 WELL-TO-WELL INVERSION EXAMPLES

4.2.1 Example with Pole-Pole Array

The original WTW inversion at the T Tank farm used the resistivity code EI3D, which has since been upgraded to accommodate large memory, multi-processor computers to EI3DCL. The EI3D code solved the WTW resistivity problem adequately, typically creating somewhat noisy results due to the incorporation of the resistivity values of the cells assigned to the well into the resistivity inversion.

The code RES3D64 has since been updated to conduct WTW inversion and a comparison of its strengths over EI3D are demonstrated below. Consider the following scenario: A simple target is placed in a background of 100 ohm-m. The target is 1 ohm-m and resides at the depths of 10 to 15m below ground surface. The larger domain is 60 by 60m and the target is 15 by 15m placed slightly off center. The pole-pole array is used for all simulations. The results of first running the forward simulation to obtain the potential measurements then inverting the potentials

to calculate the resistivity distribution is shown in Figure 4-3. The figure compares the results of RES3D64 and EI3D, with RES3D64 producing an image more similar to the initial conditions than EI3D. The EI3D results are not necessarily incorrect, but the noise surrounding the target makes the subsurface more difficult to interpret. In contrast, the target identified by RES3D64 is more coherent.

Figure 4-3. Comparison of WTW inversion with RES3DINVx64 (RES3D64) and EarthImager3D (EI3D).

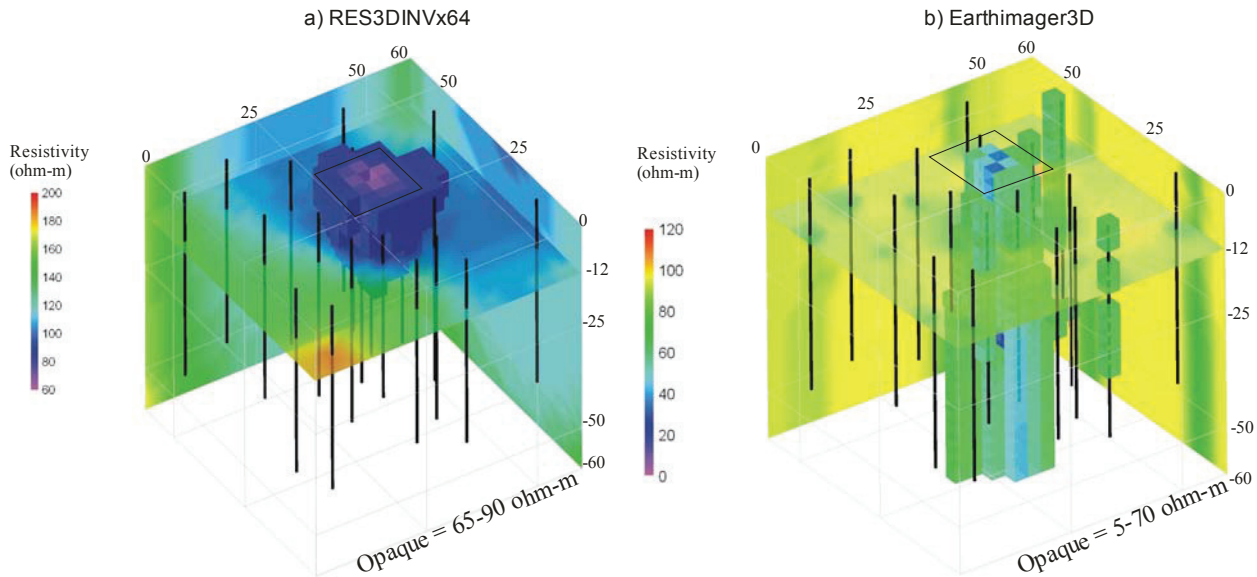

An example of the WTW inversion method showing the advantage of using wells as electrodes in infrastructure-rich areas is presented in Figure 4-4. Figure 4-4 considers the same scenario described for Figure 4-3, but comparing STS with WTW. Figure 4-4a shows the inversion results for surface electrodes only using RES3D64. The surface electrodes are evenly spaced 5m apart over the entire domain for a total of 36 electrodes and 630 measured potential values. In the figure, the higher resistivity values are peeled away to reveal the lowest values that range from 50-80 ohm-m. These values were chosen such that the footprint of the inverted target matched the footprint of the original target. For reference, a transparent horizontal color contoured layer is placed at a depth of 12m, through the center of the original target. The inverted target matches the footprint of the original target quite well with some vertical smearing that is common with this type of reconstruction.

Figure 4-4b shows the inversion results from a similar circumstance but with the use of 20 long electrodes and no surface electrodes. The parameters of the long electrodes are the same as that in Figure 4-2. The density of long electrodes (200 m^2/electrode) for the model were meant to replicate that of inside T tank farm (188 m^2/well) and the electrode arrangement placed two electrodes through the target. The inversion results show a high propensity for the long electrode technique to replicate the target but with an elevated resistivity distribution compared to Figure 4-4a. Additionally, the vertical distribution of the target is funnel shaped where the majority of the low resistivity values are at the surface. We surmise that the finite conductivity value used

for the long electrode causes much of the current density to be concentrated nearer the surface. This fact will likely cause a loss of vertical resolution when using the long electrode technique in the field.

Figures 4-4c and 4-4d show a repeat of the previous two models with the exception of a 0.25m thick, high conductivity layer (0.01 ohm-m) at a depth of 1m. The simulated infrastructure was slightly higher in resistivity than the well to replicate the fact that piping and tanks would never actually touch a well. The inversion with surface electrodes shows a thin low resistivity layer that obliterates the target below it, making the original target indistinguishable. Although only the lowest resistivity values are shown in Figure 4-4c, a cycling through the complete set of data fails to reveal any information about the original target's whereabouts. The use of long electrodes in Figure 4-4d overcomes the conductive surface layer issue and makes a good attempt to reproduce the lateral position of the target. The long electrode results with a surface layer lowers the overall resistivity values of the target and background compared to Figures 4-4a and 4-4b. Therefore, limitations can be expected with the long electrode technique when applying petrophysical models for estimations of moisture content or salt concentration, as the resistivity of the inverted target will depend on the amount of infrastructure and number of wells. The long electrode method should be applied more as a target recognition technique.

Figure 4-4. Example Models Showing the Resistivity Inversion Results for Surface and Long Electrodes.

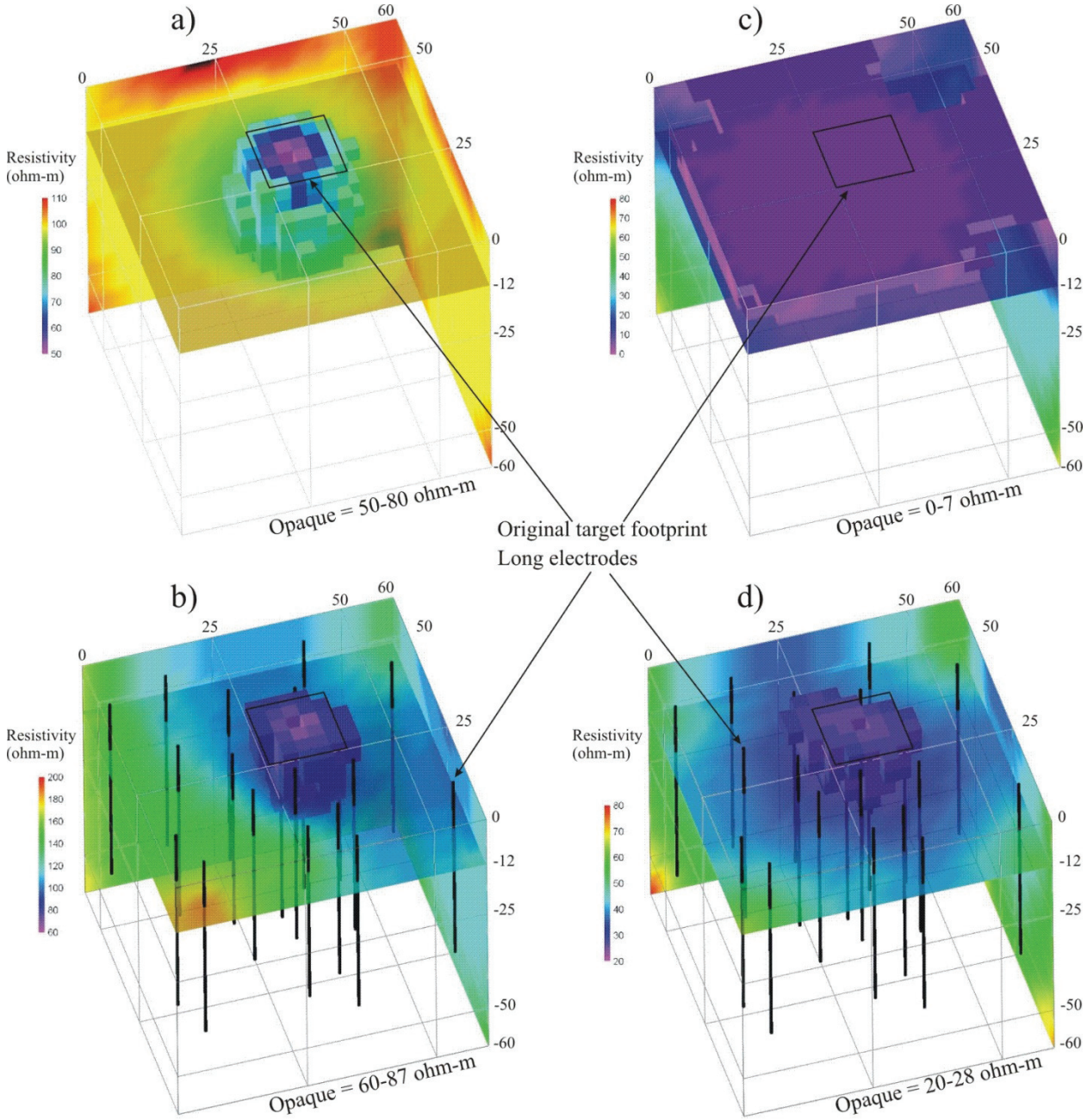

a) Surface Electrodes with Simple Target, b) Long Electrodes with Simple Target, c) Surface Electrodes with Simple Target and Conductive Surface Layer, d) Long Electrodes with Simple Target and Conductive Surface Layer. The Target Footprint is Drawn to Show the Fidelity of the Types of Electrodes to Replicate the Position of the Target

4.2.2 Example with Dipole-Dipole Array

Unlike the pole-pole array, the dipole-dipole array has no electrodes at infinity. All resistivity measurements are made with wells inside the measurement domain. Distinct advantages exists for using the dipole–dipole array, including the larger number of data measurements and no infinite electrodes. The major disadvantage of the array is the degree of measurement error, which is much higher than pole-pole. Higher errors are a consequence of the lower gradient of the electric field (i.e., voltage) when the poles are closer.

A demonstration of the WTW technique using the dipole-dipole array is given for the same simple target in an otherwise homogeneous background, described above. The pole-pole array forward model was run on this earth, and the pole-pole transfer resistance data were then used to calculate the dipole-dipole resistance data ($dd_{1,2\text{-}3,4}$) for the transmitter electrodes 1, 2 and receiver electrodes 3,4 using the formula:

$$dd_{1,2-3,4} = pp_{1,3} - pp_{1,4} - pp_{2,3} - pp_{2,4} \tag{5}$$

where $pp_{x,y}$ signifies the pole-pole transfer resistance value with pairs x,y. An example of the pole-pole transfer resistance data with and without a target is shown in Figure 4-5. The data are plotted versus distance between transmitter and receiver. The pole-pole data has a total 190 measurements and both examples show an exponential decrease of resistance with distance and a low value of 0.2 ohms. From this set, 4845 dipole-dipole measurements were calculated. Figure 4-6 shows the dipole-dipole data as a function of geometric factor. The geometric factor is the conversion factor between transfer resistance and apparent resistivity and considers the distance between the various electrodes. Approximately 75 percent of the dipole-dipole data are lower than the lowest pole-pole value.

Figure 4-5. Pole-Pole Transfer Resistance Data Used to Calculate Dipole-Dipole Data For the Example Model With and Without Any Target.

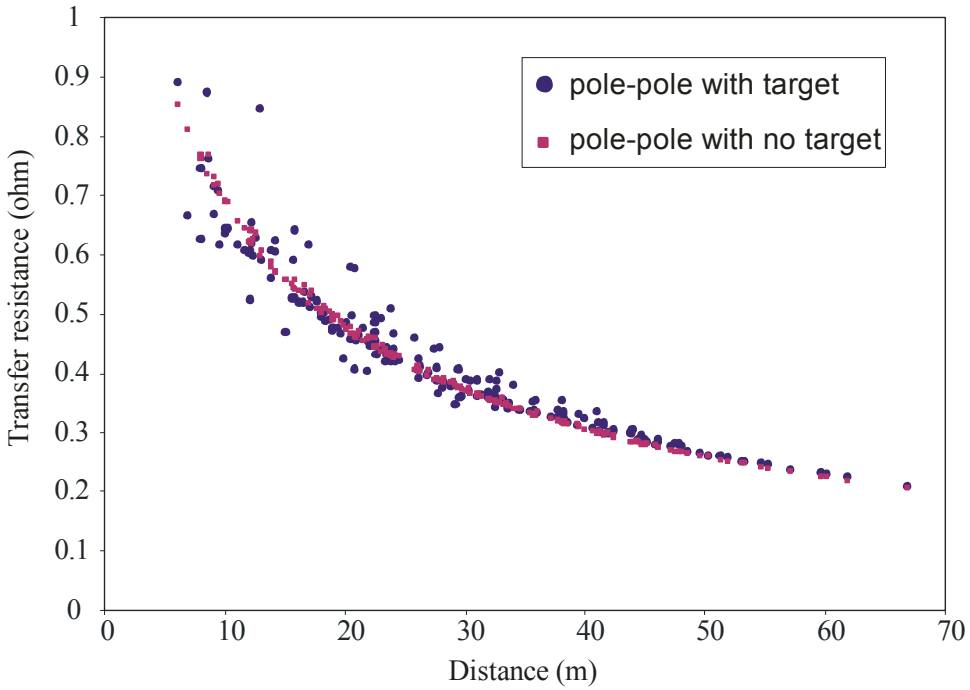

Figure 4-6. Dipole-Dipole Transfer Resistance Data With a Simple Target.

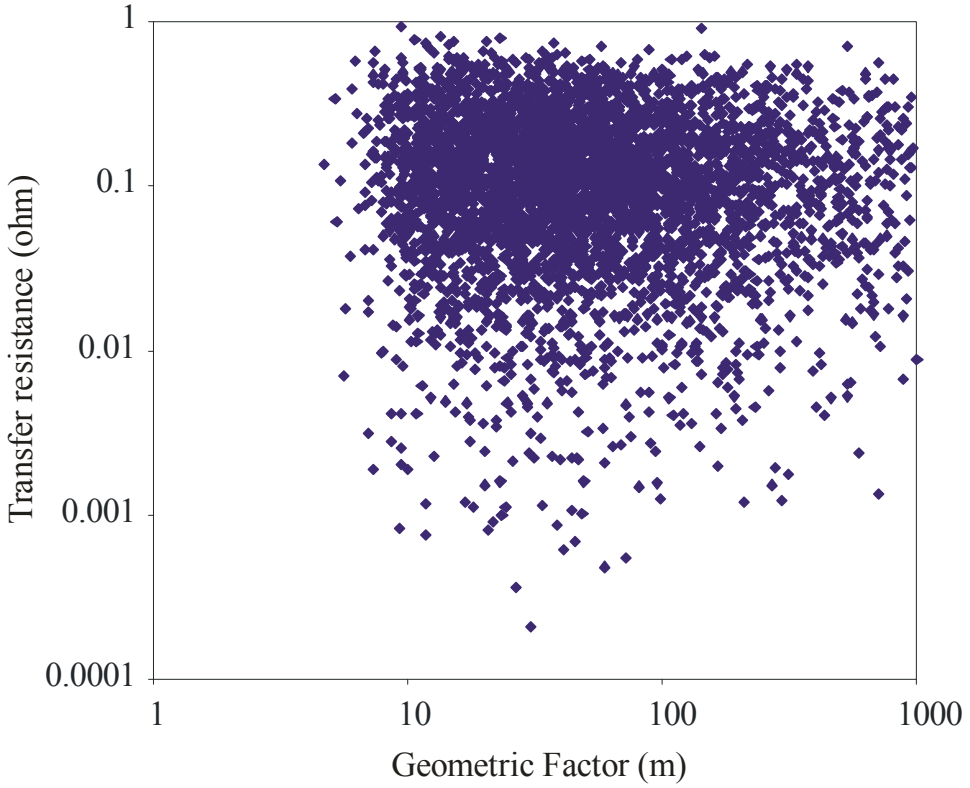

The result of inverting the dipole-dipole data is shown in Figure 4-7. Similar to the pole-pole results, the dipole-dipole array is capable of loosely defining the location of the target. However, the results are much noisier than that of the pole-pole and the overall distribution of resistivity of the subsurface is low.

Figure 4-7. Inversion Results of the Dipole-Dipole Array with a Simple Target.

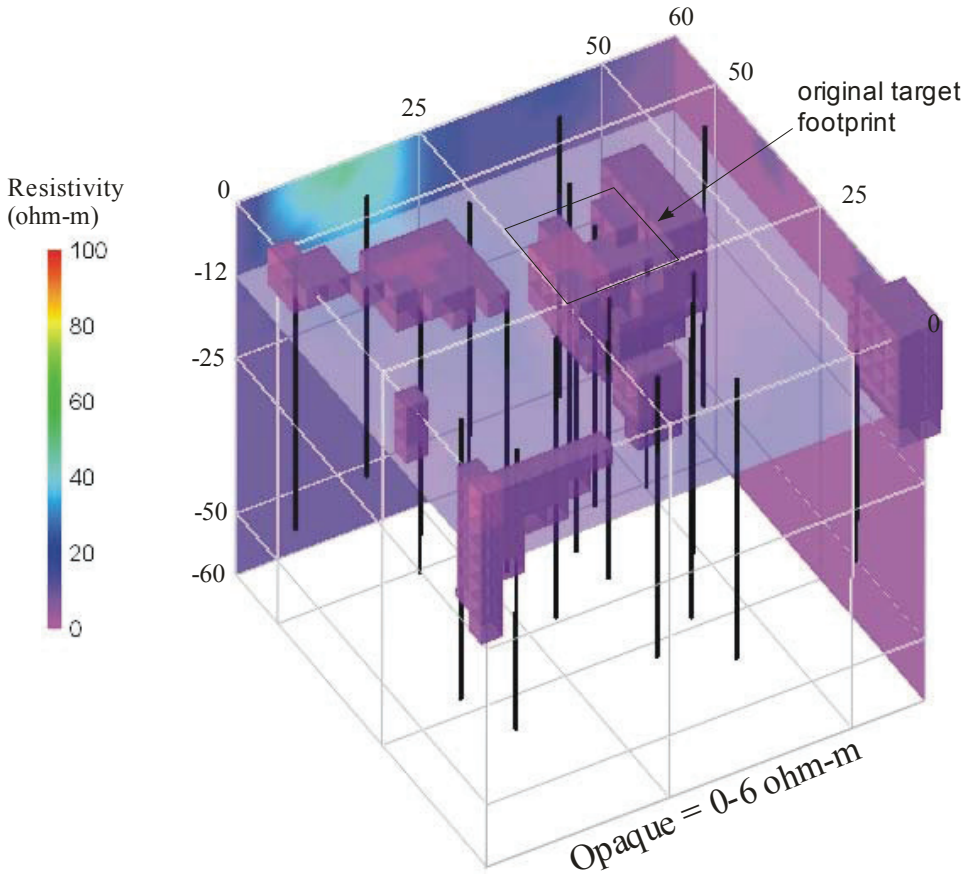

4.3 MECHANICS OF INVERSION MODELING AND VISUALIZATION

4.3.1 Geospatial Database Management and Queries

The filtered data sets from each line are used as input in the inversion modeling process. To facilitate the preparation of these data sets, all T farm resistivity data were loaded into a Microsoft Access® database. This database allows examination and evaluation of the quality control of the line layout and electrode spacing. Consistent and correct line layout and electrode coordinates are critical to the efficient functioning 3D finite difference and finite element inversion algorithms such as those used by the RES3D64.

® Microsoft Access is a registered trademark of the Microsoft Corporation.

Database queries were used to extract data for several different model domains, which are then exported from the geospatial database into the ASCII format which is used by EID3 and RES3D64 inversion software packages.

4.3.2 Inverse Modeling With RES3D Inversion Code

The automated inversion process, using the RES3D64 code, generally proceeds as described in the following five steps. These steps are also shown graphically in a flowchart provided in Figure 4-8.

1. The study site's voltage data has been measured and is discretized into grid nodes using a finite difference or finite element mesh. The meshing parameters used in either case, to design the computational grids, are dependent on electrode spacing used in site-specific data acquisition.
2. The inversion will set out to estimate the true resistivity at every grid node. An initial estimate of the subsurface properties is made based on the literal translation of the pseudo-section to a true resistivity, a constant value, or some other distribution from *a priori* information. A forward model run with these initial estimates is made to obtain the distribution of voltages in the subsurface. The root-mean-square (RMS) error is calculated between the measured voltage and the calculated voltage resulting from the forward run.
3. Based on the degree of model fit to field measurements, the initial estimate of resistivity is changed to improve the overall model fit and the forward model with the updated estimates is rerun. The iterative method linearizes a highly nonlinear problem using Newton's method. Using this method, the inversion code essentially solves the linearized problem to obtain the change in modeled resistivity (Δm) for the next iteration.
4. The resistivity model is updated using the general formula $m_{i+1} = m_i + \Delta m$, where m_{i+1} is the resistivity in a model cell at the next iteration, and the m_i is the current value.
5. Steps 3 and 4 are repeated until the RMS error change between successive iterations reaches an acceptable level.

Figure 4-8. Flowchart of the Resistivity Inversion Process With RES3D Code.

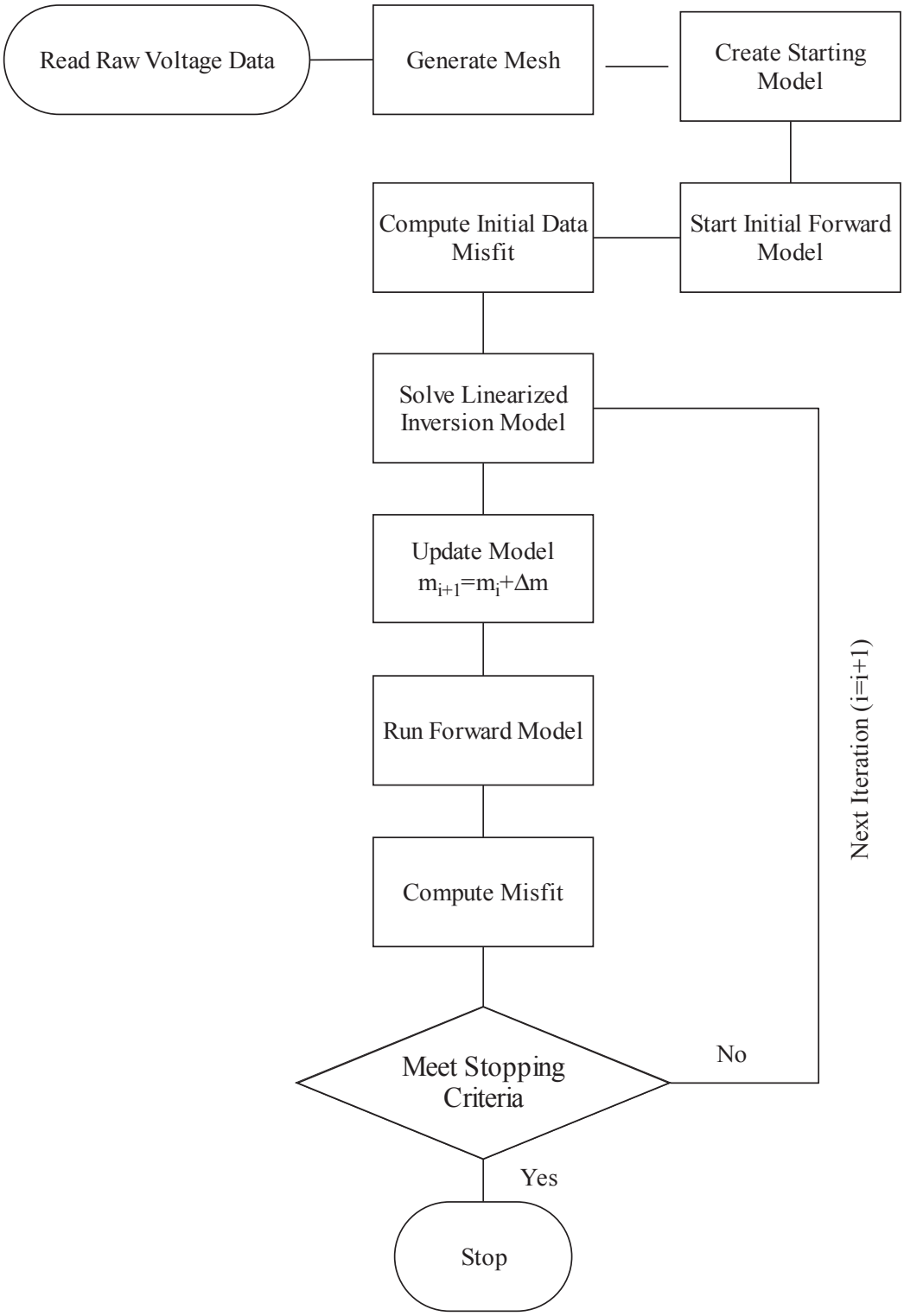

4.3.3 Inversion Parameters

Inversion software applies a series of user defined parameters to control the direction of the inversion modeling process. The following section contains a brief description of the inversion parameters used with the RES3D64 inversion software package.

4.3.3.1 Boundary Condition Type and Limit. The core mesh is a finite difference mesh with the domain limits set to the maximum distance between electrodes. The boundary mesh is a continuum of the core mesh at some distance outside of the measured region and contains the boundary condition and the remote electrodes for the pole-pole array. Numerical artifacts in the core mesh are minimized when the boundary condition is set far enough away from the current sources and sinks so that the simulated field gradients are constant at the boundaries.

RES3D64 uses a homogeneous Neumann boundary condition (i.e., specified current density) for the surface layer which has no current flow through air. This is equivalent to an insulating boundary condition. Equation (6) describes the Neumann boundary condition as applied to the surface layer of the resistivity inverse model:

$$\rho^{-1}(s)\eta \cdot \nabla\Psi = J(s) \tag{6}$$

Where:

P = resistivity of the area to be imaged

Ψ = electrical potential (i.e. voltage)

S = core mesh area

J(s) = current density.

The value of the Dirichlet boundary condition for the bottom and sides is proprietary for RES3D64.

4.3.3.2 Damping and Stabilizing Factors. The damping factors for RES3D64 include values for the initial, minimum, and first layer. These parameters are defined differently than the EI3D code and the exact implementation of these factors is proprietary (Loke 2006, Personal communication via email.). Each of these parameters can be automatically optimized by RES3D64 so that a minimum RMS model fit error is achieved.

4.3.3.3 Initial Condition of the Inverse Model. An initial value is needed to start the calculation of the partial differential equation of the predicted value at a given point in the domain of the solution. For the T tank farm resistivity inverse model, the starting value was a homogenous solid earth set to the average apparent resistivity of the measured data.

4.3.3.4 Inverse Modeling Methodology . RES3D64 supports the L_2 normalized damped least-squares inverse objective function (Equation (3). Compared to the damped least squares method with no normalization or with L_1 normalization (or robust inverse modeling), the L_2

normalization is optimal at resolving naturally smooth varying electrical properties as expected for conductive plumes and most hydrologic problems.

Refer to:

- *Geophysical Prospecting*, 2004, "A numerical comparison of 2D resistivity imaging with 10 electrode arrays"
- *Exploration Geophysics*, 2003
- *Geophysics*, 2004, "Inversion of magnetotelluric data for 2D structure with sharp resistivity contrasts
- *Geophysics*, 1990, "Occam's inversion to generate smooth, two-dimensional models from magnetotelluric data."

The L_2 normalization objective function is less likely to over fit smooth field measured data, in theory, reflecting a closer representation of the true conductive plume boundaries (*Geophysics*, 1990).

hydroGEOPHYSICS , Inc. uses the pole–pole electrode configuration due to its high signal strength at the deepest exploration depths relative to other array types, while collecting the widest horizontal coverage for a given array length (*Journal of Applied Geophysics*, 1999) The L_2 norm also appears to work well in conjunction with the pole-pole array (*Geophysics*, 1990.)

4.3.3.5 Inverse Modeling Stop Criteria. The RMS error used in RES3D64 is defined in Equation (7). When the code completes an inversion, the difference in the logarithms of the measured and calculated apparent resistivity values will be similar to the relative error.

$$RMS = \sqrt{\sum_{i=1}^{N} \frac{(\log(d_{meas}) - \log(d_{pred}))^2}{N} \times 100} \tag{7}$$

Where:

dmeas = measured apparent resistivity

dpred = predicted apparent resistivity

N = the number of measurements.

If the change of RMS error between two successive inversion iterations is less than the selected value, then the inversion codes will stop. Using an RMS change stop criteria of 5 to 10 percent is recommended by Geotomo Software for field-measured surface data sets with 5 percent as the default value in both codes. In general, the percent change stop condition of 5 percent stops Geotomo Software codes as the model RMS values plateau.

4.3.3.6 Inverted Value. RES3D64 uses the apparent resistivity as the data input for inversion. Transfer resistance and apparent resistivity are equivalent quantities that can be converted back and forth using a geometric factor. However, the different inverted value is

significant for WTW problems, where the geometric factor to convert transfer resistance to apparent resistivity does not exist. In this case, the apparent resistivity of a point electrode is assumed.

4.3.3.7 Inverted Output. The output from RES3D64 are in terms of X, Y, Z and modeled resistivity.

4.3.3.8 Jacobian Matrix Calculation. The Jacobian Matrix is the matrix of all first-order partial derivatives of a vector-valued function relative to the model parameter. This calculation provides the best linear approximation to a differentiable function near a given point. The quasi-Newton or partial Jacobian Matrix calculation is a method of slightly lower accuracy, but requires less computational power. Refer to the two Geophysical Prospecting articles:

- *Geophysical Prospecting*, 1996a, "Practical techniques for 3D resistivity surveys and data inversion,"
- *Geophysical Prospecting*, 1990, "Methods for calculating Fréchet derivatives and sensitivities for the non-linear inverse problem: a comparative study."

RES3D64 offers the option to enable the full Jacobian Matrix calculation using the Gauss-Newton method with each model update.

4.3.3.9 Model Layer Thickness Increase with Depth. The sensitivity of surface resistivity decreases with distance from the electrodes. A telescoping mesh is applied by RES3D64 so that lower layers are not overly resolved by the modeling process. The telescoping mesh layer thickness increases by a factor of 1.15 per layer for the T farm resistivity inverse models.

4.3.3.10 Mesh and Solver Type. RES3D64 incorporate finite difference and finite element mesh designs in their codes. Finite difference and finite element methods solve for electrical properties by breaking the problem area (i.e., domain) into many small elements (e.g., squares as in the finite difference or triangles, tetrahedra, etc. in finite element) and solving the equation for each element (all electrical properties are assumed constant or linearly variable within an element). The finite element method discretizes the model domain optimally for complex topographic surfaces as expected when resistivity is measured over hills and valleys. The finite difference method discretizes the model domain into block elements, which are significantly faster to compute during the inversion process. The finite difference and finite element approximation leads to an implicit set of equations that must be solved using linear algebra.

The finite difference method is used for the T farm resistivity inverse models as this is an optimal method for the SGE sites, which are relatively flat and involve large computationally intensive model domains. The solver type used by RES3D64 is proprietary, though it is very likely to be either the Cholesky Decomposition or the Conjugate Gradient solver. Both the Cholesky Decomposition and Conjugate Gradient solver are numerically equivalent, robust, and stable methods. The Cholesky Decomposition solver is generally faster and requires more memory than the Conjugate Gradient method. Refer to *Matrix Computations, 3rd Edition.*

4.3.3.11 Model Depth of Investigation. The deepest model layer as calculated from the array type and electrode geometry using an empirical method was proposed by L. S. Edwards (*Geophysics*, 1977, "A Modified Pseudo-Section for Resistivity and IP".) RES3D64 use a parameter called Depth Factor. For the T farm resistivity inverse models, a value of 0.7 was

used, which allowed for an appropriate model layer calculation given the array type and geometry.

4.3.3.12 Model Nodes. The number of model nodes per electrode spacing controls the density of the model mesh. A mesh with more than four nodes per electrode spacing is finer than the resolution of the resistivity method, but reduces numerical approximation errors within the mathematical model relative to coarser grids. For the T farm resistivity inverse models, the number of model nodes was set to a factor of four. Larger values directly increase the number of cells and subsequently the amount of computer memory required.

4.3.3.13 Model Resistivity Limits. The upper and lower resistivity limits are based on the reasonably expected values for a particular field area. These limits are imposed in order to reduce the chance of equivalent solutions that are outside the bounds of the true material properties. RES3D64 uses an upper and lower limit factor that is multiplied by the average apparent resistivity of the pseudo-section. The user manual for RES3D64 describes the limits as a soft constraint, which is not strictly applied.

4.3.4 Resistivity Visualization

2D inversion data are represented in color contour cross-section form using Surfer®. Three-dimensional inversion data are interpolated and visualized using RockWorks™. Examples of these plots are found in Appendix A and Section 6.0 of this report.

4.3.5 Resistivity Color Scales

A varying color scale was used for the T farm work based on the different types of datasets and their respective ranges and gradients. All plots have an identified color scale, which is mainly used to highlight targets. The different color scales do not allow a direct comparison of resistivity values from one plot to the next.

The color scales are composed of a continuous spectrum of colors similar to a rainbow. This spectrum uses cool colors (blue) to represent lower values and hot colors (red) to represent higher values. Figure 4-9 shows a histogram of data from an inverse model of the resistivity and log resistivity at T farm. The histogram of resistivity values from T farm exhibits a log normal distribution which can be difficult to visualize using a linear color scale. The log method improves color differentiation by placing a higher number of contrasting colors where values are clustered, such as the 0 to 300 ohm-m range.

® Surfer is a registered trademark of Golden Software, Inc.
™ RockWorks is a trademark of Rockware, Inc.

Figure 4-9. Example Histogram of Inversion Model Resistivity Data .

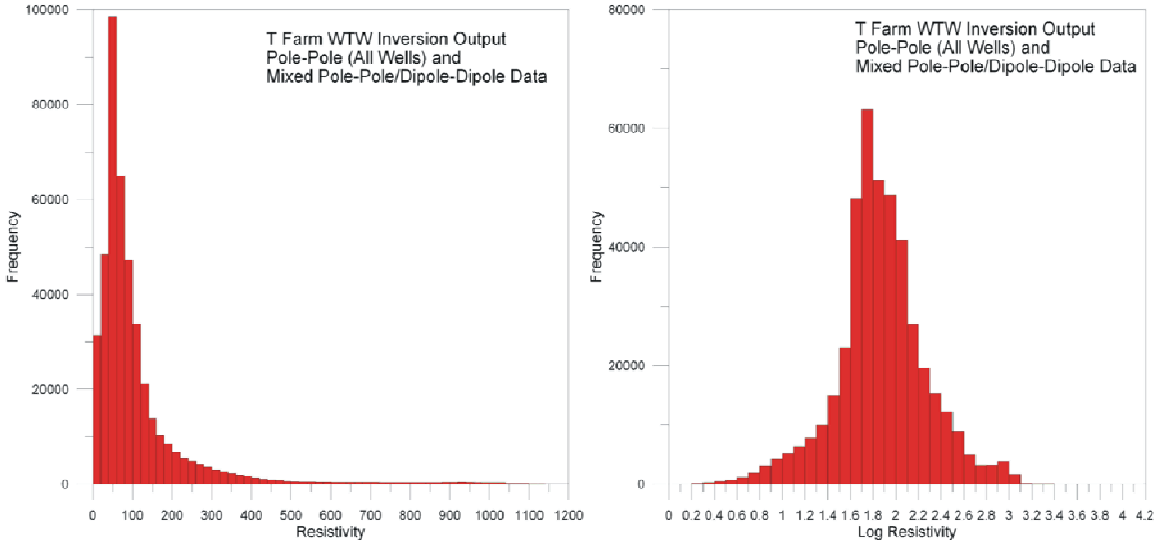

Using a Normal Resistivity Scale (Left) and a Log Normal Resistivity Scale (Right)

5.0 METHODOLOGY

This section describes the equipment and methodology used to collect, manage, and process electrical resistivity data in order to generate visualizations of conductive anomalies in and around the T tank farm for evaluation as potential contaminant plumes.

5.1 RESISTIVITY EQUIPMENT

Resistivity data for the WTW, STS, and WTS data were acquired using a SuperSting R8™ in pole-pole and dipole-dipole array configuration. For STS, the array used 72 smart electrodes or 84 passive electrodes with inter-electrode spacing ranging from 3 to 6m (9.8 to 19.7 ft). Figure 5-1 shows a standard deployment of the resistivity equipment.

Figure 5-1. Resistivity Equipment Showing Use of Lockout/Tagout Safety Equipment.

Left: Electrode Switch Boxes Center: SuperSting control unit. Right: Lockout/Tagout cable jacket and battery lock box

Two grounded remote reference electrode arrays were used for the pole-pole acquisition. The remotes were located at the following coordinates in Washington State Plane South, meters, and datum NAD83: Tx = (568395, 137725) and Rx = (566100, 137859). Each remote reference electrode array consisted of six 0.9m (3 ft) long stainless steel rods, driven into the ground and connected together with wire as shown in Figure 5-2. To reduce contact resistance, 19 liters (5 gallons) of water was added to each receiver remote electrode and 19 liters (5 gallons) of salt solution was added to each transmitter remote electrode. Wire was placed from each remote reference electrode array to just north of the T tank farm fence, where it was connected to the resistivity instrument.

™ SuperSting R8 and SuperSting R8 IP are trademarks of Advanced Geosciences, Inc., Austin, Texas.

Figure 5-2. Setup of Remote Electrodes for Pole-Pole Acquisition.

Left: Remote reference electrode array; Right: Stainless rod connected with ground wire.

For the WTW and WTS acquisition, individual wires had to be connected between each well and the SuperSting R8. The connection required a patch panel of banana clips that allowed the SuperSting R8 control of which well acted as a transmitter and receiver. Figure 5-3a shows the patch panel developed by HGI. Two 56-channel patch panels were necessary for connection with 110 wells. Figure 5-3b shows a wire terminated and connected to a well.

Figure 5-3. Physical Connection of Wells for Acquisition.

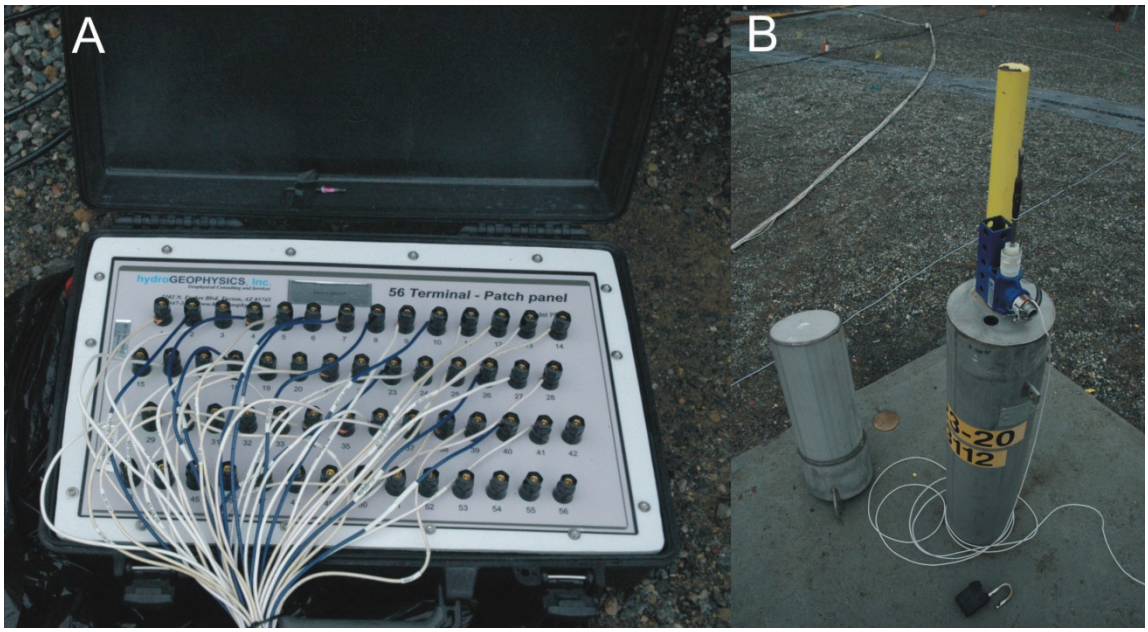

Figure 5-4 shows a typical layout of STS survey lines with use of smart electrode cables outside of the T tank farm, passive electrode cables inside the tank farm, and depth-limited surface electrodes. The electrodes were limited to depths less than 12 inches, eliminating the need for

excavation permits. However, unlike SGE projects conducted after T farm, the electrodes were not left permanently in place for later occupation.

Figure 5-4. Location of the Completed High-Resolution Resistivity Survey Lines.

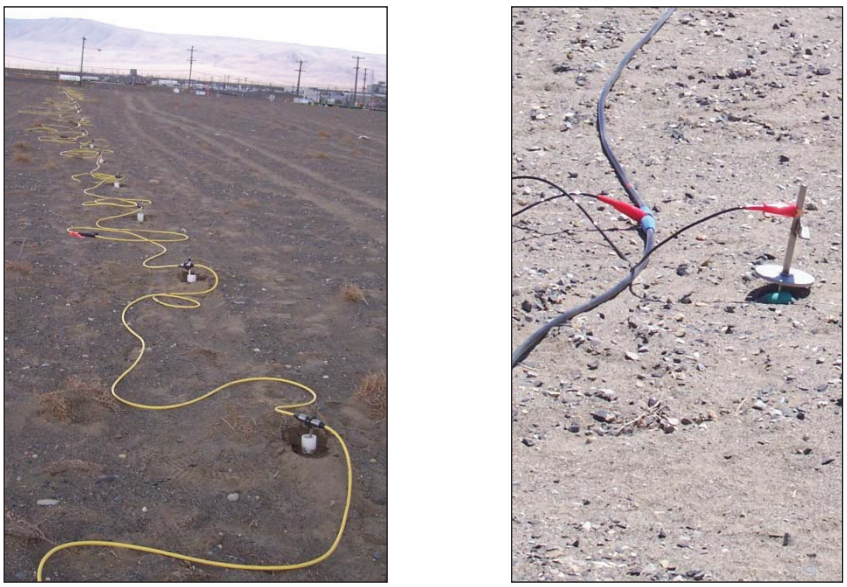

Note: Left: Ex-farm deployment of smart electrode cables, Middle: In-farm deployment of passive cables, and Right: In-farm deployment of depth limited surface electrode.

5.2 SURVEY AREA AND LOGISTICS

A summary of the resistivity data collection methods and survey coverage area can be viewed in Table 5-1 and Figure 5-5, Figure 5-6, and Figure 5-8.

Table 5-1. Summary of Resistivity Acquisition Stats at the T Tank Farm.

Geometry	Array	Date of Acquisition	Number of Lines	Number of Electrodes / Wells	Number of Raw Data Acquired
WTW	Pole-pole	January 16, 2006	N/A	110	10,635
WTW	Dipole-dipole	January 16, 2006	N/A	110	8,530
STS	Pole-pole	June 10, 2005	27	4,005	122,541
WTS	Pole-pole	January 20, 2006	N/A	112* / 110**	23,557

WTW = well-to-well; **WTS** = well-to-surface; **STS** = surface-to-surface

* number of surface electrodes in WTS

** number of wells in WTS

5.2.1 Task 1 – Well-to-Well Measurements

Onsite WTW activities commenced on January 16, 2006, with the preparation of wells that were selected for collecting WTW data. A total of 110 wells were used for data collection, including 93 drywells, and 17 groundwater wells. Figure 5-5 shows the wells used in the analysis.

Figure 5-5. Wells Used in the WTW Data Collection at T Tank Farm.

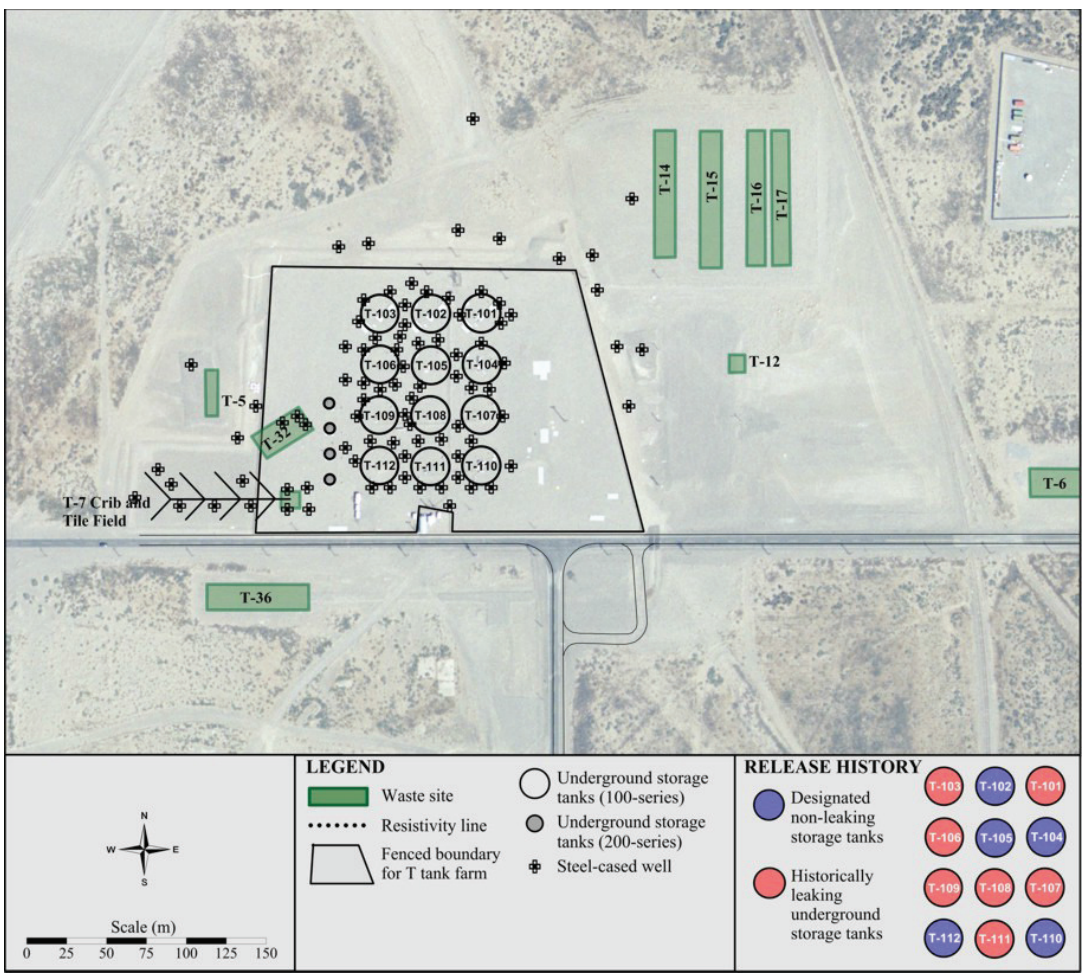

For the WTW survey, both pole-pole and dipole-dipole measurements were collected. The acquisition command file created for the pole-pole array sequenced through each possible pair for transmitter and receiver. The dipole-dipole command file sequenced through a subset of data due to the extremely large possible number of combinations. For example, a simple 27-well survey would have 351 pole-pole measurements and 52,650 dipole-dipole measurements. The dipole-dipole subset of data combinations was chosen randomly.

5.2.2 Task 2 – Surface-to-Surface Resistivity Mapping

The surface resistivity survey began on June 10, 2005 and was completed on July 27, 2005. Resistivity lines were acquired outside the tank farm first. Figure 5-6 shows the resistivity line layout and the labels for the lines are identified at each line's end.

Figure 5-6. STS Resistivity Line Layout for STS Data Collection at T Tank Farm.

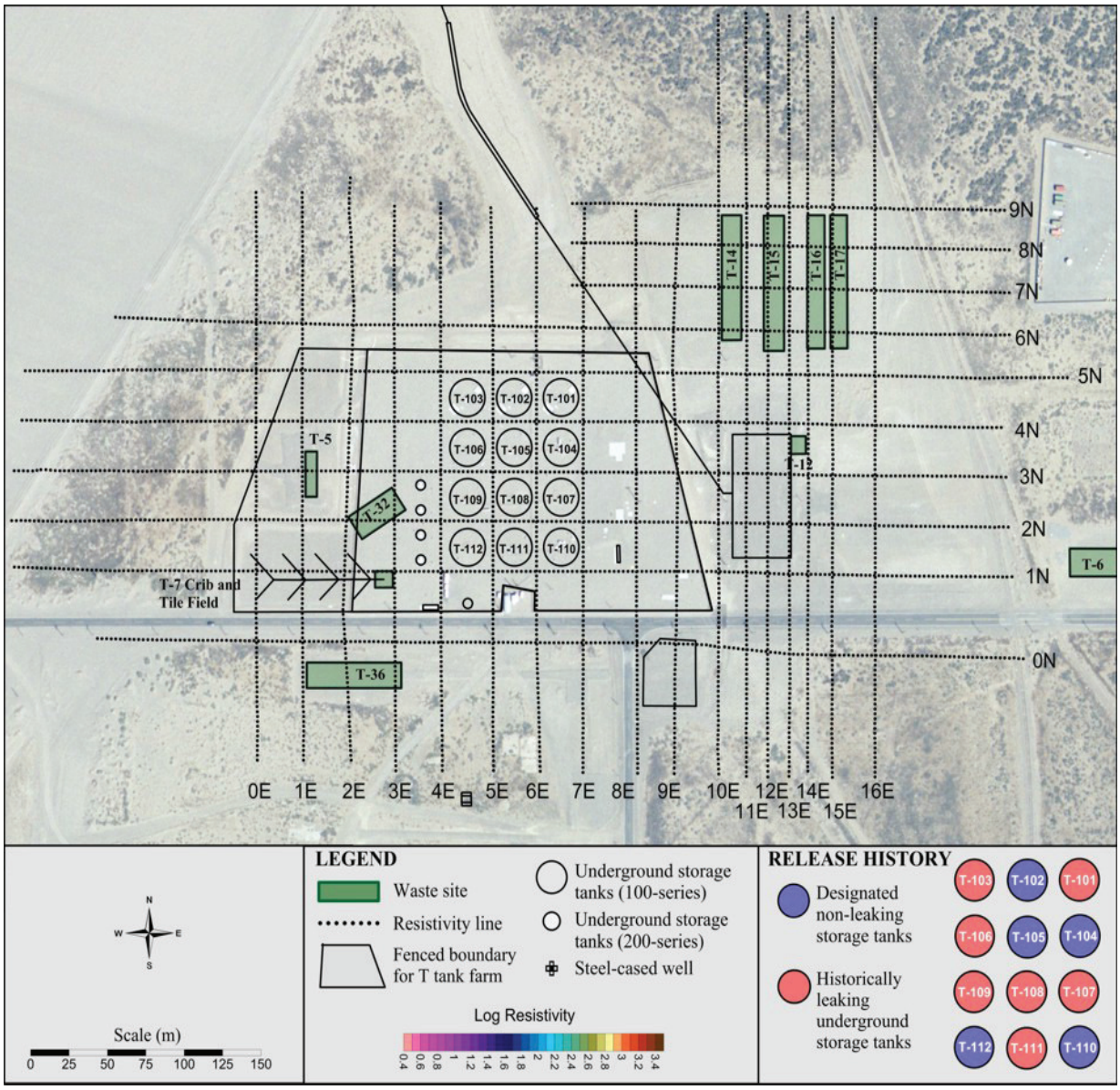

Several lines crossed major roads and road crossing tactics were employed to prevent damage to the equipment while allowing safe passage for vehicular traffic. Traffic control personnel were deployed where a Yellow Jacket® crossed 23rd Street (the street just south of T farm.) A high strength metal conduit was used to add extra cable protection. Figure 5-7 shows an example of a road crossing setup. No electrodes were installed in asphalt roads.

® Yellow Jacket is a registered trademark of Peterson Systems.

Figure 5-7. Example of Road Crossing Setups.

Note: Left: Adhesive road tape covering SO cord, used to allow remote reference cable to cross road; Right: Yellow Jacket® used to allow smart cables to cross road. ®Yellow Jacket is a registered trademark of Peterson Systems.

5.2.3 Task 3 – Well-to-Surface Measurements

In addition to the 110 wells, two surface electrode survey lines were deployed to compare WTW measurements with WTS. Fifty six electrodes were placed at 6-meter (20-ft) spacing along resistivity lines 5E and 5N. Data acquisition was performed between January 20, 2006, and January 25, 2006. Figure 5-8 shows the layout of the WTS acquisition.

Figure 5-8. Line Layout and Wells Used in WTS Data Collection in the T Tank Farm.

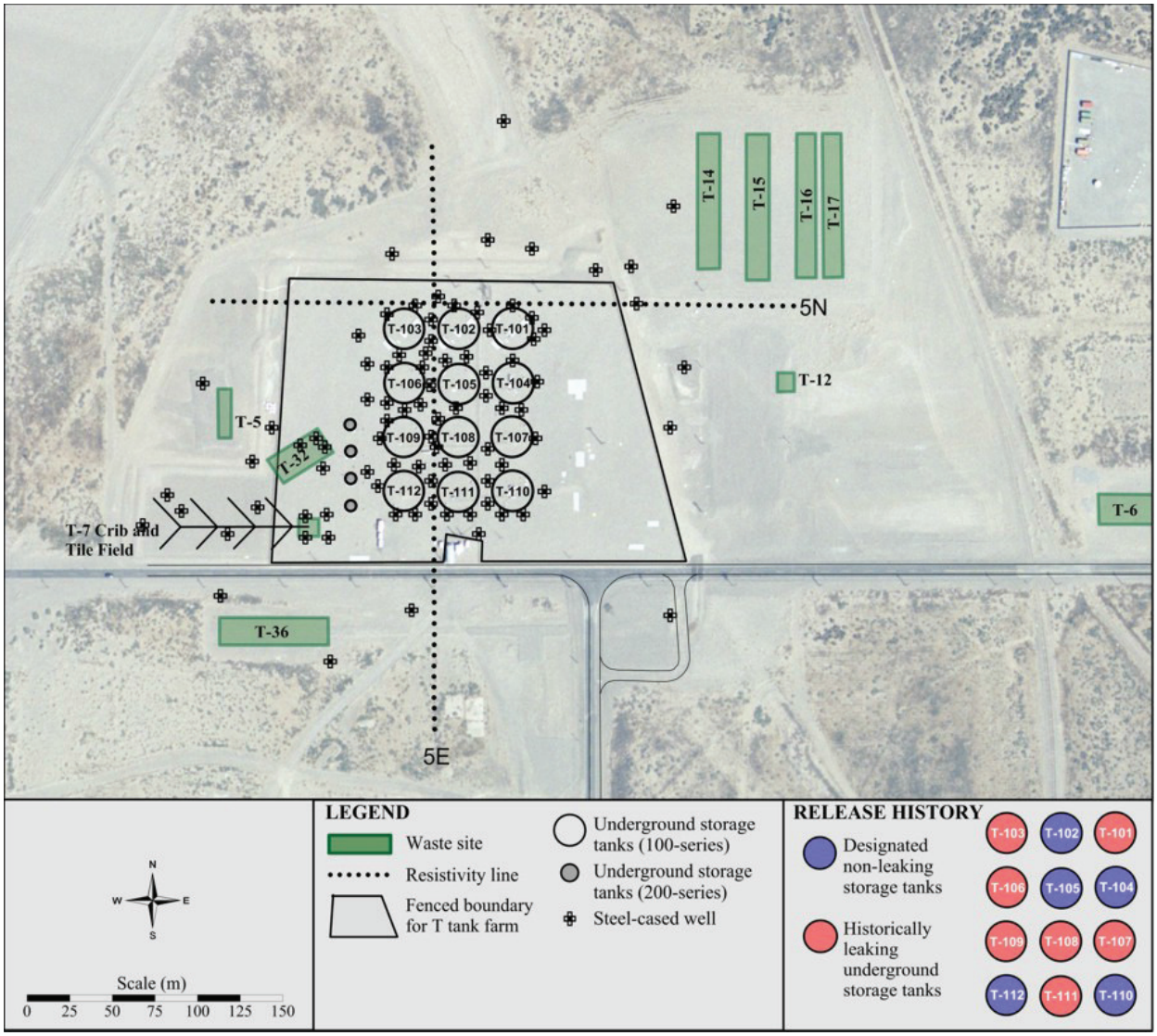

5.3 DATA PROCESSING

5.3.1 Task 1 – WTW Processing

5.3.1.1 Data Downloading, Parsing, and Quality Control. Each day, individual binary . data files were downloaded and exported to a laptop computer. The data were reviewed before removing the resistivity equipment from the field. Each file was parsed into usable columns (e.g., Record No., Date, Current, Normalized Potential, Error, Apparent Resistivity, Geometry,

Transmitter Gain) using Microsoft Excel®. Data inspection consisted of a numerical and graphical evaluation of the signal-to-noise ratio, percent error, and data scatter in comparison to neighboring wells. The object of the data inspection was not to reject erroneous points, but to ensure adequate data quality before continuing the next day. This process also allowed the operator to refine data acquisition parameters as the survey migrated from one area of the site to another.

5.3.1.2 Data Processing and Plotting. WTW processing required a multi-step procedure.

1. The first step was to apply the proper coordinates and well information to the channels. Additional information needed for WTW inversion included the type of well and casing length.
2. The second step included a quality check of the data. Repeat errors were assessed for quality, negative data were removed, and the remaining data were plotted as normalized potential versus separation distance between transmission and receiving well. Plotting allowed an assessment of relative quality. In general, the normalized potential should have decreased as the spacing between wells increased. If the opposite occurred, then it was removed. Low grounding potential due to casing contact with the surrounding soil may have had negative effects on the data.
3. The third step was to remove wells that were in close proximity to each other. A cut-off of 6m was used, where wells closer than 6m were evaluated for noise and one was removed. With the processing steps two and three, 87 of the 110 wells were used for final inversion. Figure 5-9 shows the WTW data set used for inversion.

® Microsoft Excel is a registered trademark of the Microsoft Corporation.

Figure 5-9. Transfer Resistance Measured in WTW Data Collection.

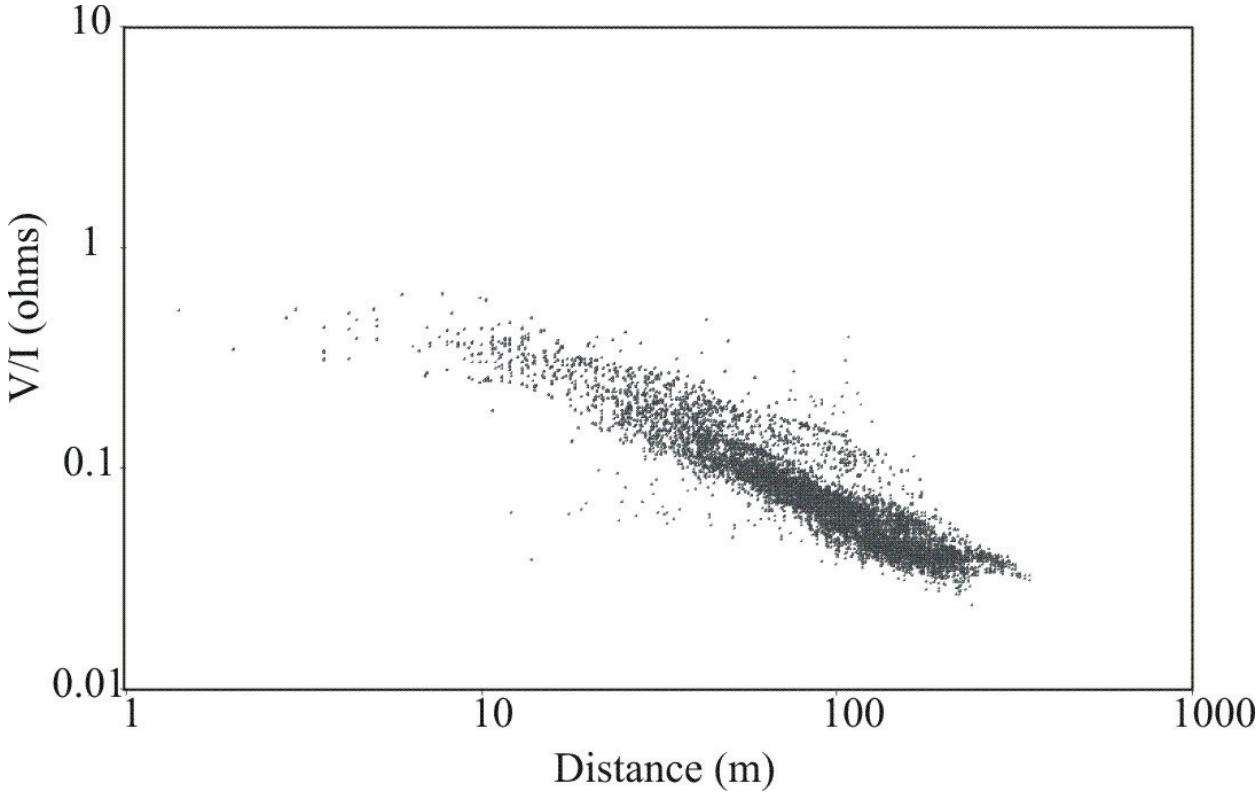

4. The fourth step was to import the voltage measurement data file with RES3D64. The inversion program goes through another set of quality checks to look for data collected with low voltage or low current. The code's inversion parameters are modified in various trials to find the best model convergence and reliability.

5. The fifth step was data visualization. The resistivity data were interpolated onto a 2D slice in Surfer, and plotted on a site infrastructure map. The lower resistivity values represent higher contaminant concentration.

5.3.2 Task 2 – STS Processing

STS evaluation involved data collection, processing, and visualization of both resistivity and GPS data. The resistivity data was acquired with the SuperSting R8 system with both passive and smart cables. The GPS data provided control points and geo-referenced resistivity data for accurate placement of data relative to tank farm features.

5.3.2.1 Data Downloading, Parsing, and Quality Control. Each day, individual binary data files were downloaded and exported to a laptop computer. The data were reviewed before moving the resistivity equipment to the next survey line. Each file was parsed into usable columns (e.g., Record No., Date, Current, Normalized Potential, Error, Apparent Resistivity,

Geometry, Transmitter Gain) using Excel. Data inspection consisted of a numerical and graphical evaluation of the signal-to-noise ratio, percent error, and data scatter in comparison to neighboring lines. The object of the data inspection was not to reject erroneous points, but to ensure adequate data quality before continuing the next day. This process also allowed the operator to refine data acquisition parameters as the survey migrated from one area of the site to another. Data acquisition parameters are permanently recorded within the headers of the downloaded files. See Table 5-2.

Table 5-2. STS Resistivity Data Acquisition Parameters.

Date	Line Number	Orientation	Length (meters)
July 27, 2005	0E	South to North	345
July 14, 2005	1E	South to North	321
July 18, 2005	2E	South to North	353
July 19, 2005	3E	South to North	334
July 20, 2005	4E	South to North	334
July 21, 2005	5E	South to North	335
July 22, 2005	6E	South to North	343
July 25, 2005	7E	South to North	343
July 26, 2005	8E	South to North	336
July 25, 2005	9E	South to North	343
June 13, 2005	10E	South to North	466
June 28, 2005	11E	South to North	463
June 23, 2005	12E	South to North	463
June 24, 2005	13E	South to North	463
June 27, 2005	14E	South to North	463
June 29, 2005	15E	South to North	463
June 30, 2005	16E	South to North	462
July 29, 2005	0N	West to East	600
July 13, 2005	1N	West to East	642
July 12, 2005	2N	West to East	643
July 11, 2005	3N	West to East	643
July 8, 2005	4N	West to East	643
July 6, 2005	5N	West to East	679
June 11, 2005 (August 1, 2005)	6N	West to East	686
June 11, 2005	7N	West to East	283
June 11, 2005	8N	West to East	283
June 10, 2005	9N	West to East	283

5.3.2.2 Data Downloading, Parsing, Quality Control. STS processing required a multi-step procedure. Step 1 involved making sure that all GPS and STS data were converted to read-only files so that the files could not be changed.

Step 2 involved filtering and editing. Filtering refers to data reduction. The reduction processes are based on several criteria of error (a statement of data quality), current transmission, and out-of-range resistivity data (such as negative apparent resistivity). The error was calculated internally by the hardware by measuring the resistivity multiple times for a single receiver and transmission pair (called stacking). The standard error is calculated from multiple stacks. Filtering removes values with an error greater than a calculated cut-off.

Editing refers to identification of trends within data after filtering. The normalized measured potential is plotted as function of space (i.e., the distance between the transmission and receiving electrode). This plot shows normalized measured potential versus distance along the line. Multiple lines are then plotted together on a single graph to observe trends and smoothness. As the spacing increases, the normalized potential decreases, and the plot shows distinct lines that rarely overlap. Infrastructure and other anomalies appear within the plot, allowing for their removal. Figure 5-10 shows the edited V/I data used for Step 3 – inversion. Although transfer resistance data are shown, data input for RES3D64 requires apparent resistivity, which is calculated by:

$$\rho_a = 2\pi a \frac{V}{I}$$

Where: a is the distance between transmitter and receiver.

Appendix A demonstrates graphically the complete process of filtering and editing for STS data.

Figure 5-10. Transfer Resistance Data Measured in STS Data Collection.

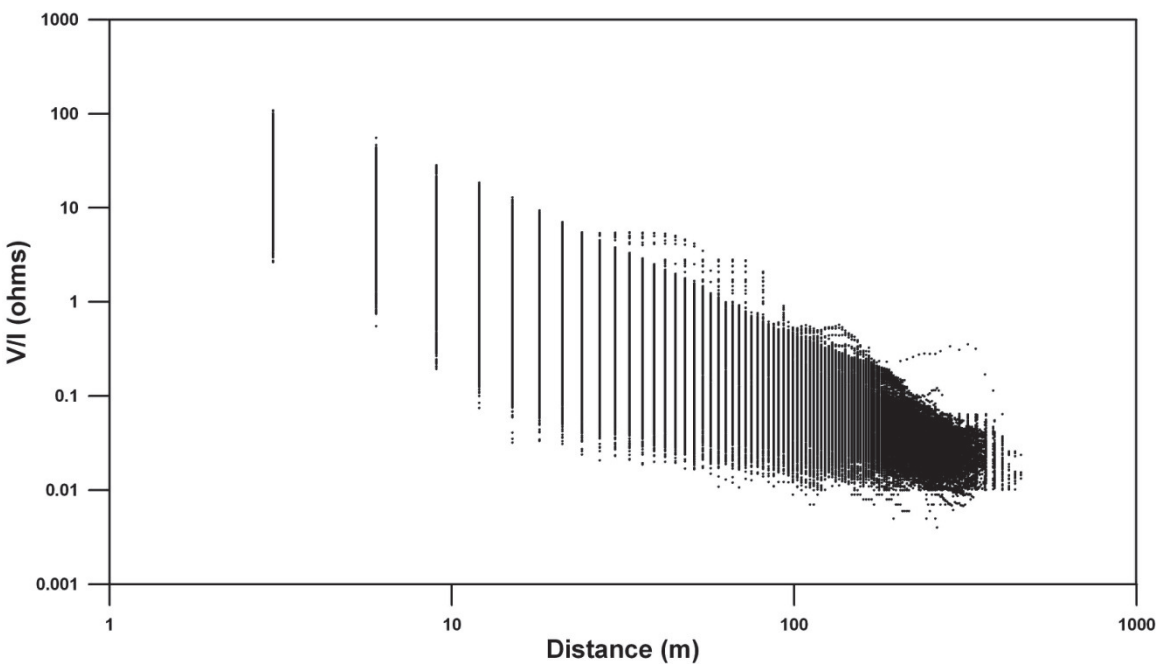

Step 3 involves inverting the apparent resistivity using RES3D64. Inversion uses an inverse algorithm to estimate the electrical resistivity of the earth based on measurements of voltage potential and current. Several researchers have used these models to determine the electrical resistivity distribution for both hydrologic and geologic studies. Refer to:

- USGS Open File Report 2004-1319, "*Direct Current Resistivity Profiling to Study Distribution of Water in the Unsaturated Zone Near the Amargosa Desert Research Site, Nevada,"*
- *Journal of Environmental Monitoring*, "Post-remediation evaluation of a LNAPL site using electrical resistivity imaging,"
- *Journal of Environmental and Engineering Geophysics*, "Difference Inversion of ERT Data: A Fast Inversion Method for 3-D In Situ Monitoring"
- Yang, X., "Stochastic inversion of 3D ERT data."

Step 4 is the plotting step, where the inverted data are contoured based on the range of resistivity values. A coloring methodology for the contours was applied to the resistivity data based on geometry-specific histograms of information. Section 4.3.5 discusses the methodology of choosing the coloring of the contours.

5.3.3 Task 3 – WTS Processing

5.3.3.1 Data Processing and Plotting. WTS processing required a multi-step. procedure, similar to WTW.

1. The first step was to apply the proper coordinates and well information to the channels. Additional information needed for WTS inversion included the type of well and casing length.
2. The second step included a quality check of the data. Repeat errors were assessed for quality, negative data were removed, and the remaining data were plotted as normalized potential versus separation distance between transmission and receiving well. Plotting allowed an assessment of relative quality. In general, the normalized potential should have decreased as the spacing between wells increased. If the opposite occurred, then it was removed. Low grounding potential due to casing contact with the surrounding soil may have had negative effects on the data.
3. The third step was to remove wells that were in close proximity to each other. A cut-off of 6m was used, where wells closer than 6m were evaluated for noise and one was removed. With the processing steps two and three, 87 of the 110 wells were used for final inversion. Figure 5-11 shows the WTS data set used for inversion.

Figure 5-11. Transfer Resistance Measured in WTS Data Collection.

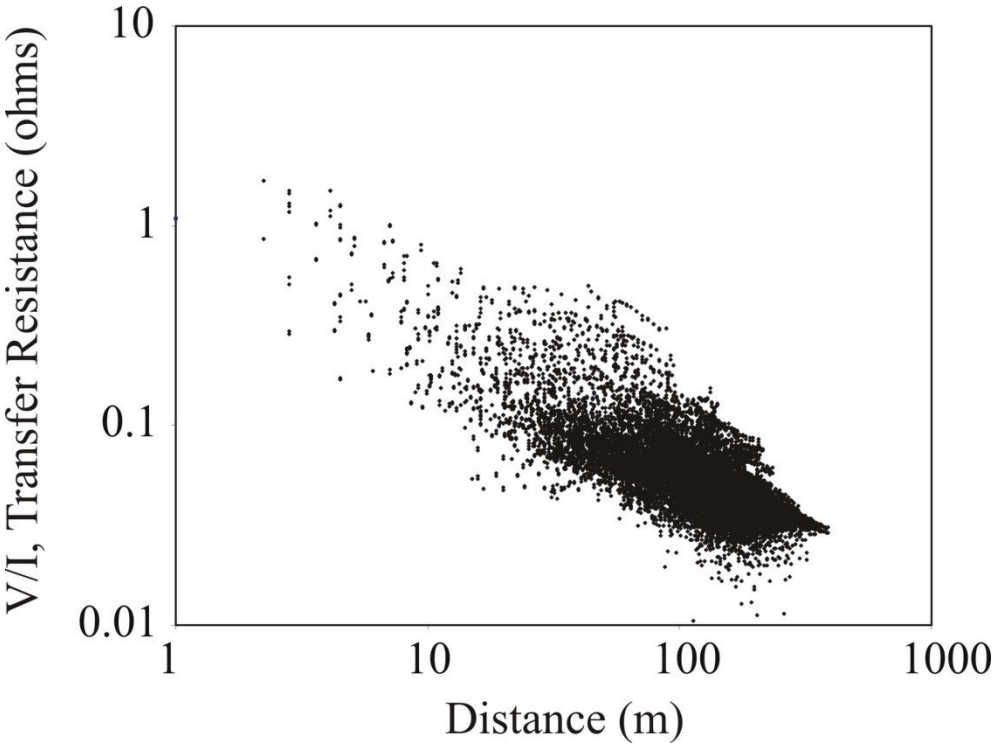

4. The fourth step was to import the voltage measurement data file with RES3D64. The inversion program goes through another set of quality checks to look for data collected with low voltage or low current. The code's inversion parameters are modified in various trials to find the best model convergence and reliability.

5. The fifth step was data visualization. The resistivity data were interpolated onto a 2D slice in Surfer, and plotted on a site infrastructure map. The lower resistivity values represent higher contaminant concentration.

6.0 RESULTS AND INTERPRETATION

6.1 PREVIOUS T FARM WELL-TO-WELL INVERSION RESULTS

For the previous T farm processing effort conducted in 2005, WTW inversion models were completed using both drywells completed in the vadose zone and groundwater wells. The code EI3D was used for the inversion, which is the 32-bit version that requires smaller model domains than its counterpart EI3DCL used in later SGE projects. Results of selected WTW inversion models from the previous effort are presented in Figures 6-1 and 6-2 below.

Figure 6-1 shows the WTW resistivity inversion results for the vadose zone wells only. The figure is an overhead shot of the resistivity distribution around the site. Since 3D information cannot be interpreted from the WTW inversion data, an overhead view is the most appropriate angle to view the data. The inversion represented in Figure 6-1 includes data collected from 83 wells, which are shown as black dots in the figure. The length of the wells varies from 7 to 46m (23 to 151 ft).

Figure 6-1. Previous T Tank Farm WTW Inversion Results Using Vadose Zone Wells Only.

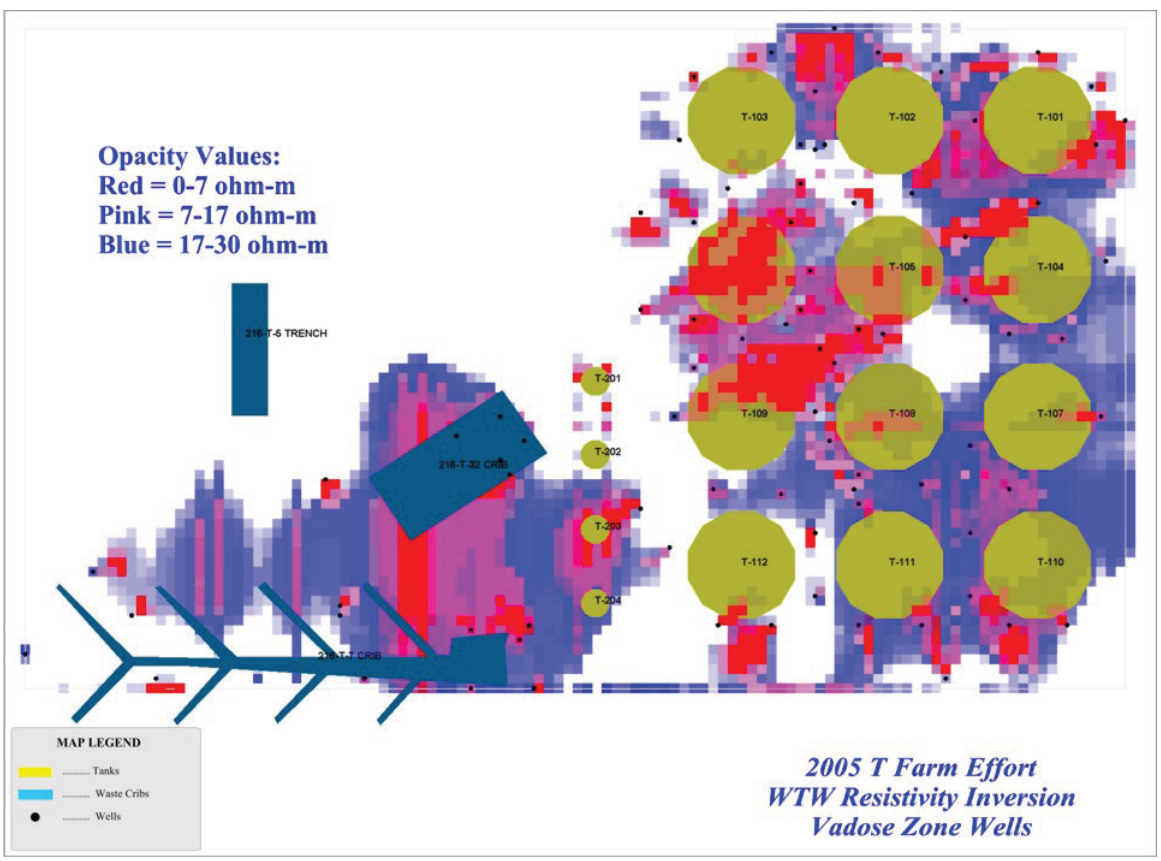

Figure 6-1 shows three levels of data. The smallest, which is represented by the lowest resistivity values from 0 to 7 ohm-m, is highlighted in red. Concentrated waste areas are enhanced by this level of contouring. The observed anomaly agrees with assumed leaks from tanks T-101, T-103, and T-106. Tank T-101, for example, shows an anomaly to the southeast and southwest of the tank that is supported by spectral gamma logging data. Tank T-103 shows a plume to the northeast of its boundary that does not correlate with spectral gamma logging data. Tank T-106 shows the largest response to the south and southeast. According to spillage reports and characterization data, the resistivity data appear to coincide with previously identified contamination from the spectral gamma logging program.

In addition to areas known to have leaked, the resistivity data show preferential hot spots that may indicate a previously unknown release. Tank T-112, for example, shows a large red anomaly to the south of its boundary. Additionally, tanks T-203 and T-204 show a response consistent with leakage near the tanks. These areas may warrant further investigation.

The other levels of contouring, outlined in pink from 7 to 17 ohm-m and 17 to 30 ohm-m, shows a larger affected area within the tank farm footprint. The pink areas tend to focus around tanks T-101 and T-106. However, tanks T-107 and T-110 show decreased resistivity that may represent leaks from these tanks, or waste migration from other sources. The blue level of contouring covers almost the entire tank farm. A few holes in the coloring suggest that these areas do not contain waste.

Although the results conform to hydrologic expectation, the degree of noise is quite high. The noise issue was discussed in Section 4.2.1 and the code EI3D produced some undesirable effects. Striping elongated in the north-south direction is a common problem seen in many past trials.

Figure 6-2 is an overhead shot of the resistivity distribution using groundwater wells. Since the wells are in direct contact with the saturated zone, the results are interpreted to be at that depth. Low resistivity values would indicate that a plume is likely in the groundwater.

Figure 6-2. Previous Results From WTW Inversion at T Tank Farm Using Groundwater Wells Only.

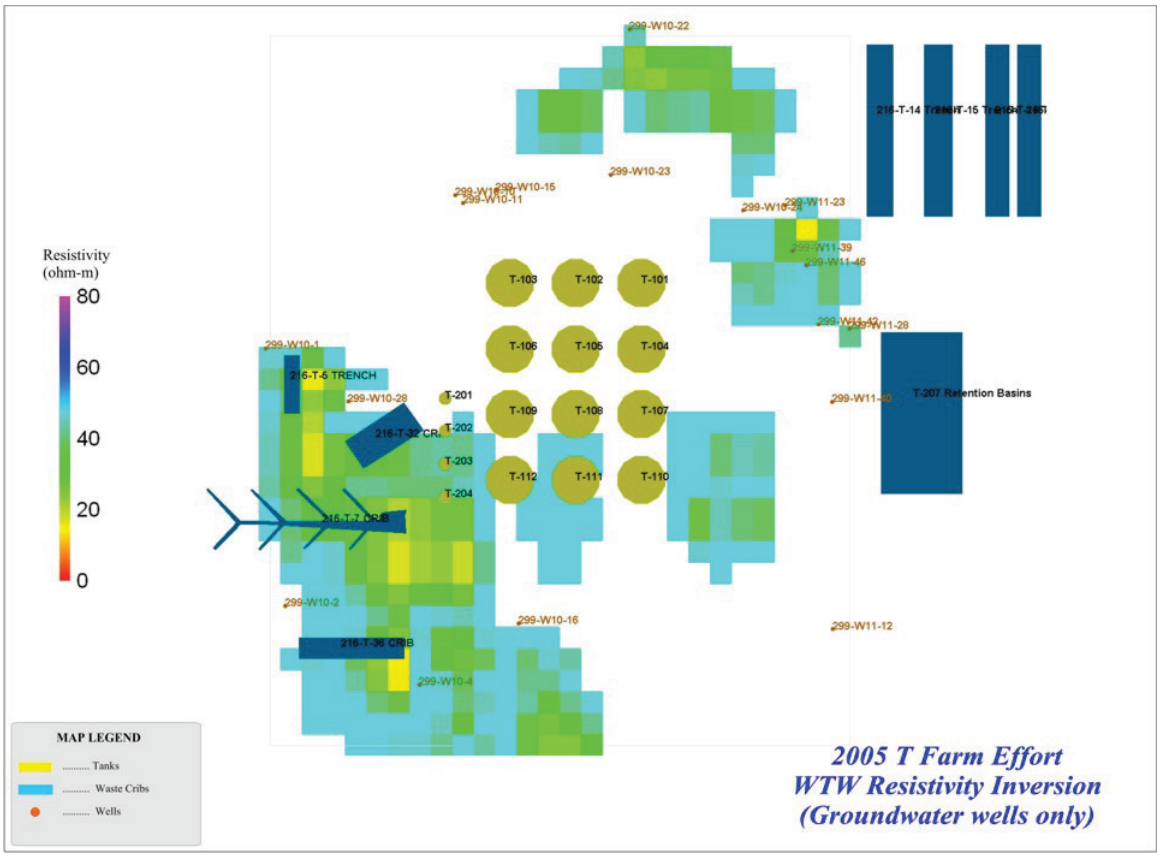

The WTW inversion, based on groundwater wells, shows that a low resistivity area exists beneath the western trenches and in the northeast corner of the fence. The lowest values, indicated in yellow, correlate with disposal trenches in the west. The values increase as the distance from these facilities increases. Wells 299-W10-4 and 299-W10-28 show nearby low values, which may fit with the high concentrations of inorganic salts measured in these wells. Additionally, the northeast corner of the site, with a large number of wells, shows a low resistivity that also coincides with known high inorganic salt concentrations. Unfortunately, the data do not pinpoint a source for the contamination.

Two unexpected resistivity anomalies also appear in the data. One appears to the north, between wells 299-W10-22 and 299-W10-23. The other is to the east of the tanks, beneath the diversion boxes. Other inversion results also show these areas as resistivity anomalies, suggesting the presence of a significant feature

6.2 REPROCESSED 3D RESISTIVITY INVERSION MODELING

A series of 3D resistivity inversion models were produced using reprocessed T farm data for select domains within the survey area, using both pole-pole and dipole-dipole WTW, pole-pole STS, and pole-pole WTS datasets. The results of all models are discussed below.

6.2.1 Task 1 – WTW Inversion Results

Convergence curves for all WTW models, based on the updated version of RES3D, are shown in Figure 6-3. A stopping criteria of six iterations was used throughout the modeling and the convergence curves in the figure show a monotonic decrease in RMS error for each successive iteration. Table 6-1 lists the details for the different models identified in the legend of Figure 6-3. From an error perspective, the most successful model was the groundwater well model, which completed with an RMS error around 5 percent. The two dipole-dipole runs also had a low RMS error.

Figure 6-3. Convergence Curves for the WTW Models.

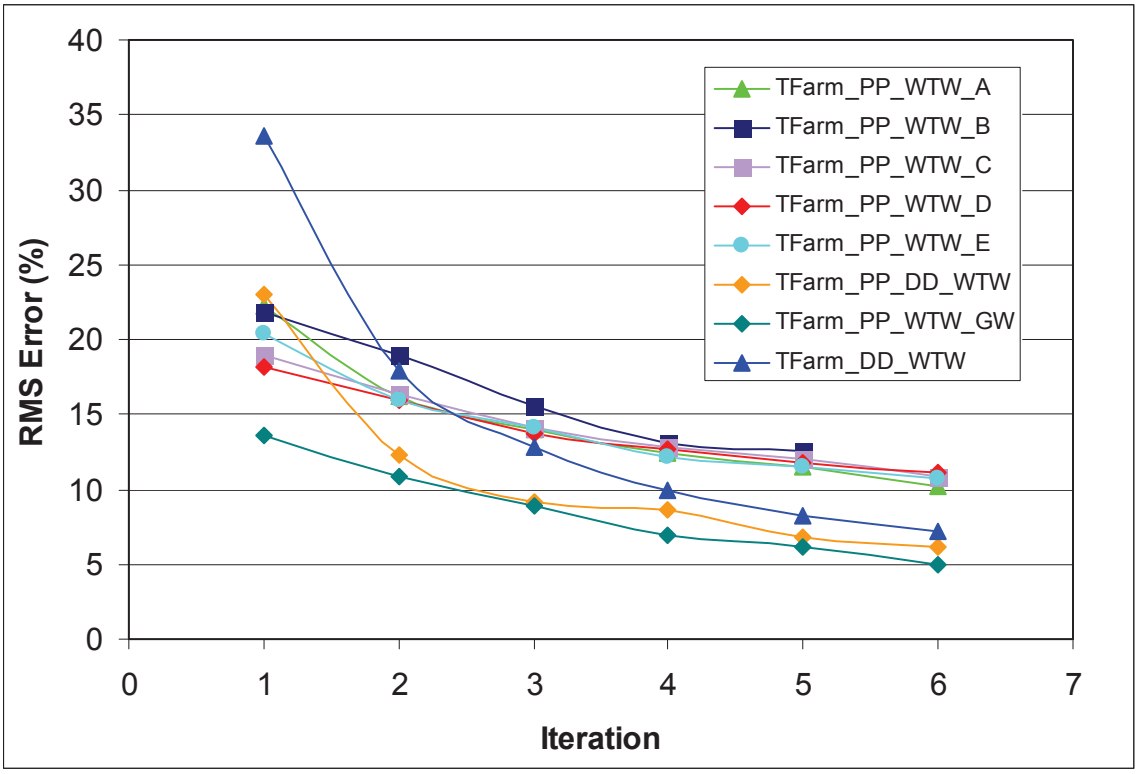

Table 6-1. Details of the WTW Models and Naming Convention.

Inversion Name	Array	Details
TFarm_PP_WTW_A	Pole-pole	Groundwater and vadose zone wells included. A priori well resistivity: 0.001 ohm-m A priori well cross sectional area: 0.04 m
TFarm_PP_WTW_B	Pole-pole	Groundwater and vadose zone wells included. A priori well resistivity: 0.001 ohm-m A priori well cross sectional area: 0.1 m
TFarm_PP_WTW_C	Pole-pole	Groundwater and vadose zone wells included. A priori well resistivity: 0.05 ohm-m A priori well cross sectional area: 0.5 m
TFarm_PP_WTW_D	Pole-pole	Groundwater and vadose zone wells included. A priori well resistivity: 0.1 ohm-m A priori well cross sectional area: 0.5 m
TFarm_PP_WTW_E	Pole-pole	Groundwater and vadose zone wells included. A priori well resistivity: 0.006 ohm-m A priori well cross sectional area: 0.1 m
TFarm_PP_DD_WTW	Mixed pole-pole and dipole-dipole	Groundwater and vadose zone wells included. A priori well resistivity: 0.006 ohm-m A priori well cross sectional area: 0.1 m
TFarm_PP_WTW_GW	Pole-pole	Groundwater wells only. A priori well resistivity: 0.006 ohm-m A priori well cross sectional area: 0.1 m
TFarm_DD_WTW	Dipole-dipole	Groundwater and vadose zone wells included. A priori well resistivity: 0.006 ohm-m A priori well cross sectional area: 0.1 m

6.2.1.1 WTW Inversion Models Based on a Pole-Pole Array Using Vadose and Groundwater Wells. Five new WTW 3D inversion models were run using pole-pole data collected from vadose zone wells and groundwater wells together. The results, located in the northwest part of the survey, are shown in Figures 6-4 through 6-8. The color scale is kept constant for each WTW plot to assist in plot comparison. The domain for these models encompasses the area over the T tank farm, tile field, T-5, T-32, and T-7 cribs. A-priori well resistivity values (Ohm-m) and cross sectional area (meters) were varied within the models to test the effect of these parameters on the resulting 3D models.

In general, all five of the WTW models evaluated show several low resistivity targets around known disposal areas. The most significant target is found in the southwest corner of the grid around cribs T-5, T-7, and T-32. Given the large volume of disposal for these trenches, the target is consistent with hydrogeologic expectations at these sites. The exact shape and position of the large target, however, is likely influenced by the distribution and density of the wells.

Another significant target is found at the southeast corner of the T-106 tank, which matches the conceptual model discussed in RPP-23752, *Field Investigation Report for Waste Management Areas T and TX-TX*. In general, this target is elongated from the northwest corner of T-106 directly south of T-103 and to the northwest corner of T-111.

Figure 6-4 displays results for inversion model TFarm_PP_WTW_A, which used an a priori well resistivity of 0.001 ohm-m and well diameter of 0.04m. The low resistivity target located in the

southwest corner of the grid around cribs T-5, T-7, and T-32 is resolved using the a priori setting for this model, however, the results appear to have a smaller spatial footprint and generally higher resistivity values when compared with models B, C, D, and E. The target located at the southeast corner of the T-106 tank shows a primary low resistivity body reaching just to the north east corner of T-108, with additional low resistivity areas spreading out to the south and east of the tank farm. In general, these a priori well settings appear to resolve the targets with minimal noise in surrounding areas with resistivity values slightly higher than in other models.

Figure 6-4. WTW Inversion Results for Reprocessed Data Using Well Resistivity of 0.001 OHM-M and Well Diameter of 0.04M.

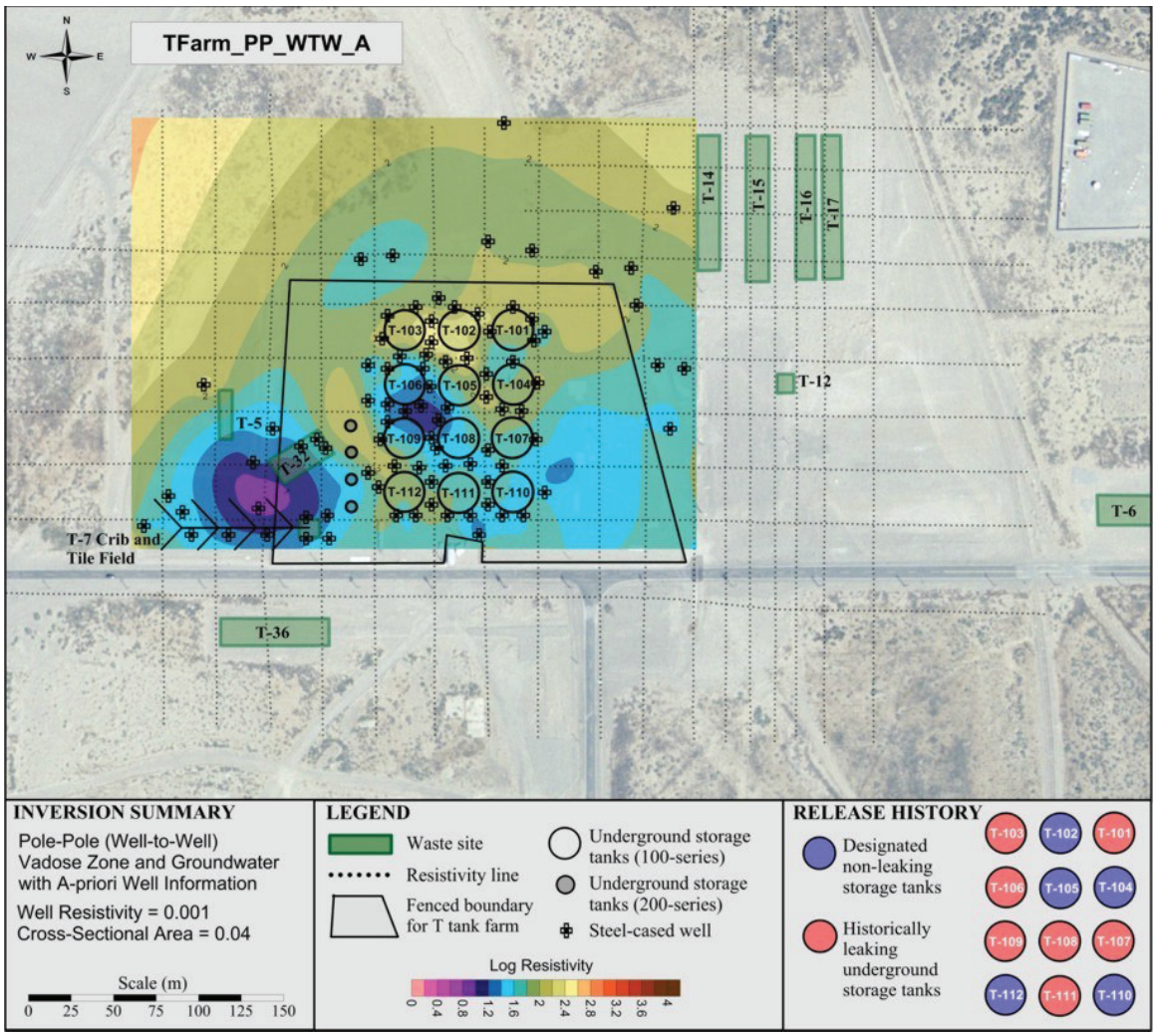

Figure 6-5 shows results for model TFarm_PP_WTW_B, which used an a priori well resistivity of 0.001 ohm-m and a larger well diameter of 0.1m. The larger well diameter was meant to reduce the total number of cells used in the forward model and explore the numerical accuracy compared to a well size of 0.04m. The low resistivity target located in the southwest corner of the grid around cribs T-5, T-7, and T-32 is well resolved and appears to have a larger spatial footprint and generally lower resistivity values when compared with TFarm_PP_WTW_A. The target located in the vicinity of the T-106 tank extends out to the north and west and remains centered over

tanks T-106, T-108 and T-109. The low resistivity area to the southeast of the tank farm seen in TFarm_PP_WTW_A is not present in TFarm_PP_WTW_B. In general, these a priori well settings appear to produce well isolated targets with minimal noise in surrounding areas. Resistivity values are slightly higher overall when compared with Model TFarm_PP_WTW_A.

Figure 6-5. WTW Inversion Results for Reprocessed Data Using Well Resistivity of 0.001 OHM-M and Well Diameter of 0.1M.

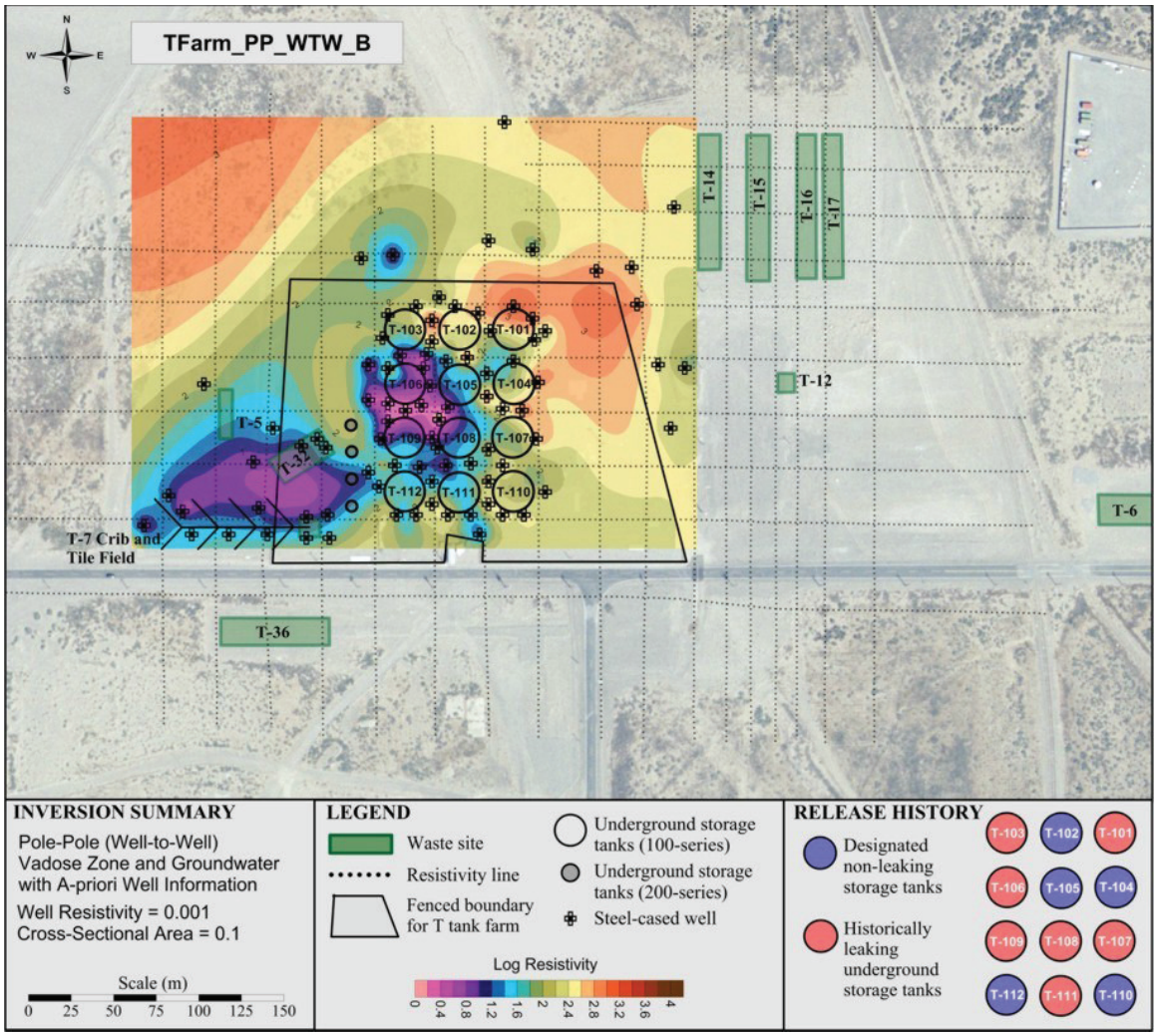

Figure 6-6 shows results for model TFarm_PP_WTW_C, which used an a priori well resistivity of 0.05 ohm-m and a larger well diameter of 0.5m. This inversion was meant to test higher well resistivity values with larger diameters compared to the previous two inversions. As demonstrated in Figure 4-2, larger diameter wells should produce more inaccurate solutions and the results of Figure 6-6 likely confirm this fact with high degrees of noise seen throughout the domain. For example, many wells have isolated low resistivity features that extend only a few tens of meters from the measurement location. In particular, the north and northeast area shows

small features around almost every groundwater well. If there were a real low resistivity feature here, then it should be contiguous from well to well.

Figure 6-6. WTW Inversion Results for Reprocessed Data Using Well Resistivity of 0.05 OHM-M and Well Diameter of 0.5M.

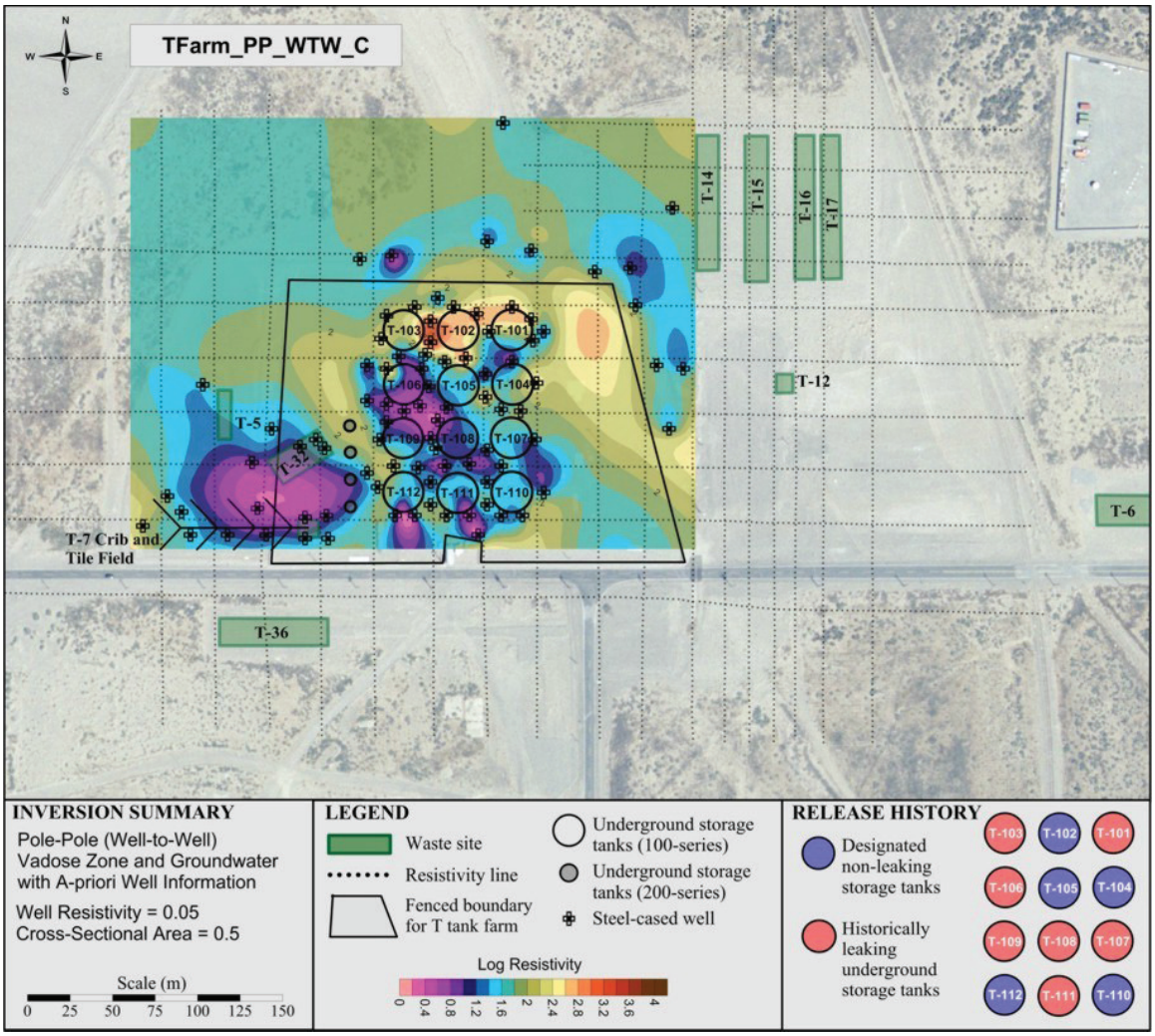

Figure 6-7 shows results for model TFarm_PP_WTW_D, which used an a priori well resistivity of 0.1 ohm-m and a larger well diameter of 0.5m. Similar to TFarm_PP_WTW_C, these results show isolated noisy targets and the resistivity values are generally lower around these targets. Perhaps the lowered target resistivity is an overcompensation for higher well resistivity.

Figure 6-7. WTW Inversion Results for Reprocessed Data Using Well Resistivity of 0.1 OHM-M and Well Diameter of 0.5M.

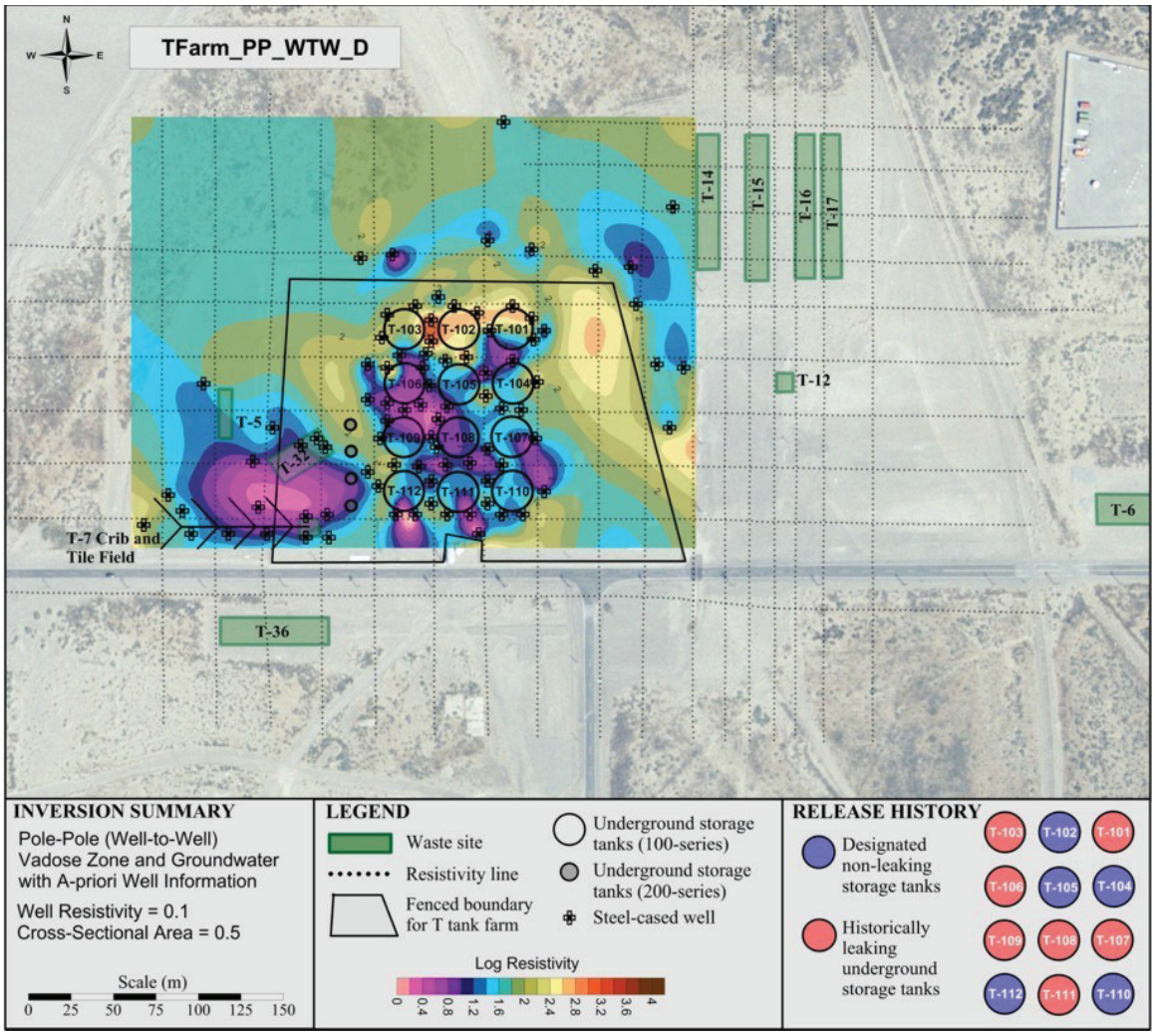

The last trial for this subset is shown in Figure 6-8, which represents model TFarm_PP_WTW_E. This simulation used an a priori well resistivity of 0.006 ohm-m and a larger well diameter of 0.1m. The well resistivity and diameter values were chosen based on the analytic solution comparisons in Figure 4-2. The results for this inversion are similar to the last two, where low resistivity noise is observed around various wells. The values and size of the noisy features are smaller than the previous two, somewhat confirming the suspicion of overcompensation.

Even though the analytic solution compared best to the well resistivity and diameter values of 0.006 ohm-m and 0.1m, respectively, it is hypothesized that the best values are chosen based on the contrast with background and not absolute values. The background resistivity of the T Tank Farm is slightly lower than the 100 ohm-m used in the analytic model. Therefore, a slightly lower resistivity for the well would work best as demonstrated by the degree of noise in

larger resistivity values. When choosing the resistivity of wells for future models, the background resistivity must be considered.

Figure 6-8. WTW Inversion Results for Reprocessed Data Using Well Resistivity of 0.006 OHM-M and Well Diameter of 0.1M.

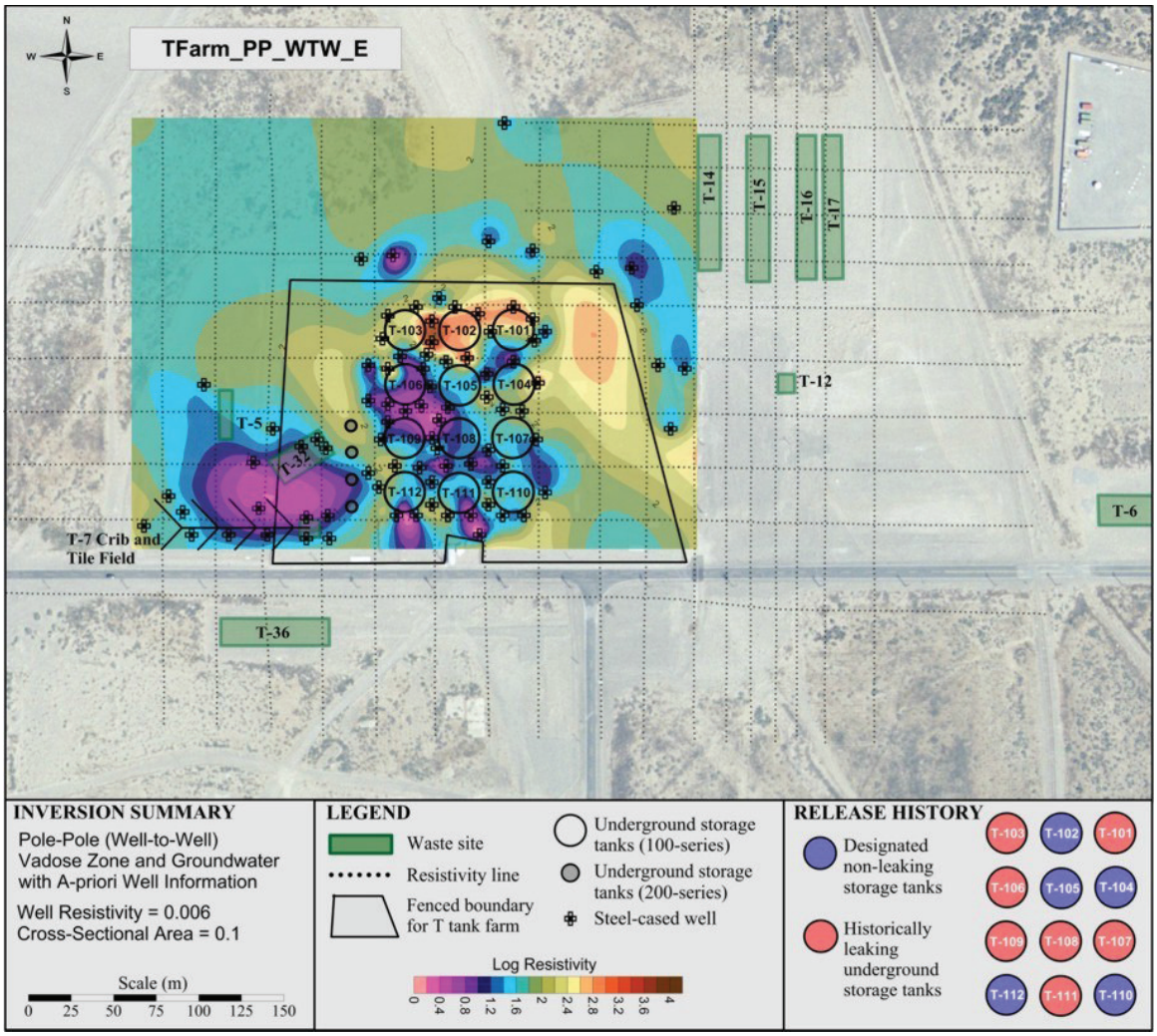

6.2.1.2 WTW Inversion Model Based on Pole-Pole Array Using Only Groundwater Wells. A WTW inversion model was run using data from select groundwater wells located on the periphery of the T tank farm. Fifteen wells were used in the inversion, mostly concentrated in the northeast and southwest portion of the site. The density of the wells is much lower, with a value of 5530m^2/well versus the 188m^2/well for the vadose zone wells inside the fence of the tank farm. To accommodate the lower resolution of the groundwater well simulation, cell sizes were increased to 100m^2. For comparison, the models TFarm_PP_WTW_A-E used a cell size of 16m^2. As shown in Figure 6-3, the groundwater well inversion finished in six iterations with an RMS around 5 percent.

Figure 6-9 shows the results of the inversion based only on groundwater wells. Values for the wells include a resistivity of 0.006 ohm-m and a diameter of 0.1m. The most striking feature in the figure is the large low resistivity anomaly below the T-36 trench. It is suspected that this trench did not receive much waste and it is odd to see the target this far south. The majority of the waste was disposed in the T-7 crib and tile field. Unfortunately, no groundwater wells exist in the immediate vicinity of T-7, so it is possible that there could be lower resistivity values north of T-7.

Figure 6-9. WTW Inversion Results for Reprocessed Data Using Groundwater Wells Only With Well Resistivity of 0.006 OHM-M And Well Diameter of 0.1M.

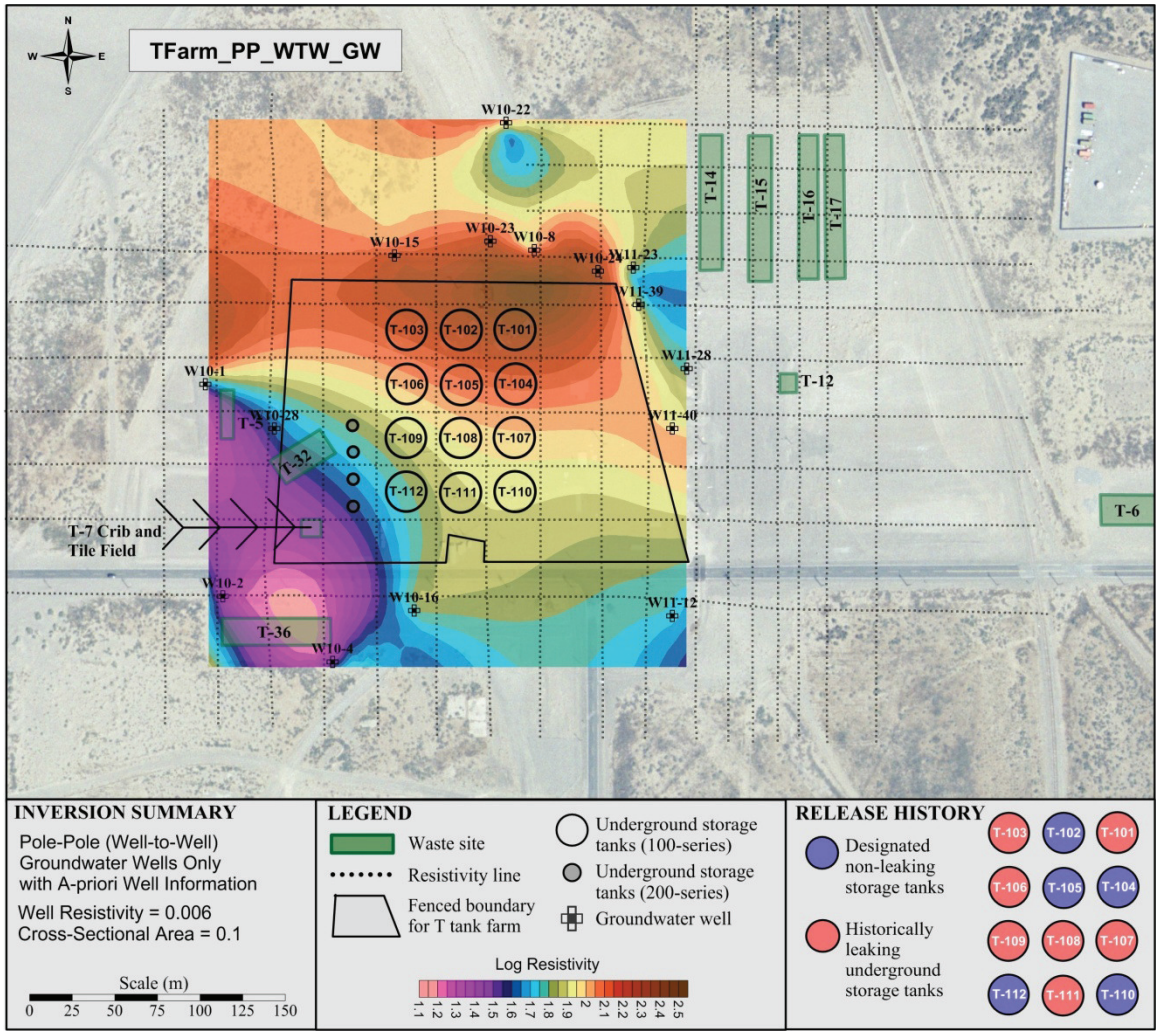

Fortunately, historical groundwater monitoring data are available for select wells around the site. Figure 6-10 shows the nitrate concentration data in milligrams per liter (mg/L) for several wells as a function of time. The figure is divided between the southwest set of wells and the northeast set, and the two plots have different scales in both concentration and time line. Just as the resistivity data of Figure 6-9 shows a large feature to the southwest, the nitrate in groundwater is significantly higher in the southwest. In particular, W10-4 and W10-28 are shown to be increasing significantly in the time before the survey, with W10-1 being relatively flat during this late time period. This well is at the northern edge of the anomaly. Historically, W10-2 is shown to be quite high and its location is near the very low resistivity feature beneath T-36.

Figure 6-10. Nitrate in Groundwater for Select Wells Around the T Tank Farm.

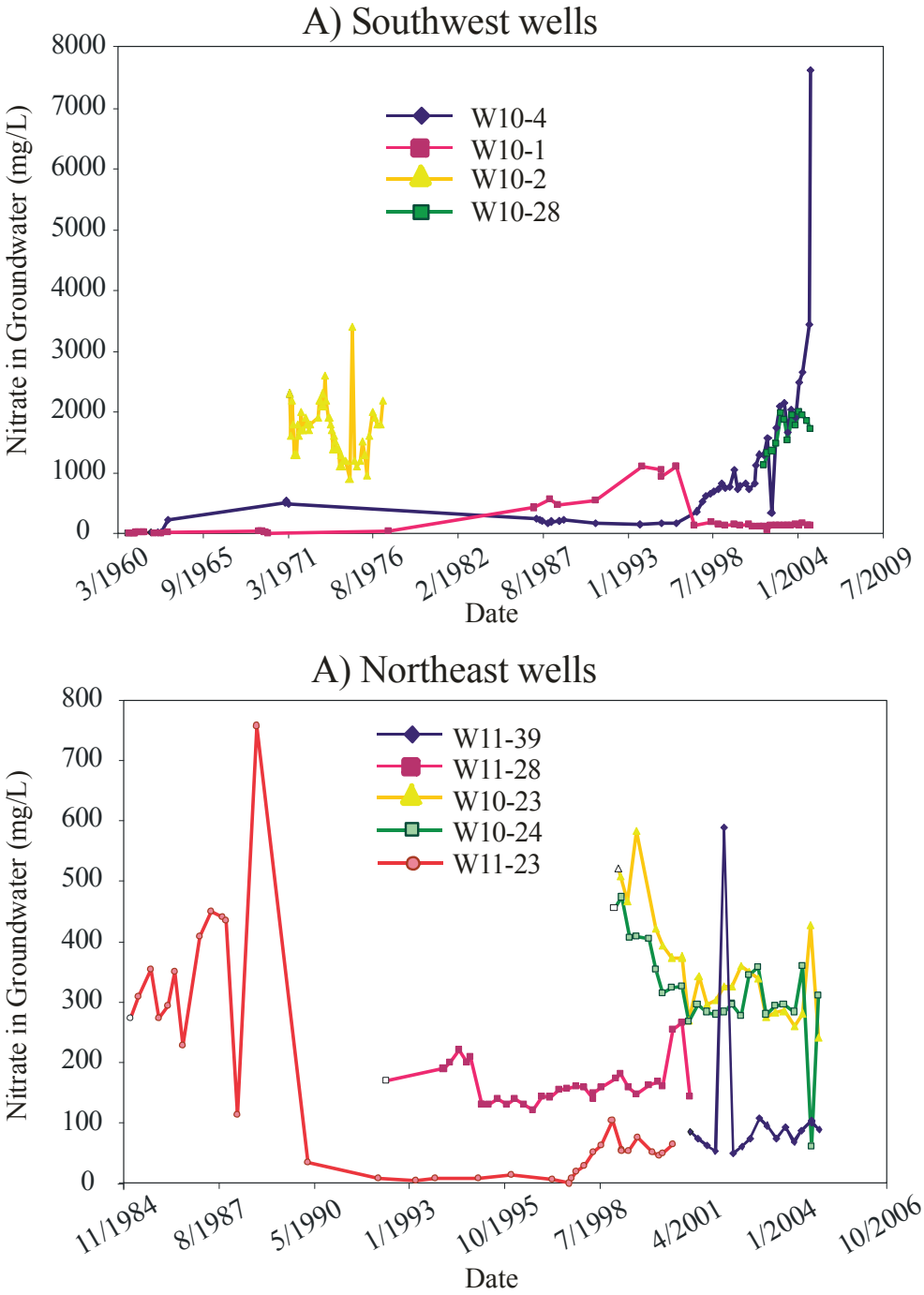

The nitrate concentration in the northeastern wells is shown to be much lower than the southwestern wells. The data are also relatively stable, varying over 200-300 mg/L and dropping. The resistivity data do show some isolated low resistivity values in the northeast, but these are more likely noise and not a geochemical target.

Another aspect to consider is the source locations for the low resistivity targets around the site. Figure 6-11 shows the ratio of nitrate to technetium in groundwater for three wells. The ratio was used because both analytes are transported through Hanford soils similarly. The plot shows that there are potentially three different sources and perhaps more. For the W10-4, the ratio is steadily increasing over time perhaps from the mixing of a new plume that is coming in contact with an older plume. The newer plume would have a lower technetium concentration relative to the nitrate compared to the older plume. The ratio for the W10-28 appears steady but slight decreasing. The ratio for W11-39, however, is several orders of magnitude lower than the wells in the southwest due to the high technetium concentrations. It appears unlikely that contamination at this location is a result of the sources to the west. Although this northeastern well clearly shows technetium contamination, the volume of the leak causing the contamination and the low nitrate concentration makes a poor target for resistivity.

Figure 6-11. Ratio of Nitrate to Technetium in Groundwater for Select Wells.

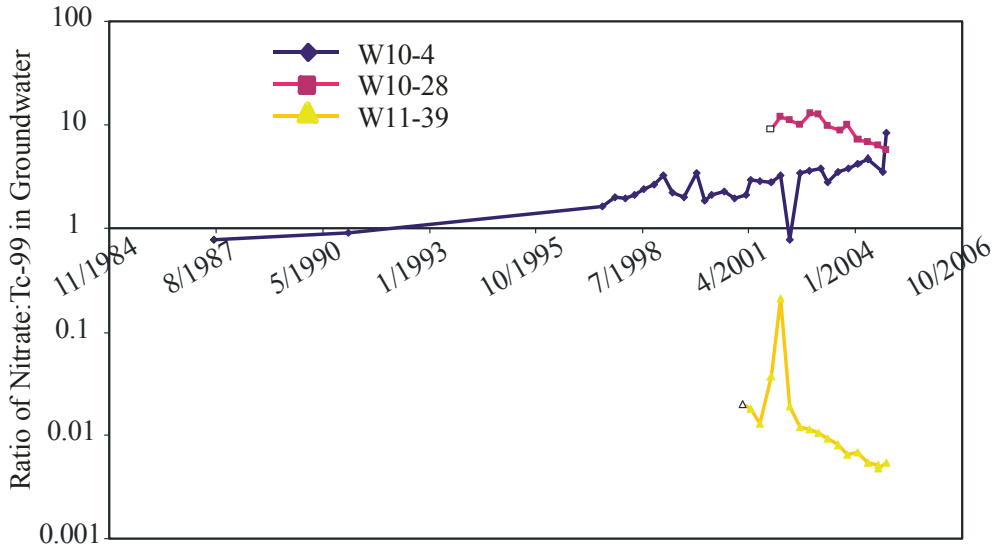

6.2.1.3 WTW Inversion Model Based on Dipole-Dipole Array Using Vadose Zone and Groundwater Wells. A WTW inversion was conducted for the dipole-dipole data and Figure 6-12 shows the resistivity distribution. In general, the dipole-dipole data are prone to higher noise simply due to lower signal strength. This higher noise in the data translates to higher noise in the inversion and the inversion results of Figure 6-12 reflect this. Within the model domain there are several low resistivity targets, with the main target in the southwestern corner. The southwestern target has been identified in several WTW inversions already, so its existence is not a surprise. Additionally, the T-106 and T-101 leaks appear as relatively large features.

Figure 6-12. WTW Inversion Results for Dipole-Dipole Array Reprocessed Data Using Well Resistivity of 0.006 OHM-M and Diameter of 0.1M.

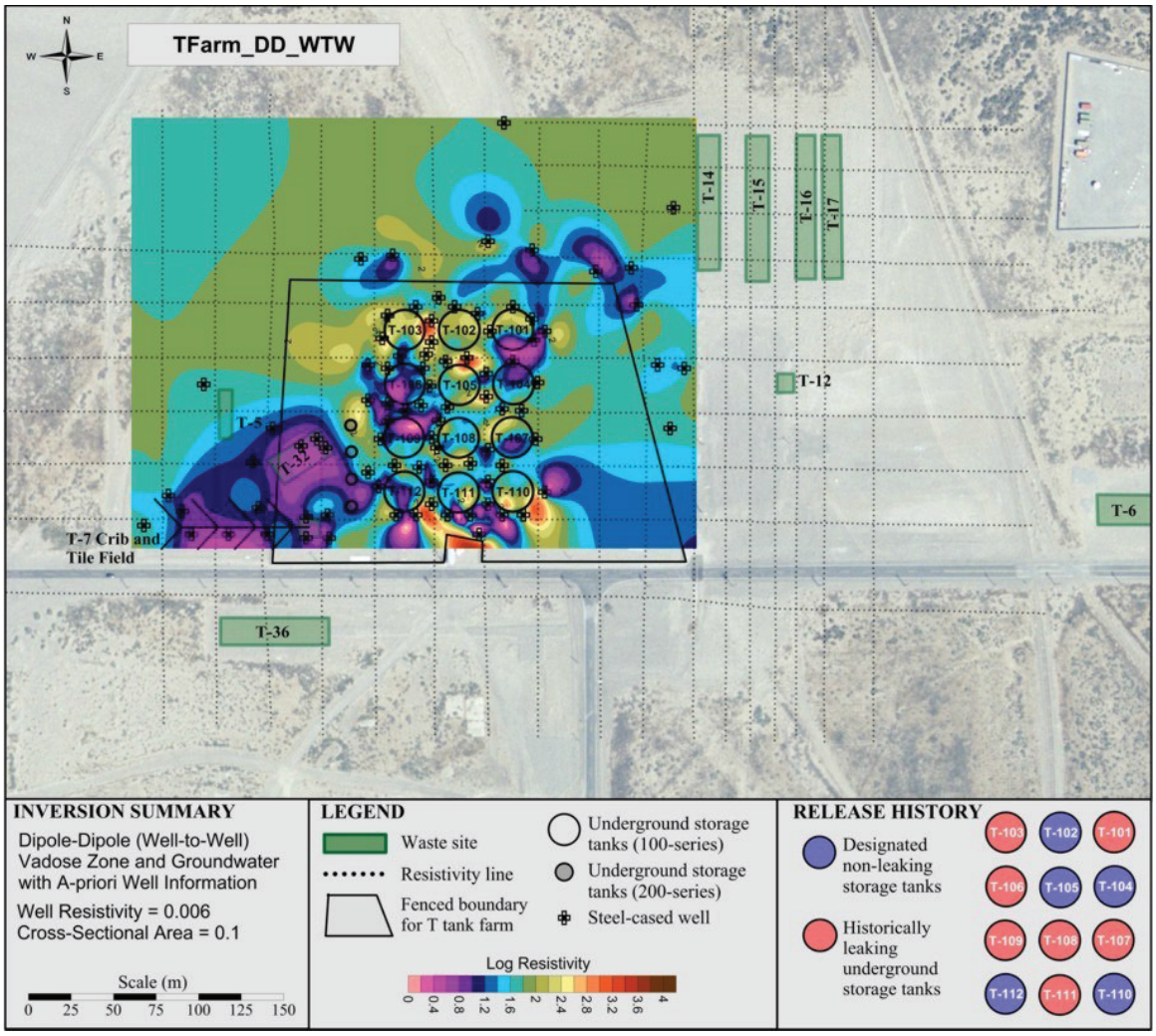

From these results, the dipole-dipole acquisition of WTW data is less than ideal compared to pole-pole. The dipole-dipole method can recognize the major sources of contamination, but it also creates what are likely a significant number of false-positives. Therefore, dipole-dipole acquisition is not recommended at Hanford unless insurmountable logistical challenges prevent

acquisition with the pole-pole array. The challenges may include the inability to find a suitable remote electrode location or difficulty in maintaining electrical contact with the remote.

6.2.1.4 WTW Inversion Model Based on Mixed Pole-Pole and Dipole-Dipole Arrays Using Vadose Zone and Groundwater Wells. The final WTW inversion includes both pole-pole and dipole-dipole data. Although it is clear that the dipole-dipole data are noisy, it was hoped that the inclusion of the pole-pole data would mitigate the noise problem while providing more data into the model. Figure 6-13 shows the results of the mixed data set. The distribution of resistivity appears more noisy than dipole-dipole data alone. Again, major targets are identified in the mixed inversion. However, what were minor targets in Figure 6-12 have become major targets for this inversion.

Figure 6-13. WTW Inversion Results for Mixed Pole-Pole and Dipole-Dipole Array Reprocessed Data Using Well Resistivity of 0.006 OHM-M and Well Diameter of 0.1M.

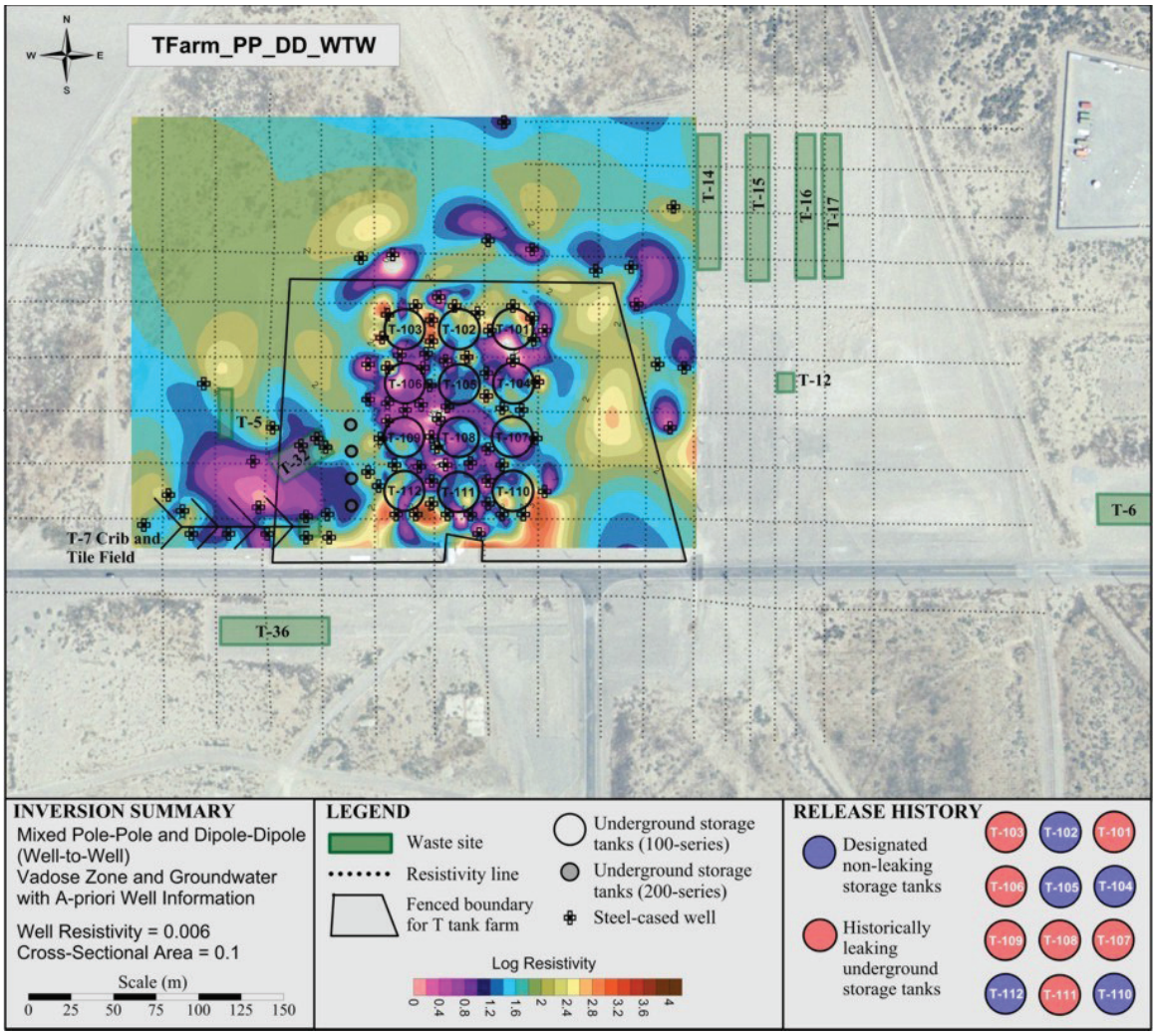

6.2.2 Task 2 – STS Inversion Model Results

Past attempts at modeling the T Farm STS data necessitated the domain to be split into multiple subdomains using EI3D. Remodeling of the STS data was conducted with RES3D64, with the expressed goal of the using all data from the entire T Farm domain in a single inversion. While the entire domain was modeled, test models were also run in areas of minimal infrastructure. In total, three inversion models were generated, and included the western region, northeast region, and the entire domain. Figure 6-14 shows the outline of the domain boundaries for the three models.

Figure 6-14. Domain Boundaries for the STS Inversion Models.

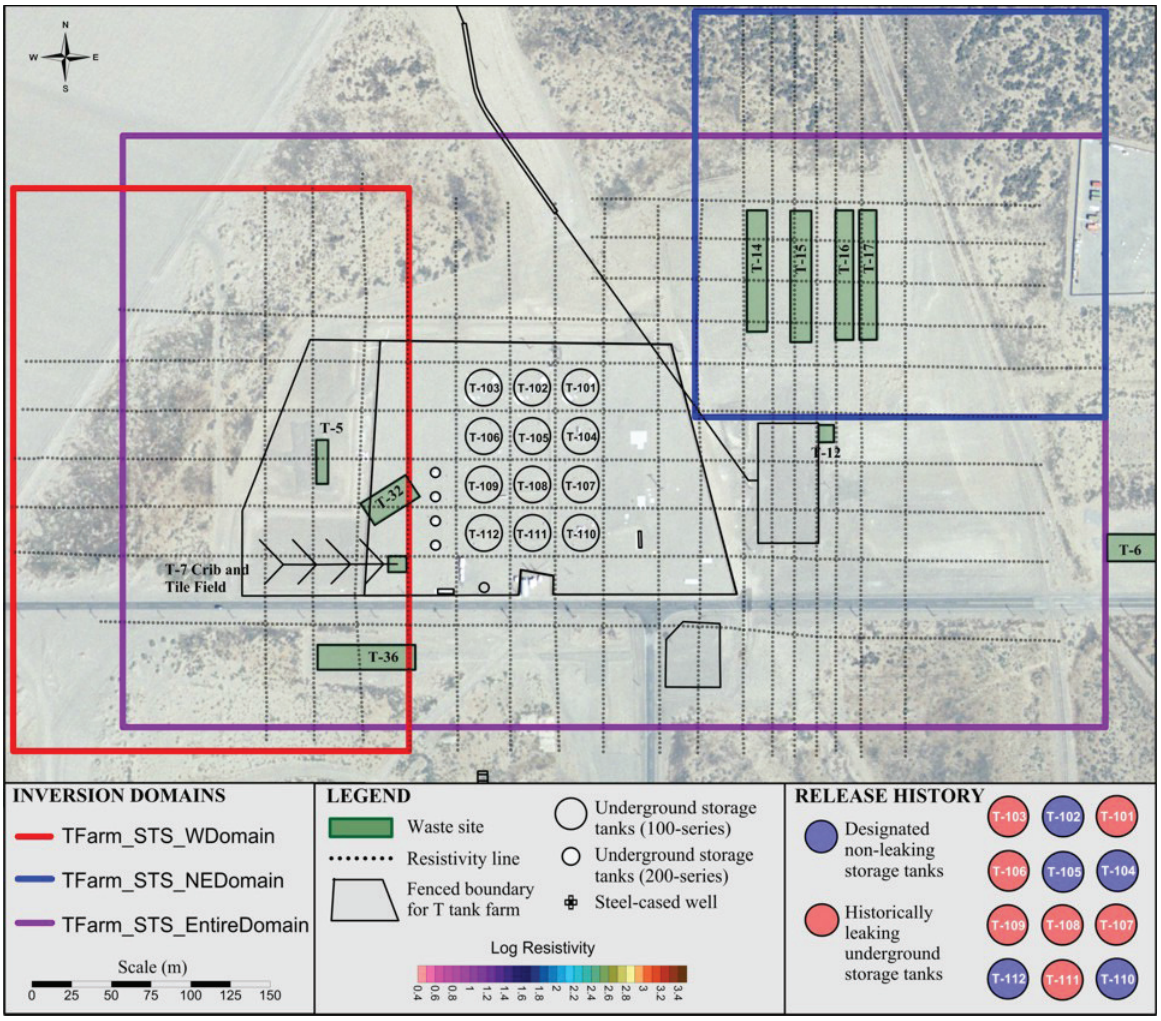

The success of the inversions, from the standpoint of minimizing the error between modeled and measured data as reflected by the RMS error statistic, were satisfactory for the northeastern domain, marginal for the western domain, and poor for the entire domain. The convergence curves for all three models, shown in Figure 6-15, indicate a decrease in RMS with each successive iteration. The starting resistivity distribution model for the inversion is set to the average apparent resistivity and the initial error for each domain reflects how well that average

value represents much of the subsurface. The northeastern region started with the lowest RMS error at around 27 percent. There appears to be a correlation with starting RMS and final RMS error. The specific results and resistivity distribution for each domain are discussed below.

Figure 6-15. Convergence Curves for the STS Models.

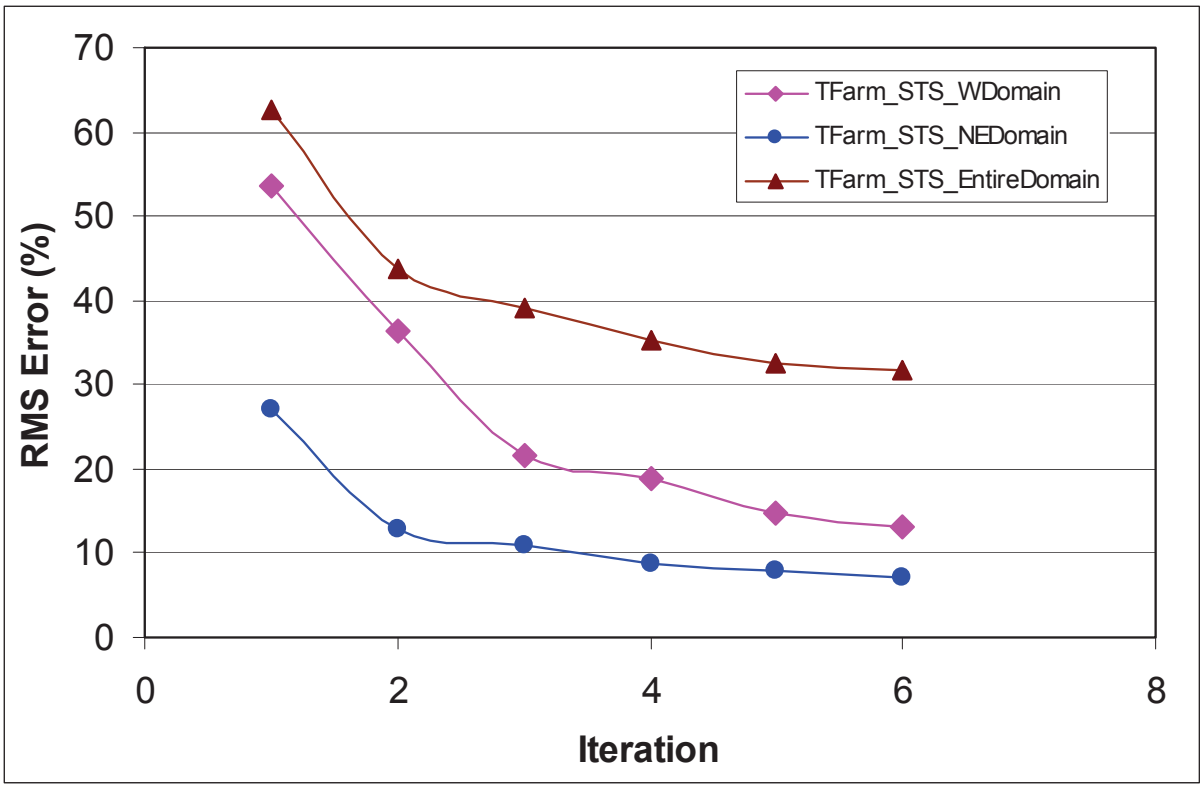

6.2.2.1 STS Inversion Model for the Western Region. The inversion input file of the model for the western region consists of all data west (and including) line 3E. A total 22,971 data values were used for the inversion. The results of the modeling are shown as a series of horizontal slices at different depths in Figures 6-16 through 6-20. The top two slices are fairly shallow and show smaller low resistivity targets near the waste disposal facilities. There appears to be some banding of high and low resistivity in the uppermost slice as a result of lines spaced fairly far apart. Gharibi and Bentley also noticed this problem and recommended that parallel lines be no further apart than 3-4 times the minimum intra-line electrode spacing. (Refer to *Journal of Environmental and Engineering Geophysics,* "Resolution of 3-D Electrical Resistivity Images from Inversions of 2-D Orthogonal Lines.") Given the 3m electrode spacing at T Farm, parallel lines should be spaced no further than 12m apart. Recognizing that line spacing is mostly dictated by economics and many scientists will stretch out the survey lines to acquire less data over larger areas, Farquharson suggested to improve inversion model results and reduce the banding by modifying the roughness filter so that it has components in the diagonal directions as well in the x-y plane. (Refer to *Geophysics*, 2008, "Constructing piecewise-constant models in multidimensional minimum-structure inversions.") The degree of banding decreases by 16m depth and is altogether a nonissue by 38m.

Figure 6-16. Horizontal Slice Showing Resistivity Distribution at 5M for the Western Region STS Inversion Model.

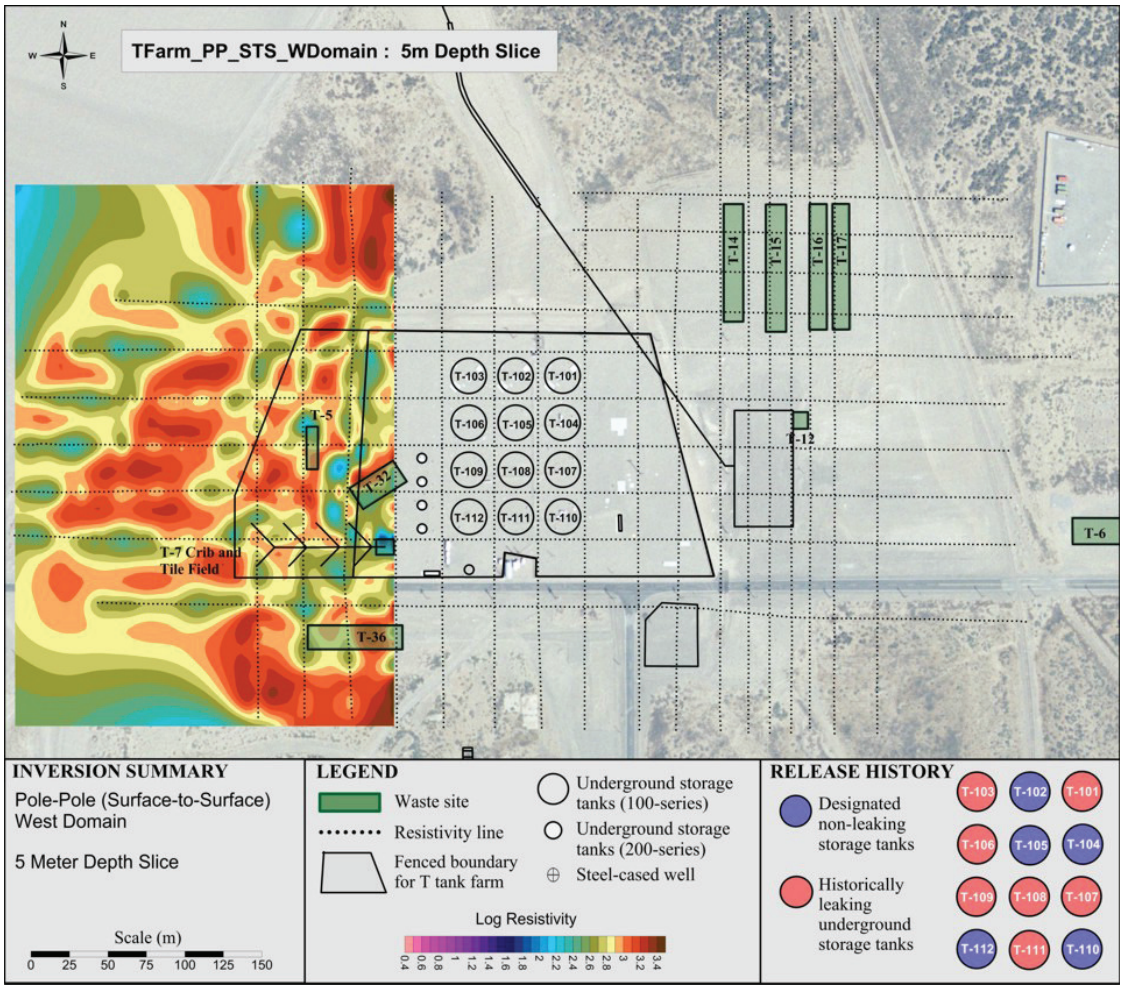

Figure 6-17. Horizontal Slice Showing Resistivity Distribution at 16M For The Western Region STS Inversion Model.

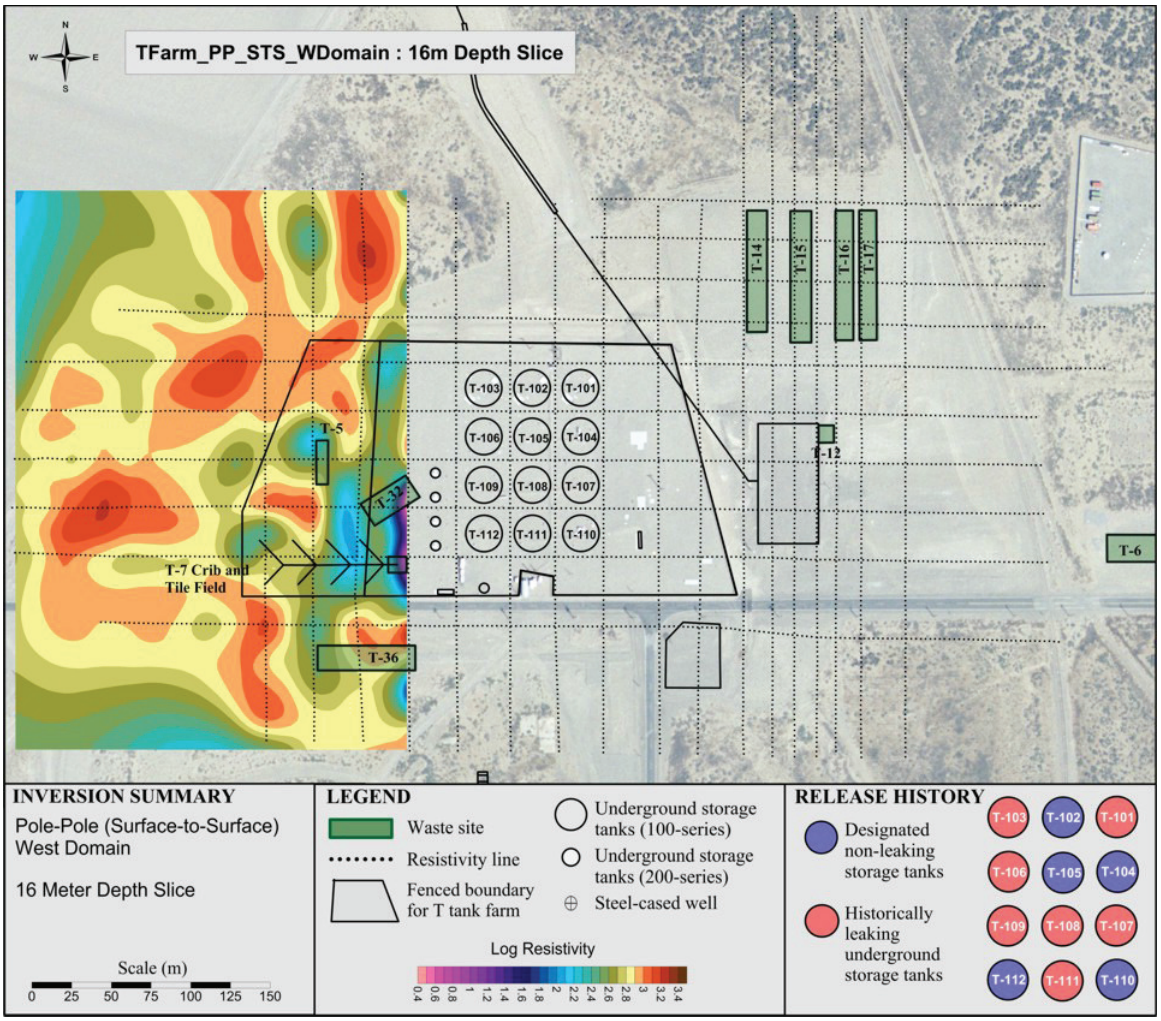

The depth slices for the 38m, 56m, and 78m show a significant low resistivity feature coincident with the waste disposal sites. The area below the T-7 and T-32 cribs appears to have the lowest resistivity. The low resistivity also extends partially to T-5. All of the WTW inversion results showed a low resistivity anomaly at this location. However, due to the well's extended coverage to the east, the vadose plume is shown to potentially encompass the soil beneath the 200-series tanks. Trials were conducted with the western region to include an extra line 4E, however, the results were considerably less than desirable due to the infrastructural interference.

Figure 6-18. Horizontal Slice Showing Resistivity Distribution at 38M for the Western Region STS Inversion Model.

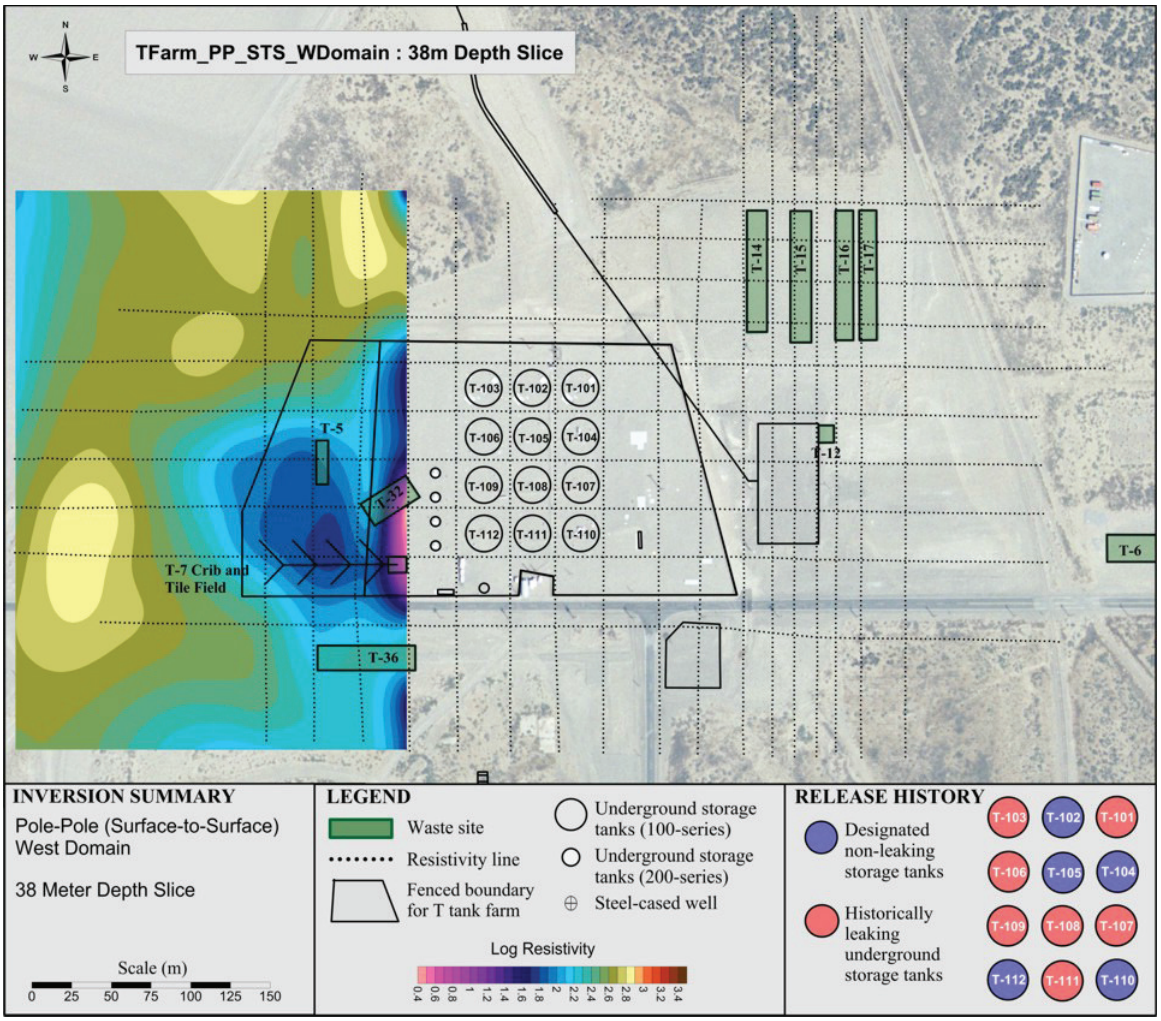

Figure 6-19. Horizontal Slice Showing Resistivity Distribution at 56M for the Western Region STS Inversion Model.

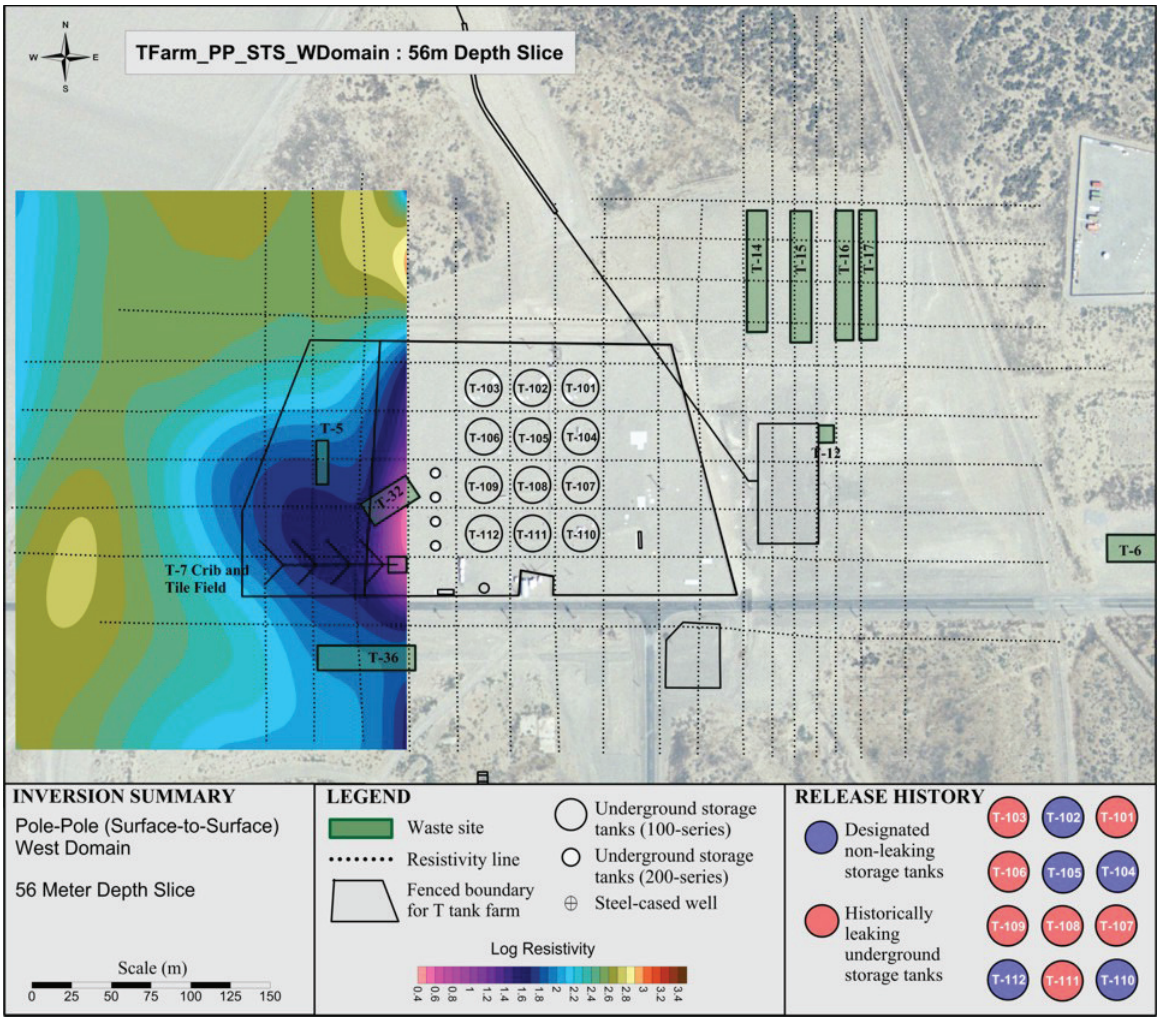

The last slice at 78m should represent the resistivity distribution at the water table. The epicenter for the resistivity mass for this slice is between the T-7 and T-32 cribs. For the WTW inversion with groundwater wells only, however, the epicenter is beneath T-36. The WTW groundwater plume is south of the STS groundwater plume, which could be due to spatial well coverage or loss of sensitivity by the STS from having a nearer surface low resistivity plume. That is, if a low resistivity feature exists at a shallower depth, the information below is essentially masked and secondary plumes may be hidden in the shallow plume's "shadow".

Figure 6-20. Horizontal Slice Showing Resistivity Distribution at 78M for the Western Region STS Inversion Model.

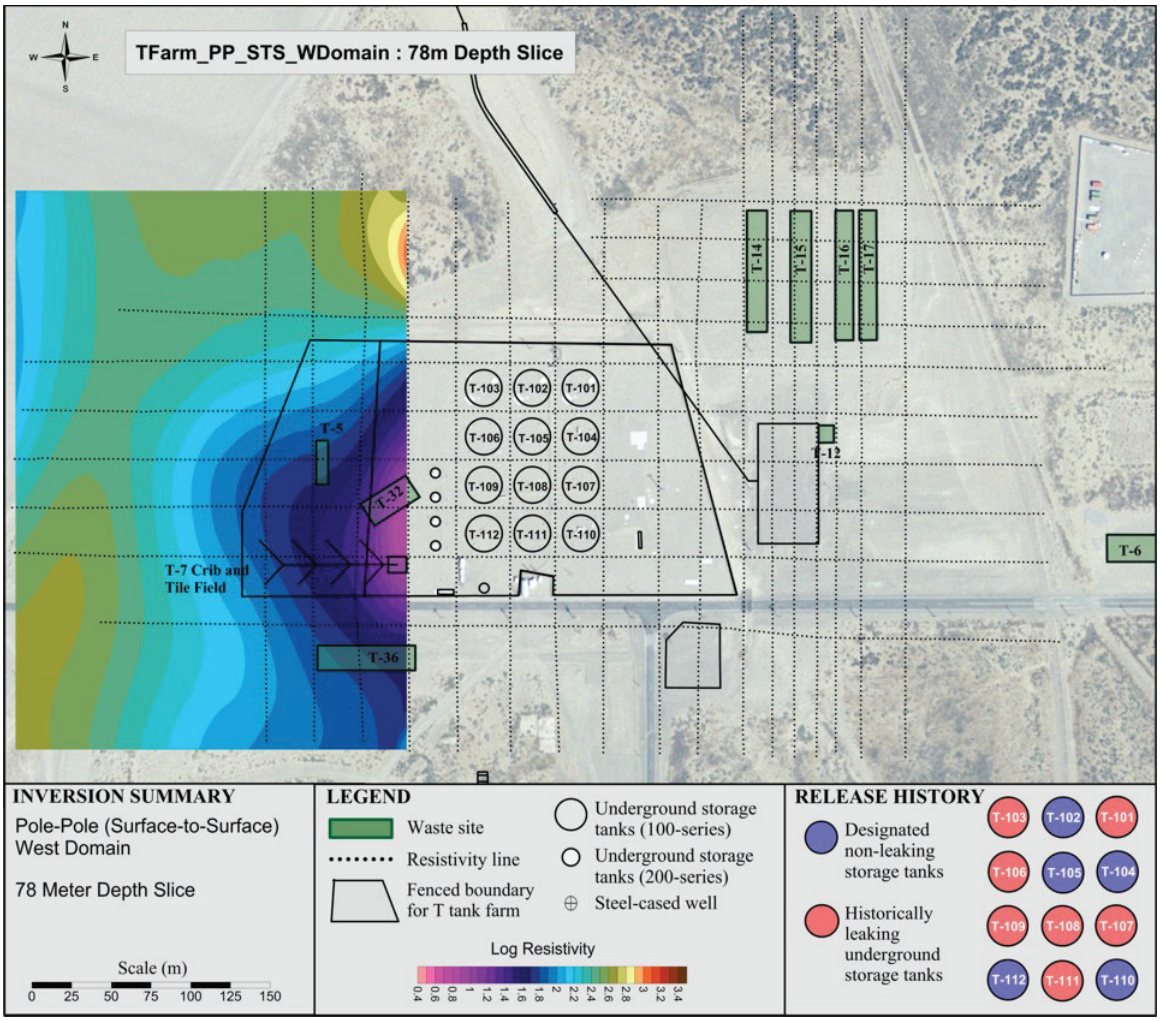

6.2.2.2 STS Inversion Model of the Northeastern Region. Results for the inversion of the STS for the northeastern region are shown as horizontal slices in Figure 6-21 through 6-26. The model was conducted in hopes to better define the waste plume that likely exists beneath trenches T-14 through T-17. About one million gallons of liquid waste were disposed in these trenches. This sizeable volume should be a good target for SGE, especially since infrastructure is minimal.

Figure 6-21. Horizontal Slice Showing resistivity Distribution at 5M for the Northeast Region STS Inversion Model.

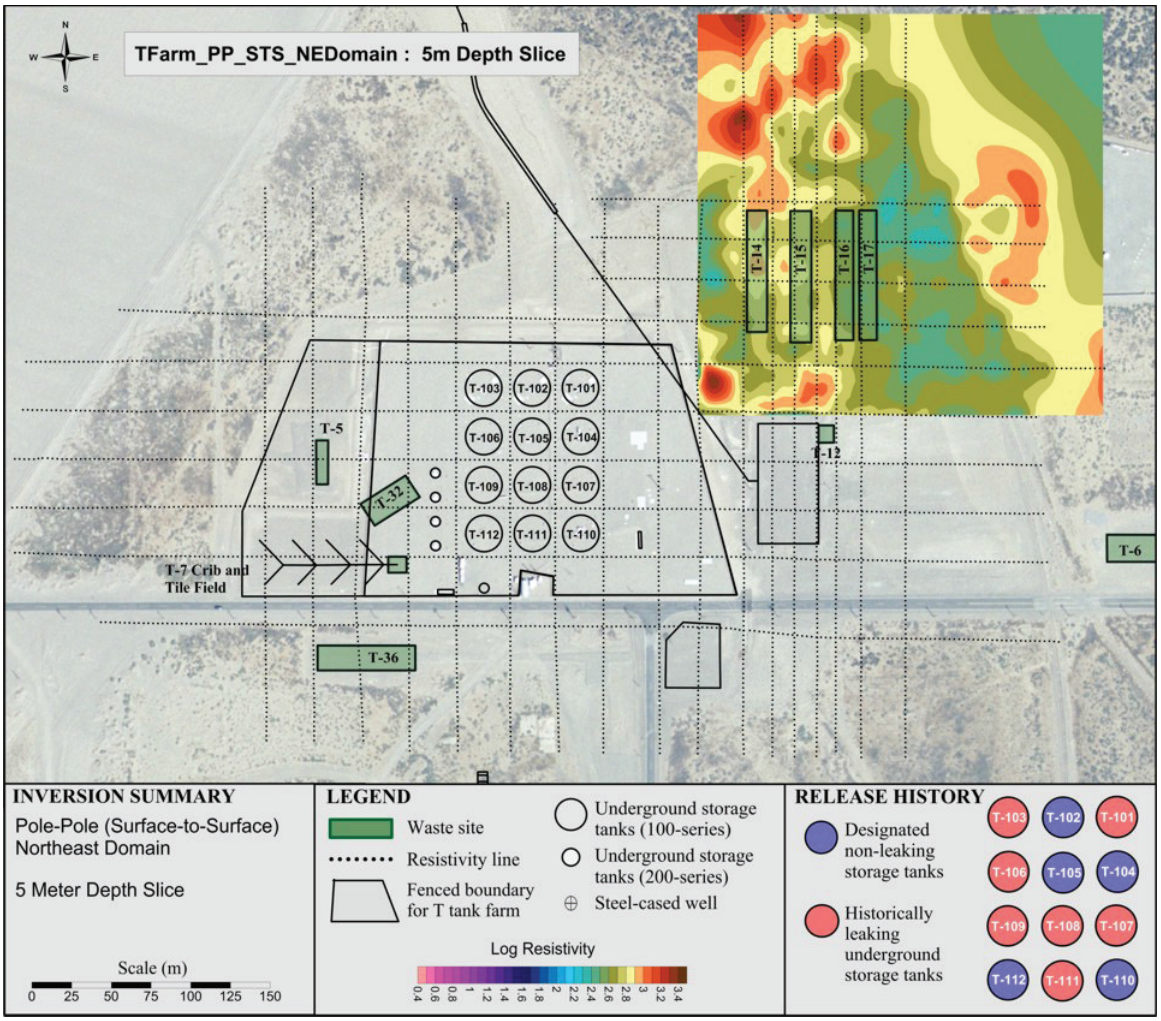

The northeastern STS model used data east of (and including) line 9E and north of line 5N. The far northeast corner of the model had no line coverage and results in this area should be viewed with great skepticism. The final input data count for the model was 17,638.

The top layer at 5m (Figure 6-21) shows a fairly noisy pattern in the resistivity distribution, typical of most upper layers for inversion models. The banding effect is not as prevalent as the western region model, but does exist to some degree. By 16m depth, shown in Figure 6-22, the banding has minimized and a target is starting to take shape beneath trenches T-16 and T-17.

Figure 6-22. Horizontal Slice Showing Resistivity Distribution at 16M for the Northeast Region STS Inversion Model.

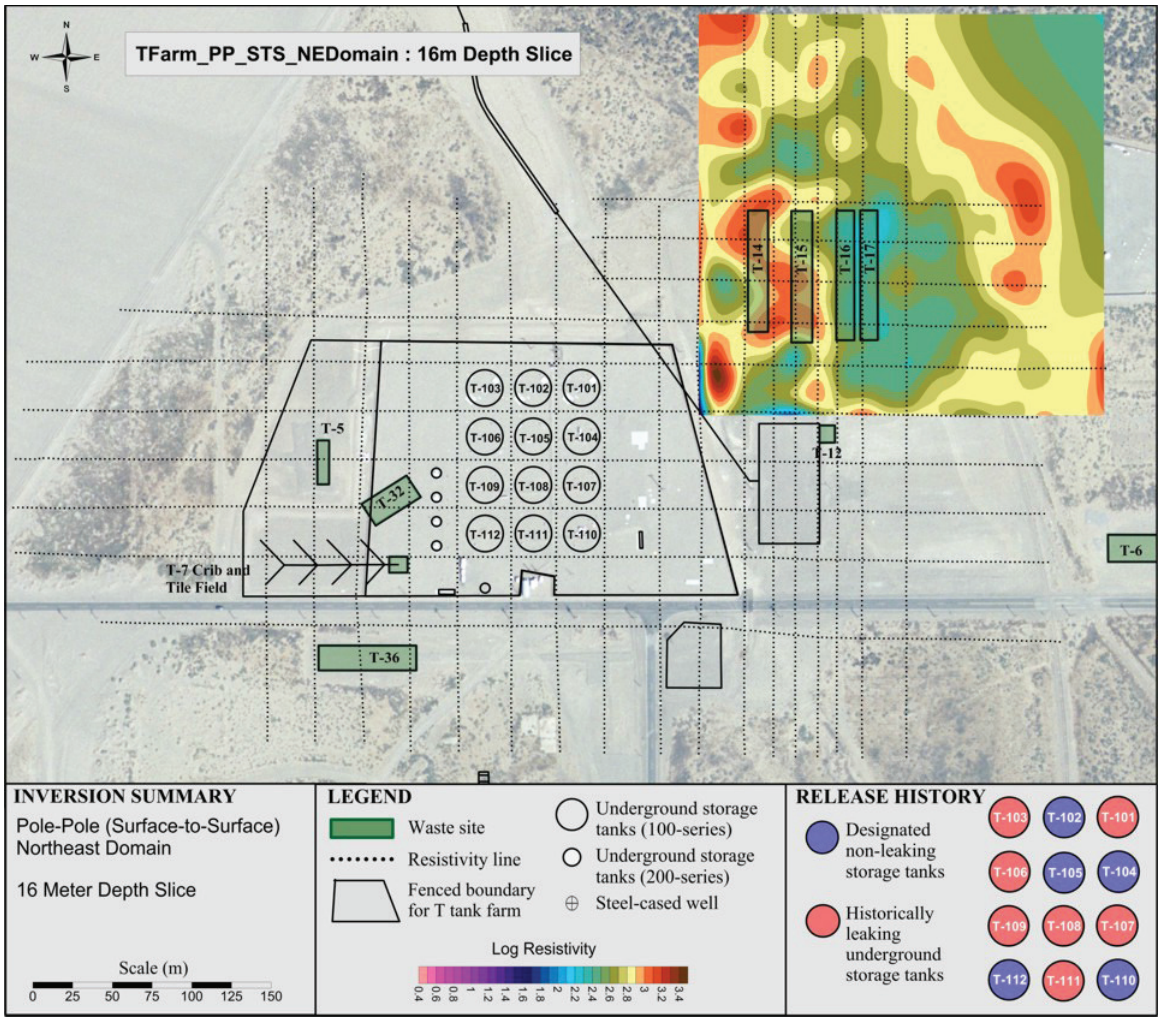

The depth slices at 26m and 38m in Figures 6-23 and 6-24, respectively, show the low resistivity target take shape more formally beneath trenches T-16 and T-17. For comparison, the direct characterization data presented in Figure 2-8 shows well W11-45 immediately south of trenches T-15 and T-17 with high nitrate between 20 and 40m depth. The highest value is at 22m and calculations show a concentration of 65,000 mg/L. The resistivity shows the highest value around 38m. Mismatches in depth estimation by the resistivity method is not uncommon, and methodologies have been developed to obtain better depth estimates by either acquiring data in true three dimensions or by placing depth electrodes in the domain.

Figure 6-23. Horizontal Slice Showing Resistivity Distribution at 26M for the Northeast Region STS Inversion Model.

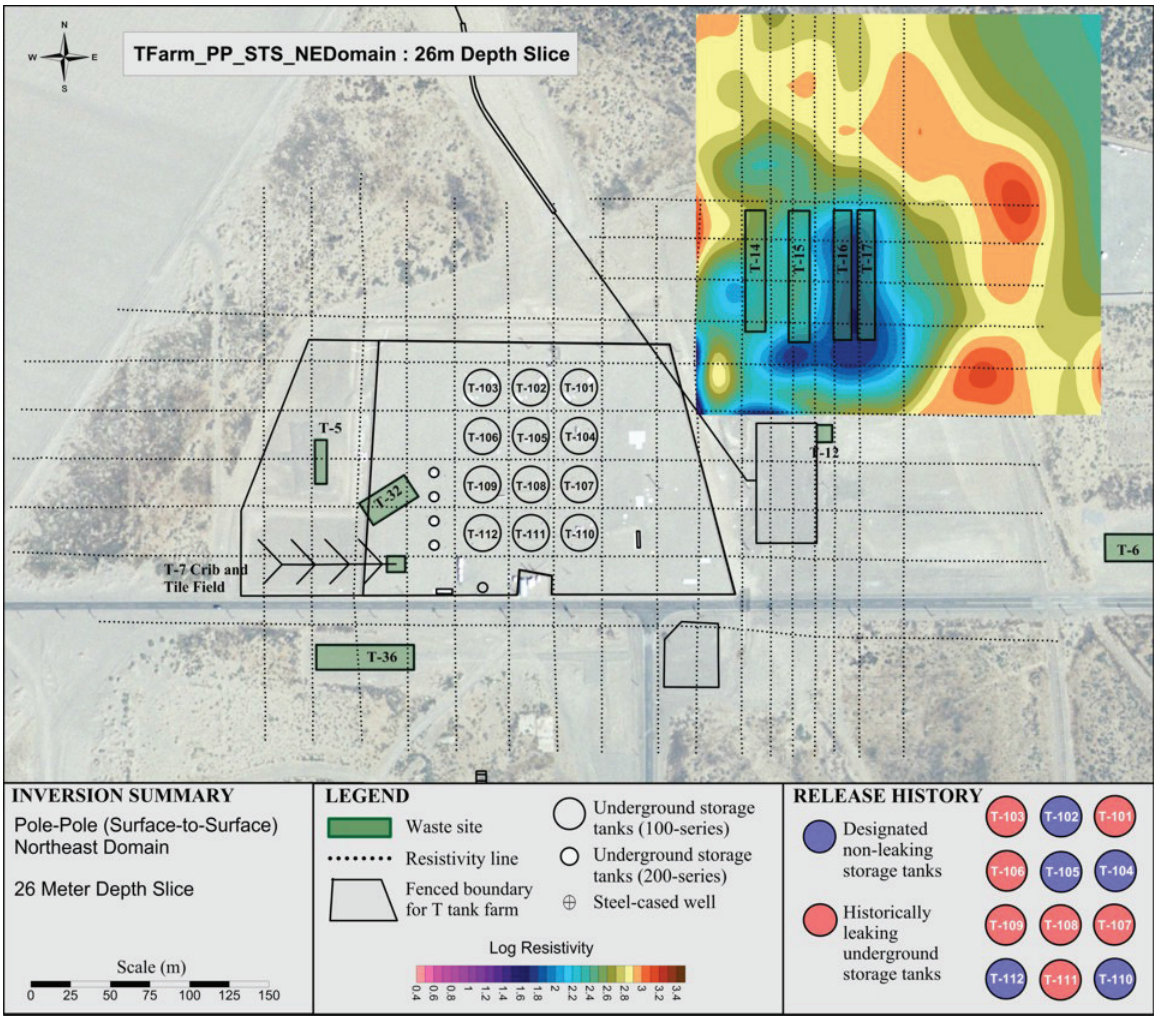

Figure 6-24. Horizontal Slice Showing Resistivity Distribution at 38M for the Northeast Region STS Inversion Model.

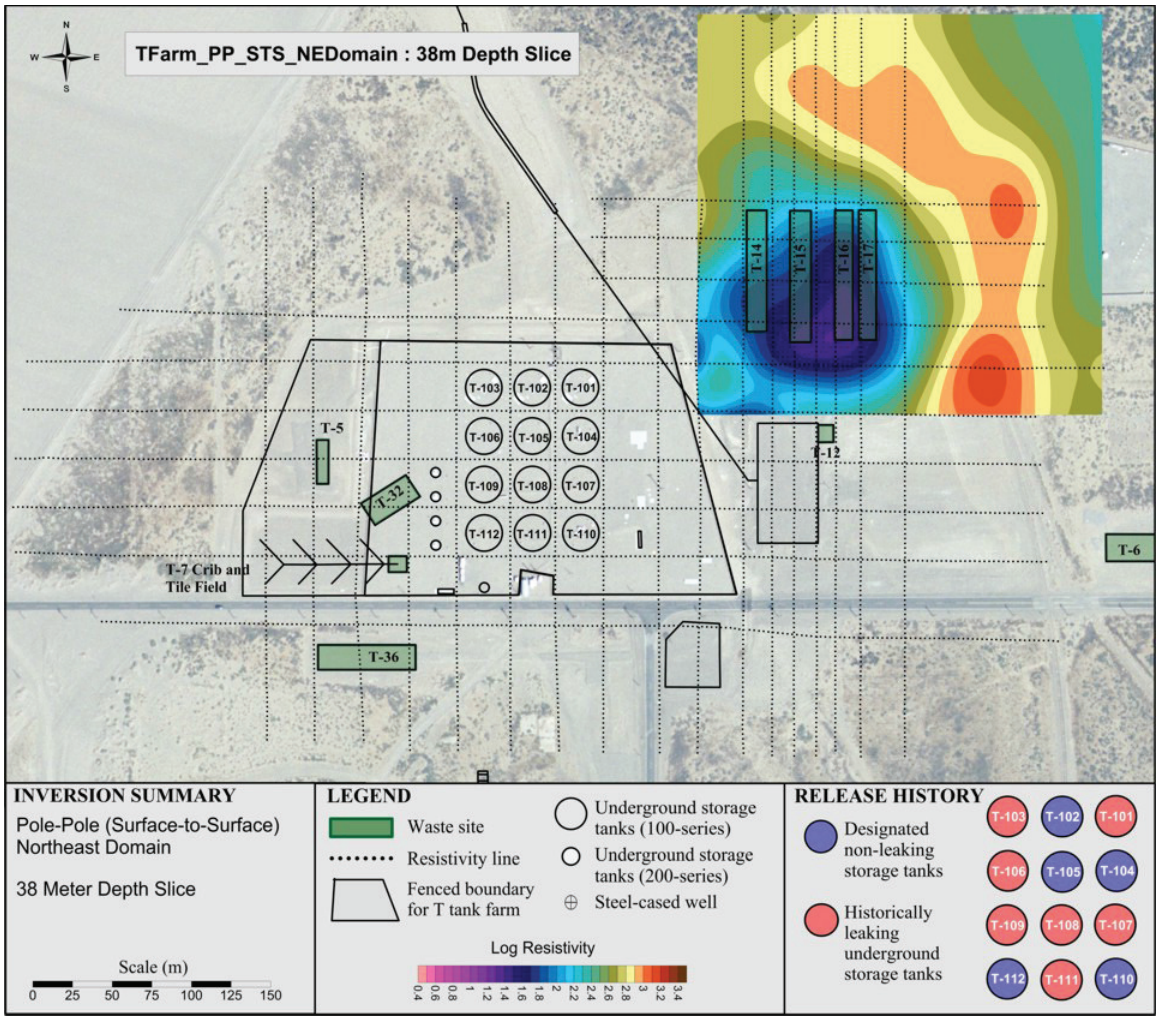

The resistivity slice at 56m is presented in Figure 6-25 and shows the resistivity values that represent the target increase compared to the upper layers. Experience at other waste sites at Hanford have shown that the resistivity value is slow to return to what is normally considered a background condition (i.e., very high resistivity) below a conductive target. This observation is likely true from the data in Figure 6-25, where low resistivity values persist. For this snapshot in 2005, the ionic porewater from legacy waste disposal activities is likely confined to depths above 56m. Looking even deeper in Figure 6-26 to 78m, which is below the water table, the low resistivity target appears to persist. By itself, the figure could be misleading and show that the solution reached the water table. This is likely not the case and the horizontal slices must be viewed in context with one another.

Figure 6-25. Horizontal Slice Showing Resistivity Distribution at 56M for the Northeast Region STS Inversion Model.

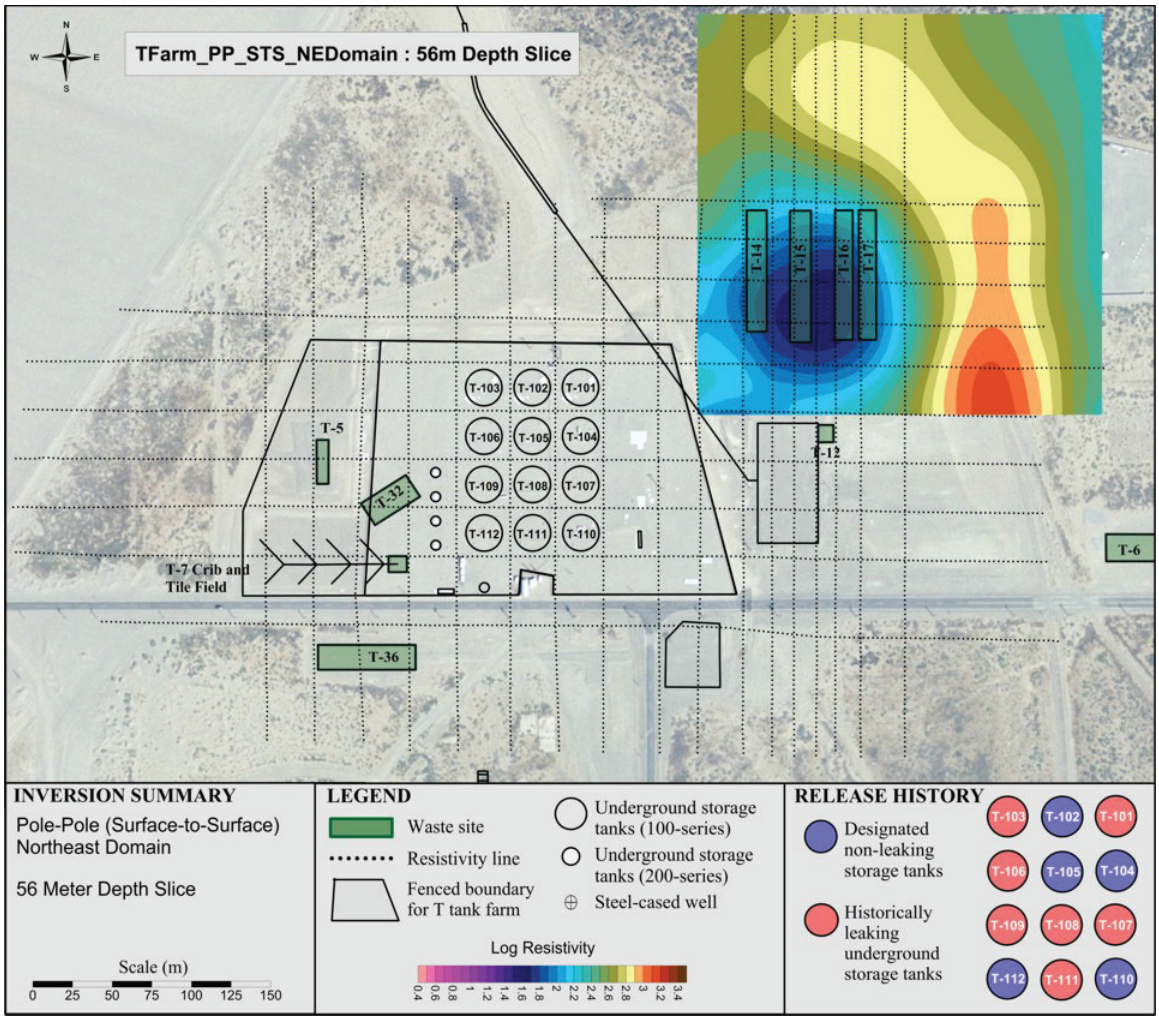

Figure 6-26. Horizontal Slice Showing Resistivity Distribution at 78M for the Northeast Region STS Inversion Model.

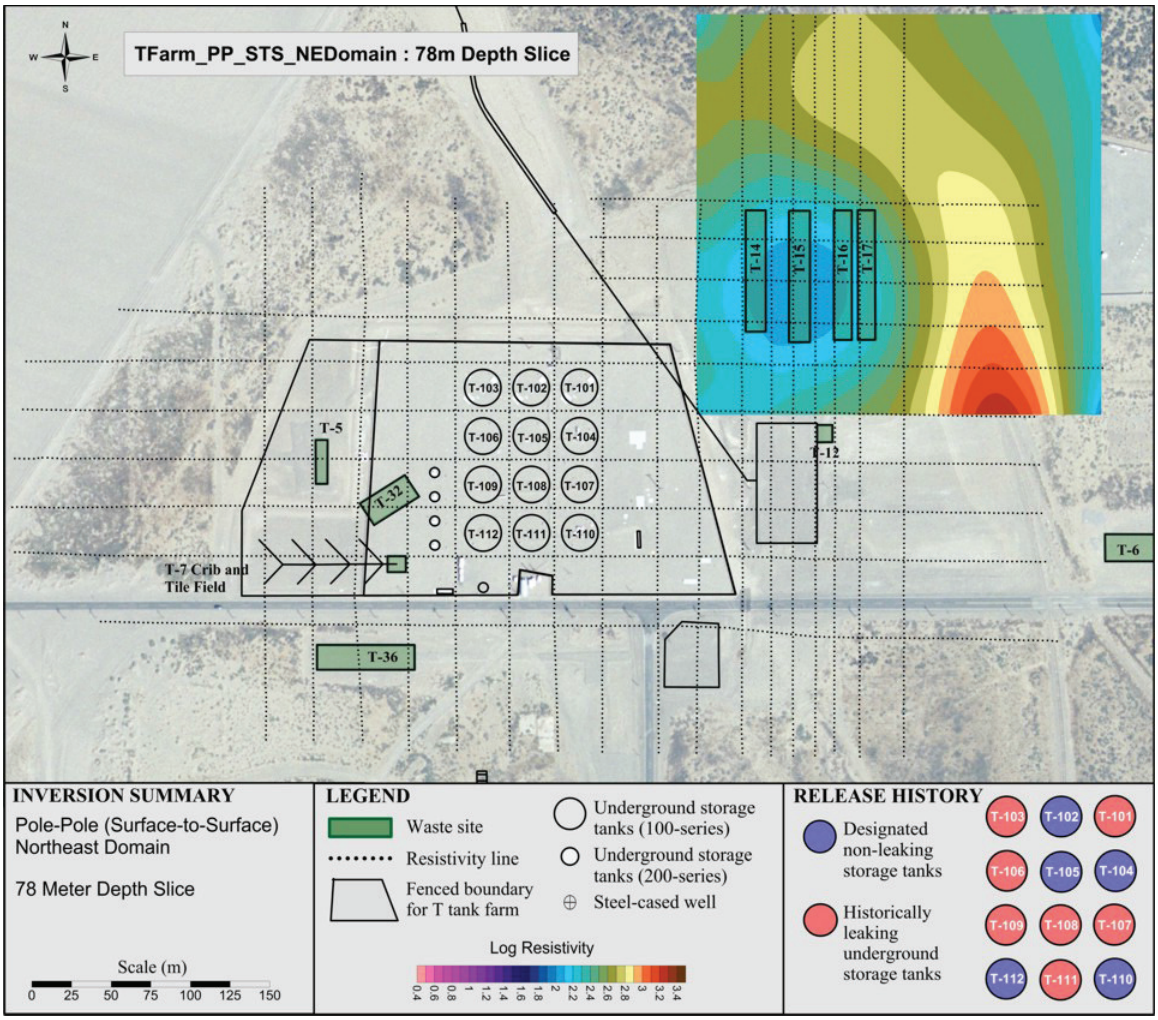

6.2.2.3 STS Inversion Model of the Entire T Farm. The main objective for the STS modeling was to use the entire dataset in one large inversion. The models for the previous efforts in 2005 were forced to be split into subdomains using EI3D because that was the state of the art at the time. Since then, both software and hardware have been developed to accommodate the larger models.

Modeling of the entire domain required combining all processed STS data from the individual lines into one large file. The methodology for processing the lines can be seen in Appendix A. The final data count for the entire domain inversion model was 88,508 which is much less than the filtered dataset. This is due to the fact that a logical rectilinear boundary was drawn around the site that eliminated ends of lines that had no cross line support.

A 3m cell size was chosen for the inverse modeling, based on the initial intra-line electrode spacing. For the boundary shown in Figure 6-14, this discretization created 184 cells in the x-direction and 125 in the y-direction. In total, considering the layering, there were 363,023

inverse model cells on which to calculate the true resistivity. The final model chosen for the report took approximately 32 hours to complete using RES3D64 on a computer that had 16 individual processers and 128GB of RAM.

Figures 6-27 through 6-32 show the depth slices for the inversion results. The slices were taken at select intervals throughout the domain to give a representative view of the results. The uppermost slice at 5m (Figure 6-27) generally shows lower resistivity inside the tank farm fence line and higher resistivity outside the farm fence line. Unfortunately, the resistivity distribution shows severe banding from cross-line data. Interline spacing was generally set to 30m and the large spacing has adverse effects on the model. For example, the northwest area, just outside the fence, shows high resistivity that should generally be contiguous from line to line. However, where the resistivity line crosses through the region, the resistivity is lowered and contours are pinched. The effect can also be seen just west of the fence, where pinching in both directions creates a pattern of high resistivity dots, or squares, surrounded by low resistivity at the electrodes. The effect is seen in the tank farm where tanks standout as conductive anomalies. The effect is significantly minimized in the east due to the interline spacing shrinking to 15m.

The low resistivity values inside and to the south-southwest of the farm are likely the result of near surface infrastructure and not tank waste. Low resistivity features appear to coincide with all tanks even though the WTW inversions only showed low resistivity targets around a select few tanks. For example, see Figure 6-5. The WTW inversion results confirmed the original hydrogeologic conceptual model that was developed based on the past disposal practices and known leaks. The STS model appears not to discriminate the tanks based on leaks. Results for the inversion of the STS for the northeastern region are shown as horizontal slices in Figure 6-21.

Figure 6-27. Horizontal Slice Showing Resistivity Distribution at 5M for the Entire T Farm.

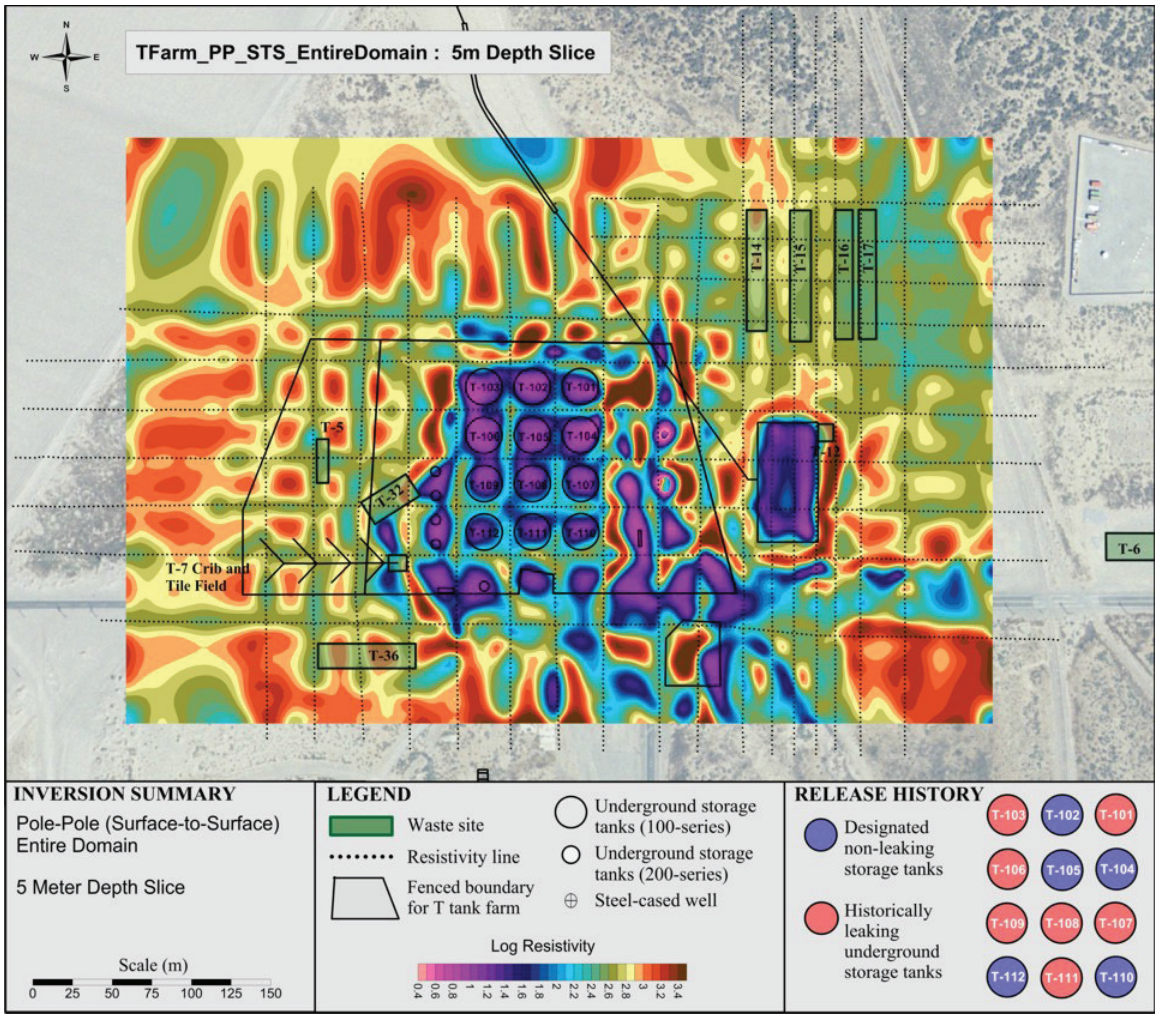

At the 16m depth, the banding issues persist. Figure 6-28 shows the depth slice, and the examples highlighted above are still noticeable with the exception of the tank farm. The low resistivity feature inside the farm has more or less blended into a larger target. Again, these low resistivity values are likely the result of infrastructure. The high resistivity values (seen as thin red bands) encircling the tank farm help to support this hypothesis. Hydrologic-based features tend to show a gradual transition from target to background as demonstrated in the northeastern model. Here, however, the abrupt change of low resistivity to high resistivity over a short distance is indicative of metal in the ground.

Figure 6-28. Horizontal Slice Showing Resistivity Distribution at 16M for the Entire T Farm.

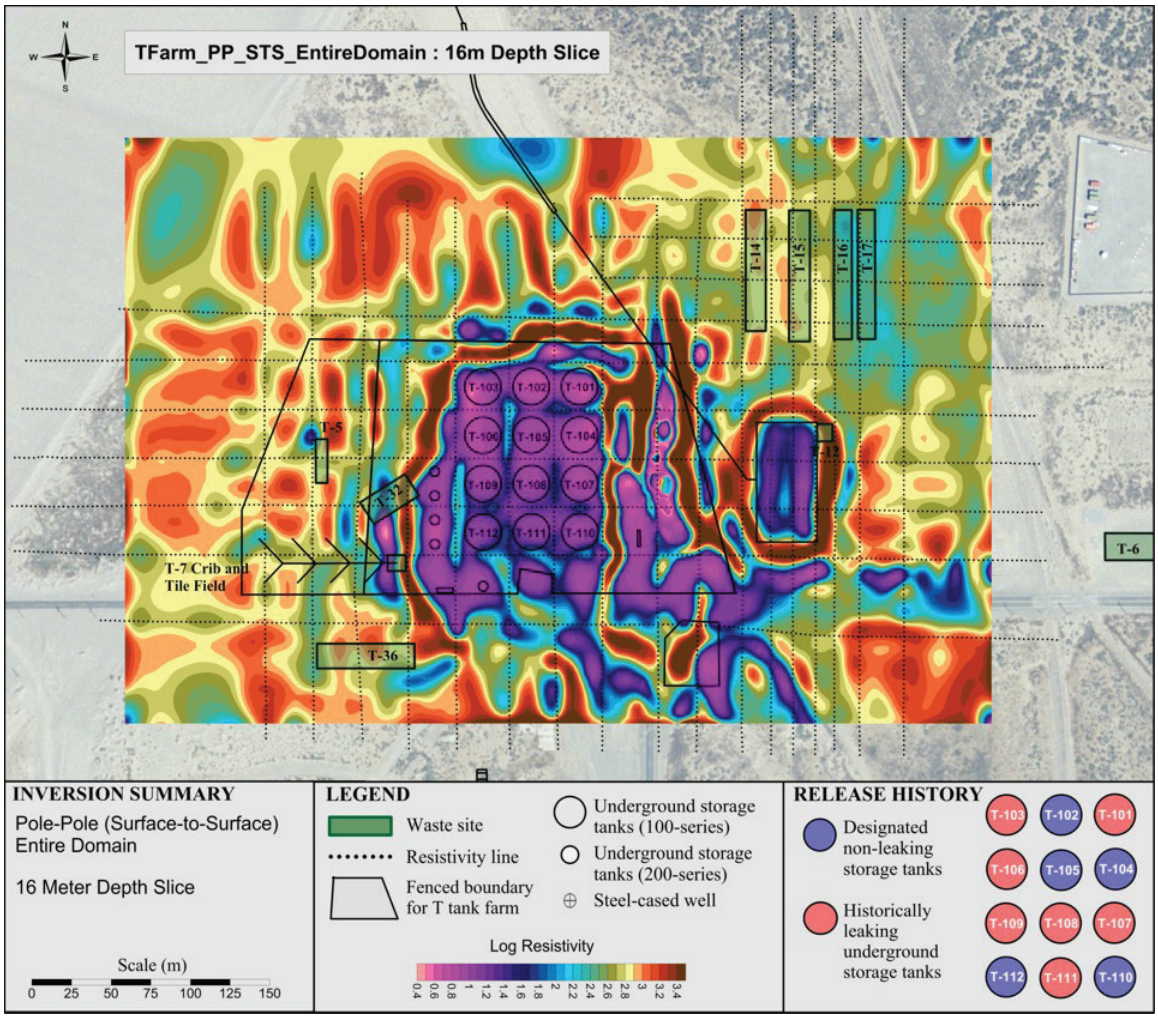

Figure 6-29 shows the depth slice at 26m. The low resistivity values of the tank farm are essentially a monolith and there is no distinguishing individual tank leaks within the area. Directly east of the tanks is another low resistivity feature that appears to coincide with support infrastructure that delivered waste from the T plant to the T farm, including divergence boxes and piping manifolds. Low resistivity patterns south and southwest of the farm also exhibits linear shapes that are likely pipelines that have been identified in electromagnetic induction and magnetic gradiometry mapping.

What is disappointing is that the noisy data from inside the farm are affecting the outcome of the clean areas outside the farm. The resistivity beneath the northeast trenches, for example, has a different distribution for this model compared to the model of the region by itself. The western cribs and trenches show a more severe difference.

Figure 6-29. Horizontal Slice Showing Resistivity Distribution at 26M for the Entire T Farm.

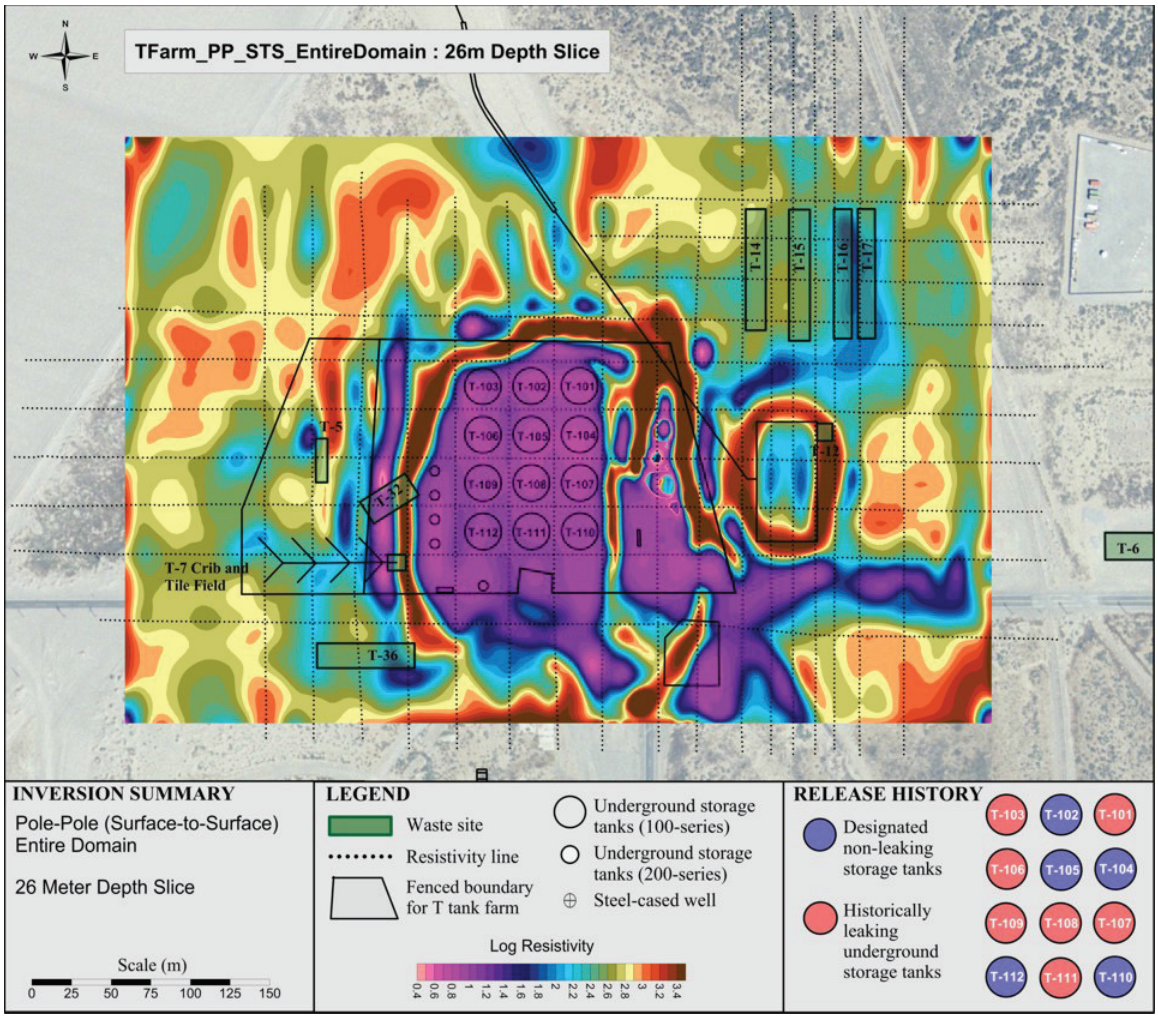

The last three slices in Figures 6-30 through 6-32 continue the same trend observed in the 26m slice. Low resistivity features tend to coincide with infrastructure and not with the expected location of waste plumes.

Figure 6-30. Horizontal Slice Showing Resistivity Distribution at 38M for the Entire T Farm.

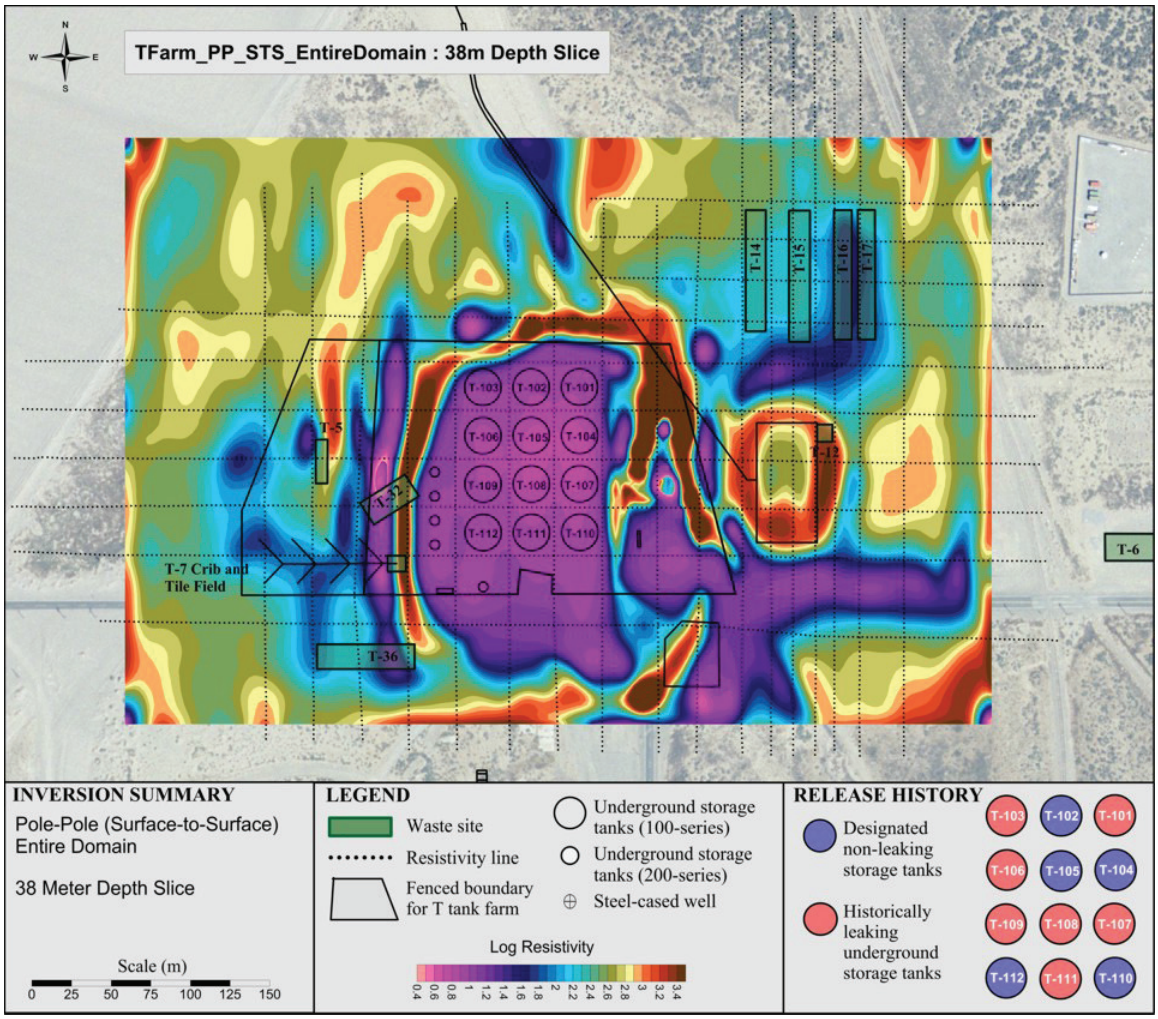

Figure 6-31. Horizontal Slice Showing Resistivity Distribution at 56M for the Entire T Farm.

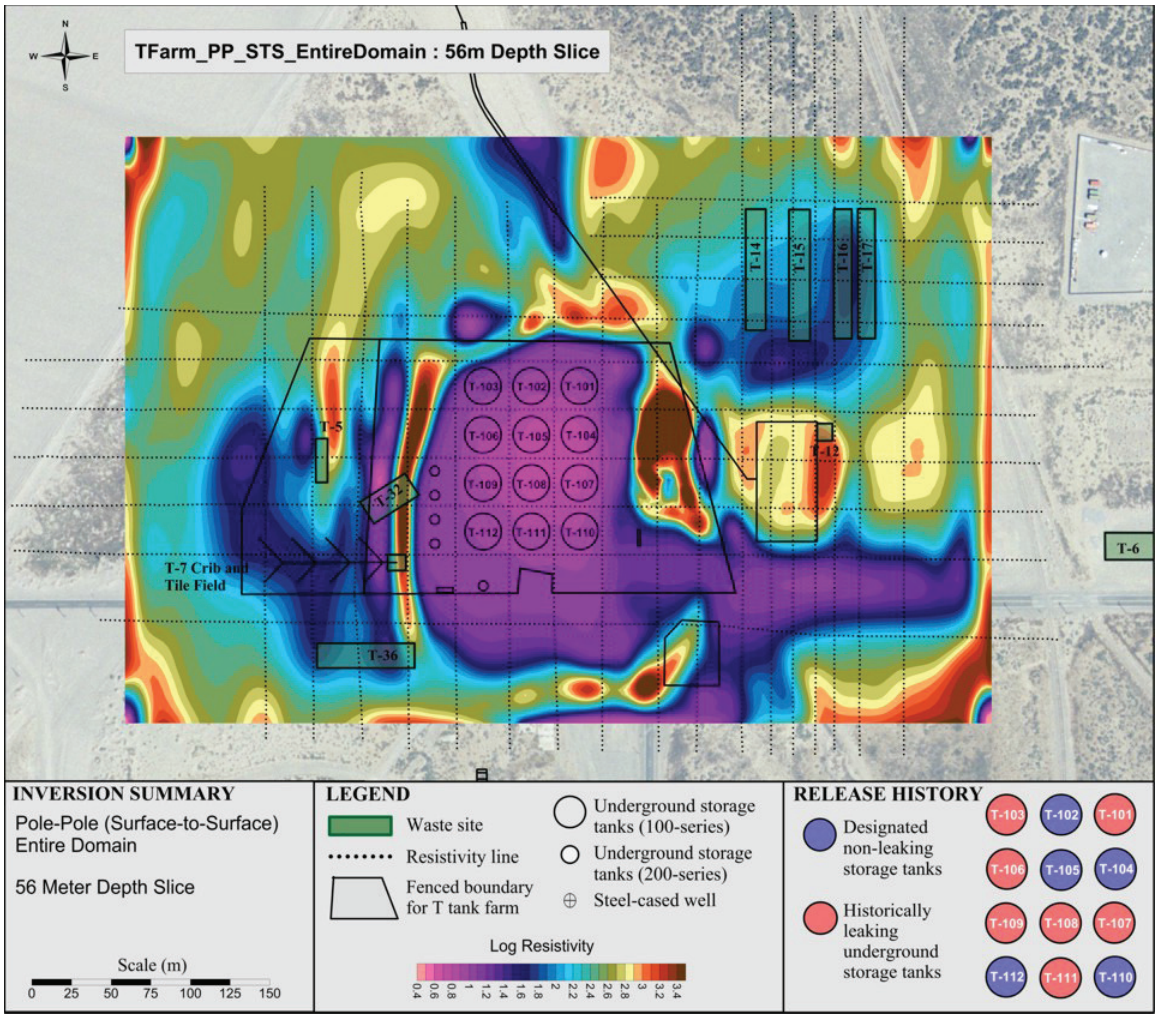

Figure 6-32. Horizontal Slice Showing Resistivity Distribution at 78M for the Entire T Farm.

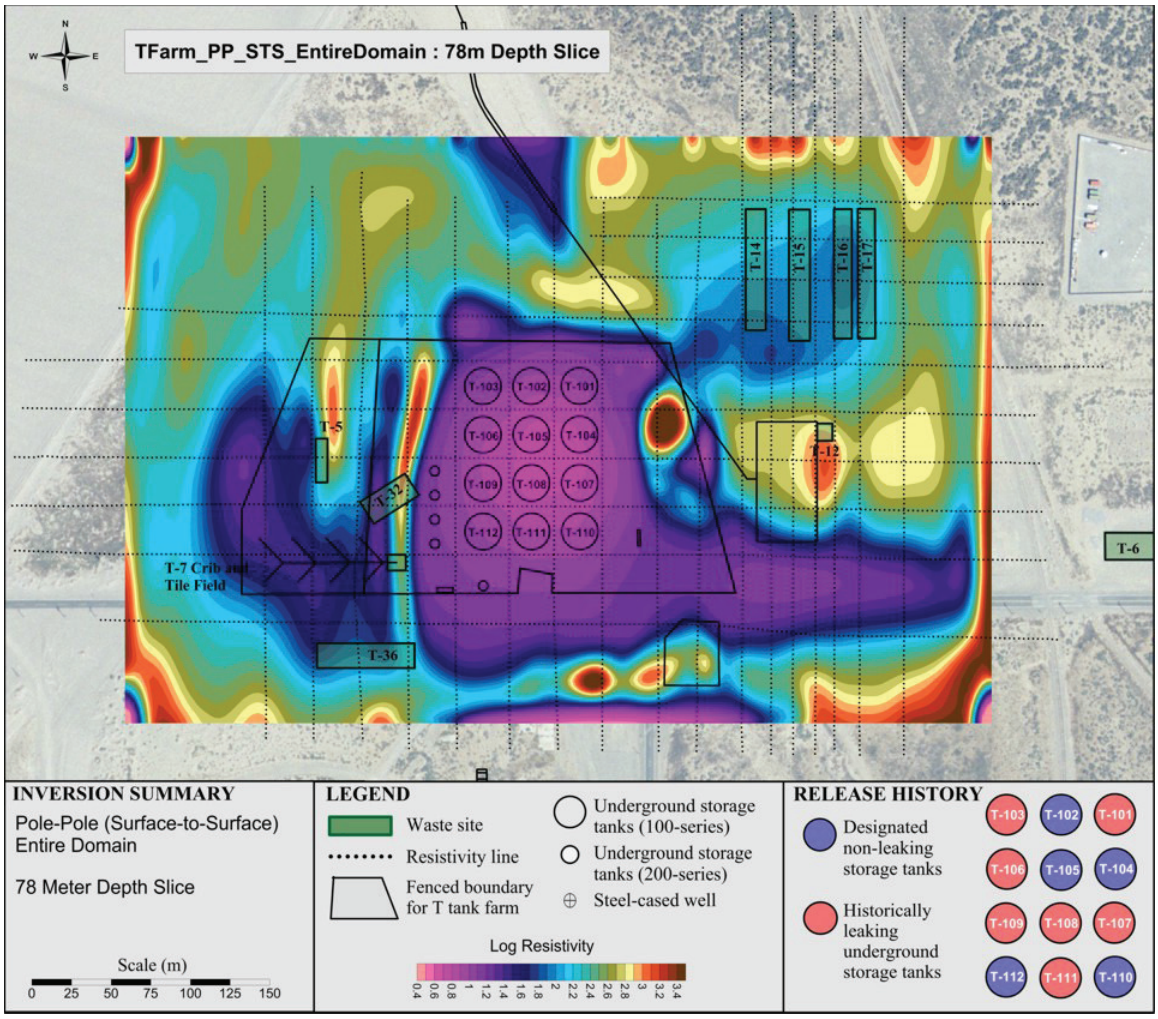

6.2.3 Task 3 – WTS Inversion Model Results

Three WTS inversions were performed with select wells and surface electrodes using the pole-pole array. The first model, TFarm_PP_WTS, applied strictly WTS data and the second and third, TFarm_PP_WTS+WTW and TFarm_PP_WTS+WTW partial, used a combination of WTS and WTW data. The last model used a partial subset of the surface electrodes outside of the farm fence.

The code RES3D64 was used for the three WTS-based inversions and the success of each inversion iteration is shown in Figure 6-33. A model stopping criteria of six iterations was used throughout the modeling and the convergence curves in the figure show a monotonic decrease in RMS error for each successive iteration. From an error perspective, the most successful model was the WTS+WTW partial model, which completed with an RMS error around 14.7 percent, while the WTS completed at 16.5 percent and WTS+WTW reached a final RMS error

around 19.5 percent. However, compared to the successful WTW models, these WTS models are marginal.

Figure 6-33. Convergence Curves for the WTS Models.

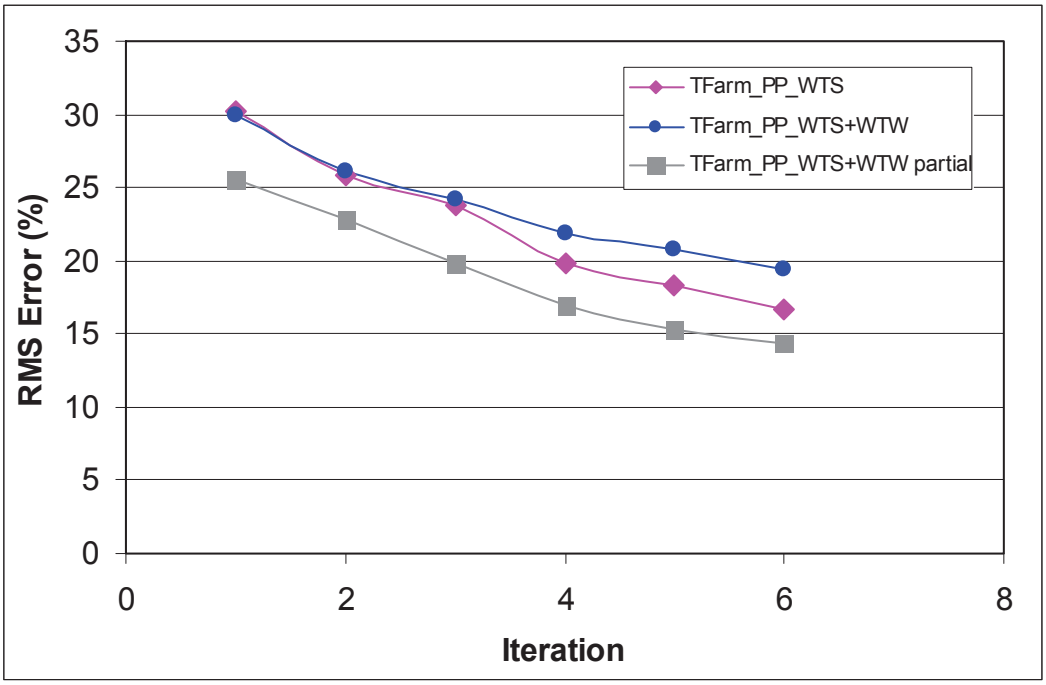

6.2.3.1 Resistivity Model for WTS Inversion Model. The WTS model used primarily the same set of wells as the WTW models presented in Section 6.2.1.1. A couple of WTW wells were taken out of the WTS model and a few were added to the model for a net gain of one well for a total of 88 for the model. The surface lines were placed along the original location of lines 5N and 5E with an electrode spacing of 6m. Reciprocal data were acquired, where both surface electrodes and wells acted as transmitters. A total of 18,424 data values were used for the model.

Figure 6-34 shows the results of the resistivity distribution with the WTS data. The WTS results are displayed similar to the WTW results, with the uppermost layer color contoured to view the entire range of resistivity values. Large low resistivity targets are seen distributed throughout the domain. The target beneath the T-7 and T-32 cribs appear to match other results from WTW and STS.

Unfortunately, the resistivity distribution in the tank farm is quite noisy and interpreting potential waste plumes is a challenge. Compared to successful WTW inversions, the WTS results show more targets that are likely false positives. The low resistivity values in the regions south of T-106 and T-101 match hydrologic expectations. However, the low resistivity targets at T-108 and east of T-107 are not substantiated by other models.

In addition to inside the tank farm, regions outside the farm also appear to have large low resistivity targets that are not substantiated by the WTW. The region north of the farm shows an east-west trending low resistivity anomaly that coincides with the north side of each well. The

location of the target is too suspicious to consider real. To the south of the farm fence are two anomalies that are split by the location of the north-south surface line. The shape and location make this target suspicious as well.

Figure 6-34. WTS Inversion Model Results.

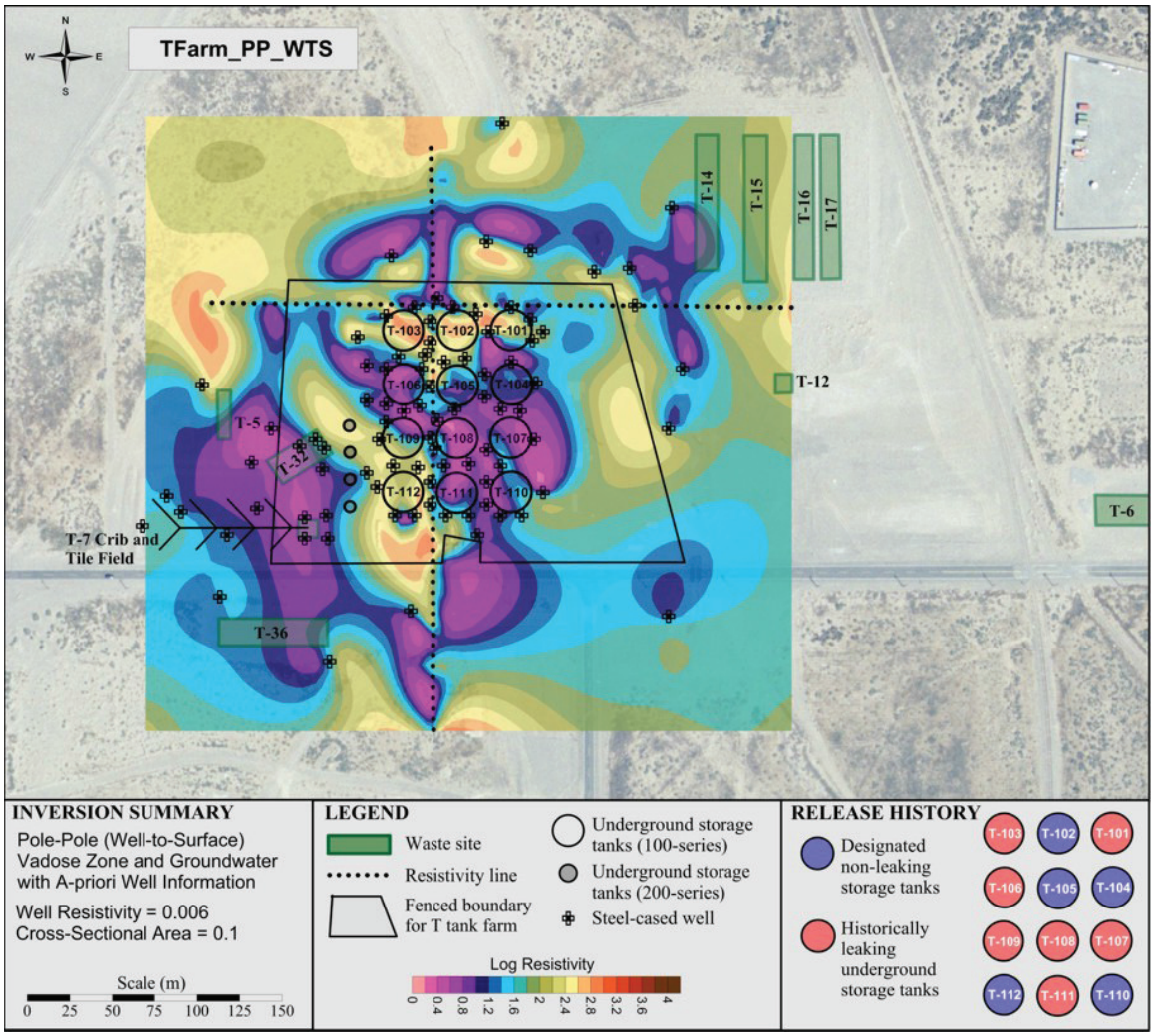

The quality of the WTS inversion is most likely the direct result of the quality of the surface line data and not the method. The surface lines are placed mostly inside the tank farm fence where near surface infrastructure may influence the transmitted current or received voltage. Surface lines placed on the periphery of the farm in areas of no infrastructure would likely produce better results.

6.2.3.2 Mixed Well-to-Surface Inversion Model and Well-to-Well Inversion Model. Another trial of the WTS method was tried by incorporating WTW data with WTS data in a single inversion model. It was hoped that the problems in the WTS inversion alone would have been minimized by adding the WTW data. For this model, the data count increased to 25,013 and the well count increased to 92.

Figure 6-35 shows the results of the combined WTS and WTW inversion model. The results look quite similar to the WTS data with the target beneath the T-7 and T-32 cribs well defined and others suspect. The low data count by the WTW dataset may not have been sufficient to reduce the number of artifacts in the data. Overall, combining the WTW with the WTS added little value to the analysis because of the strong effects from noisy surface electrodes inside the farm.

Figure 6-35. Results of Combined WTS and WTW Inversion Model.

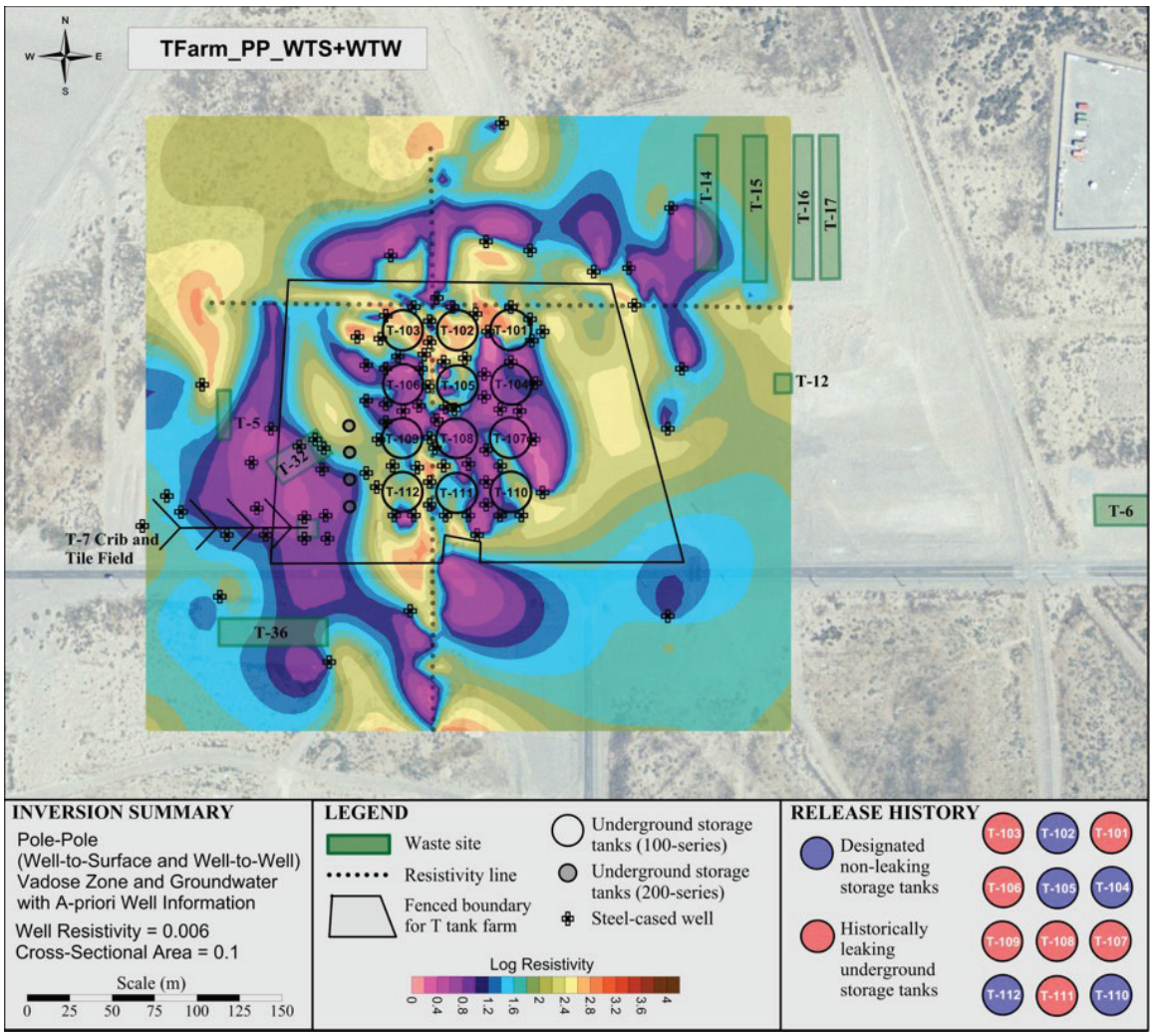

The last model for the WTS trials was conducted using the WTW+WTS with a subset of surface electrodes that are outside the farm fence. The trial was to test the hypothesis that the surface

electrodes inside the farm are contributing to the majority of noise in the inversion results seen in the previous two trials. Figure 6-36 shows the results of the modeling, which had 12,922 data values for model input.

Figure 6-36. Mixed WTS and WTW Inversion Model Results Using a Subset Of Surface Electrodes.

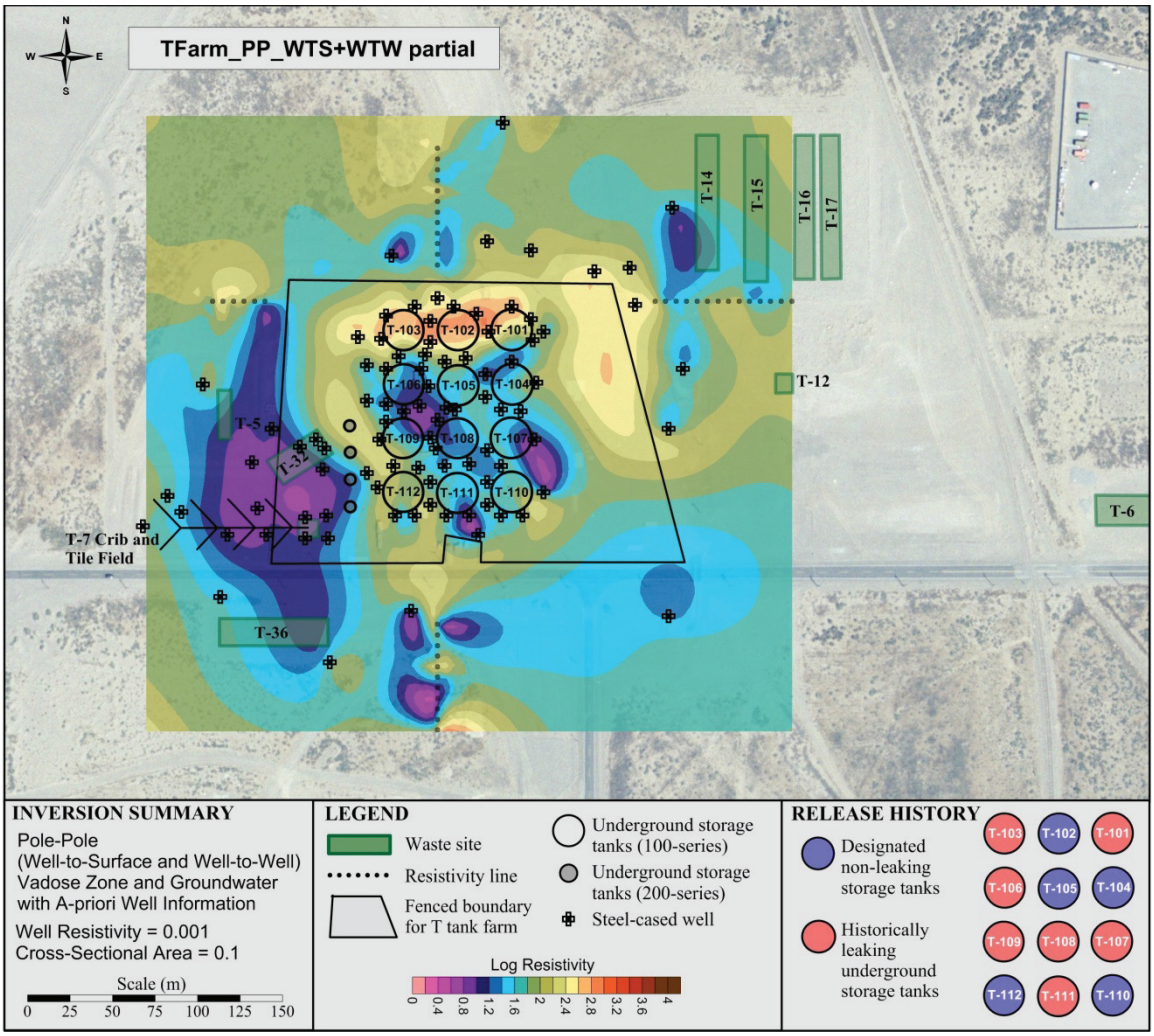

The results from using a partial subset of measurements from surface electrodes outside the farm had a positive effect on the outcome of the model. Inside the tank farm, the low resistivity targets are logically located near known leaks. The leak at T-106, for example, shows prevalently in the resistivity. A few smaller targets are identified around tanks T-101, T-107 and T-111.

Outside the fence line, the large low resistivity target beneath T-7 and T-32 is consistent with other models with the exception of an elongated north-south trend. Near the northeast trenches, a low resistivity target is seen to the west and south of the trench footprint. The location of the target is different from the STS model most likely due to the location and number of electrodes

in this model. The low resistivity target south of the fence that is bisected by the north-south set of electrodes is a curious feature and could possibly be a false positive.

7.0 CONCLUSIONS

Electrical resistivity data acquired in the T tank farm was reprocessed using advanced software algorithms and enhanced computer hardware. The resistivity datasets for T tank farm included STS data acquired in the summer of 2005, and WTW and WTS acquired in January 2006. The state-of-the-art for software and hardware at the time of acquisition was a 32-bit version of EI3D and computers limited with 2GB of usable memory and a single processor. The limitations in both software and hardware forced the modeling effort in 2006 to split the T farm domain into smaller subsets.

Since the initiation of the SGE program, significant advances have been made to model the resistivity data that encompass large tank farm domains in one single inversion model on computers with expanded memory and processors. The current scope of reprocessing the T tank farm data included reprocessing the WTW, STS, and WTS data using these enhanced tools with the RES3D64 code on computers with up to 128GB of RAM and 16 processors. The RES3D64 has been upgraded from its 32-bit version to accommodate multiple processors and large computer memory. Additionally, the code went through a significant upgrade to properly model the WTW and WTS datasets. Model tests and benchmarks were conducted to ensure the accuracy of the results with synthetic data.

The reprocessing of the T farm data was divided into three tasks. The first task was to model the WTW data. Several subsets of the WTW data were modeled, including a pole-pole array dataset of all groundwater and vadose zone wells, pole-pole dataset for groundwater wells alone, dipole-dipole data for both groundwater and vadose zone wells, and a mixed pole-pole with dipole-dipole for groundwater and vadose zone wells. Several trials for pole-pole data on all well types were completed to test the effects of various well parameters on the final resistivity distribution and error statistics. Model TFarm_PP_WTW_B (Figure 6-5) produced the best results, which showed targets that were coherent and met hydrologic expectations compared to the site conceptual model and direct characterization data. Additionally, the outcome with the RES3D64 model was far superior to the previous outcome using EI3D. The inversion model using only groundwater wells also showed logical low resistivity targets compared to groundwater monitoring data. Unfortunately, the dipole-dipole data were not useful due to the high degree of noise in the data. Dipole-dipole data are typically prone to higher noise from the lower signal strength compared to pole-pole.

The second task was to model the STS data. The effort was divided into three subtasks to investigate the western trenches area, northeastern trenches area, and the entire domain. The first two subtasks were meant to investigate areas of minimal infrastructure to ensure a good model with reasonable error statistics could be generated in simple areas, before moving on to complex areas. The model of the western trenches showed a significant target beneath T-7 and T-32 cribs. These cribs received approximately 35 million gallons of liquid waste and it was expected that a large low resistivity target would be located here. The model of the northeastern trenches also showed a significant target, which appeared to match with reasonable fidelity information from the sole characterization well in the area (W11-45). The last model for STS was completed on the entire domain, and included apparent resistivity data that went directly through the tank farm.

The T tank farm has a considerable amount of infrastructure that could cause interference with electrical resistivity measurements. The resistivity results reflect much of this infrastructure in that the low resistivity appears to coincide with the footprint of the tanks. Unlike the WTW models that could identify segregated areas of low resistivity, the STS model of the entire domain shows only large undifferentiated targets that do not match hydrologic expectations. This has been problematic in some but not all tank farms (e.g., S farm). See Section 8.2.1 for additional discussion.

The third task was to model the WTS data. The surface lines for the WTS acquisition coincided with the locations of 5N and 5E from the STS acquisition. The results showed a high degree of incoherency, or noise, that may or may not coincide with historical leaks. These noise sources are likely due to a majority of the surface electrodes running directly through the tank farm where metallic infrastructure could be causing interference. A few trials were conducted with the WTS geometry including adding WTW data and removing surface electrodes that were within the tank farm (leaving electrodes outside the farm intact). Adding WTW data did not affect the outcome of the resistivity distribution. However, removing a subset of surface electrodes had a profound effect. Many low resistivity targets were shown to be at logical locations with respect to known contamination sources. A few low resistivity targets were seen at unexpected locations which could mean that even though the electrodes were outside the farm fence, piping could still be causing significant noise. If placed properly, the WTS method could expand the success of the WTW method to areas of no or minimal well coverage. An example is the TX/TY tank farm SGE project, where surface electrodes were placed on the periphery of the domain.

In summary, the reprocessing of T tank farm SGE resistivity data was a success. The WTW models showed greater coherency and targets matched conceptual models. The STS models of domains in areas of minimal infrastructure were also quite successful. It is recommended, at the minimum, to reprocess all previous WTW data from the various SGE project using RES3D64.

8.0 LIMITATIONS AND RECOMMENDATIONS

The T tank farm area, as with all SGE project sites, provided a challenging environment for surface geophysical characterization of subsurface soil conditions. This section describes impacts to the resistivity method caused by limitations of data acquisition and processing, and presents recommendations that may help resolve a few limitations on future deployments.

8.1 DATA ACQUISITION

8.1.1 Logistics

The T Tank farm was the first SGE project within a tank farm environment. Acquisition parameters and procedures established for subsequent tank farms were not yet in place. For example, permanent electrodes are now installed in all tank farms, except the T tank farm. The permanent electrodes are typically larger diameter than the temporary electrodes used in T farm. The advantage of the permanent electrode, even if the resistivity survey is never conducted again, is a larger current density that would reduce noise.

The main advantage to using permanent electrodes, however, is the ability to conduct time-lapsed imaging for monitoring plume movement. Some tank farms are known to be dynamic systems with possible transient plume movement both in the vadose zone and groundwater. For example, nitrate concentrations in groundwater around the T farm have shown significant increases within the last several years. To monitor such plume movement, we recommend that permanent electrodes be placed in T Farm and periodic resistivity surveys be performed in the vicinity of those identified tank farms. The current practices of leaving permanent electrodes installed will provide for improved data quality for subsequent acquisition of time-series data.

Other electrode geometries should also be considered if data acquisition is to be conducted again in T farm. The geometry that is most likely to succeed for the tank farm environment is cross-borehole, where multiple electrodes are nested vertically in two or more boreholes placed below the infrastructure.

8.1.2 Equipment

The STS data were acquired using 2D survey lines with no measurements between survey lines. This approach was logistically easier, more expedient, and consequently more cost effective due to the reduced equipment requirements compared to full 3D data acquisition. Future deployment should consider full 3D acquisition to help resolve targets with higher fidelity.

The SuperSting R8 is limited to 2 amps of transmitter power and the resolution of the data acquisition card is limited to a minimum of 30 nanovolts (SuperStingR8 Specifications – Advanced Geosciences, Inc.). The limited electrode grounding surface-area caused by limiting the permanent electrodes to less than 11 in. (28 centimeters), due to site safety restrictions, prevented the R8 from attaining optimal transmitter current. Although this did not prevent data

acquisition, it decreased the signal-to-noise ratio. Future projects may consider testing a higher powered transmitter that could improve the signal to noise ratio.

8.2 DATA PROCESSING

8.2.1 Infrastructure Interference

Areas with substantial infrastructure continue to present the most difficulties with regard to inverse modeling and associated interpretation of estimated resistivity distributions. It is recommended that new models be developed to more effectively deal with the effect of the infrastructure on inverse modeling results. The new models should make use different modeling methods, such as the analytic element method, filtering, or some other technique that would help to better approximate the effects of infrastructure in inverse models.

All estimates of resistivity distributions resulting from inversion models need to be viewed and evaluated in terms of whether they are consistent hydrologically with site conditions. For conceptual models of tanks that are assumed to be leakers, the results of the inversion process should be validated against independent observations of vadose zone and/or groundwater contamination. However, the resistivity inversion process does not incorporate any aspect of hydrology. It is recommended that a joint inversion model be developed that would make use of both resistivity and unsaturated zone measurements.

8.2.2 Inversion Modeling

The biggest enhancement with the use of RES3D64 is the increased functionality for WTW inversion. Previous WTW inversion modeling with EI3D and EI3DCL produced marginal results that were noisy. The results from the EarthImager series of models were also presented by removing high resistivity values and showing a partial distribution of the remaining low resistivity values. This was necessary because a target may have been hidden below a high resistivity layer and simply showing a slice though the domain may have missed important features. The new T farm WTW model is shown to be much more resolved and less prone to noise than the previous models. Targets appear to be more coherent and match reasonably well with site conceptual models. Additionally, the presentation of the results has been enhanced by showing the full range of resistivity in contour plots. It is recommended that all tank farms be remodeled using RES3D64, especially those that had multiple domains (e.g., C farm).

9.0 REFERENCES

"Hazardous Waste Management Act," RCW 70.105, *Revised Code of Washington*, as amended.

40 CFR 141, "National Primary Drinking Water Regulations," *Code of Federal Regulations*, as amended.

ARH-LD-135, 1976, *Geology of the 241-T Tank Farm*, Atlantic Richfield Hanford Company, Richland, Washington.

CEES-0338, 2006, *Software Management Plan for Surface Geophysical Exploration Projects*, Revision 0, Columbia Energy & Environmental Services, Inc., Richland, Washington.

Ellis, R.G., and D.W. Oldenburg, 1994, Applied geophysical inversion: Geophysical Journal International, 116, 5-11.

Exploration Geophysics, 2003, 34, 182-187, "A comparison of smooth and blocky inversion methods in 2D electrical imaging surveys," Loke, M.H., I. Acworth, and T. Dahlin.

Furman, A., A.W. Warrick, and T.P.A. Ferré, 2002, Electrical potential distributions in response to applied current in a heterogeneous subsurface, solution for circular inclusions: Vadose Zone Journal, 1, 273–280.

Geophysical Prospecting, 1990, 38(5): 499-524, "Methods for calculating Fréchet derivatives and sensitivities for the non-linear inverse problem: a comparative study," McGillivray, R. and D.W. Oldenburg.

Geophysical Prospecting, 1996a, 44(3): 499-523, "Practical techniques for 3D resistivity surveys and data inversion," Loke, M.H. and R.D. Barker.

Geophysical Prospecting, 2004, Volume 52, pp. 379-398, "A numerical comparison of 2D resistivity imaging with 10 electrode arrays," Dahlin, T. and B. Zhou.

Geophysics (in review), 2009, "Electrical resistivity characterization of an industrial site using long electrodes," Rucker, D.F., M. H. Loke, M.T. Levitt, and G. Noonan.

Geophysics , 2009, 3, F31-F43, "Explicit expressions for the Fréchet derivatives in 3D anisotropic resistivity inversion, " Greenhalgh, S.A., B. Zhou, M. Greenhalgh, L. Marescot, and T. Wiese.

Geophysics, 1977, Volume 43(5): 1020-036, "A Modified Pseudo-Section for Resistivity and IP," Edwards, L. S.

Geophysics, 1979, Volume 44(4): 753-780, "Resistivity modeling for arbitrarily shaped three-dimensional structures," Dey, A. and H.F. Morrison.

Geophysics, 1989, Volume 54, 254-262, "Two-dimensional joint inversion of magnetotelluric and dipole-dipole resistivity data," Sasaki, Y.

Geophysics, 1990, Volume 55(12): 1613-1624, "Occam's inversion to generate smooth, two-dimensional models from magnetotelluric data," deGroot-Hedlin, C. and S. Constable.

Geophysics, 1995, Volume 60(6):1682-1690, "Least-squares deconvolution of apparent resistivity pseudosections," Loke, M.H., and R.D. Barker.

Geophysics, 2002a, Volume 67(6): 1692-1700, "A 3-D resistivity investigation of a contaminated site at Lernacken, Sweden," Dahlin, T., C. Bernstone, and M.H. Loke.

Geophysics, 2004, Volume 69(1): 78-86, "Inversion of magnetotelluric data for 2D structure with sharp resistivity contrasts," deGroot-Hedlin, C. and S. Constable.

Geophysics, 2007, Volume 72: H1-H10, "RESINVM3D: A 3D resistivity inversion package," Pidlisecky, A., E. Haber, and R. Knight.

Geophysics, 2008, Volume 73: K1-K9, "Constructing piecewise-constant models in multidimensional minimum-structure inversions," Farquharson, C.G.

GJO-HAN-27, 1999, *Hanford Tank Farms Vadose Zone: T Tank Farm Report*, GJO-99-101-TAR, U.S. Department of Energy, Grand Junction Office, Grand Junction, Colorado.

Halihan, T., S. Paxton, I. Graham, T. Fenstemaker, and M. Riley, 2005, "Post-remediation evaluation of a LNAPL site using electrical resistivity imaging," *Journal of Environmental Monitoring*, 7:283–287.

HGI-2005-062, 2006, *Geophysical Characterization of the PUREX Facility*, hydroGEOPHYSICS, Inc., Tucson, Arizona.

HNF-5183, 2007, *Tank Farms Radiological Control Manual (TFRCM)*, Revision 2, CH2M HILL Hanford Group, Inc., Richland, Washington.

HNF-EP-0182, 1999, *Waste Tank Summary Report for Month Ending December 31, 1998*, as revised, Fluor Hanford, Inc., Richland, Washington.

Johnston, R.H., F.N. Trofimenkoff, and J.W. Hasslett, 1987, Resistivity response of a homogeneous earth with a finite-length contained vertical conductor: IEEE Transactions on Geoscience and Remote Sensing, GE-25, 414-421.

Journal of Applied Geophysics, 1999, Volume 41(4), pp. 313-333, "The location of infinite electrodes in pole-pole electrical surveys: Consequences for 2D imaging, " Robain, H., Y. Albouy, M. Dabas, M. Descloitres, C. Camerlynck, P. Mechler, Pierre and A. Tabbagh.

Journal of Applied Geophysics, 2002, Volume 49, pp. 149-162, "A comparison of Gauss-Newton and quasi-Newton methods in resistivity imaging inversion," Loke, M.H. and T. Dahlin

Journal of Environmental and Engineering Geophysics, December 2005, 10(4):339-350, "Resolution of 3-D Electrical Resistivity Images from Inversions of 2-D Orthogonal Lines," Gharibi and Bentley.

LaBrecque, D.J., and X. Yang, 2001, "Difference Inversion of ERT Data: A Fast Inversion Method for 3-D In Situ Monitoring," *Journal of Environmental and Engineering Geophysics*, V6(2):83-89.

Loke, 2006, Personal communication via email.

Matrix Computations, 3rd Edition. Johns Hopkins Press, 2006, Golub, G.H. and C.F. van Loan.

PNL-6820, 1989, *Hydrogeology of the 200 Areas Low-Level Burial Grounds – An Interim Report*, Pacific Northwest Laboratory, Richland, Washington.

PNL-7336, 1990, *Geohydrology of the 218-W-5 Burial Ground, 200 West Area, Hanford Site*, Pacific Northwest Laboratory, Richland, Washington.

PNNL-11809, 1998, *Results of Phase 1 Groundwater Quality Assessment for Single-Shell Tank Waste Management Areas T and TX-TY at the Hanford Site*, Pacific Northwest National Laboratory, Richland, Washington.

PNNL-14849, 2008, *Characterization of Vadose Zone Sediments Below the T Tank Farm: Boreholes C4104, C4105, 299-W10-196, and RCRA Borehole 299-W11-39,* Revison 1, Pacific Northwest National Laboratory, Richland, WA, Serne, R.J.; Bjornstad, B.N.; Horton, D.G.; Lanigan, D.C.; Schaef, H.T.; Lindenmeier, C.W.; Lindberg, M.J.; Clayton, R.E.; Legore, V.L.; Geiszler, K.N.; Baum, S.R.; Valenta, M.M.; Kutnyakov, I.V.; Vickerman, T.S.; Orr, R.D. and Brown, C.F.

PNNL-14948, 2004, *Plume Delineation in the BC Cribs and Trenches Area*, Pacific Northwest National Laboratory, Richland, Washington.

PNNL-15070, 2005, *Hanford Site Groundwater Monitoring for Fiscal Year 2004*, Pacific Northwest National Laboratory, Richland, Washington.

RHO-ST-23, 1979, *Geology of the Separations Areas, Hanford Site, South Central Washington*, Rockwell Hanford Operations, Richland, Washington.

RPP-20303, 2004, *Preliminary Data from 216-B-26 Borehole in BC Cribs Area*, Revision 0, CH2M HILL Hanford Group, Inc., Richland, Washington.

RPP-23405, 2005, *Tank Farm Vadose Zone Contamination Volume Estimates*, CH2M HILL Hanford Group, Inc., Richland, Washington.

RPP-23748, *Geology, Hydrogeology, Geochemistry, and Mineralogy Data Package for the Single-Shell Tank Waste Management Areas at the Hanford Site*, Revision 0, CH2M HILL Hanford Group, Inc., Richland, Washington.

RPP-23752, 2005, *Field Investigation Report for Waste Management Areas T and TX-TX*, Revision 0-A, D.A. Myers, CH2M HILL Hanford Group, Inc., Richland, Washington.

RPP-34974, *Verification and Testing of the EarthImager Series of Electrical Resistivity Inversion Codes – A Benchmark Comparison*, Revision 0, CH2M HILL Hanford Group, Inc., Richland, Washington.

RPP-7123, 2001, *Subsurface Conditions Description of the T and TX-TY Waste Management Areas*, Revision 0, CH2M HILL Hanford Group, Inc., Richland, Washington.

RPP-7578, 2002, *Site-Specific SST Phase 1 RFI/CMS Work Plan Addendum for WMAs T and TX-TY*, Revision 2, CH2M HILL Hanford Group, Inc., Richland, Washington.

RPP-8531, 2001, *Vadose Zone Geology of Boreholes 299-W10-27 and 299-W11-39 T-TX-TY Waste Management Area, Hanford Site, South-Central Washington*, Revision 0, CH2M HILL Hanford Group, Inc., Richland, Washington.

RPP-RPT-28955, 2006, *Surface Geophysical Exploration of T Tank Farm*, Revision 0, CH2M HILL Hanford Group, Inc., Richland, Washington.

Rucker, D.F., J.B. Fink, M.T. Levitt, D.R. Glasser II, and C.A. Baldyga, 2005, "High Resolution Resistivity (HRR) delineation of a liquid waste plume at a former radioactive waste disposal site, Hanford, Washington," *Proceedings of the Waste Management 2005 (WM05) Conference*, February 27 – March 3, Tuscon, Arizona.

Soil Science , 1976, 122:181-187, "Predicting specific conductance and salt concentration in dilute aqueous solutions," Marion, G.M., and K.L. Babcock.

Soil Science, 1973, 116:26-30, "Estimation of activity coefficients from the electrical conductivity of natural aquatic systems and soil extracts," Griffin, R.A., and J.J. Jurinak.

USGS Open File Report 2004-1319, 2004, , "*Direct Current Resistivity Profiling to Study Distribution of Water in the Unsaturated Zone Near the Amargosa Desert Research Site, Nevada,"* Abraham, J.D., and Lucius, E.

WAC 173-303, "Dangerous Waste Regulations," *Washington Administrative Code*, as amended.

Water Resources Research, May 1999, Volume 35, Number 5, pp. 1425-1433, "Effects of source cavity shape on steady, three-dimensional flow of soil gases, " Warrick, A.W. and Rojano, A.

WHC-MR-0227, 1991, *Tank Wastes Discharged Directly to the Soil at the Hanford Site*, Westinghouse Hanford Company, Richland, Washington.

WHC-SD-EN-AP-132, 1993, *Interim-Status Groundwater Quality Assessment Plan for the Single-Shell Tank Waste Management Areas T and TX-TY*, Revision 0, Westinghouse Hanford Company, Richland, Washington.

WHC-SD-EN-TI-014, 1992, *Hydrogeologic Model for the 200 West Groundwater Aggregate Area*, Revision 0, Westinghouse Hanford Company, Richland, Washington.

Yang, X., 1999, *Stochastic inversion of 3D ERT data*, Ph.D. Dissertation, Department of Mining and Geological Engineering, University of Arizona, Tucson, Arizona.

APPENDIX A

DATA PROCESSING AND REDUCTION

TABLE OF CONTENTS

A1.0 INTRODUCTION A-1
A1.1 DATA REDUCTION A-1
A1.2 DATA FILTERING STATISTICS FOR T FARM DATA A-7

A2.0 REFERENCES A-9

LIST OF FIGURES

A-1. Schematic Flowchart for the SGE Data Acquisition and Processing Steps Contributing to the Analysis and Presentation of Resistivity Data A-2
A-2. Example of Noisy Data Removal using Repeat Error (left image) and Electrical Current (right image) A-3
A-3. Example of Data Scatter (Plotted as Linear Pseudo-Section) Before and After Noisy Data Rejection A-4
A-4. Example of Spike Rejection of Transfer Resistance A-5
A-5. Data Filtering Example A-6
A-6. Example HRR Section A-7
A-7. Data Distribution A-9

LIST OF TABLES

A-1. Data Reduction Statistics for All T Farm HRR Lines A-8

LIST OF TERMS

3D	three-dimensional
EM	electro-magnetics
GPR	ground penetrating radar
GPS	global positioning system
HRR	high resolution resistivity

This page is intentionally left blank.

A1.0 INTRODUCTION

Data processing and reduction steps involve processing and visualization of resistivity and global positioning system (GPS) data. The GPS data provide accurate control points and geo-referencing so that the resistivity data can be accurately located relative to trenches, cribs and tank farm features. Data reduction involves the post-acquisition identification and removal of spurious data values that do not conform to the overall data population or that violate potential theory.

A1.1 DATA REDUCTION

Resistivity data are collected along two-dimensional transects in order to best satisfy data processing, site layout logistics and equipment. Data processing is performed on an individual line basis and then combined into a three-dimensional (3D) data set using the GPS data. Figure A-1 presents a flowchart of the data acquisition and processing steps contributing to and resulting in the final analysis and presentation of the high resolution resistivity (HRR) data.

Pre-survey and background geophysical properties were acquired using ground penetrating radar (GPR), electro-magnetics (EM), and magnetics surveying to determine the location of subsurface infrastructure or other buried metallic debris. The results of these surveys are presented in two separate reports:

1. RPP-RPT-36893, Revision 0, *Surface Geophysical Exploration of TX and TY Tank Farms at the Hanford Site: Results of Background Characterization with Magnetics and Electromagnetics*, CH2M HILL Hanford Group, Inc., Richland, Washington.
2. RPP-RPT-38104, Revision 0, *Surface Geophysical Exploration of TX-TY Tank Farms at the Hanford Site: Results of Background Characterization with Ground Penetrating Radar*, CH2M HILL Hanford Group, Inc., Richland, Washington.

Each day, individual binary data files are downloaded and exported to a laptop computer where the data are reviewed to ensure adequate data quality before moving the resistivity equipment to the next survey line. This process also allows the operator to refine data acquisition parameters as the survey migrates from one area of the site to another. Each file is parsed into usable columns (e.g., record no., date, current, normalized potential, error, apparent resistivity, geometry, transmitter gain) using Microsoft Excel®. Numerical and graphical evaluation of the signal-to-noise ratio, percent error, and scatter in collected data in comparison to neighboring lines were conducted as a part of the data inspection process.

After data are downloaded from the resistivity instrument and parsed into a usable spreadsheet format, data filtering techniques are used to identify and remove: data spikes, or anomalous data caused by data acquisition card instabilities, or extraneous current sources. Data filtering is performed by copying the parsed raw data into an Excel data filtering template that contains a series of graphs showing the various data parameters. The process of filtering identifies and eliminates data points, but no data modification such as rounding, averaging, smoothing, or

® Excel is a registered trademark of the Microsoft Corporation.

splining is permitted. The rationale is to seek out and remove spurious points that do not conform to the data population or points that violate potential theory.

Figure A-1. Schematic Flowchart for the SGE Data Acquisition and Processing Steps Contributing to the Analysis and Presentation of Resistivity Data.

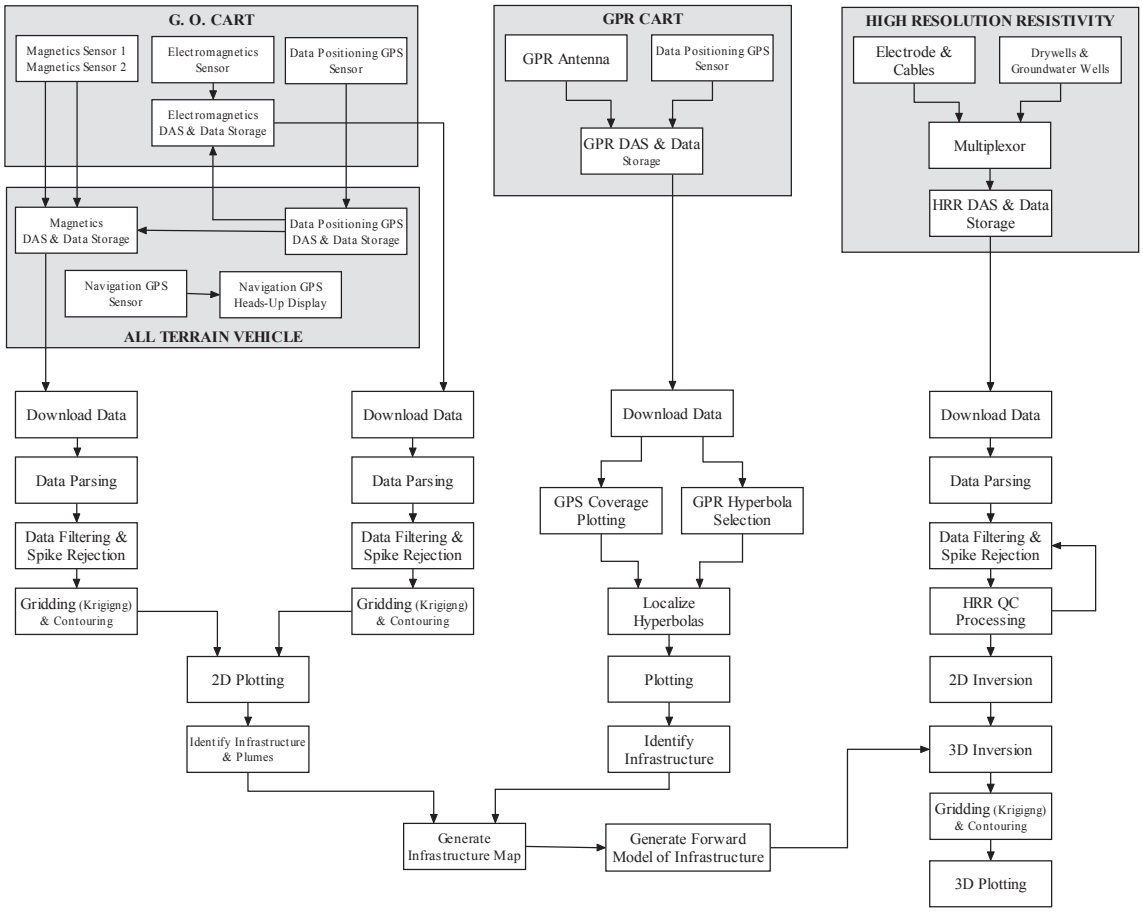

Several data parameters are plotted with respect to the x-axis plane along the line (i.e., pseudo-sectional format) to inspect data quality and consistency. Data parameters that are assessed during this step include: apparent resistivity (calculated by the measurement instrument), normalized potential (V/I), repeat error, and electrical current. Auto-filter (filtering technique within Microsoft Excel that easily segregates specific groups of data records based on user criteria, e.g., measured normalized voltage values below 0.001 ohms) is then applied to the data fields. The auto-filtering allows an operator to quickly interrogate a specific data range for each parameter. The data plots for all quality fields are linked to the auto-filters, and only show the resulting data that remains after a filter is applied. To remove any unsatisfactory data points, an operator selects the appropriate auto-filter range, determines which data points do not conform to the surrounding data population or conflict with potential theory, and then deletes the rows that contain the unsatisfactory points.

The following discussion provides a specific example data set to illustrate the general filtering process:

3. Figure A-2 shows an example of data that are targeted for removal. The low transmitted current produced measured data with high error (in relation to the data population). To ensure that the original data are retained and error removal can be repeated, the raw and edited data are saved to different folders with different file names. Data editing statistics are retained for QA purposes.

Figure A-2. Example of Noisy Data Removal using Repeat Error (left image) and Electrical Current (right image).

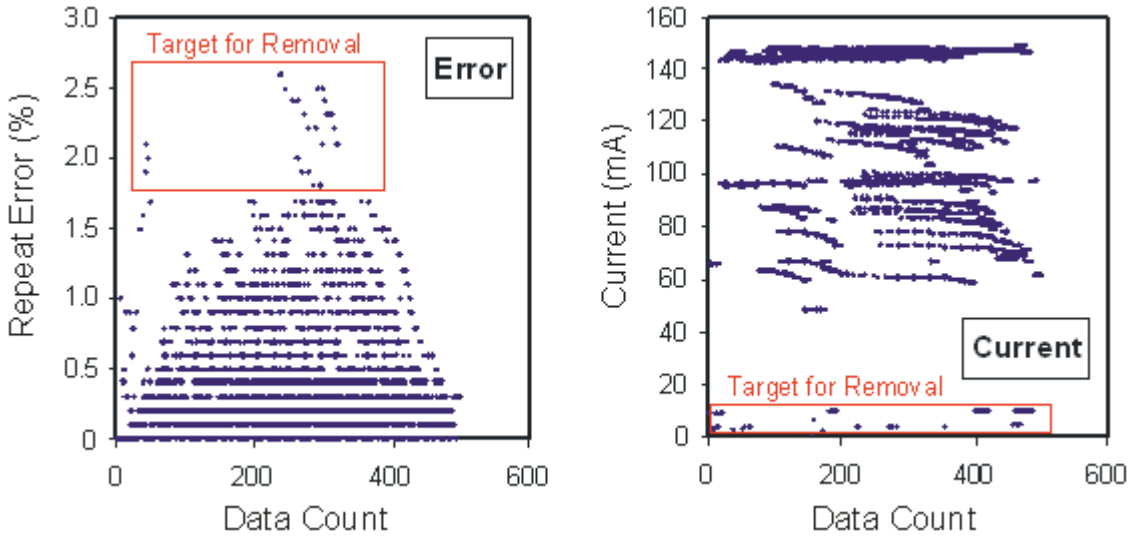

4. The result of the data removal in Step 1 is shown in Figure A-3. The data are plotted spatially according to the standard pseudo-section methodology. The left plot of Figure A-3 shows the distribution of all measurements and the right plot of Figure A-3 shows the distribution of data after removal of noisy data from Step 1.

Figure A-3. Example of Data Scatter (Plotted as Linear Pseudo-Section) Before and After Noisy Data Rejection.

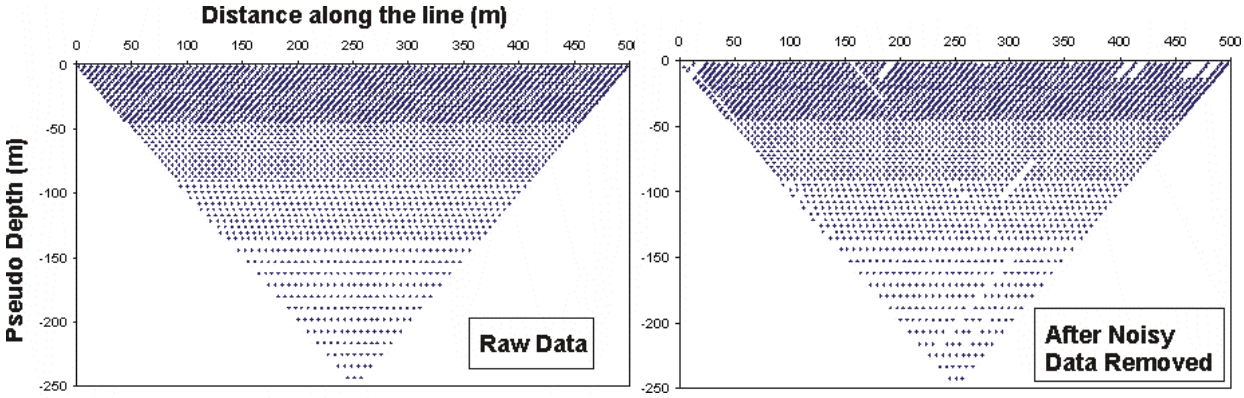

5. After data rejection is completed based on noise or error, data are evaluated for physical impossibilities as they relate to potential field theory. This step requires that the transfer resistance (V/I) for each transmitter electrode be plotted with all of the receiver electrodes. The plot should show a smoothly varying function as the separation of the transmitter and receiver electrode increases. Large spikes in the function are associated with suspect data points that represent physical impossibilities in natural media. In this case, these data are removed from the overall data set. Figure A-4 demonstrates an example of a data spike that is targeted for removal as it violates potential theory. The process involves individually assessing each data "sweep" based on transmitter and then repeating the process based on each receiver "sweep."

Figure A-4. Example of Spike Rejection of Transfer Resistance.

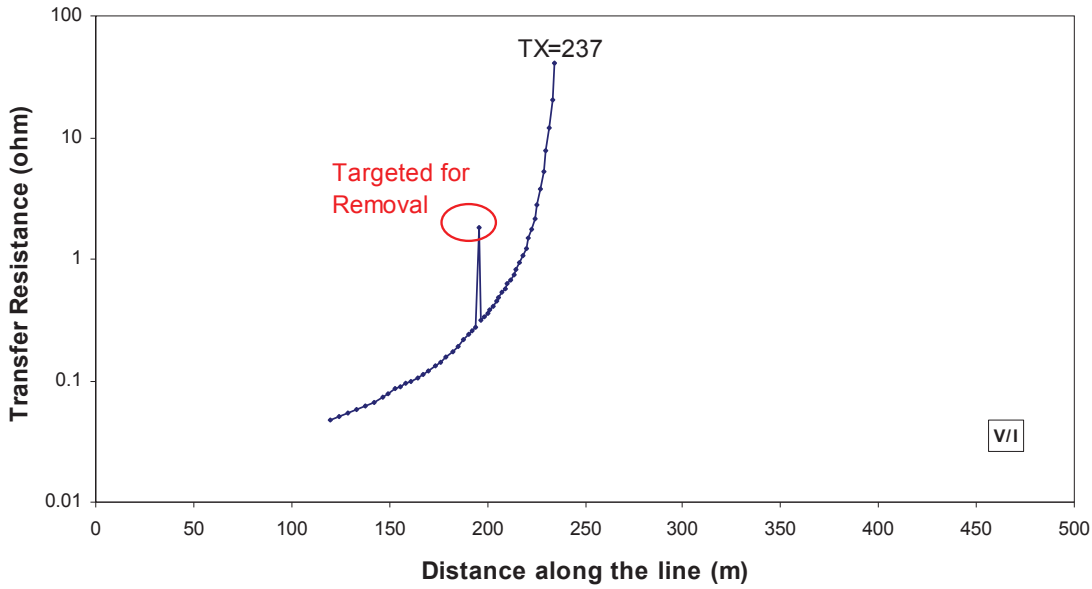

Filtering is accomplished by plotting all receivers associated with a particular transmitter. Using Figure A-5A as a guide, a single transmitter is shown with a series of receivers. The distance between a transmitter-receiver pair will dictate the depth at which the data point is represented. Figure A-5B shows how the entire subsurface is populated when considering all transmitter-receiver pairs. Figure A-5C shows a plot of the actual normalized voltage potential (V/I in ohms [transfer resistance]) associated with a transmitter. Within this plot are two example sets representing different types of spurious data: Line A, transmitter number 240 (Tx 222) with all receivers and Line B, Tx 234 with all receivers.

In the case of Line A, a single spike is evident on only one receiver when transmitting on transmitter number 240. The single point spike violates potential field theory and is therefore likely due to measurement error. Potential field theory, in summary, conveys that if the spike would have been from a very resistive layer, it would also have influence on all other measurements at larger separations. This is not the case in Figure A-5C. For filtering, this spike is removed from the data set due to its non-conformance. Often, spikes of this nature are associated with one bad receiver and will carry through a series of transmitters. In such a case, all data from the affected receiver may be removed from the data set. Conversely, these spikes may carry through a series of receivers and may be associated with one transmitter. Line A represents a fairly clean data set.

Line B presents multiple suspect data points. Little confidence can be placed in these data values for this particular transmitter. As a result, many points at multiple receiver locations would be removed during the filtering. Line B represents a relatively noisy data set.

Figure A-5D shows how the removal process affects the overall data coverage. The plot representing Line B shows that approximately 35 percent of the data are removed. This

represents a highly edited resistivity line. Line A, on the other hand, shows that approximately 3 percent of the data have been removed, representing a more lightly edited resistivity line.

Figure A-5. Data Filtering Example.

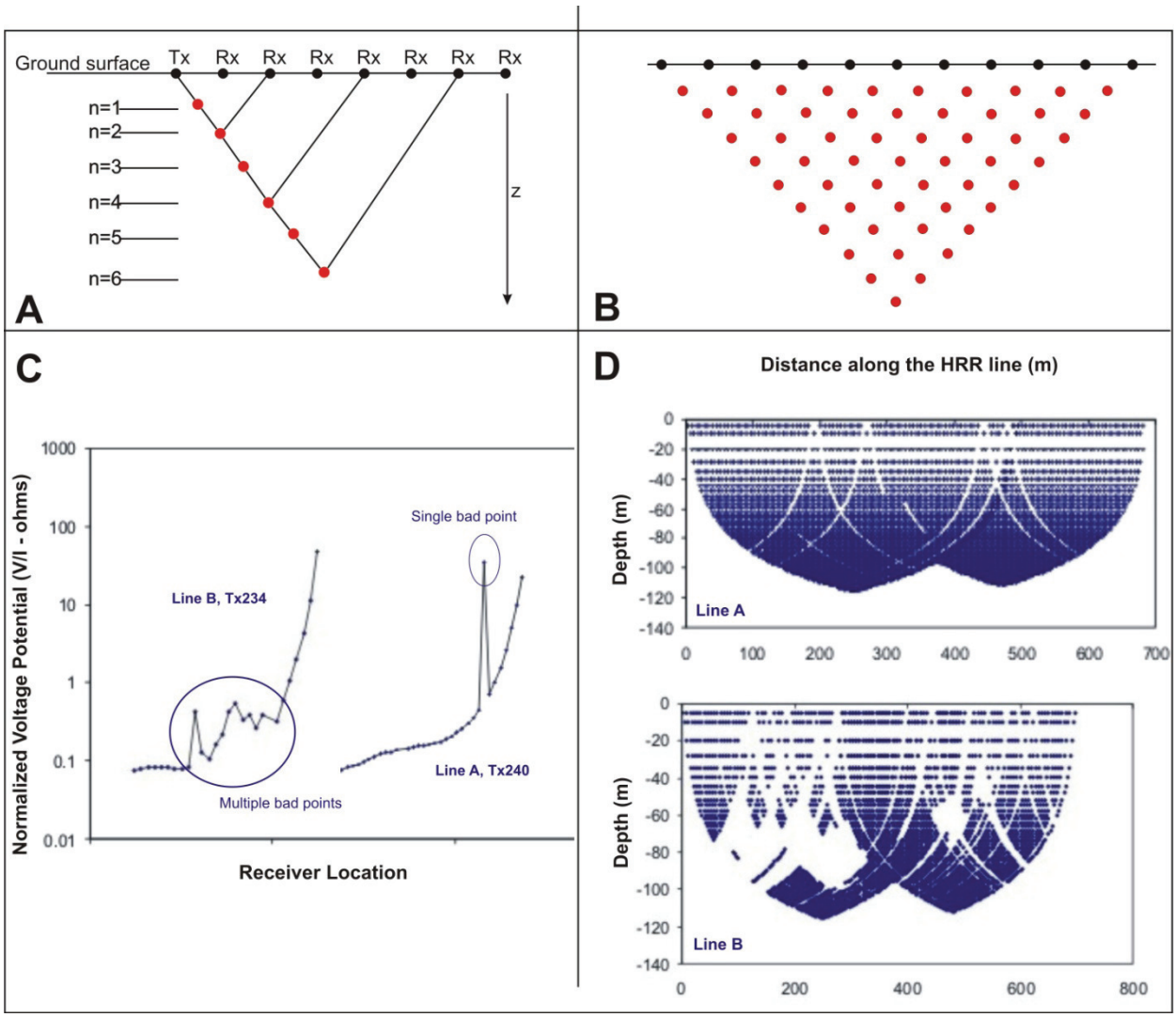

6. After eliminating all data that are considered low quality, the data are then passed through a processing algorithm that uses a geometric inversion technique. Measured normalized potential values are converted to an apparent resistivity at a depth that represents the highest sensitivity. The depth is a logarithmic function of electrode spacing. The HRR routine places the measured apparent resistivity value at a depth below ground surface that best represents its location.

7. The data are then plotted as HRR color-contoured cross-sections in Surfer® (Golden Software, Inc). The plot can be used as a quality check of data acceptability and data coverage, while also providing an approximation to the depth of the target. Refer to RPP-RPT-28955, 2006, *Surface Geophysical Exploration of T Tank Farm*, Revision 0, CH2M HILL Hanford Group, Inc., Richland, Washington for an explanation of resistivity theory and HRR. Figure A-6 displays an example of a contoured cross section.

Figure A-6. Example HRR Section.

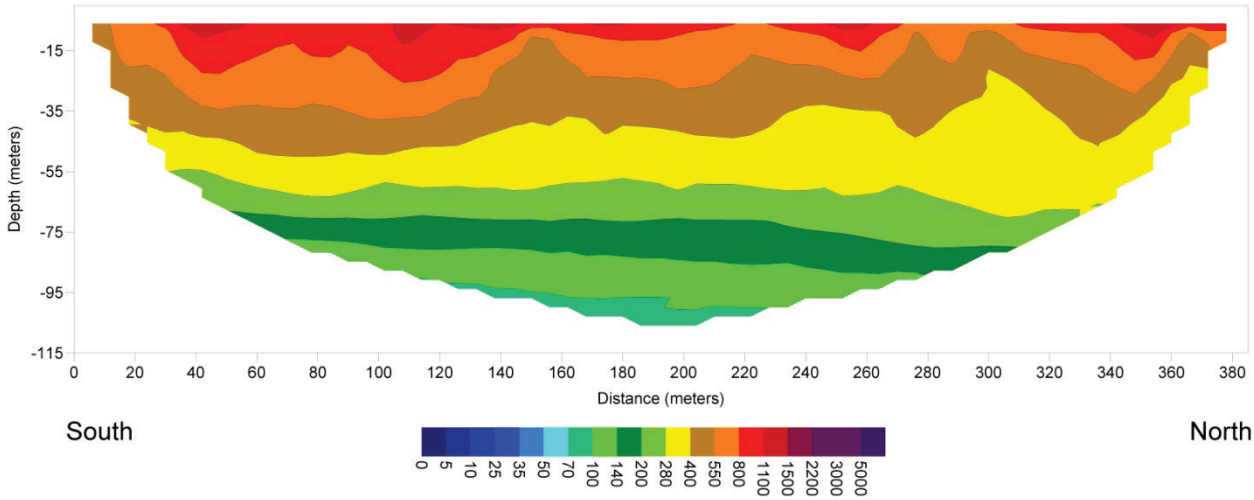

A1.2 DATA FILTERING STATISTICS FOR T FARM DATA

The T farm Data were filtered for inversion and data reduction statistics were recorded. Table A-1 displays statistics for data reduction performed on all twenty-seven T farm resistivity lines, detailing both the number and percentage of data points removed for each line. Approximately 15 percent of the total data were removed in the filtering process, with a minimum of 1.27 percent and a maximum of 46.26 percent removed on a line by line basis.

® Surfer is a registered trademark of Golden Software, Inc., Golden, Colorado.

Table A-1. Data Reduction Statistics for All T Farm HRR Lines.

Line	No. Data Points (Raw)	No. Data Points (Filtered)	No. Data Points Removed	Percent Data Removed
0E	3921	2539	1382	35.25
1E	1398	1107	291	20.82
2E	1623	1495	128	7.89
3E	5035	2706	2329	46.26
4E	4939	2957	1982	40.13
5E	4163	4010	153	3.68
6E	6439	6216	223	3.46
7E	6439	6322	117	1.82
8E	6391	6225	166	2.60
9E	6427	5202	1225	19.06
10E	3056	2767	289	9.46
11E	2353	2155	198	8.41
12E	2241	1879	362	16.15
13E	2149	2002	147	6.84
14E	2398	2041	357	14.89
15E	2469	2105	364	14.74
16E	2057	1595	462	22.46
0N	3201	2203	998	31.18
1N	7910	6926	984	12.44
2N	7920	5700	2220	28.03
3N	8686	7817	869	10.00
4N	7207	6339	868	12.04
5N	14483	11625	2858	19.73
6N	2972	2792	180	6.06
7N	1264	1248	16	1.27
8N	1272	1187	85	6.68
9N	4128	3859	269	6.52

The distribution of the total data set is shown below in Figure A-7, plotted as the log of the apparent resistivity versus the distance in meters between electrode pairs. For comparison, the distribution is presented pre- and post-filter. A dramatic reduction in noisy data is evident after data editing.

Figure A-7. Data Distribution.

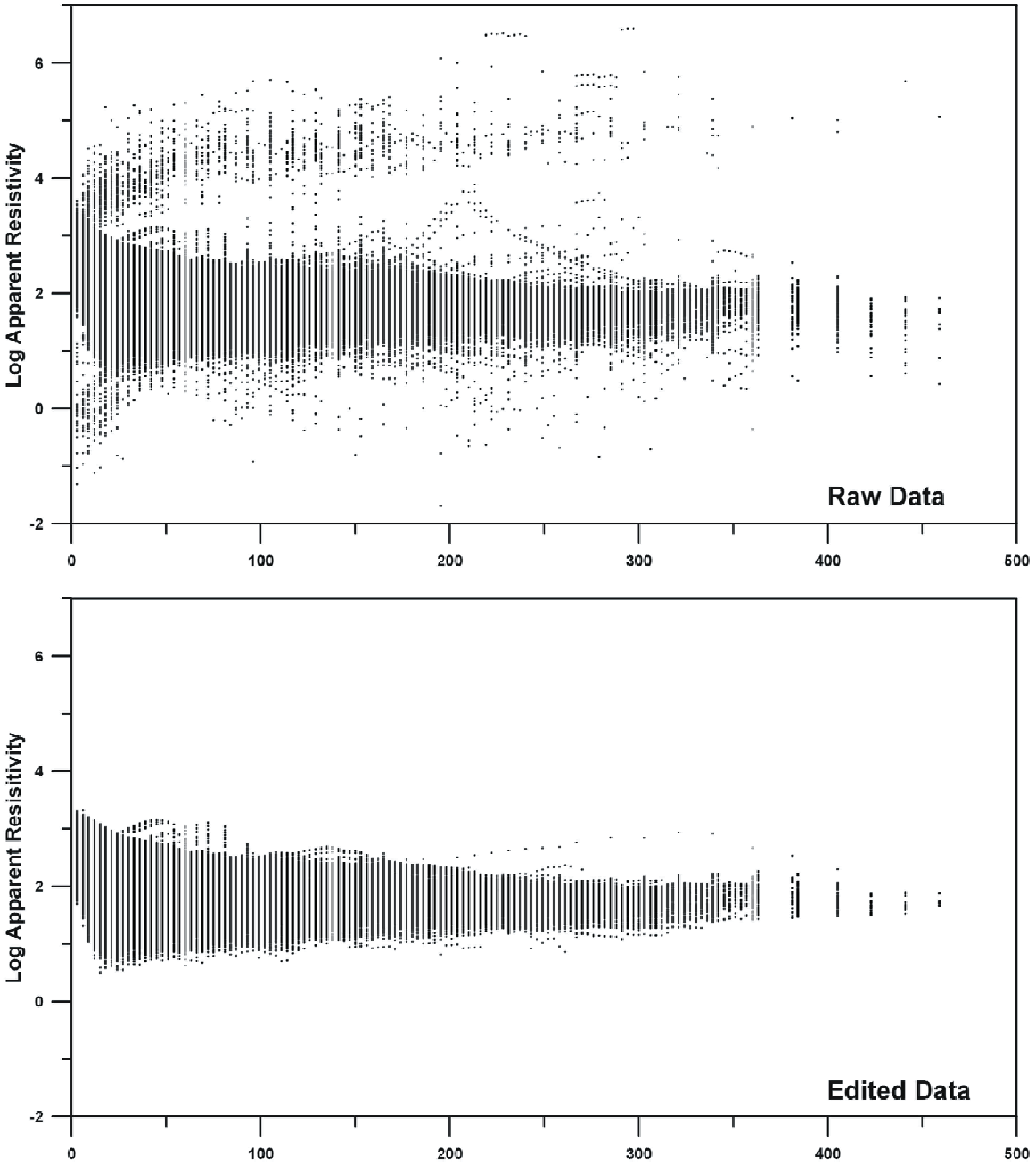

A2.0 REFERENCES

RPP-RPT-28955, 2006, *Surface Geophysical Exploration of T Tank Farm*, Revision 0, CH2M HILL Hanford Group, Inc., Richland, Washington.

RPP-RPT-36893, Revision 0, *Surface Geophysical Exploration of TX and TY Tank Farms at the Hanford Site: Results of Background Chracterization with Magnetics and Electromagnetics*, CH2M HILL Hanford Group, Inc., Richland, Washington.

RPP-RPT-38104, Revison 0, *Surface Geophysical Exploration of TX-TY Tank Farms at the Hanford Site: Results of Background Characterization with Ground Penetrating Radar*, CH2M HILL Hanford Group, Inc., Richland, Washington.

APPENDIX B

ELECTRICAL RESISTIVITY INVERSION FORMS

HGI hydroGEOPHYSICS	RES3D Inversion Model Tracking and Statistics			Page 1 of 2
	Date:	9/12/2009	Project Name:	Reprocessing of T Farm Resistivity
	Inversion Operator:	Dale Rucker	Project Number:	2009-020

ITEM	PARAMETER	REVIEWER Initial & DATE
Inversion Model Name	TFarm_PP_WTW_A	GN 9/12/09
Inversion Model Folder	\\snowwhite\Temp_Models\T Farm	
Data Processing Server Name	Happy	
Purpose or Description of Inversion Model	Characterization of T Farm and surrounding areas using compiled WTW data with a-priori well information.	
Raw Data File(s) & Location	\\snowwhite\2009-020 Reprocessing of T Farm Resistivity Data\Data\WTW\Raw WTW Data\WELDIPA.stg	GN 9/12
Input File Name & Location	\\snowwhite\Temp_Models\T Farm\TFarm PolePole LongElectrode Form.dat	GN 9/12
Description of Filtering/Editing Applied to Input File	For wells within 5 meters of each other one was chosen for data input, due to code restrictions and meshing requirements. Filtered very low and very high resistivity values. Filtered based on homogenous halfspace model using 95 ohm-meters as upper threshold and 19 ohm-meters as lower threshold.	
Inversion Parameter File Name & Location	\\snowwhite\Temp_Models\T Farm\TFarm PolePole LongElectrode Form.dat\Tfarm.ivp	
Output File Name & Location	\\snowwhite\Temp_Models\T Farm\TFarm PolePole LongElectrode Form_a.inv	GN 9/12
Start Date	Batch mode - Not available	GN 9/12
Start Time	Batch mode - Not available	
End Date	Batch mode - Not available	
End Time	Batch mode - Not available	
Avg. Hours per Iteration	10.26	
Total Running Hours	61.53	
System Pause Time (Hours)	0	
Northing Range(m)	235	GN 9/12
Easting Range(m)	306	
Easting Min (UTM)	566,629	
Northing Min (UTM)	136,648	
Easting Max (UTM)	566,935	
Northing Max (UTM)	136,883	
Domain Area (Sq meters)	71,910	
Domain Area (Acres)	17.8	
Software Name	RES3DINVx64	GN 9/12
Software Version	v.3.01.07	
Electrode Type	WTW	GN 9/12
No. Data Points	6,522	
No. Model Blocks	5,022	
Notes	Well Resistivity = 0.001, Cross sectional area = 0.04	GN 9/12

hydroGEOPHYSICS

RES3D Inversion Model Tracking and Statistics

Page 2 of 2

Date:	9/12/2009	**Project Name:**	Reprocessing of T Farm Resistivity
Inversion Operator:	Dale Rucker	**Project Number:**	2009-020

Iteration Number	RMS %	L2	Hrs	Min	Sec	D.Hr	Elapsed Time (D.Hr)
1	22.2577				44382	12.328	12.328
2	16.2556				88390	24.553	24.553
3	13.927				117967	32.769	32.769
4	12.3745				147632	41.009	41.009
5	11.4853				177277	49.244	49.244
6	10.1861				221525	61.535	61.535
7							
8							
9							
10							

CONVERGENCE CURVE

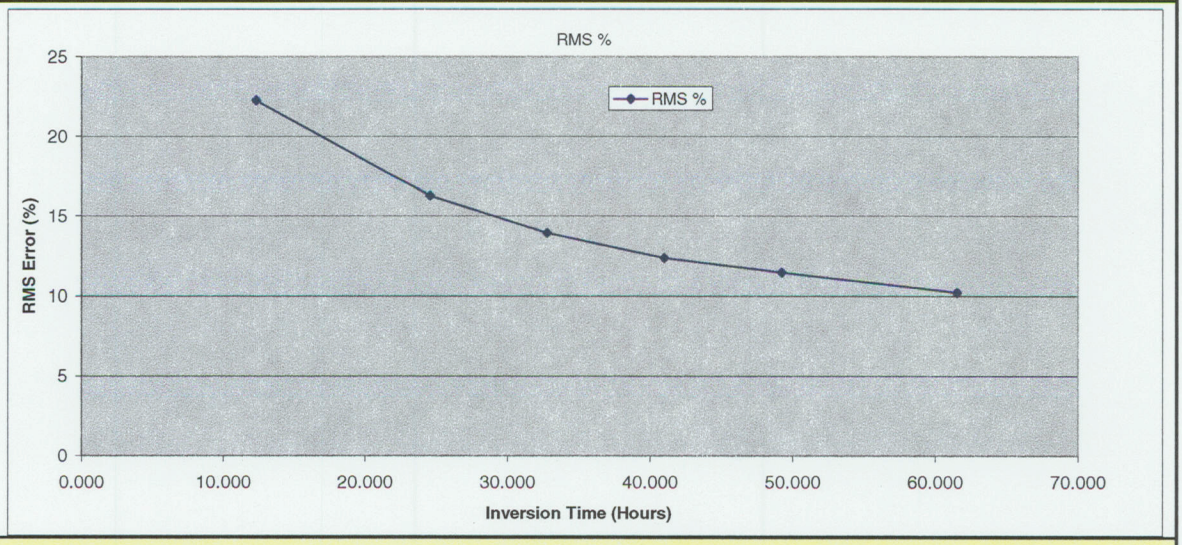

SIGNATURE

Inversion Operator Signature

9/12/09
Date

Reviewer Signature

Billian Noonan
Reviewer Name

9/12/09
Date

Project Manager Signature

James B. Fink
Project Manager Name

28 Sept 2009
Date

HGI hydroGEOPHYSICS	RES3D Inversion Model Tracking and Statistics			Page 1 of 2
	Date:	8/26/2009	Project Name:	Reprocessing of T Farm Resistivity
	Inversion Operator:	Dale Rucker	Project Number:	2009-020

ITEM	PARAMETER	REVIEWER Initial & DATE
Inversion Model Name	TFarm_PP_WTW_B	GN 8/26/09
Inversion Model Folder	\\snowwhite\Temp_Models\T Farm	
Data Processing Server Name	Happy	
Purpose or Description of Inversion Model	Characterization of T Farm and surrounding areas using compiled WTW data with a-priori well information.	
Raw Data File(s) & Location	\\snowwhite\2009-020 Reprocessing of T Farm Resistivity Data\Data\WTW\Raw WTW Data\WELDIPA.stg	GN 8/26
Input File Name & Location	\\snowwhite\Temp_Models\T Farm\TFarm PolePole LongElectrode Form.dat	GN 8/26
Description of Filtering/Editing Applied to Input File	For wells within 5 meters of each other one was chosen for data input, due to code restrictions and meshing requirements. Filtered very low and very high resistivity values. Filtered based on homogenous halfspace model using 95 ohm-meters as upper threshold and 19 ohm-meters as lower threshold.	
Inversion Parameter File Name & Location	\\snowwhite\Temp_Models\T Farm\Tfarm.ivp	
Output File Name & Location	\\snowwhite\Temp_Models\T Farm\TFarm PolePole LongElectrode Form_b.inv	GN 8/26
Start Date	Batch mode - Not available	GN 8/26
Start Time	Batch mode - Not available	
End Date	Batch mode - Not available	
End Time	Batch mode - Not available	
Avg. Hours per Iteration	9.29	
Total Running Hours	46.46	
System Pause Time (Hours)	0	
Northing Range(m)	235	GN 8/26
Easting Range(m)	306	
Easting Min (UTM)	566,629	
Northing Min (UTM)	136,648	
Easting Max (UTM)	566,935	
Northing Max (UTM)	136,883	
Domain Area (Sq meters)	71,910	
Domain Area (Acres)	17.8	
Software Name	RES3DINVx64	GN 8/26
Software Version	v.3.01.07	
Electrode Type	WTW	GN 8/26
No. Data Points	6,522	
No. Model Blocks	5,022	
Notes	Well Resistivity = 0.001, Cross sectional area = 0.1	GN 8/24

hydroGEOPHYSICS

RES3D Inversion Model Tracking and Statistics

Page 2 of 2

Date:	8/26/2009	Project Name:	Reprocessing of T Farm Resistivity
Inversion Operator:	Dale Rucker	Project Number:	2009-020

Iteration Number	RMS %	L2	Hrs	Min	Sec	D.Hr	Elapsed Time (D.Hr)
1	21.8852				38745	10.763	10.763
2	18.9024				64688	17.969	17.969
3	15.5084				90465	25.129	25.129
4	13.0862				116228	32.286	32.286
5	12.5518				167249	46.458	46.458
6							
7							
8							
9							
10							

CONVERGENCE CURVE

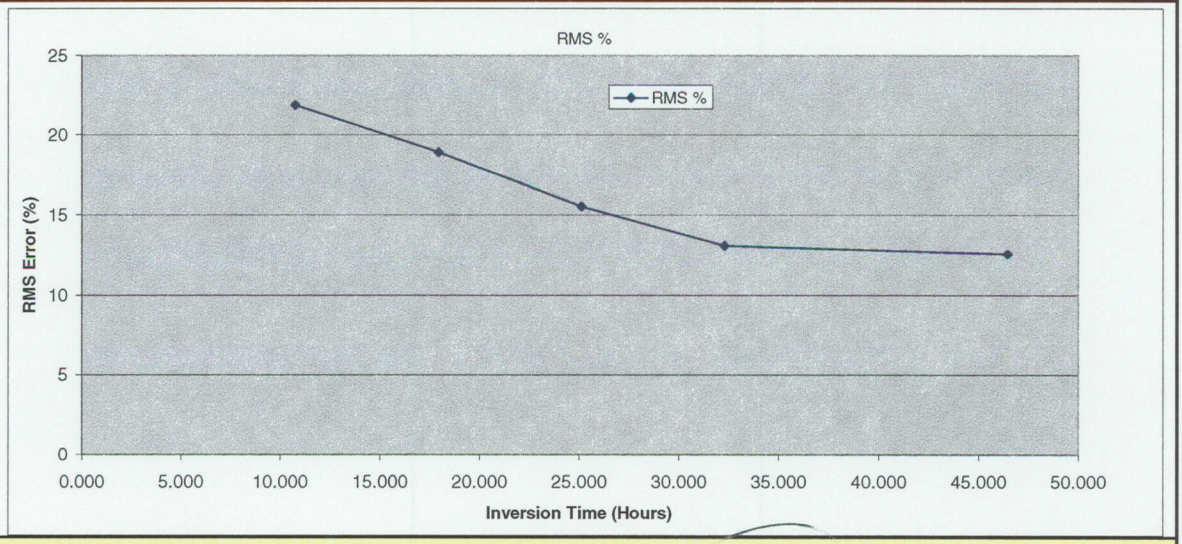

SIGNATURE

Inversion Operator Signature

8/26/09
Date

Reviewer Signature

Gillian Noonan
Reviewer Name

8/26/09
Date

Project Manager Signature

James B. Fink
Project Manager Name

28 Sept 2009
Date

HGI hydroGEOPHYSICS

RES3D Inversion Model Tracking and Statistics

Page 1 of 2

Date: 8/31/2009 **Project Name:** Reprocessing of T Farm Resistivity

Inversion Operator: Dale Rucker **Project Number:** 2009-020

ITEM	PARAMETER	REVIEWER Initial & DATE
Inversion Model Name	TFarm_PP_WTW_C	GN 8/31/09
Inversion Model Folder	\\snowwhite\Temp_Models\T Farm	
Data Processing Server Name	Happy	
Purpose or Description of Inversion Model	Characterization of T Farm and surrounding areas using compiled WTW data with a-priori well information.	
Raw Data File(s) & Location	\\snowwhite\2009-020 Reprocessing of T Farm Resistivity Data\Data\WTW\Raw WTW Data\WELDIPA.stg	GN 8/31
Input File Name & Location	\\snowwhite\Temp_Models\T Farm\TFarm PolePole LongElectrode Form.dat	GN 8/31
Description of Filtering/Editing Applied to Input File	For wells within 5 meters of each other one was chosen for data input, due to code restrictions and meshing requirements. Filtered very low and very high resistivity values. Filtered based on homogenous halfspace model using 95 ohm-meters as upper threshold and 19 ohm-meters as lower threshold.	
Inversion Parameter File Name & Location	\\snowwhite\Temp_Models\T Farm\Tfarm.ivp	
Output File Name & Location	\\snowwhite\Temp_Models\T Farm\TFarm PolePole LongElectrode Form_c.inv	GN 8/31
Start Date	Batch mode - Not available	GN 8/31
Start Time	Batch mode - Not available	
End Date	Batch mode - Not available	
End Time	Batch mode - Not available	
Avg. Hours per Iteration	10.26	
Total Running Hours	61.55	
System Pause Time (Hours)	0	
Northing Range(m)	235	GN 8/31
Easting Range(m)	306	
Easting Min (UTM)	566,629	
Northing Min (UTM)	136,648	
Easting Max (UTM)	566,935	
Northing Max (UTM)	136,883	
Domain Area (Sq meters)	71,910	
Domain Area (Acres)	17.8	
Software Name	RES3DINVx64	GN 8/31
Software Version	v.3.01.07	
Electrode Type	WTW	GN 8/31
No. Data Points	6,522	
No. Model Blocks	5,022	
Notes	Well Resistivity = 0.05, Cross sectional area = 0.5	GN 8/31

HGI hydroGEOPHYSICS

RES3D Inversion Model Tracking and Statistics

Page 2 of 2

Date:	8/31/2009	Project Name:	Reprocessing of T Farm Resistivity
Inversion Operator:	Dale Rucker	Project Number:	2009-020

Iteration Number	RMS %	L2	Hrs	Min	Sec	D.Hr	Elapsed Time (D.Hr)
1	18.9327				44332	12.314	12.314
2	16.3184				73770	20.492	20.492
3	14.166				103245	28.679	28.679
4	12.8257				147830	41.064	41.064
5	11.9857				177438	49.288	49.288
6	10.9112				221577	61.549	61.549
7							
8							
9							
10							

CONVERGENCE CURVE

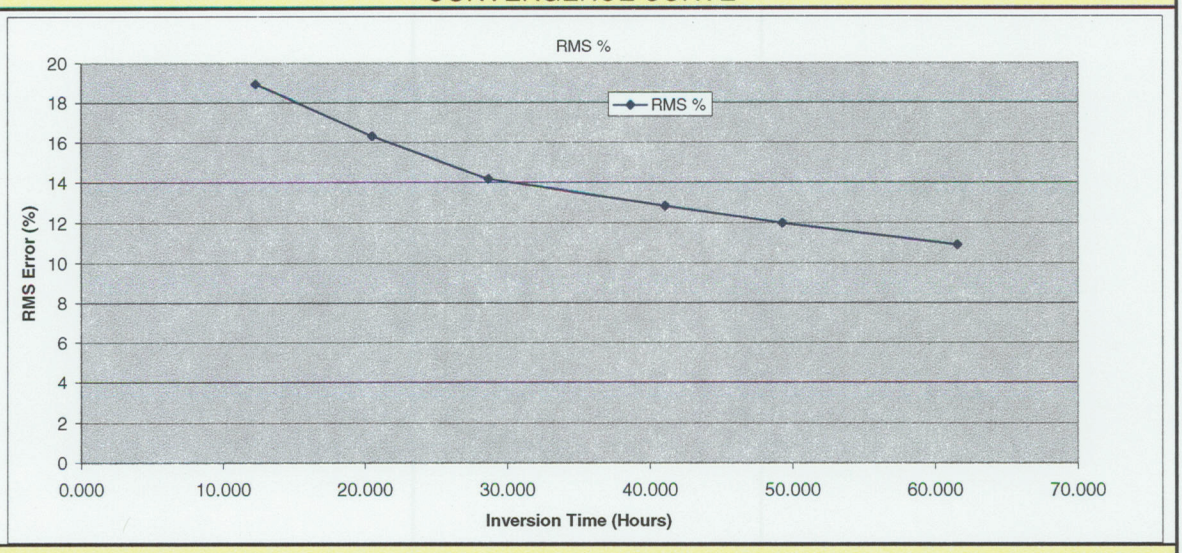

SIGNATURE

Inversion Operator Signature

8/31/09

Date

Reviewer Signature

Gillian Noonan

Reviewer Name

8/31/09

Date

Project Manager Signature

James B. Fink

Project Manager Name

28 Sept 2009

Date

HGI hydroGEOPHYSICS	RES3D Inversion Model Tracking and Statistics			Page 1 of 2
	Date: 9/3/2009	Project Name:	Reprocessing of T Farm Resistivity	
	Inversion Operator: Dale Rucker	Project Number:	2009-020	

ITEM	PARAMETER	REVIEWER Initial & DATE
Inversion Model Name	TFarm_PP_WTW_D	GN 9/3/09
Inversion Model Folder	\\snowwhite\Temp_Models\T Farm	
Data Processing Server Name	Happy	
Purpose or Description of Inversion Model	Characterization of T Farm and surrounding areas using compiled WTW data with a-priori well information.	
Raw Data File(s) & Location	\\snowwhite\2009-020 Reprocessing of T Farm Resistivity Data\Data\WTW\Raw WTW Data\WELDIPA.stg	GN 9/3
Input File Name & Location	\\snowwhite\Temp_Models\T Farm\TFarm PolePole LongElectrode Form.dat	GN 9/3
Description of Filtering/Editing Applied to Input File	For wells within 5 meters of each other one was chosen for data input, due to code restrictions and meshing requirements. Filtered very low and very high resistivity values. Filtered based on homogenous halfspace model using 95 ohm-meters as upper threshold and 19 ohm-meters as lower threshold.	
Inversion Parameter File Name & Location	\\snowwhite\Temp_Models\T Farm\Tfarm.ivp	
Output File Name & Location	\\snowwhite\Temp_Models\T Farm\TFarm PolePole LongElectrode Form_d.inv	GN 9/3
Start Date	Batch mode - Not available	GN 9/3
Start Time	Batch mode - Not available	
End Date	Batch mode - Not available	
End Time	Batch mode - Not available	
Avg. Hours per Iteration	9.59	
Total Running Hours	57.51	
System Pause Time (Hours)	0	
Northing Range(m)	235	GN 9/3
Easting Range(m)	306	
Easting Min (UTM)	566,629	
Northing Min (UTM)	136,648	
Easting Max (UTM)	566,935	
Northing Max (UTM)	136,883	
Domain Area (Sq meters)	71,910	
Domain Area (Acres)	17.8	
Software Name	RES3DINVx64	GN 9/3
Software Version	v.3.01.07	
Electrode Type	WTW	GN 9/3
No. Data Points	6,522	
No. Model Blocks	5,022	
Notes	Well Resistivity = 0.1, Cross sectional area = 0.5	GN 9/3

HGI hydroGEOPHYSICS

RES3D Inversion Model Tracking and Statistics

Page 2 of 2

Date: 9/3/2009 **Project Name:** Reprocessing of T Farm Resistivity

Inversion Operator: Dale Rucker **Project Number:** 2009-020

Iteration Number	RMS %	L2	Hrs	Min	Sec	D.Hr	Elapsed Time (D.Hr)
1	18.1697				44505	12.363	12.363
2	15.9215				74039	20.566	20.566
3	13.6901				103639	28.789	28.789
4	12.6271				147766	41.046	41.046
5	11.7797				177425	49.285	49.285
6	11.1021				207038	57.511	57.511
7							
8							
9							
10							

CONVERGENCE CURVE

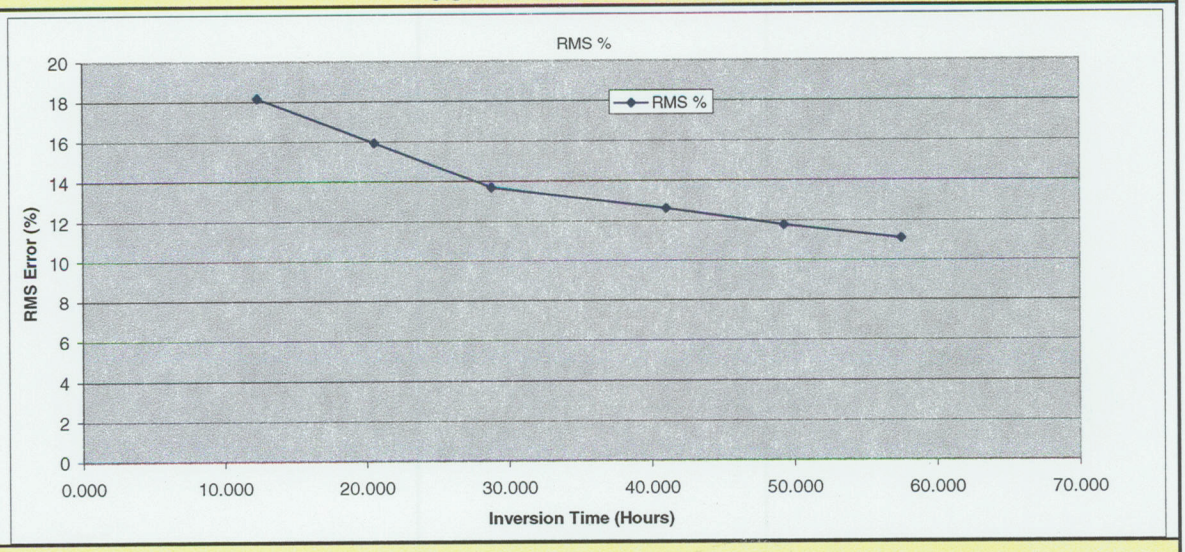

SIGNATURE

Inversion Operator Signature

9/5/09
Date

Reviewer Signature

Gillian Noonan
Reviewer Name

9/3/09
Date

Project Manager Signature

James B. Fink
Project Manager Name

28 Sept 2009
Date

HGI hydroGEOPHYSICS	RES3D Inversion Model Tracking and Statistics			Page 1 of 2
	Date: 9/5/2009	Project Name:	Reprocessing of T Farm Resistivity	
	Inversion Operator: Dale Rucker	Project Number:	2009-020	

ITEM	PARAMETER	REVIEWER Initial & DATE
Inversion Model Name	TFarm_PP_WTW_E	GN 9/5/09
Inversion Model Folder	\\snowwhite\Temp_Models\T Farm	
Data Processing Server Name	Happy	
Purpose or Description of Inversion Model	Characterization of T Farm and surrounding areas using compiled WTW data with a-priori well information.	
Raw Data File(s) & Location	\\snowwhite\2009-020 Reprocessing of T Farm Resistivity Data\Data\WTW\Raw WTW Data\WELDIPA.stg	GN 9/5
Input File Name & Location	\\snowwhite\Temp_Models\T Farm\TFarm PolePole LongElectrode Form.dat	GN 9/5/09
Description of Filtering/Editing Applied to Input File	For wells within 5 meters of each other one was chosen for data input, due to code restrictions and meshing requirements. Filtered very low and very high resistivity values. Filtered based on homogenous halfspace model using 95 ohm-meters as upper threshold and 19 ohm-meters as lower threshold.	
Inversion Parameter File Name & Location	\\snowwhite\Temp_Models\T Farm\Tfarm.ivp	
Output File Name & Location	\\snowwhite\Temp_Models\T Farm\TFarm PolePole LongElectrode Form_e.inv	GN 9/5
Start Date	Batch mode - Not available	GN 9/5
Start Time	Batch mode - Not available	
End Date	Batch mode - Not available	
End Time	Batch mode - Not available	
Avg. Hours per Iteration	10.24	
Total Running Hours	61.41	
System Pause Time (Hours)	0	
Northing Range(m)	235	GN 9/5
Easting Range(m)	306	
Easting Min (UTM)	566,629	
Northing Min (UTM)	136,648	
Easting Max (UTM)	566,935	
Northing Max (UTM)	136,883	
Domain Area (Sq meters)	71,910	
Domain Area (Acres)	17.8	
Software Name	RES3DINVx64	GN 9/5
Software Version	v.3.01.07	
Electrode Type	WTW	GN 9/5
No. Data Points	6,522	
No. Model Blocks	5,022	
Notes	Well Resistivity = 0.006, Cross sectional area = 0.1	GN 9/5

hydroGEOPHYSICS

RES3D Inversion Model Tracking and Statistics

Page 2 of 2

Date:	9/5/2009	Project Name:	Reprocessing of T Farm Resistivity
Inversion Operator:	Dale Rucker	Project Number:	2009-020

Iteration Number	RMS %	L2	Hrs	Min	Sec	D.Hr	Elapsed Time (D.Hr)
1	20.371				44318	12.311	12.311
2	15.988				88255	24.515	24.515
3	14.1341				117746	32.707	32.707
4	12.0973				147281	40.911	40.911
5	11.4444				176907	49.141	49.141
6	10.7688				221081	61.411	61.411
7							
8							
9							
10							

CONVERGENCE CURVE

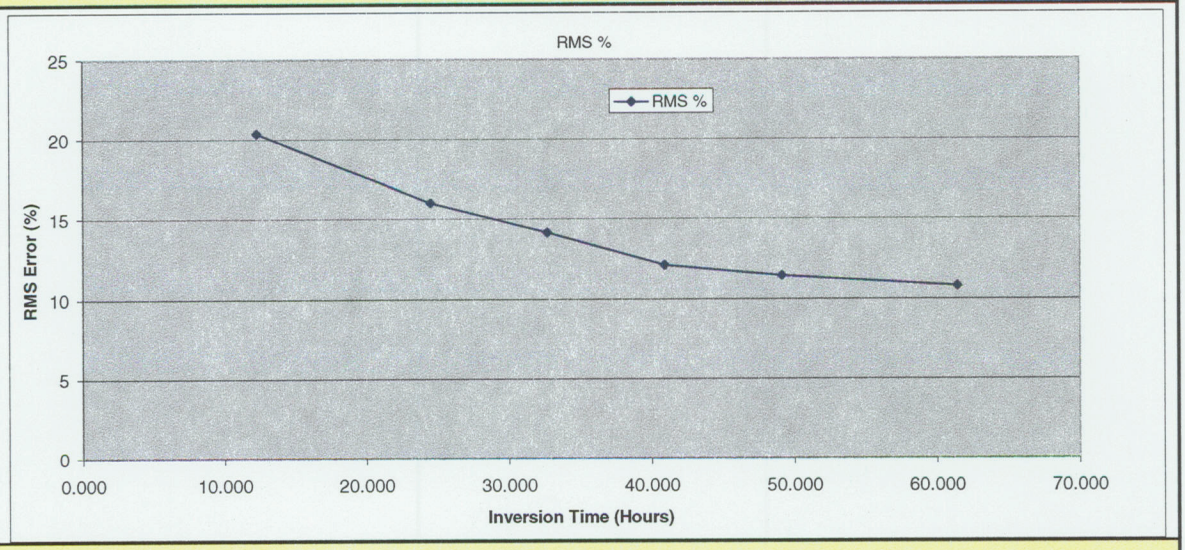

SIGNATURE

Inversion Operator Signature

9/5/09
Date

Reviewer Signature

Gillian Noonan
Reviewer Name

9/5/09
Date

Project Manager Signature

James B. Fink
Project Manager Name

28 Sept 2009
Date

HGI hydroGEOPHYSICS	RES3D Inversion Model Tracking and Statistics	Page 1 of 2
	Date: 9/9/2009 Project Name: Reprocessing of T Farm Resistivity	
	Inversion Operator: Dale Rucker Project Number: 2009-020	

ITEM	PARAMETER	REVIEWER Initial & DATE
Inversion Model Name	TFarm_PP_DD_WTW	GN 9/9/09
Inversion Model Folder	\\snowwhite\Temp_Models\T Farm	
Data Processing Server Name	Happy	
Purpose or Description of Inversion Model	Characterization of T Farm and surrounding areas using compiled mixed pole pole and dipole dipole WTW data with a-priori well information.	
Raw Data File(s) & Location	\\snowwhite\2009-020 Reprocessing of T Farm Resistivity Data\Data\WTW\Raw WTW Data\WELDIPA.stg and DIPDIPA.stg	GN 9/9/09
Input File Name & Location	\\snowwhite\Temp_Models\T Farm\TFarm LongElectrode mixed data.dat	GN 9/9/09
Description of Filtering/Editing Applied to Input File	For wells within 5 meters of each other one was chosen for data input, due to code restrictions and meshing requirements. Filtered very low and very high resistivity values. Filtered based on homogenous halfspace model using 95 ohm-meters as upper threshold and 19 ohm-meters as lower threshold. For dipole dipole, also removed duplicates and negative apparent resistivity data.	
Inversion Parameter File Name & Location	\\snowwhite\Temp_Models\T Farm\Tfarm.ivp	
Output File Name & Location	\\snowwhite\Temp_Models\T Farm\TFarm LongElectrode mixed data.inv	GN 9/9
Start Date	Batch mode - Not available	GN 9/9
Start Time	Batch mode - Not available	
End Date	Batch mode - Not available	
End Time	Batch mode - Not available	
Avg. Hours per Iteration	8.95	
Total Running Hours	53.69	
System Pause Time (Hours)	0	
Northing Range(m)	235	GN 9/9
Easting Range(m)	306	
Easting Min (UTM)	566,629	
Northing Min (UTM)	136,648	
Easting Max (UTM)	566,935	
Northing Max (UTM)	136,883	
Domain Area (Sq meters)	71,910	
Domain Area (Acres)	17.8	
Software Name	RES3DINVx64	GN 9/9
Software Version	v.3.01.07	
Electrode Type	WTW	GN 9/9
No. Data Points	7,303	
No. Model Blocks	5,022	
Notes	Well Resistivity = 0.006, Cross sectional area = 0.1	GN 9/9

hydroGEOPHYSICS

RES3D Inversion Model Tracking and Statistics

Page 2 of 2

Date: 9/9/2009 **Project Name:** Reprocessing of T Farm Resistivity

Inversion Operator: Dale Rucker **Project Number:** 2009-020

Iteration Number	RMS %	L2	Hrs	Min	Sec	D.Hr	Elapsed Time (D.Hr)
1	22.974				44466	12.352	12.352
2	12.2878				73940	20.539	20.539
3	9.1667				103506	28.752	28.752
4	8.595				133280	37.022	37.022
5	6.813				163199	45.333	45.333
6	6.1182				193271	53.686	53.686
7							
8							
9							
10							

CONVERGENCE CURVE

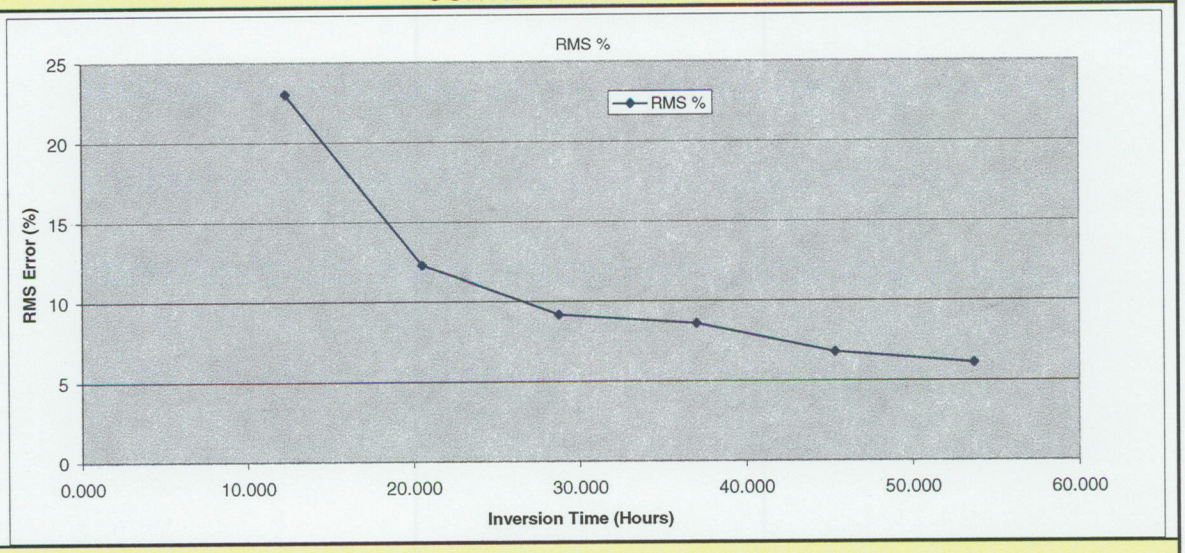

SIGNATURE

Inversion Operator Signature

9/9/09

Date

Reviewer Signature

Gillian Noonan

Reviewer Name

9/9/09

Date

Project Manager Signature

James B. Fink

Project Manager Name

28 Sept 2009

Date

HGI hydroGEOPHYSICS	RES3D Inversion Model Tracking and Statistics	Page 1 of 2
	Date: 9/9/2009 Project Name: Reprocessing of T Farm Resistivity	
	Inversion Operator: Dale Rucker Project Number: 2009-020	

ITEM	PARAMETER	REVIEWER Initial & DATE
Inversion Model Name	TFarm_PP_WTW_GW	GW 9/9/09
Inversion Model Folder	\\snowwhite\Temp_Models\T Farm	
Data Processing Server Name	Happy	
Purpose or Description of Inversion Model	Characterization of T Farm and surrounding areas using compiled pole pole WTW data with groundwater wells only.	
Raw Data File(s) & Location	\\snowwhite\2009-020 Reprocessing of T Farm Resistivity Data\Data\WTW\Raw WTW Data\WELDIPA.stg	GW 9/9
Input File Name & Location	\\snowwhite\Temp_Models\T Farm\T Farm GW Wells.dat	GW 9/9
Description of Filtering/Editing Applied to Input File	For wells within 5 meters of each other one was chosen for data input, due to code restrictions and meshing requirements. Filtered very low and very high resistivity values. Filtered based on homogenous halfspace model using 95 ohm-meters as upper threshold and 19 ohm-meters as lower threshold.	
Inversion Parameter File Name & Location	\\snowwhite\Temp_Models\T Farm\Tfarm.ivp	
Output File Name & Location	\\snowwhite\Temp_Models\T Farm\T Farm GW Wells.inv	GW 9/9
Start Date	Batch mode - Not available	GW 9/9
Start Time	Batch mode - Not available	
End Date	Batch mode - Not available	
End Time	Batch mode - Not available	
Avg. Hours per Iteration	0.33	
Total Running Hours	1.99	
System Pause Time (Hours)	0	
Northing Range(m)	305	GW 9/9
Easting Range(m)	272	
Easting Min (UTM)	566,663	
Northing Min (UTM)	136,578	
Easting Max (UTM)	566,935	
Northing Max (UTM)	136,883	
Domain Area (Sq meters)	82,960	
Domain Area (Acres)	20.5	
Software Name	RES3DINVx64	GW 9/9
Software Version	v.3.01.07	
Electrode Type	WTW	GW 9/9
No. Data Points	183	
No. Model Blocks	896	
Notes	Well Resistivity = 0.006, Cross sectional area = 0.1	GW 9/9

hydroGEOPHYSICS

RES3D Inversion Model Tracking and Statistics

Page 2 of 2

Date:	9/9/2009	Project Name:	Reprocessing of T Farm Resistivity
Inversion Operator:	Dale Rucker	Project Number:	2009-020

Iteration Number	RMS %	L2	Hrs	Min	Sec	D.Hr	Elapsed Time (D.Hr)
1	13.5381				1653	0.459	0.459
2	10.8527				2754	0.765	0.765
3	8.9135				3854	1.071	1.071
4	6.9783				4953	1.376	1.376
5	6.0902				6052	1.681	1.681
6	4.9205				7153	1.987	1.987
7							
8							
9							
10							

CONVERGENCE CURVE

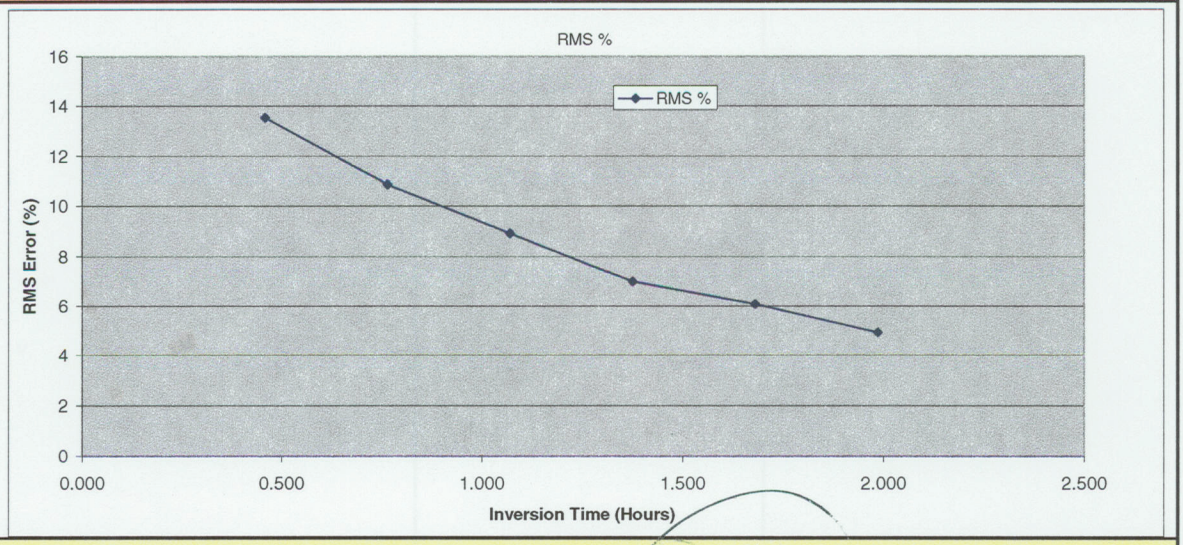

SIGNATURE

Inversion Operator Signature

9/9/09
Date

Reviewer Signature

Gillian Noonan
Reviewer Name

9/9/09
Date

Project Manager Signature

James B. Fink
Project Manager Name

28 Sept 2009
Date

HGI hydroGEOPHYSICS	RES3D Inversion Model Tracking and Statistics			Page 1 of 2
	Date:	8/27/2009	Project Name:	Reprocessing of T Farm Resistivity
	Inversion Operator:	Dale Rucker	Project Number:	2009-020

ITEM	PARAMETER	REVIEWER Initial & DATE
Inversion Model Name	T Farm Pole-Pole W Domain	GN 8/27/09
Inversion Model Folder	\\happy\Data\T Farm\WDomain	
Data Processing Server Name	Happy	
Purpose or Description of Inversion Model	Characterization of Area West of T Farm using compiled STS data.	
Raw Data File(s) & Location	Y:\2009-020 Reprocessing of T Farm Resistivity Data\Data\STS\Alldata_coords_ROUNDED.txt	GN 8/27
Input File Name & Location	\\happy\Data\T Farm\WDomain\Wdomain_RES3D_3E.dat	GN 8/27
Description of Filtering/Editing Applied to Input File	Filtered negative, high error and outlying resistivity values. Removed repeated TX/RX data. GPS locations were rounded to fit a 3 meter grid.	
Inversion Parameter File Name & Location	\\happy\Data\T Farm\WDomain\TFarm.ivp	
Output File Name & Location	\\happy\Data\T Farm\WDomain\Wdomain_RES3D_3E.inv	GN 8/27
Start Date	Batch mode - Not available	GN 8/27
Start Time	Batch mode - Not available	
End Date	Batch mode - Not available	
End Time	Batch mode - Not available	
Avg. Hours per Iteration	1.54	
Total Running Hours	9.23	
System Pause Time (Hours)	0	
Northing Range(m)	354	GN 8/27
Easting Range(m)	249	
Easting Min (UTM)	566,481	
Northing Min (UTM)	136,536	
Easting Max (UTM)	566,730	
Northing Max (UTM)	136,890	
Domain Area (Sq meters)	88,146	
Domain Area (Acres)	21.8	
Software Name	RES3DINVx64	GN 8/27
Software Version	v.3.01.07	
Electrode Type	STS	GN 8/27
No. Data Points	17,910	
No. Model Blocks	9,794	
Notes		GN 8/27

HGI hydroGEOPHYSICS

RES3D Inversion Model Tracking and Statistics

Page 2 of 2

Date:	8/27/2009	Project Name:	Reprocessing of T Farm Resistivity
Inversion Operator:	Dale Rucker	Project Number:	2009-020

Iteration Number	RMS %	L2	Hrs	Min	Sec	D.Hr	Elapsed Time (D.Hr)
1	41.7627				5109	1.419	1.419
2	26.2277				8344	2.318	2.318
3	13.5583				12970	3.603	3.603
4	11.3512				16192	4.498	4.498
5	10.9054				19410	5.392	5.392
6							
7							
8							
9							
10							

CONVERGENCE CURVE

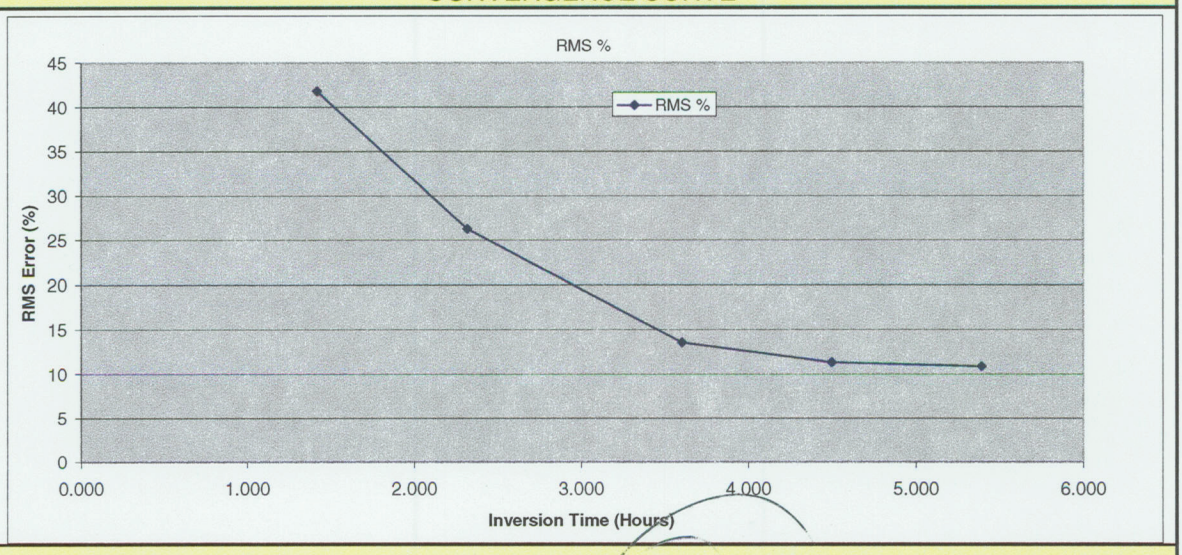

SIGNATURE

Inversion Operator Signature

8/27/09
Date

Reviewer Signature

Gillian Noonan
Reviewer Name

8/27/09
Date

Project Manager Signature

James B. Fink
Project Manager Name

28 Sept 2009
Date

HGI hydroGEOPHYSICS	RES3D Inversion Model Tracking and Statistics	Page 1 of 2
	Date: 9/5/2009 **Project Name:** Reprocessing of T Farm Resistivity	
	Inversion Operator: Dale Rucker **Project Number:** 2009-020	

ITEM	PARAMETER	REVIEWER Initial & DATE
Inversion Model Name	T Farm Pole-Pole NE Domain	GN 9/5/09
Inversion Model Folder	\\happy\Data\T Farm\NEDomain	
Data Processing Server Name	Happy	
Purpose or Description of Inversion Model	Characterization of Area Northeast of T Farm using compiled STS data.	
Raw Data File(s) & Location	Y:\2009-020 Reprocessing of T Farm Resistivity Data\Data\STS\Alldata_coords_ROUNDED.txt	GN 9/5
Input File Name & Location	\\happy\Data\T Farm\NEDomain\NEdomain_RES3D.dat	GN 9/5
Description of Filtering/Editing Applied to Input File	Filtered negative, high error and outlying resistivity values. Removed repeated TX/RX data. GPS locations were rounded to fit a 3 meter grid.	
Inversion Parameter File Name & Location	\\happy\Data\T Farm\NEDomain\TFarm.ivp	
Output File Name & Location	\\happy\Data\T Farm\NEDomain\NEdomain_RES3D.inv	GN 9/5
Start Date	Batch mode - Not available	GN 9/5
Start Time	Batch mode - Not available	
End Date	Batch mode - Not available	
End Time	Batch mode - Not available	
Avg. Hours per Iteration	8.01	
Total Running Hours	48.06	
System Pause Time (Hours)	0	
Northing Range(m)	255	GN 9/5
Easting Range(m)	258	
Easting Min (UTM)	566,910	
Northing Min (UTM)	136,746	
Easting Max (UTM)	567,168	
Northing Max (UTM)	137,001	
Domain Area (Sq meters)	65,790	
Domain Area (Acres)	16.3	
Software Name	RES3DINVx64	GN 9/5
Software Version	v.3.01.07	
Electrode Type	STS	GN 9/5
No. Data Points	17,638	
No. Model Blocks	7,310	
Notes		

hydroGEOPHYSICS

RES3D Inversion Model Tracking and Statistics

Page 2 of 2

Date:	9/5/2009	Project Name:	Reprocessing of T Farm Resistivity
Inversion Operator:	Dale Rucker	Project Number:	2009-020

Iteration Number	RMS %	L2	Hrs	Min	Sec	D.Hr	Elapsed Time (D.Hr)
1	21.5043				37593	10.443	10.443
2	13.2534				62297	17.305	17.305
3	10.1446				87005	24.168	24.168
4	8.497				123485	34.301	34.301
5	7.4188				148269	41.186	41.186
6	6.5087				173013	48.059	48.059
7							
8							
9							
10							

CONVERGENCE CURVE

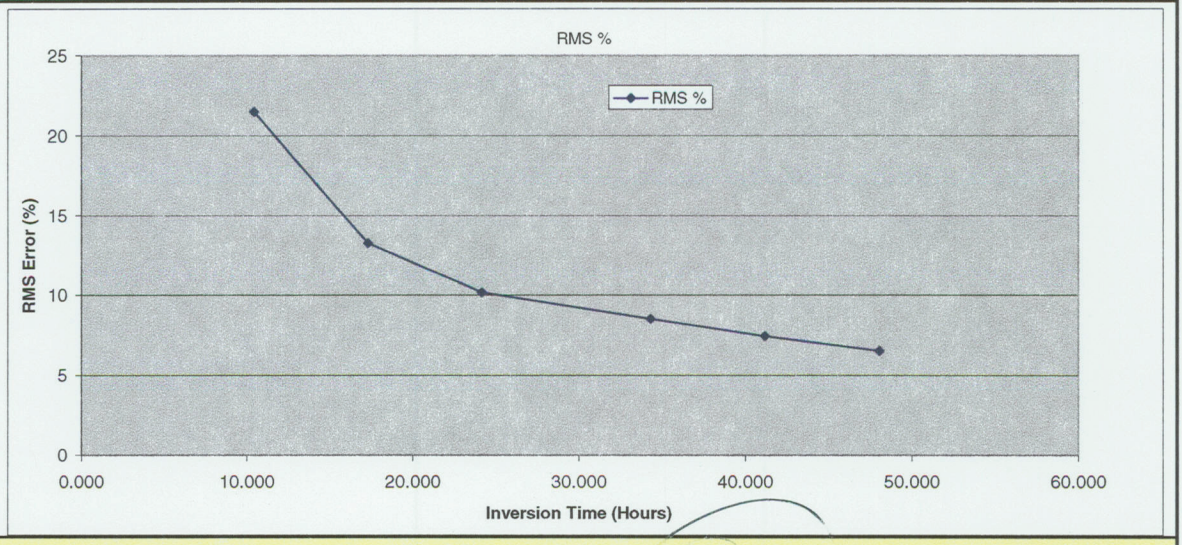

SIGNATURE

Inversion Operator Signature

9/5/09
Date

Reviewer Signature

Billian Noonan
Reviewer Name

9/5/09
Date

Project Manager Signature

James B. Fink
Project Manager Name

28 Sept 2009
Date

HGI hydroGEOPHYSICS	RES3D Inversion Model Tracking and Statistics			Page 1 of 2
	Date:	9/12/2009	Project Name:	Reprocessing of T Farm Resistivity
	Inversion Operator:	Dale Rucker	Project Number:	2009-020

ITEM	PARAMETER	REVIEWER Initial & DATE
Inversion Model Name	T Farm Pole-Pole Entire Domain	GN 9/12/09
Inversion Model Folder	\\happy\Data\T Farm\Entire Domain	
Data Processing Server Name	Happy	
Purpose or Description of Inversion Model	Characterization of T Farm and surrounding areas using compiled STS data.	
Raw Data File(s) & Location	Y:\2009-020 Reprocessing of T Farm Resistivity Data\Data\STS\Alldata_coords_ROUNDED.txt	GN 9/12
Input File Name & Location	\\happy\Data\T Farm\Entire Domain\TFarm_EntireDomain.dat	GN 9/12
Description of Filtering/Editing Applied to Input File	Filtered negative, high error and outlying resistivity values. Removed repeated TX/RX data. GPS locations were rounded to fit a 3 meter grid.	
Inversion Parameter File Name & Location	\\happy\Data\T Farm\Entire Domain\entire domain.ivp	
Output File Name & Location	\\happy\Data\T Farm\Entire Domain\TFarm_EntireDomain.inv	GN 9/12
Start Date	Batch mode - Not available	GN 9/12
Start Time	Batch mode - Not available	
End Date	Batch mode - Not available	
End Time	Batch mode - Not available	
Avg. Hours per Iteration	5.38	
Total Running Hours	32.27	
System Pause Time (Hours)	0	
Northing Range(m)	372	GN 9/12
Easting Range(m)	549	
Easting Min (UTM)	566,550	
Northing Min (UTM)	136,551	
Easting Max (UTM)	567,099	
Northing Max (UTM)	136,923	
Domain Area (Sq meters)	204,228	
Domain Area (Acres)	50.5	
Software Name	RES3DINVx64	GN 9/12
Software Version	v.3.01.07	
Electrode Type	STS	GN 9/12
No. Data Points	88,508	
No. Model Blocks	22,692	
Notes		

hydroGEOPHYSICS

RES3D Inversion Model Tracking and Statistics

Page 2 of 2

Date:	9/12/2009	Project Name:	Reprocessing of T Farm Resistivity
Inversion Operator:	Dale Rucker	Project Number:	2009-020

Iteration Number	RMS %	L2	Hrs	Min	Sec	D.Hr	Elapsed Time (D.Hr)
1	62.5513				31007	8.613	8.613
2	43.7093				47799	13.278	13.278
3	39.2332				64760	17.989	17.989
4	35.1395				81936	22.760	22.760
5	32.5265				98944	27.484	27.484
6	31.6589				116162	32.267	32.267
7							
8							
9							
10							

CONVERGENCE CURVE

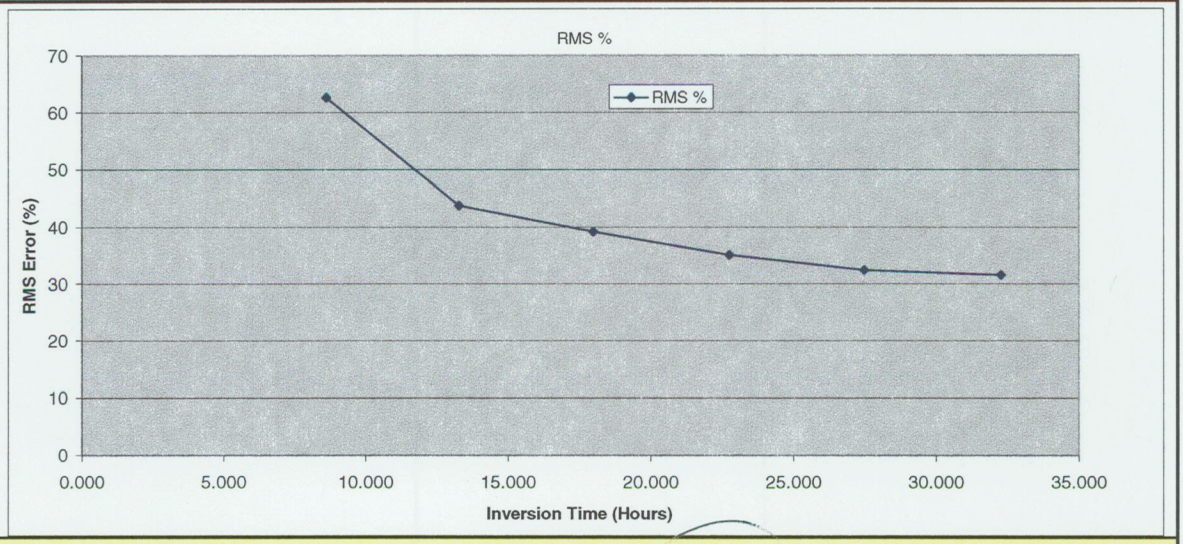

SIGNATURE

Inversion Operator Signature

9/12/09
Date

Reviewer Signature

Gillian Noonan
Reviewer Name

9/12/09
Date

Project Manager Signature

James B. Fink
Project Manager Name

28 Sept 2009
Date

HGI hydroGEOPHYSICS	RES3D Inversion Model Tracking and Statistics	Page 1 of 2
	Date: 9/23/2009 **Project Name:** Reprocessing of T Farm Resistivity	
	Inversion Operator: Dale Rucker **Project Number:** 2009-020	

ITEM	PARAMETER	REVIEWER Initial & DATE
Inversion Model Name	TFarm_PP_WTS	GN 9/23
Inversion Model Folder	\\snowwhite\Temp_Models\T Farm	
Data Processing Server Name	snowwhite	
Purpose or Description of Inversion Model	Characterization of T Farm and surrounding areas using compiled pole pole WTS data.	
Raw Data File(s) & Location	\\snowwhite\jobs\2009-020 Reprocessing of T Farm Resistivity Data\Data\WTS\Original Work	GN 9/23
Input File Name & Location	\\snowwhite\Temp_Models\T Farm\TFarm WTS.dat	GN 9/23
Description of Filtering/Editing Applied to Input File	Filtered negative, high error and outlying resistivity values. Removed repeated TX/RX data. GPS locations of the surface electrodes were rounded to fit a 3 meter grid. For wells within 5 meters of each other one was chosen for data input, due to code restrictions and meshing requirements. Filtered very low and very high resistivity values. Removed duplicates, removed close proximity wells, removed negative app res data.	
Inversion Parameter File Name & Location	\\snowwhite\Temp_Models\T Farm\TFarm WTS.ivp	
Output File Name & Location	\\snowwhite\Temp_Models\T Farm\TFarm WTS.inv	GN 9/22
Start Date	Batch mode - Not available	GN 9/23
Start Time	Batch mode - Not available	
End Date	Batch mode - Not available	
End Time	Batch mode - Not available	
Avg. Hours per Iteration	3.89	
Total Running Hours	23.35	
System Pause Time (Hours)	0	
Northing Range(m)	347	GN 9/23
Easting Range(m)	365	
Easting Min (UTM)	566,629	
Northing Min (UTM)	136,536	
Easting Max (UTM)	566,994	
Northing Max (UTM)	136,883	
Domain Area (Sq meters)	126,655	
Domain Area (Acres)	31.3	
Software Name	RES3DINVx64	GN 9/22
Software Version	v.3.01.07	
Electrode Type	WTS	GN 9/23
No. Data Points	18,424	
No. Model Blocks	3,658	
Notes	Well Resistivity = 0.006, Cross sectional area = 0.1	GN 9/23

hydroGEOPHYSICS

RES3D Inversion Model Tracking and Statistics

Page 2 of 2

Date: 9/23/2009 **Project Name:** Reprocessing of T Farm Resistivity

Inversion Operator: Dale Rucker **Project Number:** 2009-020

Iteration Number	RMS %	L2	Hrs	Min	Sec	D.Hr	Elapsed Time (D.Hr)
1	30.1907				16939	4.705	4.705
2	25.8704				33400	9.278	9.278
3	23.8574				44625	12.396	12.396
4	19.823				55912	15.531	15.531
5	18.3542				72661	20.184	20.184
6	16.6966				84077	23.355	23.355
7							
8							
9							
10							

CONVERGENCE CURVE

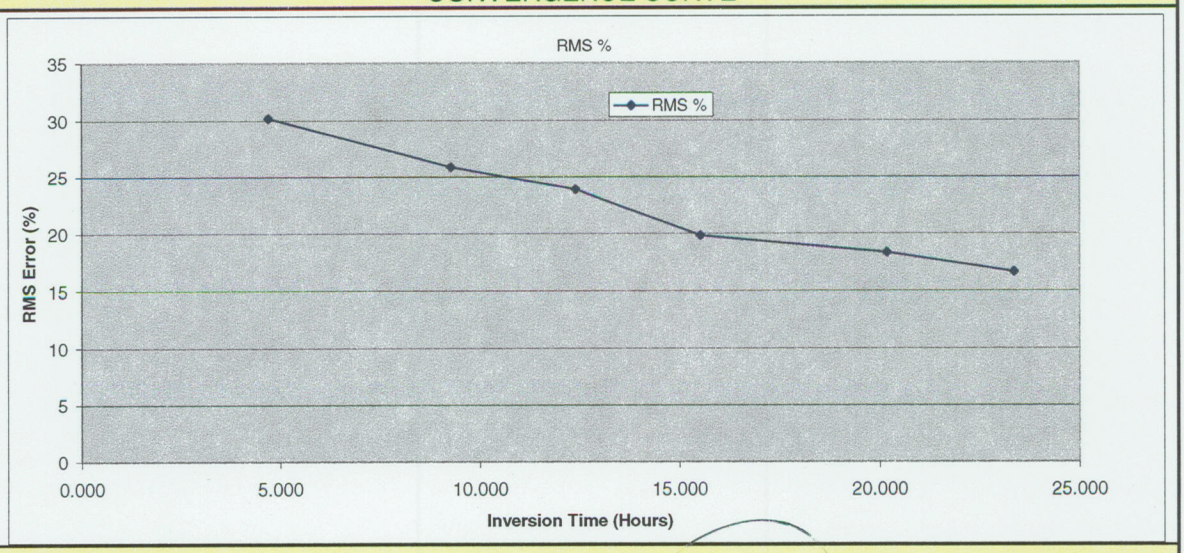

SIGNATURE

Inversion Operator Signature

9/23/09
Date

Reviewer Signature

Gillian Noonan
Reviewer Name

9/23/09
Date

Project Manager Signature

James B. Fink
Project Manager Name

28 Sept 2009
Date

hydroGEOPHYSICS	RES3D Inversion Model Tracking and Statistics	Page 1 of 2
	Date: 9/25/2009 **Project Name:** Reprocessing of T Farm Resistivity	
	Inversion Operator: Dale Rucker **Project Number:** 2009-020	

ITEM	PARAMETER	REVIEWER Initial & DATE
Inversion Model Name	TFarm_PP_WTS+WTW	GW 9/25
Inversion Model Folder	\\snowwhite\jobs\2009-020 Reprocessing of T Farm Resistivity Data\Data\WTS\Res3D	
Data Processing Server Name	snowwhite	
Purpose or Description of Inversion Model	Characterization of T Farm and surrounding areas using compiled pole pole WTS and WTW data.	
Raw Data File(s) & Location	\\snowwhite\jobs\2009-020 Reprocessing of T Farm Resistivity Data\Data\WTS\Original Work and \\snowwhite\2009-020 Reprocessing of T Farm Resistivity Data\Data\WTW\Raw WTW Data\WELDIPA.stg	GW 9/25
Input File Name & Location	\\snowwhite\jobs\2009-020 Reprocessing of T Farm Resistivity Data\Data\WTS\Res3D\Tfarm WTS+WTW.dat	GW 9/25
Description of Filtering/Editing Applied to Input File	Filtered negative, high error and outlying resistivity values. Removed repeated TX/RX data. GPS locations of the surface electrodes were rounded to fit a 3 meter grid. For wells within 5 meters of each other one was chosen for data input, due to code restrictions and meshing requirements. Filtered very low and very high resistivity values. Removed duplicates, removed close proximity wells, removed negative app res data.	
Inversion Parameter File Name & Location	\\snowwhite\jobs\2009-020 Reprocessing of T Farm Resistivity Data\Data\WTS\Res3D\Tfarm WTS+WTW.ivp	
Output File Name & Location	\\snowwhite\jobs\2009-020 Reprocessing of T Farm Resistivity Data\Data\WTS\Res3D\Tfarm WTS+WTW.inv	GW 9/25
Start Date	Batch mode - Not available	GW 9/25
Start Time	Batch mode - Not available	
End Date	Batch mode - Not available	
End Time	Batch mode - Not available	
Avg. Hours per Iteration	3.93	
Total Running Hours	23.61	
System Pause Time (Hours)	0	
Northing Range(m)	347	GW 9/25
Easting Range(m)	365	
Easting Min (UTM)	566,629	
Northing Min (UTM)	136,536	
Easting Max (UTM)	566,994	
Northing Max (UTM)	136,883	
Domain Area (Sq meters)	126,655	
Domain Area (Acres)	31.3	
Software Name	RES3DINVx64	GW 9/25
Software Version	v.3.01.07	
Electrode Type	WTS	GW 9/25
No. Data Points	25,013	
No. Model Blocks	3,658	
Notes	Well Resistivity = 0.006, Cross sectional area = 0.1	GW 9/25

hydroGEOPHYSICS

RES3D Inversion Model Tracking and Statistics

Page 2 of 2

Date: 9/25/2009 **Project Name:** Reprocessing of T Farm Resistivity

Inversion Operator: Dale Rucker **Project Number:** 2009-020

Iteration Number	RMS %	L2	Hrs	Min	Sec	D.Hr	Elapsed Time (D.Hr)
1	29.9566				17234	4.787	4.787
2	26.1369				33841	9.400	9.400
3	24.1677				45210	12.558	12.558
4	21.8836				56620	15.728	15.728
5	20.7201				73432	20.398	20.398
6	19.4744				84990	23.608	23.608
7							
8							
9							
10							

CONVERGENCE CURVE

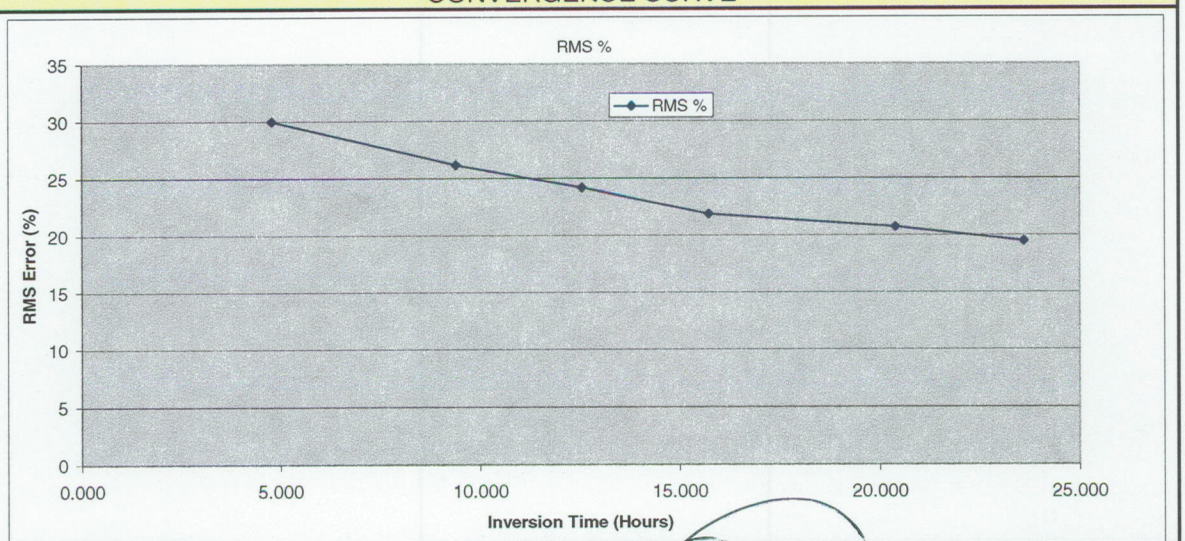

SIGNATURE

Inversion Operator Signature

9/25/09

Date

Reviewer Signature

Gillian Noonan

Reviewer Name

9/25/09

Date

Project Manager Signature

James B. Fink

Project Manager Name

28 Sept 2009

Date

HGI hydroGEOPHYSICS	RES3D Inversion Model Tracking and Statistics			Page 1 of 2
	Date:	9/28/2009	Project Name:	Reprocessing of T Farm Resistivity
	Inversion Operator:	Dale Rucker	Project Number:	2009-020

ITEM	PARAMETER	REVIEWER Initial & DATE
Inversion Model Name	TFarm_PP_WTS+WTW_partial	GW 9/28
Inversion Model Folder	\\snowwhite\jobs\2009-020 Reprocessing of T Farm Resistivity Data\Data\WTS\Res3D	
Data Processing Server Name	snowwhite	
Purpose or Description of Inversion Model	Characterization of T Farm and surrounding areas using a subset of compiled pole pole WTS and WTW data.	
Raw Data File(s) & Location	\\snowwhite\jobs\2009-020 Reprocessing of T Farm Resistivity Data\Data\WTS\Original Work and \\snowwhite\2009-020 Reprocessing of T Farm Resistivity Data\Data\WTW\Raw WTW Data\WELDIPA.stg	GW 9/28
Input File Name & Location	\\snowwhite\jobs\2009-020 Reprocessing of T Farm Resistivity Data\Data\WTS\Res3D\TFarm WTS+WTW partial.dat	GW 9/28
Description of Filtering/Editing Applied to Input File	Filtered negative, high error and outlying resistivity values. Removed repeated TX/RX data. GPS locations of the surface electrodes were rounded to fit a 3 meter grid. For wells within 5 meters of each other one was chosen for data input, due to code restrictions and meshing requirements. Filtered very low and very high resistivity values. Removed duplicates, removed close proximity wells, removed negative app res data.	
Inversion Parameter File Name & Location	\\snowwhite\jobs\2009-020 Reprocessing of T Farm Resistivity Data\Data\WTS\Res3D\Tfarm WTS+WTW partial.ivp	
Output File Name & Location	\\snowwhite\jobs\2009-020 Reprocessing of T Farm Resistivity Data\Data\WTS\Res3D\Tfarm WTS+WTW partial.inv	GW 9/28
Start Date	Batch mode - Not available	GW 9/28
Start Time	Batch mode - Not available	
End Date	Batch mode - Not available	
End Time	Batch mode - Not available	
Avg. Hours per Iteration	1.47	
Total Running Hours	8.81	
System Pause Time (Hours)	0	
Northing Range(m)	347	GW 9/28
Easting Range(m)	365	
Easting Min (UTM)	566,629	
Northing Min (UTM)	136,536	
Easting Max (UTM)	566,994	
Northing Max (UTM)	136,883	
Domain Area (Sq meters)	126,655	
Domain Area (Acres)	31.3	
Software Name	RES3DINVx64	GW 9/28
Software Version	v.3.01.07	
Electrode Type	WTS	GW 9/28
No. Data Points	12,922	
No. Model Blocks	3,658	
Notes	Well Resistivity = 0.001, Cross sectional area = 0.1	GW 9/28

hydroGEOPHYSICS

RES3D Inversion Model Tracking and Statistics

Page 2 of 2

Date:	9/28/2009	Project Name:	Reprocessing of T Farm Resistivity
Inversion Operator:	Dale Rucker	Project Number:	2009-020

Iteration Number	RMS %	L2	Hrs	Min	Sec	D.Hr	Elapsed Time (D.Hr)
1	25.5295				6499	1.805	1.805
2	22.7728				12715	3.532	3.532
3	19.7992				16968	4.713	4.713
4	16.9876				21218	5.894	5.894
5	15.2892				27459	7.628	7.628
6	14.3236				31724	8.812	8.812
7							
8							
9							
10							

CONVERGENCE CURVE

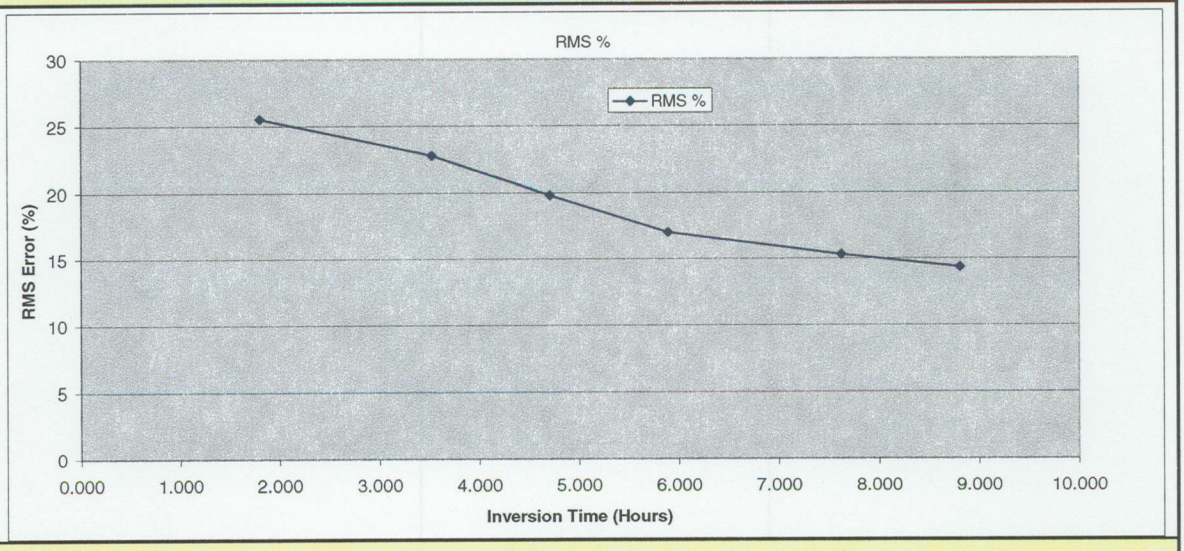

SIGNATURE

Inversion Operator Signature

9/28/09
Date

Reviewer Signature

Gillian Noonan
Reviewer Name

9/28/09
Date

Project Manager Signature

James B. Fink
Project Manager Name

28 Sept 2009
Date